Tampere University

HIEN LE

A Novel Synthetic Agonist of P2Y1

Purinergic Receptor Acts as An Anticancer Agent for Prostate Cancer Treatment

Tampere University Dissertations 720

Tampere University Dissertations 720

HIEN LE

A Novel Synthetic Agonist of P2Y1

Purinergic Receptor Acts as An Anticancer Agent for Prostate Cancer Treatment

ACADEMIC DISSERTATION
To be presented, with the permission of
the Faculty of Medicine and Health Technology
of Tampere University,
for public discussion at Tampere University
on 20th December 2022, at 15 o'clock.

ACADEMIC DISSERTATION
Tampere University, Faculty of Medicine and Health Technology
Finland

Responsible supervisor
Adjunct Professor
Meenakshisundaram Kandhavelu
Tampere University
Finland

Supervisor
Professor Olli Yli-Harja
Tampere University
Finland

Pre-examiners
Associate Professor
Srivatsan (Sri) Kidambi
University of Nebraska-Lincoln
USA

Professor
Israel V. Muthu Vijayan Enoch
Karunya Institute of Technology and Sciences
India

Opponent
Professor Arun K. Sharma
Penn State College of Medicine
USA

Custos
Professor Olli Yli-Harja
Tampere University
Finland

The originality of this thesis has been checked using the Turnitin OriginalityCheck service.

Cover design: Roihu Inc.

ISBN 978-952-03-2691-3 (print)
ISBN 978-952-03-2692-0 (pdf)
ISSN 2489-9860 (print)
ISSN 2490-0028 (pdf)
http://urn.fi/URN:ISBN:978-952-03-2692-0

HIILINEUTRAALI PAINOTUOTE
ClimateCalc CC-000025/FI
PunaMusta Printing

Carbon dioxide emissions from printing Tampere University dissertations have been compensated.

PunaMusta Oy – Yliopistopaino
Joensuu 2022

This thesis is dedicated to my little angle.

ACKNOWLEDGEMENTS

This thesis work was carried out during 2018-2022 at Molecular Signaling Lab, Faculty of Medicine and Health Technology, Tampere University. This thesis was funded by Tampere University and TUT-RAE for financial support and instrumental facility grant support, which has enabled me to carry out the study, widened my academic perspective, and attended international conferences. The financial support is truly meaningful. I would like to thank all the people who have helped me through the years and made the thesis become possible.

Foremost, I would like to express my sincere gratitude to my supervisor, Adjunct Professor Meenakshisundaram Kandhavelu for his guidance, encouragement, and continuous support for my research. His patience, motivation, enthusiasm, and knowledge have always impressed me and encouraged me to face any challenges in the research. Besides my advisor, I am truly grateful to my co-supervisor, Professor Olli Yli-Harja for sharing his valuable guidance, inspiration, and support to succeed in my thesis. I am thankful to my instructor, Professor Frank Emmert-Streib for the enlightening and inspiring discussion about computational biology parts, which helped me to understand and finalize my thesis. I also wish to thank Professor Nuno Rafael Candeias for his expert work in the world of chemical synthesis. With his nice support, I could continue my research experiments for over 4 years. I want to thank the pre-examiners for this thesis, Associate Professor Srivatsan (Sri) Kidambi and Professor Dr. Israel V. Muthu Vijayan Enoch for their valuable comments and encouragement. I would like to thank Professor Arun K. Sharma for his agreement to become the opponent in my Ph.D. defense.

During my doctoral degree, I am also truly grateful to all my other co-authors for their help, contributions, and advice that made these publications belonging to this thesis possible. Especially, I would like to thank Ph.D. Akshaya Murugesan for proofreading my manuscripts and giving me a lot of scientific concern during my research. I also wish to thank Ph.D. Aliyu Musa and MSc. Vili Sipilä for their expert help in bioinformatics and image analysis. I would like to thank Ph.D. Thiyagarajan Ramesh for sharing his wide expertise in protein complex analysis.

Furthermore, my sincerest thanks go also to Professor Sayeon Cho for his kind comments and advice regarding my study. With his encouragement, I became

confident to pursue higher steps in my study and career after finishing my master's degree in 2017.

Special thanks are reserved to my present and past members at Molecular Signaling Lab, Ph.D. Anisha Viswanathan, Ph.D. Phuong Doan, MSc. Tien Nguyen, MSc. Nga Nguyen, MSc. Giulia Seba. You have made a pleasant atmosphere working environment and I am thankful for all the great co-works and memories we have made together.

I would like to thank my senior, Ph.D. Huiyun Seo for her advice, love, and care since I studied for my master's degree in Korea and now almost have completed my Ph.D. degree. I also thank my friends, Nga Nguyen, Huyen Phan, and Paulli Ruuska for their help, support, and care during my journey in Finland. For the support in bioinformatics, special thanks are reserved for MSc. Anja Hartewig for her nice guidance and help whatever I ask.

Last but not the least, I would like to thank my family in Viet Nam, especially, my parents for giving birth to me in the first place and supporting me spiritually throughout my life. My parents-in-law have truly supported and shared my concerns by giving me lots of care and encouragement. Also, my sweet sister, Thao Le, thank you so much for your love, faith, and helps when I live far away from Viet Nam. I wish to thank my husband, Anh Hoang, who has stood by me through all my travails and challenges. He has given me love and help and prevented several wrong turns in my decisions. He also helps me take care of the family during much of my Ph.D. degree. **Finally, this thesis is dedicated to my little angle**. He makes me stronger, better, and more fulfilled than I could have ever imagined. I love you more than words can say!

Tampere, August 2022

Hana-Hien Le

ABSTRACT

Prostate cancer (PCa) is one of the most common tumors and the fifth leading cause of death in men worldwide. The high incidence of PCa all over the world has thrown up the challenge of developing new drugs and/or drug combinations that target various signaling pathways, DNA repair mechanisms, and specific epigenetic mechanisms. Despite the wealth of research focused on investigating potential compounds to tackle PCa, its treatment still demands novel therapeutic approaches to overcome castration resistance and metastasis.

One of the most promising approaches to overcoming castration resistance and metastasis is the use of G protein-coupled receptors (GPCRs). These receptors are the largest family of cell surface receptors, and they respond to extracellular nucleotides. They also modulate various physiological functions during cancer progression and treatment. Among this eight-member receptor family, it has been observed that the activation of the purinergic receptor 1 (P2Y1R) induces apoptosis and cell death, not only in negative-androgen PCa cells but also in other cancer cells. This indicates that P2Y1 is a potential target for the treatment of PCa. Furthermore, a combination of MRS2365 and P2Y1R both inhibited cell proliferation and increased the apoptotic response through increased caspase 3 activity and higher lactate dehydrogenase levels in the PC3 cells. However, no detailed investigation of the molecular mechanisms occurring in P2Y1R and its agonists in negative-androgen PCa has yet been carried out.

Thus, this thesis focuses on investigating the molecular mechanisms that occur when potential ligands target P2Y1R, particularly those mechanisms that inhibit the growth and proliferation of PCa cells. Docking analysis of about 900 ligands as substituents of 1-indolinoalkyl 2-phenols with P2Y1R reveals 1-(2-Hydroxy-5-nitrophenyl) (4-hydroxyphenyl) methyl) indoline-4-carbonitrile) (HIC) and Methyl 4-((4-cuamoimdolin-1-yl) (2,5-dihydroxyphenyl) methyl) benzoate (MB) to be the two top ligands with the highest docking score. Both of these compounds increase the intracellular calcium level in two of the PCa cells, PC3 and DU145. They have thus been identified as potent agonists of P2Y1R. Although both ligands were able to suppress cell proliferation in a dose- and time-dependent manner, HIC effectively

and selectively inhibits cell proliferation at lower concentrations and is thus selected for further analysis.

A molecular dynamics simulation specifically confirms the stable binding of HIC-P2Y1R, and this is validated through siRNA analysis. In addition, our results reveal that HIC could reduce and inhibit the cancer's adherence properties, its ability to form colonies and cancer metastasis, and it could also interrupt the cell progression of both PC3 and DU145 cells at G1/S phase arrest. Gene expression analysis also indicates that HIC is able to induce DNA damage, the activation of p53 and p21signaling-mediated apoptosis, and cell cycle arrest in PCa cells. It achieves these effects by modulating the expression of significant genes like *PARPs*, *BAX*, *CDKs*, and *MDMs*. The data also indicates HIC to be a potent anti-cancer agent through its ability to inhibit mitochondrial membrane activity and the glutathione levels in PCa cells.

During the development of PCa therapy, combination chemotherapy has emerged as a mainstay in the treatment of cancer cells with a reduced risk of incurring drug resistance. The effect of combining HIC and abiraterone acetate (AA), a chemotherapeutic drug for PCa, was investigated for its anti-cancer effects on PCa cells. The synergistic effect of HIC and AA increases the cytotoxicity in PCa cells more effectively than each drug did on its own. Moreover, a combination of HIC and AA also induces apoptosis via p53 and p21 signaling, cell cycle arrest, caspase 3/7 activation, increased ROS levels, and the inhibition of migrated and invaded cancer cells. Thus, combination treatment with HIC and AA could contribute to the development of new strategies for PCa treatment.

HIC could be seen as multiple molecular targets through their inhibition of the *MDMs* and *PARPs* in PCa cells. The activation of P2Y1R might also benefit patients with lower AR expression levels and metastasis cancer. In addition, the synergy of HIC and AA could facilitate the targeted inhibition of PCa cells more effectively than monotherapy. All in all, the results shed light on the important role HIC-P2Y1 agonist play in inhibiting the development and progression of PCa through their ability to promote p53 and p21 signaling. However, further preclinical investigation on in-vivo models and patients' samples should be carried out to evaluate the efficacy of adopting a combinatorial therapeutic approach with HIC in the future.

TABLE OF CONTENTS

List of Figures

List of Tables

ABBREVIATIONS

AA	Abiraterone acetate
AKT	Protein kinase B
AR	Androgen receptor
BAX	BAX
BAX	BAX
CaMKIIα	calmodulin-dependent protein kinase II
cAMP	Cyclin adenosine monophosphate
CI	Combination index
CRPC	Castration-resistant prostate cancer
DGE	Gene expression levels
DMEM	Dulbecco's modified eagle medium high glucose
ERBT	External-beam radiotherapy
FDA	Food and drug administration
GPS	Genomic prostate score
GSH	Glutathione
Gscore	GlideScore
H2DCFA	Fluorescent 2',7-dichlorodihydroglurescein diacetate
H_2O_2	Hydrogen peroxide
HIC	1-(2-Hydroxyl-5-notrophenyl)(4-hydroxyphenyl)indoline-4-carbonitrite
HPS	Heat shock protein
HTSeq	High-throughput sequencing data
IC_{50}	Half maximal inhibitory concentration
IMRT	Intensity-modulated radiation therapy
IP3	Inositol trisphosphate
KEGG	Kyoto encyclopedia of genes and genomes
LPC	Local prostate cancer
MB	Methyl 4-((4-cyanoindolin-1-yl)(2,5-dihydroxyphenyl) methyl) benzoate
MAPKs	Mitogen-activated protein kinases
mCRPC	Metastasis CRPC

MDM2	E3 ubiquitin protein ligase
MEF	Fibroblast cell line
MtMP	Mitochondiral membrane potential
NCCN	National Comprehensive Cancer Network
P2Y1R	Purinergic receptor 1
PARP	Poly(adenosine diphosphate-ribose) polymerase
PCa	Prostate cancer
PCR	Polymerase chain reaction
PI3K	Phosphoinositide 3-kinase
PIP2	Phosphatidylinositol 4,5-bisphosphate
PIP3	Phosphatidylinositol (3,4,5)-triphosphate
PLC	Phospholipase C
PLDN	Pelvic lymåhadenectomy
PSA	Prostate specific antigen
PTEN	Phosphatase and tensin homolog
TGFβ	Transforming growth factor beta
TNF-α	Tumor necrosis factor
ROS	Reactive oxygen species

ORIGINAL PUBLICATIONS

Publication I H. Le, T. Rimpiläinen, S. K. Mani, A. Murugesan, O. Yli-Harja, N. R. Candeias, and M. Kandhavelu, "Synthesis and preclinical validation of novel P2Y1 receptor ligands as a potent anti-prostate cancer agent", Scientific reports (2019), 9, 18938, DOI: 10.1038/s41598-019-55194-8

Publication II H. Le, A. Murugesan, T. Ramesh, O. Yli-Harja, K. M. Saravanan, and M. Kandhavelu, "Molecular interaction of HIC, an agonist of P2Y1 receptor, and its role in prostate cancer apoptosis", International Journal of Biological Macromolecules (2021), 189, DOI: 10.1016/j.ijbiomac.2021.08.103

Publication III H. Le, A. Murugesan, N. R. Candeias, O. Yli-Harja, and M. Kandhavelu, "Functional characterization of HIC, a P2Y1 agonist, as a p53 stabilizer for prostate cancer cell death induction", Future medicinal chemistry (2021), 13, 21, DOI: 10.4155/fmc-2021-0159

Publication IV H. Le, A. Murugesan, N. R. Candeias, T. Ramesh, O. Yli-Harja, and M. Kandhavelu, "P2Y1 agonist HIC in combination with androgen receptor inhibitor abiraterone acetate impairs cell growth of prostate cancer", Apoptosis (2022): 27,3, DOI: 10.1007/s10495-022-01716-1

AUTHOR CONTRIBUTIONS

Publication I	S. K. Mani executed the docking analysis and computational analysis. T. Rimpiläinen and N. R. Candeias conceived the chemical synthesis. H. Le performed biological and biochemical experiments to evaluate the effects of HIC and MB on PCa cells. N. R. Candeias, O. Yli-Harja, and M. Kandhavelu managed and provided feedback to the research. All the authors contributed to writing the manuscript.
Publication II	T. Ramesh and K. M. Saravanan conducted the docking and computational analysis. H. Le performed biological and biochemical experiments to evaluate the effects of HIC on PCa cells and handled statistical analysis. H. Le, A. Murugesan, and K. M. Saravanan involved in editing the manuscript. O. Yli-Harja, K. M. Saravanan, and M. Kandhavelu conceived and guided the research. All the authors contributed to writing the manuscript.
Publication III	H. Le conducted the biological and biochemical experiments to investigate the anti-cancer effect of HIC on PCa cells and also managed the statistical analysis. H. Le and M. Kandhavelu supported each other to perform computational analysis. A. Murugesan was involved in the results discussion and manuscript editing. N. R. Candeias provided the chemical synthesis. O. Yli-Harja and M. Kandhavelu managed the research. All the authors contributed to writing the manuscript.
Publication IV	H. Le defined the methods to evaluate the combinational drugs in PCa cells and statistical analysis. T. Ramesh gave the critical feedback. A. Murugesan and T. Ramesh provided further critical feedback and were involved in technical discussions. N. R. Candeias provided the chemical synthesis. O. Yli-Harja and M. Kandhavelu controlled the research. All the authors contributed to writing the manuscript.

1 INTRODUCTION

Prostate cancer (PCa) is one of the most common non-cutaneous cancers and is the fifth leading cause of male deaths worldwide (Sandhu et al., 2021). GLOBOCAN estimates that there were 1,414,259 new cases of PCa in 2018, 3.8% of which resulted in death. It is reported that the 5-year survival rate of patients with local or territorial PCa is nearly 95% (Lehto et al., 2017). However, in patients diagnosed with castration-resistant or metastasis PCa in other organs in the body, the five-year survival rates and the quality of life are lower. Further investigation of these mysterious molecular mechanisms that underly the progression and treatment of PCa could greatly improve the quality of life of PCa patients.

One of the more effective approaches in the diagnosis and prognosis of PCa is the identification of novel molecular markers. These have great potential as targets for chemotherapy treatment (Alford et al., 2017). During drug discovery for PCa, an extensive diagnosis of potential molecular markers was used as a model for improving the efficacy of PCa treatment. Nowadays the identification of biomarkers is recognized as an important approach to finding treatments for both PCa and for localized PCa (LPC). As such, it is nearly always part of the primary treatment plan (Loeb and Ross, 2017).

There are many commercially produced diagnostic kits that utilize these biomarkers. For example, ConfirmMDx, Prolaris, OncotypeDx, Decipher, and Promark are primary tests that are all based on the changes in specific genes and proteins in prostate biopsy tissue. A number of surveys have shown that the tests do have value, certainly as far as clinicians and doctors are concerned. Opinion surveys have consistently shown that doctors feel more confident in making decisions about PCa treatment plans when they have the results of these tests available, particularly for patients with LPC (López et al., 2017). Among the known biomarkers for PCa, the androgen receptor (AR) has long been regarded as a primary biomarker for LPC as well as for advanced PCa. However, a recent study described a prostate tumor that resisted the treatment of AR mutations and metastasis cancer with negative-AR expression (Ahmed et al., 2014). To prevent the development and progression of PCa more effectively, especially in negative-AR expression conditions, we need to

investigate any new molecules with the potential to act as anti-cancer agents in PCa through mechanism signaling.

G protein-coupled receptors (GPCRs), the largest family of functionally active receptors on cell membranes, are considered to have the most potential as a target for drug discovery (Sriram and Insel, 2018). In fact, one-third of current clinical drugs and nearly two-thirds of drugs in development use GPCRs. The association between GPCRs, tumor metastasis and cancer survival has been proven over the past few decades (Lappano and Maggiolini, 2011). As members of the GPCR family, purinergic receptors (P2YRs) are one of three families of extracellular receptors suitable to act as purine and pyrimidine nucleotides (Jacobson et al., 2020). Researchers have already discovered some promising characteristics of the P2YR range. Based on the differences in the P2YR's gene sequences, protein structures, and functions, there are 8 receptor subtypes: P2Y1, P2Y2, P2Y4, P2Y6, P2Y11, P2Y12, P2Y13, and P2Y14 (Campos-Contreras et al., 2020; Jacobson et al., 2020). Of these, the P2Y1 protein's expression is higher in PC3 and DU145 cells, and also in cancer cells with low AR expression, than it is in non-cancerous controls (Janssens et al., 1996; Li et al., 2013; Shabbir et al., 2008; Wei et al., 2011). According to Wan et al., (2016) different biological responses to P2Y1R activity on cell phenomena have been recorded for ligands and cell types, such as cell proliferation and apoptosis. Even before that study, Wei et al had reported that a combination of the selective agonist MRS2365 and P2Y1R could induce apoptosis and inhibit the proliferation of PC3 cells (Wei et al., 2011). However, other research into the mechanisms behind the inhibitory effect of P2Y1R activation in PCa is still inconclusive, so this study will investigate P2Y1R and its ligands, with a detailed investigation of the molecular targets in DU145 and PC3 cells.

Phenolic compounds have been shown to inhibit cancer cell proliferation and induce cell death in a number of studies (Anantharaju et al., 2016; Wahle et al., 2010). Since phenolic compounds have properties that impede cancer cell survival, a number of the substituents of 1-indolinoalkyl 2-phenols were used as the original library for the docking analysis with P2Y1R. Two of the synthesized ligands, 1-(2-Hydroxyl-5-notrophenyl)(4-hydroxyphenyl)indoline-4-carbonitrite (HIC) and Methyl 4-((4-cyanoindolin-1-yl)(2,5-dihydroxyphenyl) methyl) benzoate (MB) have been found to be stronger with P2Y1R than MRS2500, a known antagonist of the receptor. More specifically, the present study documents the use of a novel ligand, HIC. This has great potential as an anti-cancer drug as it causes PCa cell death and induces an apoptotic response. The insight mechanism of HIC in prostate models was addressed in order to explain its anti-cancer effects through DNA damage,

apoptosis, and cell arrest analysis. The effects of HIC in PCa cells are noted in the form of an increase in p53 stabilization and a decrease in both poly- (ADP ribose) polymerase (PARP) and the transforming growth factor beta (TGFβ). Furthermore, combination therapy using the new ligand HIC with AA, a clinical drug that targets AR, was performed in negative- or low-expression AR cells. The combination treatment of HIC and AA is a synergistic model. These findings suggest that such combinatorial compounds should be explored as promising drugs for fighting PCa. Ultimately, this thesis provides new insight into the design of ligand-like compounds based on a P2Y1R structure. The work addresses several challenging issues in PCa treatment using molecular markers, cell signaling, and combination therapy.

2 REVIEW OF THE LITERATURE

2.1 Prostate cancer

Prostate cancer (PCa) is second only to lung cancer as being the most prevalent cancer in males worldwide. One of the problems with PCa is that some relatively mild symptoms of the disease often remain undetected until the cancer is in its later stages. (As et al., 2008; Cooperberg et al., 2011; Soloway et al., 2010; Tosoian et al., 2011) Another problem is that although up to 95% of PCa patients should survive the first 5 years, clinical studies have reported that up to 33% of males under active observation need some kind of therapeutic intervention after an average of 1.2 – 3.5 years.

There is clearly a need for new approaches to the treatment of PCa. These should be focused on improving the quality of life of PCa patients and avoiding the proliferation of treatment-resistant cancer cells. Such research will require a thorough understanding of the biomolecular mechanisms that occur in PCa cells that are being treated with anti-cancer drugs. The research must also aim to "improve the efficacy" of cancer therapy (Bergh et al., 2009; Egevad et al., 2013; McKenney et al., 2011). There follows an attempt to summarize the most notable clinical- and bio-markers in PCa progression, according to the published literature.

2.1.1 Molecular markers in prostate cancer treatment

2.1.1.1 Local prostate cancer

A local prostate cancer (LPC) is a tumor that is located on only one side of the prostate gland. It has not yet spread to any other organ in the body (Cheng et al., 2012). It is essential to use every available means to catch cancer as early as possible before it starts to spread. The results of regular cancer screening tests can also be used to help select the optimal therapies. The survival rates and quality of life for patients with an LPC can be greatly improved through early diagnosis (Cuzick et al., 2014).

Recent research by Loeb and Ross (2017) has shown that genetic tests can provide estimated prognoses for LPC patients. These prognoses can predict specific changes in genes, chromosomes, or proteins. Plenty of genomic tests have been carried out in LPC research but this study will confine itself to describing five popular commercially produced kits used to detect LPC-based biomarkers: ConfirmMDx, Prolaris, OncotypeDx, Decipher, and ProMark (Table 1). All of these kits can test biopsy tissue to predict the risk of disease. They also help clinicians make optimally therapeutic decisions for their PCa patients. Table 1 gives an overview of these products.

Table 1. Overall view of biomarkers in LPC. Five commercial kits for detecting biomarkers of prostate biopsy tissue samples in LPC. The table is modified from (Falzarano et al., 2015).

No	Test	Assay	Biomarkers
1	ConfirmMDx	Methylation via PCR	Specific targets: GSTP1, APC, RASSF2
2	Prolaris	mRNA expression	46 genes with 31 genes regulated to cell cycle and 15 housekeeping genes
3	OncotypeDx	RT-PCR	17 genes with 12 genes linked to androgen, cell proliferation, stromal response, and cellular pathways
4	Decipher	Whole trascriptome microarray	22 coding and non-coding RNAs regulated to cell differentiation, cell phase, cell adhesion and migration, androgen signaling, and immune modulation
5	Promark	Automatic fluorescent imaging platform	8 protein markers

ConfirmMDx

ConfirmMDx is a polymerase chain reaction (PCR) test that measures the methylation in cancer tissues quantitatively to detect an epigenetic field effect which shows the progression of cancer (Yonover et al., 2019). The cancer is evaluated by following any changes in the values of GSTP1, APC, and RASSF2. The methylations of APC and RASSF2 are susceptible to detecting false positives in PCa from the cancer biopsy. The methylation evaluation of ConfirmMDx in patients' samples which determined negative cancer by the biopsy detection means a positive result for suggesting a cancer region that was missed in the previous investigation. Thus, the main commercial use for the ConfirmMDx test is to evaluate cancer cases that can't be detected from biopsies with a standard microscopic evaluation by

pathologists (Kohaar et al., 2019). Recently, the test has been cited in the USA National Comprehensive Cancer Network (NCCN) guidelines for patients who have had one prior negative result in a biopsy evaluation.

Prolaris

Prolaris aims to detect the mRNA of the genes related to cell cycle progression. It is based on the changes in 46 genes in prostate biopsy tissue related to cell phase progression (Falzarano et al., 2015). The cell cycle progression scores detected in the biopsy can be used to predict the outcome effects after radiation therapy in patients receiving primary treatment for PCa. Recent studies have shown that the cell cycle progression scores are a crucial prognostic factor for biochemical recurrence and cancer metastasis in patients after they have had a prostatectomy (Bauman et al., 2017). Since then, a number of clinical studies have also investigated the topic using a variety of questionaries asking clinicians whether the results of such tests could influence clinical procedures and best practices (López et al., 2017). The results of these studies indicate that there is a 30% link between the results of the tests and changes in clinical practices. These figures are based on a survey of the consequences of Prolaris tests carried out on a tranche of 15 urologists with 294 clinical cases.

OncotypeDx

The OncotypeDx test is based on a genomic prostate score (GPS) taken from 12 genes linked to 4 different pathways: AR, cell proliferation, stromal response, and cellular progression. There is significant regulation of the GPS scores in the tumor grade and pathological stages of PCa (Table 1) (Klein et al., 2013). The efficacy of using OncotypeDx results to detect the different stages of cancer was proved in a study involving 395 PCa patients with low and intermediate-risk diseases. Later, a combination of GPS and a prostate risk assessment score were used to enhance the discrimination of adverse pathology findings. This combination was able to detect more cancer cases than were detected with the prostate risk assessment score alone (EA et al., 2014; J et al., 2015). The current thinking is that the test could be linked to decisions about the patient's management. One thing that the questionnaires do make clear is that clinicians feel more confident about making decisions when they have the GPS scores available (Badani et al., 2015).

Decipher

The Decipher test is a relatively new research tool that detects 1.4 million marker expressions per patient by analyzing the expression of 22 RNA biomarkers regulated to multiple pathways in a PCa tumor (Table 1) (Dalela et al., 2017; JL et al., 2017). The twenty-two RNA expressions are commonly detected in cell growth, cell cycle progression, cell metastasis, AR, and immune modulation. The algorithmic score of the decipher test ranges from 0 to 1, where a higher score relates to a higher chance of cancer metastasis (Marascio et al., 2019; Spratt et al., 2017). Clinical evaluation of Decipher has shown that it is more effective at predicting cancer metastasis than a traditional assessment of the patient's clinical and pathological features. The best thing about the Decipher test is that it works with only a small number of samples.

Decipher was first validated in a study of 1,010 patients who had undergone radical prostatectomy (Karnes et al., 2013). In a subsequent study, the distribution of the Decipher score was also evaluated to assess the impact of adverse pathology for radical prostatectomy in males under active surveillance (Herlemann et al., 2020). The study was carried out with 647 patients diagnosed as low risk under the NCCN categorization, or as a favorable-intermediate risk PCa on a database of multiple-institutional PCa biopsies. The aim was to determine the ability of Decipher to predict adverse pathology after radical prostatectomy in males. The analysis results suggested Decipher is a useful tool in all risk groups of PCa when used with active surveillance, as recommended by the National Comprehensive Cancer Network for patients (Kim et al., 2019).

Promark

Promark is used to detect multiple protein biomarkers. The test kit uses automated immunofluorescent images to predict the disease's aggressiveness and possible outcomes (Blume-Jensen et al., 2015; Shipitsin et al., 2014b, 2014a). The efficacy of 8 of Promark's biomarkers was shown in a National Comprehensive Cancer Network study of two independent groups totaling 657 patient biopsies (Blume-Jensen et al., 2015). The quantitative measurements of the protein biomarkers provided further useful information for the urologists. The results of the Promark tests enabled the clinicians to stratify the patients according to the state of the cancer and its aggressiveness (Shipitsin et al., 2014). Indeed, recent studies have produced promising results for Promark tests giving patients a Gleason score of 3+3=6 and 3+4=7, as well as a more detailed evaluation of the state of the PCa. However, the

differences in genomics between the different regions of one individual tumor is still a problem for the Promark test. This is because the expression of the 8 biomarkers is dependent on the location from which the biopsy was taken. Moreover, the volume of cancer samples required for this type of analysis might also be a limiting factor, particularly if used for low-risk cancer patients.

2.1.1.2 Advanced prostate cancer

Advanced prostate cancer is classed as a heterogenous disease for which the prognoses are extremely variable. Multiple therapeutic options to improve the survival rate and life quality of patients with advanced PCa have been identified. For example, AR has been used as a mandatory biomarker for advanced PCa for centuries. Nevertheless, a recent study described a prostate tumor that has shown resistance to the therapeutic progression of AR mutations (Ahmed et al., 2014; Fujita and Nonomura, 2019). So, the search for novel biomarkers continues. Any biomarkers which have the potential to improve the clinical outcomes for patients with advanced PCa are being investigated as potential targets for PCa therapy (Beltran et al., 2016; Iacovelli et al., 2020). This chapter describes some of the more common biomarkers for PCa that work on the same principle as the AR shown in Figure 1, below.

AR-Androgen receptor

The Androgen Receptor (AR), the vital control for the development of normal prostate, has been associated with the growth of prostate tumors (Fujita and Nonomura, 2019; Karantanos et al., 2015). The combination of AR and natural ligands as androgenic hormones, testosterone, and metabolite dihydrotestosterone (DHT) leads to nucleic translocations in the cytoplasm and transcriptional activation of the target genes (Figure 1). Since the ligands bind to the AR, the receptor can interact with the heat-shock proteins (HSP) in the cytoplasm. This interaction is directly linked to a conformation change of the HSP structure and replacement of the HSP protein (Culig and Santer, 2014). The AR's sequence of activation prevents the degradation of the proteasome and the ubiquitin. Dimerization between the interaction of the AR and the ligands is then transported into the nucleus to interact with the promoter or enhancer regions of the DNA. The outcomes of these interactions initiate various transcription factors and growth pathways such as cell

proliferation, an anti-apoptotic response, and androgen-regulated genes in a prostate-specific antigen (PSA).

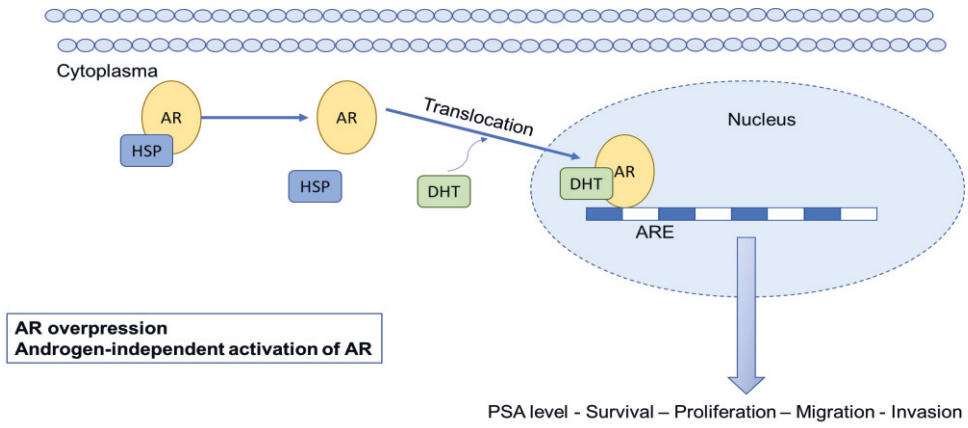

Figure 1. AR dependent signaling in PCa. Upon binding to DHT, AR releases HSP in cytoplasm and translocates to the nucleus with DHT to activate its target genes and regulate their expressions. The downstream signaling of AR induces an increase in the PSA level, an anti-apoptotic response, cell proliferation, invasion, and migration (Culig and Santer, 2014).

Based on the downstream regulation of AR activity, an AR inhibitor is potentially useful when treating PCa with chemotherapy. It is generally accepted that most advanced PCas are in an active AR state. Thus, androgen deprivation therapy is almost mandatory in such cases, as it results in improved clinical outcomes. However, some high-risk PCas develop into a more moderate castration-resistant prostate cancer (CRPC). This may be due to the AR variant, point mutations, amplification, and/or changes in its cofactors (Watson et al., 2015). To date, 22 known variants of AR have been reported. Among the twenty-two variants, AR-V7 is the most common and abundant variant detected in prostate samples with CRPC using mRNA and protein expression. The highest expression of AR-V7 was detected with immunohistochemistry from the bone biopsy of patients resistant to enzalutamide (Beltran et al., 2016). A high expression of AR-V7 proteins was detected in almost 57% of patients who had been treated with enzalutamide less than 4 months before. In contrast, no such proteins were detected in the biopsies of patients who had received enzalutamide more than 6 months earlier.

In addition, other studies indicated that patients in whom AR-V7 mutations were detected were ineffectively treated with AR inhibitors (Antonarakis et al., 2014, 2015, 2017; Scher et al., 2017). Armstrong and his colleagues reported that men with AR-V7 positive metastasis CRPC (mCRPC) had shorter radiographic progression-free

survival and lower overall survival rates than the control groups (AA et al., 2019). However, this finding couldn't be applied to all patients with mCRPC because it is unclear how accurate its predictions are. Another crucial point mutation of AR is T878A. This activates the receptor by losing the specificity binding of the agonist (Fujita and Nonomura, 2019). It is worth noting that over 15% of CRPC patients have point mutations in the AR genes, most often in the ligand-binding domain of the receptor. The T878A mutation was found in the plasma of 13% of CRPC patients who had been treated with abiraterone. Generally, the number of AR mutations in plasma is a useful guide when selecting the appropriate drugs for CRPC patients.

Finally, the activity of AR is also linked to the opening of the chromatin macromolecules at AR-binding sites, which are linked to several genes. One of the known regulated genes of AR is from the *SRC* kinase family, which includes *SRC-1*, *SRC-2*, and *SRC-3* (Chattopadhyay et al., 2017). A decrease in SRC-1 protein expression significantly inhibits cancer cell proliferation and alters the target genes for AR in PCa (Fujita and Nonomura, 2019). Experiments on mice have shown that this affects the aggressiveness and metastasis of the PCa. SRC-2 expression is amplified in both localized and advanced PCa, whereases SRC-3 expression is only inhibited in advanced cases. The downregulation of the SRC family upon AR activity inhibits tumor growth and increases the chances of survival in PCa progression.

DNA damage pathways

In general, destruction of the DNA repair pathways induces changes in the expressions and structures of genomics and impedes the normal replication mechanisms that inhibit the cancer cells' survival (Burdak-Rothkamm et al., 2020). Several studies have reported that DNA damage pathways are often limited in terms of PCa growth, anti-apoptosis, and cell cycle responses. These limitations are due to the various up- and down-expressions of the regulated genes (Carr and Jones, 2016; Matt and Hofmann, 2016; Trovesi et al., 2013).

A living organism's ability to repair damaged DNA is integral to the process of evolution, which requires specific genes such as BRCAs, HOXBs, and MSHs etc. to maintain the organism's genomic integrity. DNA repair pathways increase the risk of the PCa's aggressive progression. Nevertheless, next-generation sequencing technologies are enabling the assessment of larger genomic intervals. These are amplified in human disease so as to present a quick and comprehensive diagnosis of the disease. Based on 'big data' from 'next-generation' sequencing, some of the

mutations that occur in DNA repair pathways have also been observed in prostate tumors, and they could become mandatory clinical markers in the future. These mutations, particularly the ones in *BRCA2*, *BRCA1*, *PALB2*, *HOXB13*, *MSH2*, *MSH6*, and *ATM,* are known to be associated with an increased risk of the more aggressive forms of PCa.

Recent research has shown that the *BRAC1* and *BRAC2* mutations commonly inhibit the action of the PARP inhibitors, known anti-cancer drugs which prevent cells from repairing single- and double-strand DNA damage (Grewal et al., 2021). The potential of using PARP inhibitors as targets for treating mCRPC was investigated in a clinically effective phase III study (Adashek et al., 2019). The study also showed that the *PALB2* mutation was found in 0.29% of 5472 unselected patients with aggressive PCa while it was 0.21% for the 8016 controls (Wokołorczyk et al., 2021). The *HOXB13* mutation has also been reported from 5083 patients diagnosed with PCa and 1401 random men who were non-PCa or PCa-free according to Fisher's accurate tests and linear regression models (Ewing et al., 2012). The *HOXB13* mutation presents as an oncogene because it decreases apoptosis and promotes prostate carcinogenesis. A number of other mutated genes have been discovered in prostate tissue samples. For example, the *MSH2* and *MSH6* mutations were observed in PCa. The respective mismatch repair proteins were lost in 69% of the tumors. This is associated with increased PCa risk in Lynch syndrome carriers (Dominguez-Valentin et al., 2016).

Cell cycle arrest is another useful tool in PCa therapy. It induces a break in the cell phase amplification that allows cells to repair damaged DNA and grow. The arrest of the cell cycle is controlled by the activation of CHK2 and TP53 (Pizarro et al., 2010). The *ATM* serine/threonine kinase is recruited and activated by DNA double-strand breaks via *CHK2* and *TP53* activity, leading to cell phase arrest and apoptotic response. Altogether, the research suggests that the generation of novel drugs targeted at repairing DNA damage could also be used against PCa in the future.

PTEN/AKT pathway

One of the most common alterations during PCa treatment is the loss of the tumor suppressor, phosphatase and tensin homolog (PTEN). This occurred in around 40% of CRPC patients who had previously received AA post-docetaxel (Ferraldeschi et al., 2015). The activity of PTEN involves a number of cellular processes consisting of cell growth, migration, and invasion, as well as changes in the cellular architecture (Figure 2) (Phin et al., 2013). PTEN regulates the growth factor receptors on the cell

membrane to the transcription factors in the nucleus, and this is directly linked to other tumor suppressors and oncogenic signaling pathways.

Preclinical studies have investigated the PTEN function in the activation of the phosphoinositide 3-kinase (PI3K)/protein kinase B (AKT) pathway. This regulates the AR signaling and can result in a more negative prognosis for PCa patients. Furthermore, PTEN loss and the subsequent AKT activation increase the patient's resistance to radiation and chemotherapy. Inhibition of the active form of AKT inhibits the cancer cells' growth and invasiveness, as well as the cancer cell's survival mechanism. Further information about the development of therapies for mCRPC patients, including AR-targeted therapies and PI3K/AKT inhibitors, is available in the work of Karantanos et al., (2013). A randomized phase III clinical trial between 2017 and 2019 among 1611 mCRPC patients found that the ipatasertib-Akt inhibitor and the abiraterone-AR inhibitor promoted progression-free survival more effectively than a combinatorial therapy of placebo and abiraterone (Sweeney et al., 2021). There were no significant differences between the groups in the test population. The results of this experiment suggested that the clinical values of PTEN/AKT activities in patients with PTEN-loss mCRPC indicate a population with a poor prognosis.

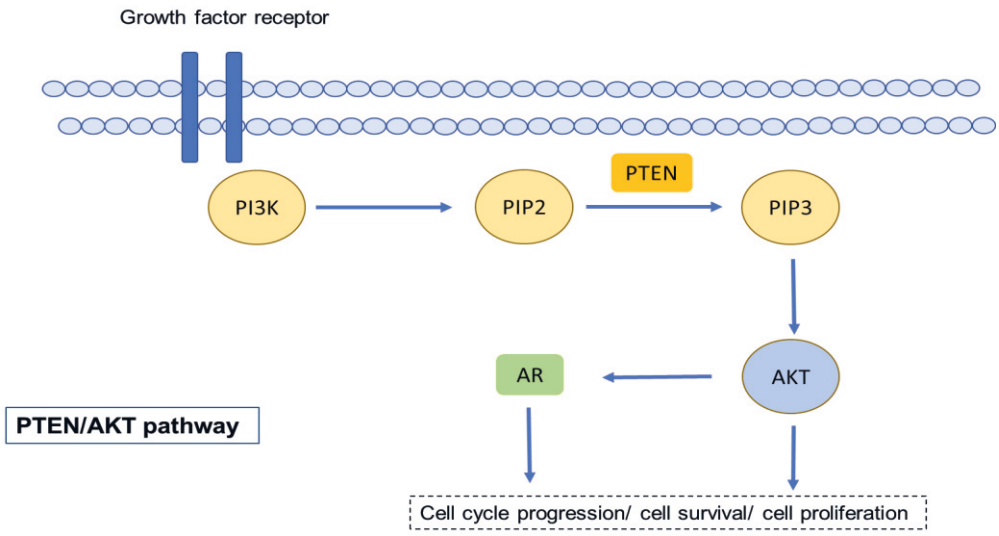

Figure 2. Overview of PTEN/AKT pathway in PCa. Upon the connection between PTEN and the growth factor receptor, AKT activity is linked to the activation of the PTEN. It then regulates the transcriptional activity of AR in the PCa model. The figure is modified according to (Phin et al., 2013). PIP2, phosphatidylinositol 4,5-bisphosphate; PIP3, phosphatidylinositol (3,4,5)-trisphosphate.

P53, a nuclear transcription factor, plays a crucial role in activating apoptosis and cell phase arrest (Ozaki and Nakagawara, 2011). In normal conditions, the expression of p53 is extremely low due to proteasomal degradation, which is regulated by the MDM2-E3 ubiquitin-protein ligase (Figure 3). Under stress conditions, a wild-type of p53 activates a pro-apoptotic function to trigger its target genes. This disrupts the tumor's progression and chemoresistance by inducing cell phase arrest and an apoptotic response, which induces cancer cell death.

However, mutations of *p53* may cause cancer cells to grow and survive. The presence of p53 mutations has been investigated as a potential biomarker for the likelihood of the disease's recurrence after a patient has had a radical prostatectomy (Rivlin et al., 2011). Other authors have found evidence of a link between the p53 mutation protein and aggressive features of the disease such as metastasis PCa, which of course decreases the patient's chance of survival (Ecke et al., 2010).

The above studies were conducted on prostate tissues. There is currently no way of determining and evaluating this biomarker in the blood, due to the instability of the p53 protein. Indeed, the answer to the question of how the p53 protein can advance PCa therapy remains elusive. There have been a few hypotheses about the TP53 mutation involved in the progression of metastasis PCa in clinical samples of mCRPC patients (Hamid et al., 2019; Laere et al., 2019). What is clear is that there is a need to establish a novel strategy to eliminate the occurrence of p53 mutations and provoke the activation of wild-type p53 for efficient chemotherapy.

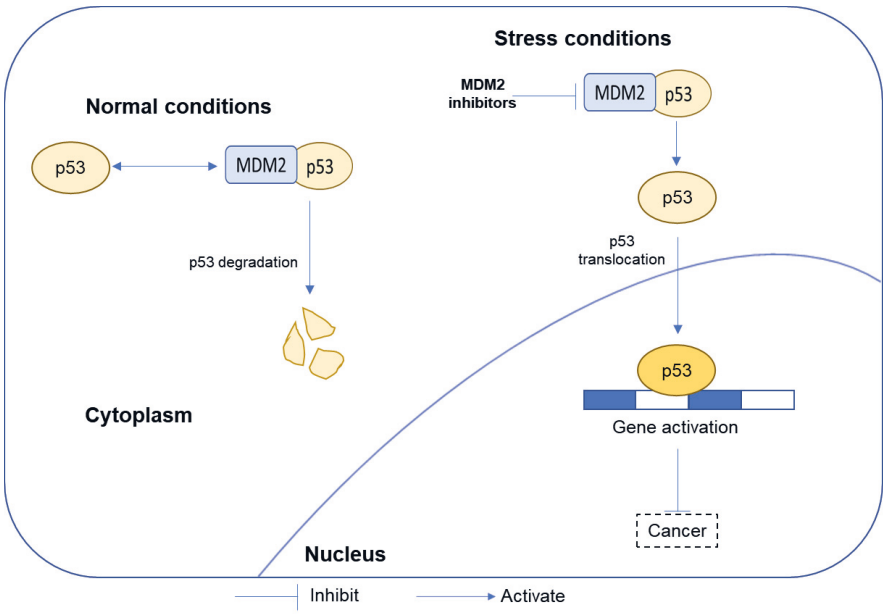

Figure 3. Overview of p53-MDM2 regulation under normal and stress conditions. Under normal conditions, the interaction between MDM2 and p53 induces p53 degradation because of the ubiquitin activity. Under stress conditions, or if there are MDM2 inhibitors, the MDM2 is unable to interact with the p53 and a wild-type p53 is translocated as a nucleus for activating the target genes which induce an apoptotic response and cell cycle arrest (Ozaki and Nakagawara, 2011).

Recent studies of the biology of advanced PCa have expanded the disease's database for drug discovery. In this regard, several research groups have been trying to identify different biomarkers in PCa progression. This study describes some of those biomarkers in terms of AR deprivation. These markers include AT-V7, AR-T878A, PTEN inhibition, and the inhibition of p53 mutations, all of which have contributed to PCa therapy, although with limited clinical outcomes. Moreover, the clinical values for the p27, SRC and BRCA mutations have been reported for the more aggressive stages of PCa, all of which have potential benefits for cancer therapy. It is sincerely hoped that a number of potential biomarkers will be discovered and incorporated into routine clinical procedures for improving the treatment and care of patients receiving PCa therapy.

2.1.2 Advances in PCa treatment

The treatment of PCa has traditionally been based on the stage of cancer, the age of the patient, and the patient's risk of death from other causes (Armstrong, 2018). Any of the treatments will have side-effects on the quality of the patients' life, so the treatment discussion is often focused on striking a balance between the benefits to be gained from successful therapy and the threats the therapy may have on the PCa patient's lifestyle. Dietary management, lifestyle, and disease history are also used to regulate the growth of PCa. In addition, several clinical studies have reported that the risk of death from other causes could outweigh the risk of death from PCa. While the optimal management of each PCa is open to discussion, this study will describe some of the more common clinical treatments and anti-cancer drugs used in PCa therapy (Figure 4).

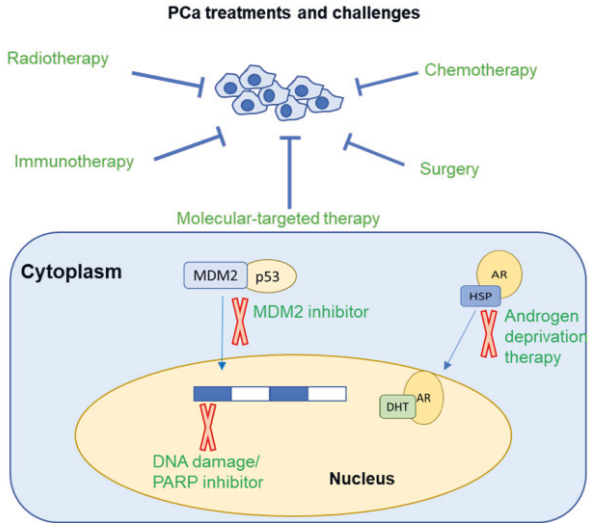

Figure 4. Overview of advances in PCa treatment. LPC patients may be treated with the expectant management approach, surgery, radiation, or a combination of these methods. The clinical options for advanced or metastasis PCa patients are usually limited to chemotherapy, immunotherapy, hormone therapy, or molecular inhibitors.

2.1.2.1 Expectant management

In general, the routine assignment of the stages in PCa follows the TNM staging classification (Cuzick et al., 2014). Males diagnosed with localized disease have three primary approaches to treatment: (i) expectant management, (ii) surgery, and (iii)

radiation. Expectant management includes watchful waiting and active surveillance. After a diagnosis of PCa, this course of action (or inaction) means deferring or avoiding treatment, relying instead on surveillance of the disease. (Briganti et al., 2018). In other words, the symptoms of PCa are merely monitored.

In contrast, active surveillance would consist of a series of laboratory tests, such as PSA grading, physical tests, and prostate biopsies to evaluate cancer progression. Compared to watchful waiting, active surveillance biopsies reduce the risk of PCa metastasis and mortality by 1.0 to 2.4% at 5 years and by 1.4-3.3% after 20 years. For example, one Johns Hopkins University study reported only 2 PCa deaths among a cohort of 1,298 males. In a recent study, Loeb et al. showed that cancer-specific and metastasis cancer survival rates were about 99.9% and 99.4%, respectively, at 15 years (Loeb et al., 2017). A very recent study of active surveillance cohorts in North America showed that the net probability of PCa death was about 1.3% at 20 years, even lower than in previous studies (Lange et al., 2020).

2.1.2.2 Surgery

Surgery and radiation have long been regarded as effective treatments for patients with more severe cancers. These cancers can be defined as those with PSA levels from 10 ng/mL to 20 ng/mL and a Gleason score lower than 8 (Stangelberger et al., 2008). According to European Urology Association guidelines, surgery and pelvic lymphadenectomy (PLDN) are two prongs of a multimodal approach to treating PCa patients with a high-risk of locally advanced prostate carcinomas. In fact, surgery has been shown to be more effective for localized cancer than watchful waiting. In some cases, surgery can reduce the risk of the cancer developing into lymphoid metastasis (Cuzick et al., 2014). The Scandinavian Prostate Cancer Group carried out a study of 695 PCa patients to compare the efficacy of surgery vs. watchful waiting (Bill-Axelson et al., 2008a). They reported that surgery reduces the mortality rate and the risk of metastasis and also inhibited the local progression of the disease. They also noted that surgery in LPC patients is more effective over time (Bill-Axelson et al., 2008b). The ensuing time interval-based data also showed reductions in the risk of cancer metastasis, local progression, and mortality in patients, even after 8 to 10 years of follow-up research.

All in all, PLDN is a common and effective surgical procedure for high-risk metastasis PCa patients (Joung et al., 2011). It clearly has therapeutic effects in preventing metastasis in the lymph nodes in PCa. However, there is still some controversy over whether PLDN is suitable for all stages and types of PCa. While

extended lymph node dissection increased the detection of positive nodes for patients with advanced PCa and increased survival in patients at high risk, the benefits of PLDN for low-risk patients are still unproven.

2.1.2.3 Radiation therapy

Radiation therapy uses multiple radiation beams that are dictated by the size of the target tumor. The dose of radiation from each beam is carefully modulated to maximize the amount of energy it deposits in the tumor. The technology of radiation therapy has advanced significantly since its introduction into modern medicine. It now causes fewer long-term reproductive problems and less damage to the urinary tract (Morgan et al., 2018). An even more recent development, hypofractionation, can shorten the length of the treatment. In this treatment, the beams of radiation are stronger, so fewer treatment sessions are needed. Two of the latest developments in this context are the use of external-beam radiotherapy (ERBT) and brachytherapy.

A recent survey of the latest treatment strategies for PCa reported multiple positive clinical outcomes over the last few decades (Li et al., 2021). Over 15 years ago, a Swedish research group developed a course of treatment for LPC sufferers which combined neo-adjuvant hormonal therapy, ERBT, and two sessions of iridium 192 source brachytherapy (Kälkner et al., 2007). This study recorded that the average follow-up time was 6.1 years in 129 patients with a range of 2.8 to 7.9 years. Thus, the study produced good clinical results showing acceptable levels of rectal toxicity.

In its current stage of development, protein beam therapy is an advanced type of ERBT. It generates beams from a cyclotron, which has higher energy proteins than ERBT (Wisenbaugh et al., 2014). The main advantage of protein beam therapy is that it is able to target the radiation dosage more accurately than other types of radiation therapy. The accelerated charged particles can be controlled so that they enter the tumor to a specified depth, which is determined by the amount of energy in the beam. The characteristics of protein beam therapy mean that it can be used to target tumors with optimal dose distribution and with no exit dose. In the interests of biochemical freedom, one study group found a significant reduction in LPC sizes by ERBT in phase III trials (Rosenthal et al., 2019).

Another advanced type of radiation therapy is intensity-modulated radiation therapy (IMRT). It can be used to assess tumors directly. It bombards the tumor with multiple photon and proton beams of radiation and can utilize even more intense beams in order to discern the tumor's shape. Dosimetrist studies have shown

that IMRT can substantially reduce the amount of radiation accidentally delivered to other organs located around the diseased prostate gland (Fischer-Valuck et al., 2018). Several phase III trials have shown that the survival rate of patients with localized prostate cancer increased with this therapy, and the patients also had lower gastrointestinal toxicities (Hatano et al., 2019; Park et al., 2021; Wang et al., 2018). Thus, the latest advances in radiation therapy have improved PCa therapy by minimizing the treatment's toxicity, avoiding damage to neighboring tissues, and generally limiting the unwanted side-effects of radiation therapy for PCa patients.

2.1.2.4 Androgen deprivation therapy

The function of ARs in the development and progression of PCa is important. One crucial anti-androgen therapy often utilized against PCa tumors largely relies on the fact that androgens regulate the production of testosterone and DHT (Brawer, 2006). The main aim of androgen deprivation therapy is to reduce testosterone levels in patients by inhibiting the androgen activity. Based on the mechanism of the AR, its activation may stimulate transcription factors and various cell growth signaling pathways such as cell proliferation, anti-apoptotic responses, and androgen-regulated genes. The advantages of androgen deprivation therapy for patients who are symptomatic of metastatic PCa are rapid and dramatic (Fujita and Nonomura, 2019). A number of studies have revealed that Androgen deprivation therapy is frequently selected as the mandatory option for PCa, particularly for locally advanced and metastatic tumors.

Another area of interest is the formation of AR splice variants. This is considered to be a major factor contributing to castration resistance in PCa therapy, and is dependent on the mutations in AR. Notably, high expressions of AR-V7 and AR-T878A have been measured in patients with advanced prostate tumors who had received surgery and pharmacological castration (Antonarakis et al., 2014, 2015, 2017). Consequently, the current targets for using AR to treat PCa are following various strategies such as inhibiting the ligand-AR interaction, AR nuclear translocation, heat shock proteins, AR gene transcription, AR and co-activators binding DNA, and steroidogenesis. Among the compounds currently under development in the targeted androgen-AR axis, both AA and enzalutamide have been approved by the US Food and Drug Administration (FDA) for clinical applications for PCa patients.

Abiraterone acetate, or AA, is an androgen biosynthesis inhibitor. It was introduced as a next-generation PCa drug whose anti-cancer effects had acceptable

toxicity levels even in post-chemotherapy settings and CRPC (Helsen et al., 2014). AA approaches the production of androgens by targeting the enzymes C17α hydroxylase and C17-C20 lyase, which suppresses cancer cell proliferation and metastasis. Several phase III tests have confirmed the inhibitory effects of AA for males suffering from CRPC and have shown longer overall survival rates (de Bono et al., 2011; Fizazi et al., 2012; Ryan et al., 2012). In 2011, AA was approved by the FDA for patients with metastatic CRPC who had already received chemotherapy. In 2018, the FDA subsequently approved a combination of AA tablets (Zytiga, Janssen Biotech Inc.) and prednisone for the treatment of CRPC patients who had previously received surgery or pharmacological castration.

In addition, orally administered enzalutamide, a second-generation AR inhibitor, blocks several critical downstream targets of the AR signaling pathway. These include the androgen binding to the AR nuclear translocation, the AR binding to the DNA as well as coactivator recruitment by the AR (Sanford, 2013). The results can be observed as a decrease in cancer cell growth and an increase in cancer cell death. Because there are no AR-ligands bindings, the receptor still splices isoform variants of AR. This is still isoform and remains the most common activity and approach in responding to metastasis in patients with mCRPC. The treatment through AR isoform may promote the PCa's ability to build up its resistance to drug treatment. Several studies have reported the anti-tumor activity of enzalutamide via the inhibition of AR isoform activity and the consequent improvement in overall survival rates in both the pre-and post-chemotherapy models in phase III trials (Davis et al., 2019; Sanford, 2013).

2.1.2.5 Chemotherapy

In general, chemotherapy is not regarded as a very effective approach to PCa due to its limitations in the treatment of more drug-resistant cancers (Nader et al., 2018). Nevertheless, recently, a combination of chemotherapy and androgen deprivation therapy has led to significant improvements in inhibiting prostate tumors, as well as decreasing the PSA levels in patients (Sun et al., 2019).

Some of the more common chemotherapy drugs approved by the FDA and used in the treatment of advanced PCa are, for example, docetaxel, cabazitaxel, mitoxantrone, and estramustine. Estramustine has been approved by the FDA as one of the front-line drugs in the battle against PCa. Recently, a commercial derivative of estramustine has been marketed under the brand name Emcyt by Pfizer. The mechanism of estramustine is similar to that of cabazitaxel (Ravery et al., 2011).

Estramustine is made from estradiol and an alkylating agent, and it binds to the microtubules, the associated proteins, and to the tubulin, thereby causing the tubules to disassemble and thus interrupt the mitosis.

Another common chemotherapy option in PCa therapy is docetaxel. It is used in cases of hormone-refractory metastatic PCa, among many other cancers (Nader et al., 2018; Antonarakis and Eisenberger, 2013). Docetaxel is one of the taxane drugs. It is extracted from the needles of the yew tree and has anti-cancer effects which work by suppressing microtubules during the mitosis process and the interphase (Nader et al., 2018). This mechanism causes the stabilization of the mitotic spindle in the mitosis phase of the cell cycle and cell proliferation. Furthermore, it has recently been reported that taxane compounds have anti-androgenic properties and could potentially block the nuclear translocation of AR (Bai et al., 2019). This means that taxanes could work independently, not only on microtubule inhibition but also on the AR.

Yet another option for chemotherapy is Cabazitaxel. Cabazitaxel also inhibits the microtubules which interact with the tubulin and promote its assembly into microtubules, while simultaneously inhibiting disassembly (Paller and Antonarakis, 2011). This helps the microtubules to stabilize and promotes the interference of mitosis in the cell cycle. Due to the interaction between cabazitaxel and the microtubules, cabazitaxel is regarded as a novel and efficacious second-line option for mCRPC treatment. It decreases a tumor's progression through imaging analysis or death in patients with mCRPC (Wit et al., 2019).

Mitoxantrone is also recommended as a chemotherapy drug for the treatment of androgen-independent metastatic PCa (Berthold et al., 2008). The mechanism of mitoxantrone activity is a type II topoisomerase inhibitor with a DNA molecule. This in turn causes single- and double-strand DNA disruptions and inhibits DNA synthesis and repair; as has been shown in phase III clinical trial test (Green et al., 2015). Green and his team confirmed that there was a symptomatic improvement in PCa patients using mitoxantrone as one of the treatment arms in phase-III randomized controlled trials, although there was no recorded improvement in survival rates (Green et al., 2015). The current findings certainly suggest the topic is worthy of further investigation with more randomized controlled patient trials in the future.

2.1.2.6 Immunotherapy

For PCa, immunotherapy works by supporting the patient's "own immune system's battle against tumors" (Graff and Chamberlain, 2014). One immune therapy approved by the FDA for patients with mCRPC is a therapeutic cancer vaccine, sipuleucel-T (Handy and Antonarakis, 2018). To stimulate the immune system, dendritic cells are collected from the patient's samples and then loaded with a specific antigen *ex vivo*. The cells' existing antigens and other blood molecules are harvested and then exposed to a recombinant fusion protein that functions as a PCa-associated antigen. The antigen-presenting cells included two crucial components, prostatic acid phosphatase, and the recombinant antigen. Prostatic acid phosphatase was indicated in more than 95% of prostate adenocarcinomas.

The mechanism involves the recombinant antigen activating the immune cells in the patient's body. The activated cells are then infused back into the patient to improve their self-immunology system. Early evidence of clinical activity for sipuleucel-T was reported in a phase-III trial, D9901, in randomized patients (Small et al., 2006). The findings indicated that immunotherapy combined with sipuleucel-T showed an overall improvement in anti-tumor efficacy and longer survival times than it did with a placebo. To follow up on the immunology research, phase III trials D9902A and IMPACT were performed to confirm the vaccine's efficacy in another group of patients (Graff and Chamberlain, 2014). However, although the efficacy of sipuleucel-T has been indicated in patient trials, it is still rarely used in clinical practice because it is so expensive for patients.

2.1.2.7 PARP inhibitors

Together, the somatic and germline variants of mutations in a DNA damage pathway account for 20% of PCa carcinogenesis and progression (Gong et al., 2021). Gene alterations caused by DNA damage can be linked to an over-reliance on PARP for DNA repair to induce cancer cell growth. The activity of PARP in cancer cell proliferation presents us with the opportunity to use a PARP inhibitor in our PCa treatment. PARP inhibitors are among the latest generation of drugs to be approved by the FDA for patients with CRPC that have continued to progress after AR-directed therapy.

One of these drugs is olaparib, a clinical PARP inhibitor. Olaparib was reported to be effective in metastatic PCa with deleterious germline or somatic homologous recombination repair gene mutations in a phase-II trial of 128 patients (J et al., 2015;

Bono et al., 2020). Next-generation sequencing was performed to detect the change in deleterious mutations in patients who had a response with orally-administered olaparib for more than 6 months. Overall, the gene analysis of the patients indicated the involvement of DNA damage in the response to olaparib treatment. In addition, Bono and his colleagues conducted a phase-III clinical study to evaluate the efficacy of Olaparib on mCRPC randomized patients who received hormone therapy with either enzalutamide or abiraterone (Bono et al., 2020). The patients who received olaparib had longer depression-free survival and better response to the treatment than the ones dosed with hormonal agents. This study has justified the FDA's approval of olaparib in *BRCA1*, *BRCA2*, or *ATM* mutations in mCRPC patients.

Finally, an organism's ability to repair DNA damage is vital for its genomic stability. It induces cell growth and replication. PARPs have a crucial role in repairing DNA damage (Rose et al., 2020; Messina et al., 2020). Oral rucaparib, a PARP inhibitor, was tested to evaluate its efficacy in mCRPC patients. The patients had previously had either hormonotherapy or chemotherapy with genomic mutations in *BRCA1*, *BRCA2*, *BRIP1*, *CDK12*, or *PALB2* (Jang et al., 2020). The outcome of this trial showed that patients who were given rucaparib tended to live longer without their cancer growing or spreading than patients treated with only AR inhibitors or chemotherapy. It was this study that led to the FDA giving its unprecedented approval of rucaparib for patients with germline or somatic mutations in *BRCAs* in 2020. With such promising results so far, the newest generation of PARP inhibitors has to be considered a target for drug discovery for patients suffering from mCRPC in the future.

2.1.2.8 MDM2 inhibitors

The wild-type p53 is an anti-tumor molecule frequently deactivated by its mutations or inhibitions in cancer (Lane and Hupp, 2003; Wan et al., 2018). Most cancer cells express wild-type p53 whose stability is controlled through the exhibition of MDM2. Due to the interaction of MDM2 and p53, several potent and selective inhibitors for MDM2 have been investigated in terms of their efficacy in eliminating cancer progression. In addition, a variety of compounds have been synthesized upon MDM2 molecules and the evidence of a number of clinical trials has resulted in FDA approval of MDM2 inhibitors for cancer therapy (Jiang and Zawacka-Pankau, 2020; Khurana and Shafer, 2019; Warner et al., 2012).

One of the most promising of these for PCa research is idasanutlin. This inhibitor is an antagonist of MDM2 and has been approved by the FDA for acute myeloid leukemia treatment. Phase-I and II clinical trials have been conducted on PCa patients and data is being collected according to the procedures laid down on ClinicalTrials.gov. In an *in vitro* PCa modelling experiment, idasanutlin suppressed tumor progression through cell cycle arrest, apoptosis, and its cytotoxic effects on cancer cells (Natarajan et al., 2019). It was also reported that RG7388, a compound of idasanutlin, induced cell death by accelerating p21 activity through p53 signaling in cancer cells. These promising results for MDM2 inhibitors might open up a new front in the battle against PCa in the future.

2.1.3 The future of combination therapies

In recent years, the inhibition of androgen activity has come to be regarded as one of the preferred therapeutic options for patients with advanced PCa (Armstrong, 2018). One way of inhibiting androgen activity is to use hormone therapy, as this inhibits the ability of the androgen to help the PCa cells survive and grow. Unfortunately, the majority of tumors eventually develop resistance to hormone therapy. Because CRPC is, by and large, incurable, combination therapy which consists of two or more therapeutic agents is the best way to fight back against such cancers and is a cornerstone for cancer treatment (Gilad et al., 2021).

A combination of anti-cancer drugs enhances the efficacy of cancer therapies better than a mono-therapeutical approach. This is due to the synergistic or additive qualities of the drugs. A combinatorial approach also helps prevent the disease's ability to build up its resistance to drugs, while simultaneously providing therapeutic anti-cancer benefits. The overall survival rates and the patients' quality of life are undoubtedly improved due to this innovation in cancer treatment. Several combinations have been new for PCa therapy. For example, combination therapy of estramustine and docetaxel increased the cytotoxicity in a prostate tumor and improved the PSA response rates (Petrylak, 2003). A patient's chances of survival and quality of life can be greatly improved with estramustine in the treatment mix, rather than in a chemotherapy regimen without it.

There have been many other examples of the efficacy of using combination treatment regimens over the past 2 decades. In a recent GETUG-12, phase-III clinical trial it was shown that docetaxel and estramustine significantly improved the median survival time in patients who had been given androgen inhibitors for 3 years for local cancer treatment (Dumont et al., 2020). In 2004 the FDA approved injected

docetaxel in combination with prednisone in metastasis-androgen independent PCa patients. Subsequently, in 2011 a combination of AA and prednisone was approved for patients with mCRPC who had received chemotherapy treatment with high cytotoxicity in the tumor and in whom cancer's resistance to drug treatment was lower. In 2017, the FDA approved a combination of cabazitaxel and prednisone for patients with metastatic hormone-refractory PCa. One research group evaluated cabazitaxel in 755 patients with mCRPC in a phase-3 TROPIC trial in 2010 (Bai et al., 2019). This trial suggested that the efficacious activity of cabazitaxel in combination with prednisolone improved the patients' clinical condition and their chances of survival compared to mitoxantrone with prednisolone. Soon after this, on February 7, 2019, the FDA approved a combination of AA with chemotherapy prednisone for patients with mCRPC.

Even more recently, a trial of a combination of PARP inhibitors with AR-directed therapies was conducted in patients with mCRPC in a phase-III clinical research study. In fact, the database of ClinicalTrials.gov lists 286 studies of active phase 1-4 clinical trials investigating PCa therapy (not including studies whose results are due after July 15, 2021). This site presents many positive results in inhibiting PCa growth. Among the 286 studies, nearly a quarter (around 60 out of 286) were studying multiple drug combinations. The search for a combination of anti-cancer drugs with a unique mechanism of action is now justified as a potential option for cancer therapy.

2.2 Overview of GPCRs

G protein-coupled receptors, GPCRs, are the largest and most varied group of membrane receptors in human prostate tissues (Xia et al., 2001). In terms of structure, GPCR proteins usually include seven hydrophobic transmembrane domains (TM) in the cell membrane. The seven domains are connected to each other by three extracellular and three intracellular loops through the cell membrane (Rosenbaum et al., 2009). GPCRs are activated by binding to the external signals of ligands. This process exerts a conformation change in the GPCRs' structures and activates the GPCRs in the cytoplasm.

The activation of the GPCRs is generally linked to three subunits. These are α, β, and γ which are second messengers to induce signal transduction (Dhyani et al., 2020; Wright et al., 2015). A single GPCR can stimulate the production of several second messenger molecules. For example, cyclin adenosine monophosphate

(cAMP) and inositol trisphosphate (IP3) are two popular molecules that are involved in intracellular signaling pathways. Two common effectors of G_{α} are cAMP and IP3. These may control the ion channels and cell phenomena, as well as the molecules of members of the protein kinase family. In contrast, the primary effectors of $G_{\beta/\gamma}$ are various ion channels such as K^+, Na^+, and Ca^{2+} (Figure 5). The activation of the second messengers of GCPRs regulates the transcription factors in the nucleus and induces a biological response.

As the largest family of functionally active receptors, GPCRs are described as the "work-horses" of physiology, with nearly 35% of the drugs that target the receptor being approved by both the FDA and the EMA-(European Medicine Agency) (Sriram and Insel, 2018). Notably, the mRNA level of prostate-specific GPCRs was detected at higher levels in epithelial cells of PCa than in normal prostate cells (Cao et al., 2015). Thus, GPCRs can be regarded as potential targets in any PCa therapeutics strategy. Several *in vitro* and *in vivo* studies have been performed to evaluate the mechanism of certain GPCRs in PCa (Paudyal et al., 2017; Pi and Quarles, 2012; Ye et al., 2017). For example, GPCR6A is easily observable in PCa, and the knock-down of its expression in PC3 cells reduces migrated and invaded cells (Ye et al., 2019). Recently, blockers of angiotensin II, a ligand of the angiotensin II type 1 receptor, presented inhibitory activity in the growth factor signaling in LNCaP and PC3 cells (Uemura et al., 2005). In addition, the knock-down of the GPR160 protein in PC3, LNCap, and DU145 cells results in an apoptotic response and cell cycle arrest (Guo et al., 2021). An antagonist of the gonadotropin-releasing hormone receptor, degarelix, has been approved for patients with advanced PCa. It has strong efficacy in suppressing tumor growth in patients (Usman et al., 2020). Two other inhibitors of GPCRs, zibotentan and atrasentan, target the endothelin A receptor. These have been investigated with promising results in clinical trials in PCa therapy (James et al., 2010). Therefore, further studies about novel ligands targeted at GPCRs could have promising results in the fight against prostate tumors.

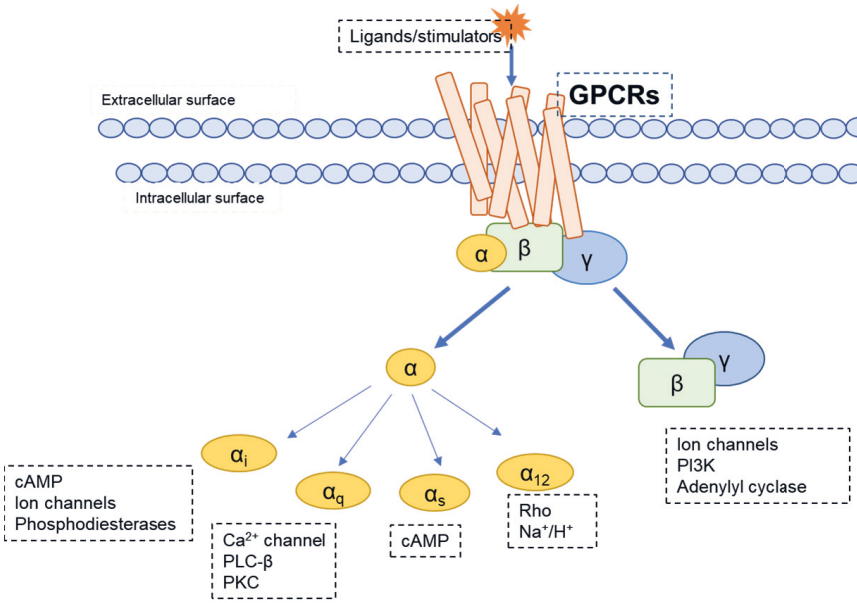

Figure 5. Activation of GPCRs. Upon the ligands binding to GPCRs, the receptors mainly divide and release subunits α, β, and γ. The subunit α, comprising four subfamilies αi, αq, αs, and α12, links to the second messengers as cAMP, ion channels, phospholipase C-PLC, phosphodiesterase, Rho, and PKC. In contrast, the subunits β and γ coexist together regulating the ion channels, PI3K, and adenylyl cyclase (Rosenbaum et al., 2009).

2.3 Overview of P2Y1R

Purinergic receptors, P2YRs, are members of the largest family of membrane receptors. The family includes 8 human subtypes, P2Y1, P2Y2, P2Y4, P2Y6, P2Y11, P2Y12, P2Y13, and P2Y14. These can be divided into two subgroups based on the way they couple to specific G proteins. Among these eight 'homo' subtypes, P2Y1R is one of the most widely distributed P2Ys in human tissue (Moore et al., 2001). Northern blot analysis has long shown researchers that the expression of P2Y1R is abundant in human prostate tissues (Janssens et al., 1996). Interestingly, it was noted that the expression of P2Y1R was observed both in PCa cells, such as PC3, and in normal prostatic cells (Janssens et al., 1996; Li et al., 2013; Shabbir et al., 2008; Wei et al., 2011). Later, $P2Y_1$ mRNA and proteins were detected in several PCa cells, such as bone-adapted castrate-resistant variant C4-2B, bone metastasis C4-2, adenocarcinoma cells LNCaP, bone metastasis PC3, and central nervous system metastasis DU145 cells (Lertsuwan et al., 2017). P2Y1R is thus clearly a suitable candidate for evaluation in this study.

Like other metabotropic GPCRs, the P2Y1R-Gαq receptor also has seven hydrophobic transmembrane domains through the cell membrane. When ligands bind to P2Y1R, the receptor acts as an extracellular Gq protein and the second messenger, in turn, acts as PLC (Dhyani et al., 2020). The activation of PLC is a direct stimulation for the hydrolysis of PIP2, which generates a new isoform IP3. This action opens the corresponding calcium channel in the cytoplasmic matrix. The IP3 released from the PIP2 associating with the IP3/Ca^{2+} channel allows the Ca^{2+} to transfer from a higher concentration level in the endoplasmic reticulum to a lower concentration in the cytosol (Berridge, 2016). This increase in Ca^{2+} levels triggers the activation of the protein kinase C, as well as the phosphorylation of the proteins in the cells targeted for cellular response. It is worth adding that the combination of ADP and P2Y1 not only leads to the activation of a G1 protein but also activates smaller monomeric G proteins known as Rac (Berridge, 2016). However, our understanding of this mechanism is still ambiguous so it will not be discussed further here.

As previously mentioned, PI3K/AKT up-regulation has been observed in various human cancer cells in which PTEN or PIP3 is absent or mutated (Yuan and Cantley, 2008). The activation of Akt encourages cell survival and invasiveness. In addition, Akt inhibits the apoptotic process via direct phosphorylation and deactivation of the components of apoptosis. Suplat et al. investigated Gq-dependent signaling. They noted that when the signaling was initiated by ADP or 2MeSADP, the P2Y1R activated the PLCβ and increased the intracellular Ca^{2+} that occurs in glioma C6 cells' serum starvation (Suplat et al., 2007). It is also worth mentioning the fact that siRNA silences the P2Y receptors, which also makes this a promising avenue of exploration in cancer therapy. The inhibition of ERK1/2 and Akt kinase phosphorylation has been observed in C6 cells that have been transfected with siRNA of P2Y1R. This accords with the Sak and Illes postulate, which asserts that cell death occurs because of the absence of P2Y1R and PI3K/Akt pathways (Sak and Illes, 2005). There is a good deal of evidence to show that P2Y1R-induced Ca^{2+} mobilization can control changes in a platelet's shape and initiate ADP-induced platelet aggregation. Finally, the activation of P2Y1R can result in chronic vascular inflammation and is associated with atherosclerosis (Jin et al., 1998).

The activity and biological responses of P2Y1R, such as cell growth and death, have been evaluated in other contexts with different disease models. As much as 20 years ago, one study investigated the anti-cancer activity of P2YRs in mouse models. In this *in vivo* mice study, ATP and ADP suppressed cancer growth in mice with CT26 tumors and extended their survival time (Rapaport and Fontaine, 1989).

However, there are certain unanswered questions from the above study regarding the degraded forms of ATP. Due to the fact that ATP can easily degrade and form ADP and adenosine in animal bodies, there is no evaluation of the individual P2YRs. ATP and ADP, the key intracellular energy currencies, were later determined to be agonists of P2Y1R (Chhatriwala et al., 2004; YK et al., 2003). In one attempt to solve this problem, *in vitro* models were carried out on different types of cancer cells. In general, these *in vitro* studies on agonists and antagonists have merely highlighted the diversity of the activity in cancer models of P2Y1R. In an experiment carried out by Wei et al., 2011 (N)-methanocarba-2-methilthioadenosine diphosphate-MRS2365, a known selective agonist of P2Y1R, was incubated in PC3 cells for 24 h. Subsequently, a decrease in cell growth and a rise in the number of apoptotic cells and increased caspase 3 activity were observed (Wei et al., 2011). One point of interest here is the phosphorylation of the ERK1/2 involved in apoptosis, which is a characteristic of prolonged receptor activation. One study reported that the calcium signaling of the P2YR agonists inhibited the growth of the androgen-independent prostate carcinoma cells, PC3 and DU145 (Fang et al., 1992; Wasilenko et al., 1997). In a later study, 2-methilthioadenosine diphosphate,2-MeSADP, a non-selective agonist of P2Y1R, promoted cell apoptosis and inhibited proliferation in 1321 N astrocytoma cells expressed recombinant human P2Y1R.

A similar anti-proliferative pattern of P2Y1R activity was recorded in A375 melanoma cells (Mamedova et al., 2006; Wan et al., 2016). In one study, incubation of the A375 cells with 2-MeSADP was linked to a decrease in the number of cells with dose- and time-dependent behavior (White et al., 2005). In another recent experiment, ADP not only induced the activation of P2Y1R and p53 stability, it also suppressed the G1 phase progression in a ZL55 Cellosaurus cell line (Muscella et al., 2018). It has been suggested that PKC-α down-regulated the signaling of P2Y1R and acted as a mediator for p53 signaling, thus playing a crucial part in eliminating cell proliferation in the presence of the agonists ADP and MeSADP. This study established a novel connection between ERK1/2 and JNK1/2 phosphorylation and the stability of the p53 protein, a known tumor suppressor in cancer.

Cancer progression involves more complex mechanisms than the mere application of ligands to cancer cells and the measurement of cell phenomena. To control cancer cell growths and deaths, it must be recognized that there are a wide variety of intracellular pathways that stimulate different cancer cells in different ways. These all need to be assessed so that PCa researchers, and other bio-researchers, can understand all the different mechanisms involved. It is in order to address some of

the structural and mechanistic questions about P2Y1R that this study will try to explain the function of this receptor and its new ligands using a PCa cell model.

2.4 Phenolic compounds

Due to the localization and expression of AR in prostate tissues, the first-line treatment of advanced PCa is to select androgen inhibitors as the primary target for treatment. This approach is aimed at decreasing the androgens and then inhibiting PCa cell growth. After intensive drug discovery studies in PCa therapy aimed at eliminating cancer resistance with drug treatment, phenolic compounds have emerged as potential targets. This is because there are numerous, wide natural distributions of these compounds and they can be synthesized in organic chemistry according to a particular molecular target (Cháirez-Ramírez et al., 2021). In organic chemistry, phenolics are defined as a type of chemical compound that includes one or more hydroxyl groups connected directly to an aromatic hydrocarbon group (Montané et al., 2020). According to the number of hydroxyl groups and phenolic rings in the structures, there are several classes and subclasses of phenolic compounds (Figure 6).

Phenolics are ubiquitous in organic chemistry and there is much evidence of their health benefits. Several studies have indicated that phenolic compounds could offer a potential approach to anti-disease drug development. A wide range of phenolic compounds has been investigated for enhanced tumor suppression in PCa. Researchers have reported that phenolic compounds have the ability to induce DNA damage, apoptosis, and cell cycle arrest and to inhibit cell migration and invasion (Costea et al., 2019). For example, in LNCaP and PC3 cells the phenolic compound apigenin decreased the expression of cyclin D1, which was followed by G0/G1 phase arrest, whereas in DU145 cells it induced G2/M phase arrest (Shukla et al., 2014; Zhu et al., 2015). Quercetin induced apoptosis through an increase in caspase 3, 8, and 9 activities and down-regulation of the matrix metallopeptidase 9 in PC3 cells (Bhat et al., 2014). According to the drug discovery from phenols, it has been hypothesized that novel polyphenols targeted at the structures of specific receptors or biomarkers would be a promising approach to the fight against PCa.

Finally, we have Gingerol, a PARP inhibitor, that induces an apoptotic response in PC3 cells and *in vivo* PCa xenograft models (Karna et al., 2012). Yet more evidence of the efficacy of polyphenol-targeted molecules emerged when it was reported that

genistein inhibited PCa growth by targeting TGF-β signaling. It also promoted apoptosis through the down-regulation of oncogenic HOX transcripts antisense RNA (Chiyomaru et al., 2013; Pavese et al., 2014). Since phenolic compounds have such a profound impact in eliminating cancer cell growth, different varieties of phenolic compounds are often adopted as an original library for designing the docking studies needed for further evaluation in PCa models.

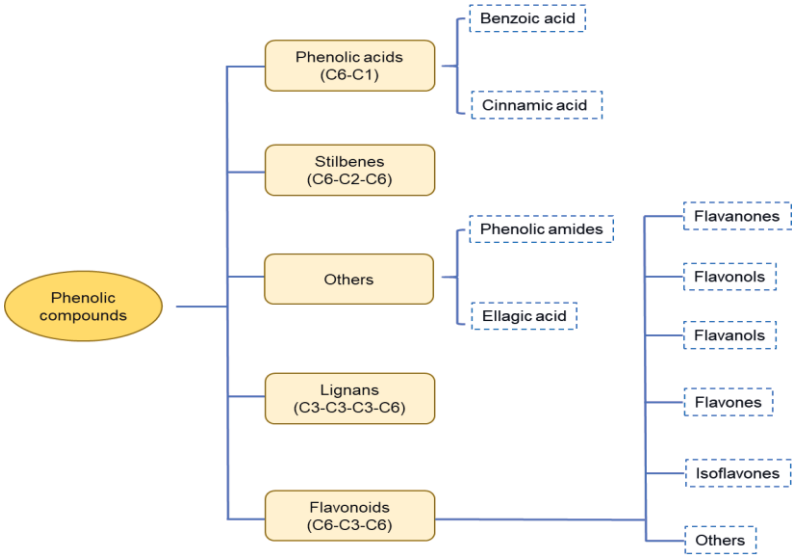

Figure 6. Classification of phenolic compounds. The classification of phenolic compounds follows (Dirimanov and Högger, 2019) with some modifications. The division is based on 5 main structural subclasses: Phenolic acids, stilbenes, lignans, flavonoids, and others.

2.5 Potential targets for drug discovery in PCa therapy

2.5.1 Cell death program

Apoptosis, a cell death program, is defined as a natural biological process for removing unwanted cells which are harmful to normal cell growth (Wolf, 2019). In general, the appearance of apoptosis involves a delicate balance between cell growth and cell death. In fact, whatever the therapy, programmed cell death is recognized as one of the main causes of death in cancerous tumor cells; this includes radiotherapy, chemotherapy and the newer hormone therapies now used in cancer treatment (Khan et al., 2010; Wolf, 2019). Drugs which are deemed to have the potential to induce apoptosis have been investigated in a number of different fields concerned with finding novel protein components and other regulators of apoptosis signaling pathways (Wolf, 2019). Apoptosis can be initiated through two distinct apoptotic pathways: intrinsic and extrinsic. Both pathways lead to cell death as shown in Figure 7.

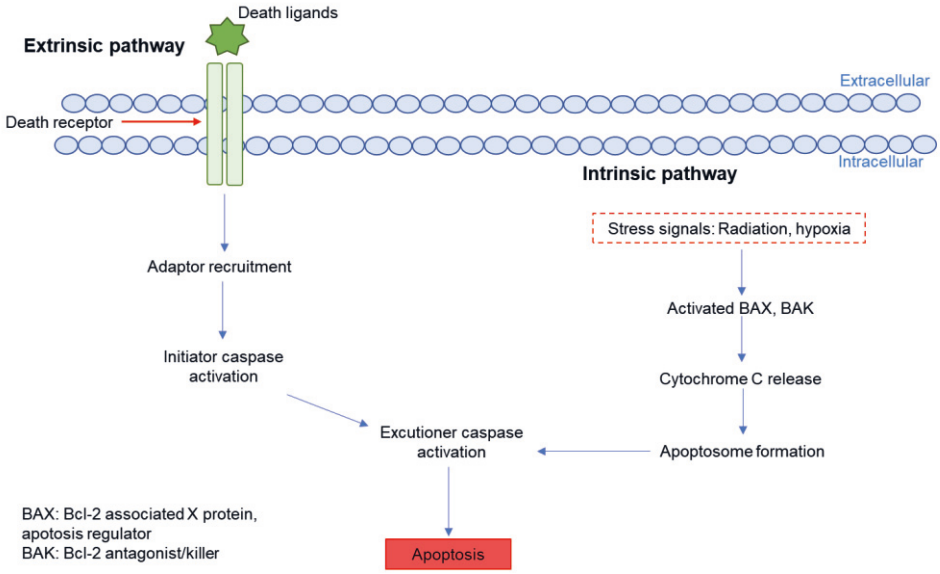

Figure 7. Extrinsic and intrinsic pathways in apoptosis. The diagram is modified according to (Mitsiogianni et al., 2019) and presents the extrinsic pathway from the death ligands binding to death receptors located on cell membranes and the intrinsic intracellular pathways under stress signals.

An intrinsic pathway is initiated after internal cell damage and hypoxia. It triggers the release of cytochrome C from the mitochondria and activates the Bcl-2 family of proteins, which are key regulators of apoptosis (Xu and Shi, 2007). In non-apoptotic cells, the key anti-apoptotic regulators of the Bcl-2 family interact with the main pro-apoptotic proteins, BAX (Bcl-2 associated X protein) and BAK (Bcl-2 antagonist). The apoptotic induction triggers apoptosis formations that activate the executioner caspases. This activation directly induces cell apoptosis. A number of studies have been conducted to investigate the activities of pro-apoptotic proteins belonging to the Bcl-2 family in apoptosis (Shamas-Din et al., 2013; Warren et al., 2019; Xu and Shi, 2007). PCa therapies such as radiation, androgen inhibition, and chemotherapy stimulate the intrinsic apoptotic pathways by causing cell stress and DNA damage through the expression of Bcl-2 and BAX.

In an extrinsic pathway, the mechanism is initiated from outside the cell membranes by death ligands. These bind to death receptors such as the tumor necrosis factor (TNF-α), tumor necrosis factor-related apoptosis-inducing ligands, and Fas receptors (Fesik, 2005; Zielinski et al., 2013). These interactions ultimately trigger the recruitment of the Fas-associated death domain and the activation of caspase. The most commonly activated is caspase 8. This induces caspase 8 cleavage which promotes caspase 3 activation and other downstream caspases. Eventually, this leads to a rise in cancer cell death characterized by DNA fragments, loss of cell volume, and cell membrane blebbing.

As well to the proteins that are directly engaged in cancer cell death, the proteins related to apoptosis could be also considered as molecular targets for anti-cancer drug discovery (Fesik, 2005). For example, MDM2 and p53 play crucial roles in apoptosis. It has been shown that p53 induces G1/S phase arrest and programmed cell death (Shadfan et al., 2012). However, p53 mutations and deactivation occur in a number of different types of cancer, demonstrating the importance of both disturbing mutated p53 signaling and stabilizing wild-type p53. The stabilization of p53 could be improved by disrupting its interaction with MDM2. Recent *in vitro* and *in vivo* studies have investigated MDM2 inhibitors as potential targets for PCa treatments, with some promising results (Endo et al., 2011). This all goes to show that promoting apoptosis is a promising strategy for anti-cancer drug discovery.

2.5.2 Cell phase checkpoint

Cell cycle arrest is a stopping phase in the cell phase progression which suppresses the cell duplication and division that could lead to cell proliferation (Matthews et al.,

2021). Cell progression usually includes the G1, S, G2, and M phases. A cell is ready to initiate DNA replication and establish DNA repair in the G1/S phases. The S phase acts as a surveillance camera to detect any problems with DNA replication or unrepaired DNA damage. After this, the replicated DNA is ready for the G2 interphase as the cell in the G2/M phases is large enough to enable the progression of mitosis and cytokinesis. The progression of the cell cycle is mediated by a series of related proteins called cyclins, the CDKs-cyclin-dependent kinase family, and the CDKs' inhibitors to cell damage (Vermeulen et al., 2003). The connection of cyclins to the CDKs shows a marked up-regulation in kinase activation and the progression of cell division through the cell cycle. The controls of the cell progression are commonly observed as a series of checkpoints through the progression from the G1 phase to the M phase (Figure 8). Cell phase progression and its checkpoints are mainly mediated through a series of signaling pathways (Bertoli et al., 2013). The activation of $p16^{INK4A}$/pRB, ataxia-telangiectasia mutation (ATM), and the ATR pathways induce G1/S phase arrest. TGF-β is another factor involved with the induction of $p16^{INK4A}$/pRB. It is related to the activation of CDK4/6 and prevents cell progression.

In contrast, the most common downstream targets of ATM are p53 and the CHK2-mediated phosphorylation of CDC25A (Hocevar and Howe, 1998). The stabilization of p53 activates p21 and inhibits the CDK2/cyclin E in the G1 phase arrest (Al Bitar and Gali-Muhtasib, 2019). At the S phase checkpoint, there are two pathways concerned with synthesis inhibition. One pathway, the ATM pathway, stimulates the activity of CDC25A and CDK2 and eliminates CDC45 activity in chromatin (Liu et al., 2006). The second pathway is induced by ionizing radiation, provoking a range of proteins in the SMCs family and DNA damage (De Zio et al., 2013).

The last key step before cell mitosis is the G2/M phase. It has recently been reported that the activation of ATM may induce the G2/M checkpoint through BRAC1, whereas TGF-β can also initiate cell cycle arrest through the induction of $p21^{WAF1/CIP1}$ (Yang et al., 2006; Yarden et al., 2002). In recognizing the important roles of DNA damage and cell cycle progression in controlling cell growth, drug discovery-induced cell phase arrest and the inhibition of DNA repair are regarded as promising targets for cancer therapy.

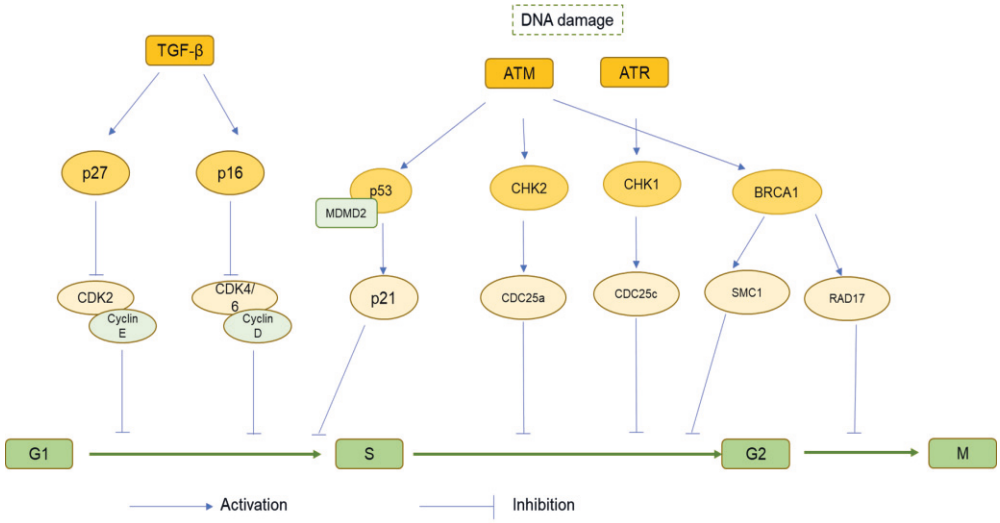

Figure 8. Schematic representation of the target genes in a cell cycle. Following DNA damage, the ATM and ATR pathways are activated. This then phosphorylates the downstream target proteins which are linked to different cell phases. Another pathway, TGF-β, triggers the activation of p27 and p16 which impede the activity of Cyclin D and E and G1/S phase progression. The diagram is modified according to (Kim et al., 2002).

3 AIMS

This thesis aims to show that P2Y1R, a GPCR-family receptor, is a novel target for regulating the apoptosis signaling pathway in prostate cancer. The research focuses on the molecular mechanism of the P2Y1R signaling activation and its effects on the downstream signaling pathway in PCa cells. In addition, the research shows that a combinatorial treatment program of HIC with AA will help settle the argument about whether using combinatorial drug treatments is better than using mono-therapeutic ones. The thesis has the following specific aims.

1. To design and develop novel ligands, phenolic derivatives, for regulating P2Y1R signaling through *in silico* and *in vitro* experiments.
2. To detect the anti-cancer effects of the leading phenolic compound, HIC, on PCa cell survival through cell and molecular biology assays integrated with image analysis.
3. To identify the downstream signaling modulation of genes and proteins involved in PCa cell metastasis, DNA damage, and cell cycle arrest.
4. To evaluate the synergistic anti-cancer activity of the combinatorial drug, HIC with AA, in PCa cells.

4 MATERIALS AND METHODS

This chapter aims to explain why certain methodologies and biological characterizations of the reagents in each experiment were selected. More detailed biological, methodological and chemical information can be found in the author's online publications, designated here by the Roman numerals (I, II, III, IV)

4.1 Designing novel ligands targeted at P2Y1R (I)

Molecular docking provides a model for the interaction between the targeted protein and various ligands. The discovery allows us to predict the behavior of small molecules when binding to the cell membranes of the targeted receptors and to examine their elemental biochemical processes. There are two main factors involved in the molecular docking approach: (i) sampling methods, and (ii) scoring schemes.

4.1.1 Sampling methods (I)

The protein sequence of P2Y1R was collected from the Protein Data Bank with the identification code 4XNW. When designing the model, hydrogen atoms were added to the P2Y1R structure to increase the number of binding sites and to remove any atomic clashes that would impede stabilization. The ligand binding sites in the P2Y1R were used as control binding sites, whereas the crystal structure of the receptor interacted with MRS2365.

This model was designed for 923 small molecules based on 1-indolinoalkyl 2-phenol derivations with 2-D structures of phenolic compounds that were designed using the RD kit library in Python. Later, the structures of the 923 molecules were translated into chemical structures following the LigPrep model, which adheres to the standard physical condition of stabilization.

4.1.2 Scoring schemes (I)

The second step was to establish a scoring scheme that could be used to rank these conformations of P2Y1R and the 923 molecules. Here, the ligands were put through Maestro in order to add hydrogen molecules and remove salt, ionization, and the generation of a low-energy ring using LigPrep. The docking was aimed at screening large numbers of ligands of unknown quality (Standard Precision). The top ligands from the final poses were given extra precision docking and a list of scores was collected in order to further refine the selection of the ligands. The docked conformers were evaluated using Glide. Glide was used to predict the protein-ligand interactions and then check the bound conformations among them with a Glide score (gscore). The two ligands with the highest gscore were selected for further experiments.

4.2 The Synthesis of P2Y1R ligands (I)

HIC
Chemical formula: $C_{22}H_{17}N_3O_4$
Molecular weight: 387.40
1-(2-Hydroxyl-5-nitrophenyl)(4-hydroxylphenyl)methyl)indoline-4-carbonitrile

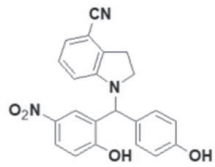

MB
Chemical formula: $C_{22}H_{20}N_2O_4$
Molecular weight: 400.43
Methyl-4-((4-cyanoindolin-1-yl)(2,5-dihyldroxyl)phenyl)nethyl)benzoate

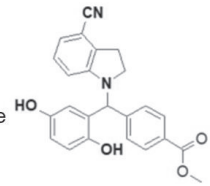

Figure 9. The chemical structures of HIC and MB. Having achieved the highest docking scores with P2Y1R, the two top compounds, HIC and MB, were selected for synthesis and evaluation in further experiments.

The reagents used in the chemical reactions were obtained from Sigma-Aldrich (St.Louis, MO, USA) and/or TCI. The ligands were synthesized in an argon atmosphere. Thin-layer and flash column chromatography were performed to detect the chemical quality of the samples and to isolate the chemicals. Nuclear magnetic resonance spectra were recorded to identify the molecular structures. A mandatory

control for suppressing the corresponding indole and triethylsilane was intoline-4-carbonitrile. The two top compounds were designed and labeled as HIC and MB (Figure 9).

4.3 Cell culture (I-IV)

Human PCa cell lines, a mouse embryonic fibroblast cell line (MEF), and the human embryonic kidney (HEK) cell line were used to select 293 cells to evaluate the cytotoxicity of the P2Y1R ligands. The cell lines were cultured in the high glucose Dulbecco's Modified Eagle Medium (DMEM) and Minimum Essential Medium Eagle (MEME), both purchased from Sigma-Aldrich (St.Louis, MO, USA) and enriched with appropriate nutrients and antibiotics.

To prepare the cells for each assay, they were first dyed with a 1X trypan blue solution (Cat no. T8154-100mL, Sigma-Aldrich, St.Louis, MO, USA). The number of cells was detected automatically using a Countess II FL automated cell counter (ThermoFisher Scientific, Waltham, MA, USA). The cells were plated in culture plates with suitable densities (Table 3).

Table 2. Cell lines. In this study, the cancer and non-cancer cells were cultured in appropriate mediums to maintain and perform the assays. The cells were cultured every 3 days using Trypsin IX purchased from Sigma-Aldrich (St.Louis, MO, USA).

No	Cell lines	Mediums	Origins
1	PC3	MEME	Bone metastasis of grade IV of prostatic adenocarcinoma
2	DU145	MEME	Brain metastasis of prostate adenocarcinoma
3	HEK293	DMEM	Human embryonic kidney
4	MEF	DMEM	Embryonic tissues

Table 3. The number of cell cultures. The number of cell cultures was designed for each assay. The cells were plated to reach a confluence of around 60-80% before carrying out the experiments.

No	Assay	Cell number	Culture plate
1	Calcium assay Toxicity assay Caspase assay Mitochondrial assay	1x 10^4 cells/well	96-well plate
2	Apoptosis assay Glutathione assay Cell cycle assay mRNA extraction assay Wound healing assay	5 x 10^5 cells/well	6-well plate
3	ROS assay	1×10^5 cells/well	6-well plate
4	Colony assay	500 cells/well	6-well plate
5	Spheroid assay	1×10^3 cells/well	12-well plate
6	Transwell migration assay Transwell invasion assay	5×10^5 cells/well	6-transwell plate

4.4 Calcium Fura-2 dynamic assay (I)

The cancer cells were seeded in a clear-bottomed 96-well black plate. The next day, the cells were washed with a 1X phosphate-buffered saline solution (PBS, Sigma-Aldrich, St. Louis, MO, USA) and then dyed with 2 μM Fura 2-AM (Cat no. 47989-1MG-F, Sigma-Alrich) for 30 min. Next, the Fure 2 AM was rinsed off and then the cells were incubated with HIC and MB to get 5 serial concentrations from 6.25 μM to 100 μM. The fluorescence levels were recorded using a Magelan™ microplate reader at 37°C every 5 min at the dual excitation/emission wavelengths 340/510 and 380/510. The fold change of Ca^{2+} was measured using the equation (1):

$$F_{340/380} = \frac{F_{340}^{tr} - F_{340}^{blank}}{F_{380}^{tr} - F_{380}^{blank}} \qquad \text{Eq.(1)}$$

The fluorescence levels of the treated samples at 340/510 nm and 380/510 nm were F_{340}^{tr} and F_{380}^{tr} respectively. The fluorescence levels of the untreated samples at 340/510 nm and 380/510 nm were F_{340}^{blank} and F_{380}^{blank} .

To further determine which ligands should be targeted to the P2Y1R, a siRNA assay was performed using the siRNA of P2Y1R, which had been predesigned by

ThermoFisher Scientifics (Cat no. AM16708, Waltham, MA, USA). The PCa cells were transfected with 20 nM of siRNA using the RNAiMAX Transfection Reagent from ThermoFisher Scientific (Waltham, MA, USA). After 48 hrs, the fold changes in the intracellular calcium levels were measured from the transfected cells according to Equation 1.

4.5 Detection of the cell toxicity (I, IV)

The activation of P2Y1R is known to induce apoptotic cells and inhibit cell growth in PC3 cells. In this experiment, a cell cytotoxicity assay was performed to determine whether the ligands have a negative effect on the PCa cell growth. Cancerous and non-cancerous cells were prepared in a 96-well plate. When the cells reached 70-80% confluence, they were treated with DMSO (vehicle control), and with serial concentrations of the compounds HIC or MB (5 μM, 10 μM, 20 μM, 50 μM, 75 μM, and 100 μM), and MRS2365 (as a positive control, cat no. 2157/1, Tocris, Abingdon, UK). After 48 hrs, MMT and a cytotoxicity assay (Cat no. BSBTAR1156, Bosterbio, CA, USA) were carried out to evaluate the cell toxicity, according to the manufacturer's protocol. The absorbance was detected at 570nm using a Magellan™ microplate reader. The experiment was repeated three times under the same conditions. The percentage of inhibition was calculated based on the manufacturer's standard equation. The cytotoxicity of the drugs used against the cancer cells was calculated using Equation 2.

$$\%\ inhibition = \frac{A_c - A_{tr}}{A_c} \times 100 \quad \text{Eq. (2)}$$

The number of cells in the untreated samples and the treated samples are A_c and A_{tr}, respectively.

The half-maximal inhibitory concentration IC_{50} values were based on the concentration-effect curve function of Graphpad Prism 8.0. A time-dependent study at 24 hrs, 48 hrs, and 72 hrs was performed using an IC_{50} concentration of the compounds on the PC3 and DU145 cells. The percentage of cell death was measured using MTT assay, as described above. The IC_{50} values of the compounds HIC and MB were used in further experiments in Studies II, III, and IV.

4.6 The detection of apoptotic activity in ligands (I-IV)

The apoptotic response is regarded as a potential target for anti-cancer drugs in cancer therapy. To investigate the capabilities of anti-cancer agents in PCa models, an apoptosis assay, a caspase 3/7 assay and a ROS induction assay were used to identify the anti-cancer effects of the agents.

4.6.1 The apoptosis assay (I, III, IV)

To assess the capabilities of the agents in cell apoptosis, an apoptosis assay was carried out using Dead Cell apoptosis kits (Cat no. V13241, TheremoFisher Scientific, Waltham, MA, USA). The cancer cells were prepared according to the method shown in Table 3. After reaching up 60-70% confluence, the cells were incubated with DMSO, HIC, MB, AA, and MRS2365 for 48 hrs. Next, the cells were washed with PBS and then stained with a dark 50 μL 1X Annexin-binding buffer included in the kit. Then the cells were incubated with 5 μL fluorescein isothiocyanate conjugated Annexin V and propidium iodide (PI) for 15 min. Florescent images of the cells were obtained using an EVOS FL microscope (ThermoFisher Scientific, Waltham, MA, USA). Semi-automated image processing and manual counting were used to assemble the colored cells according to their fluorescent intensities, after which a percentage value for the cell apoptosis and necrosis was calculated.

4.6.2 The reactive oxygen assay (I, IV)

ROS is generated in many abnormal physiological conditions of cells under endogenous and exogenous stimulation. High levels of ROS are capable of inducing an apoptotic response and cell phase arrest (Liou and Storz, 2010). Thus, ROS induction is a promising avenue of investigation for cancer treatment. To investigate the apoptotic effect of the ligands on PCa cells, a ROS production assay was performed using Fluorescent 2',7-dichlorodihydroglurescein diacetate (H2DCFA) (Cat no. D339, ThermoFisher Scientific, Waltham, MA, USA).

The cancer cells were prepared in a 6-well plate culture. After 24 hrs, the cells were treated with DMSO (a vehicle reagent), HIC, MB, AA, and hydrogen peroxide (H_2O_2) for 5 hrs. The cells were then washed with PBS and tested with H2DCFA for 30 min at 37°C. In the samples that exhibited ROS production, the H2DCFA

was oxidized into 2',7'-dichlorofluorescein. The stained wells were collected and the H2DCFA staining was washed out. They were then incubated in a normal medium for 20 min for recovery. The fluorescence of the samples was measured with a Magellan™ microplate reader with an excitation length of 485 nm and an emission length of 538 nm. The fold change of the ROS production was analyzed using Equation 3.

$$Fold\ change = \frac{F_{Drug} - F_{Blank}}{F_{Control} - F_{Blank}} \quad \text{Eq.(3)}$$

The fluorescent levels of the drug-treated samples, the untreated samples and the unstained samples are F_{Drug}, $F_{control}$, and F_{blank} respectively.

4.6.3 The caspase 3/7 activity assay (I, IV)

Caspases are known to play a part in the cellular response to apoptosis (Li and Yuan, 2008). To date, 14 caspases have been cloned and their roles in programmed cell death have been analyzed. Of these, two have great potential as targets for cancer therapy, caspases 3 and 7. When activated, caspase 3 supports DNA damage and the morphological changes of apoptosis while the activation of caspase 7 directly causes cancer cell death. To examine the anti-cancer effects of the compounds in the PCa cells, in vitro tests from Caspase-Glo® 3/7 Assay Systems (Cat no. G8091, Promega, Madison, USA) were carried out. In this assay, the PCa cells were plated on a white, 96-well plate 24 hours before the experiment. After 24 hrs, the cells were treated with DMSO, HIC, MB, and AA for 5 hrs and then incubated with a Caspase-Glo reagent for 1 hr. The luminescent signals were monitored to calculate the fold change of the caspase 3/7 as per Equation 4.

$$Fold\ change = \frac{L_{Drug} - L_{Blank}}{L_{Control} - L_{Blank}} \quad \text{Eq.(4)}$$

The luminescent densities of the drug-treated cells, the untreated cells and the unstained cells are L_{Drug}, $L_{control}$, and L_{blank} respectively.

4.7 Mitochondrial ROS generation (II)

Mitochondria are present on the cell membranes which bound the cell organelles. They produce most of the chemical energy for cell metabolism, cell proliferation,

cell death, and ROS production. Without mitochondrial activity, cancer cells are unable to grow and form new DNA strands for cancer cell proliferation.

4.7.1 Mitochondrial membrane potential assay (II)

To determine the mitochondrial activity of a cancer cell membrane under DMSO, HIC, and MRS2365 treatment, a mitochondrial membrane potential (MtMP) assay (Cat no. MAK159-1KT, ThermoFisher Scientific, Waltham, MA, USA) was carried out using a JC-10 fluorescent dye, according to the manufacture's protocol.

It is well established that upon injury, stress, or death of cells, its membrane potential decreases and JC-10 monomers are generated, resulting in a shift to green fluorescence 490/525. Therefore, our procedure was as follows. Firstly, the PCa cells were plated on a 96-well plate. The cells were then incubated with drugs at the desired concentrations for 48 hrs. Following the drug treatments, the cells were incubated with JC-10 fluorescent dye for 1 hr. The plates were then infused for 15 minutes with buffer B, included in the kit. Then they were measured with a Magellan™ microplate reader. The excitation/emission levels of the green and red fluorescence were measured at 490/525 and 540/590, respectively. The fold change of MtMP activity was calculated using Equation 5.

$$\text{Fold change} = \frac{F_{RT} - F_{RB}}{F_{GT} - F_{GB}} \qquad \text{Eq.(5)}$$

F_{RT} and F_{RB} are the fluorescent densities of the treated and untreated red samples, respectively. F_{GT} and F_{GB} are the fluorescent densities of the treated and untreated green samples, respectively. The assay was performed in triplicate under identical technical and biological conditions.

4.7.2 The glutathione assay (II)

A glutathione colorimetric detection kit (Cat no. EIAGSHC, ThermoFisher Scientific, Waltham, MA, USA) was used to measure the amount of glutathione (GSH) in the PCa cells. The experiment was carried out according to the manufacturer's guidelines. The cancer cells were treated with DMSO, HIC, and BITH for 48 hours. Next, the cancer cells were collected and re-suspended in a 5% aqueous 5-sulfo-salacylic acid dehydrate. Then, lysis solution was added to the cells for 15 mins. The lysate solution was intended to incubate with the detection reagent

and the reaction solution included in the kit. Absorbance of GSH production in the samples was detected at 405 nm. The GSH production can be calculated using the standard equation included in the kit (Equation 6).

$$\%\text{inhibition} = \frac{A_{CT} - A_{BL}}{A_{DR} - A_{BL}} \quad \text{Eq.(6)}$$

A_{CT} and A_{DR} are the concentrations of GSH products in the treated samples respectively, whereas A_{BL} is the concentration of GSH products in the untreated samples. The experiment was performed three times under identical test conditions.

4.8 Fluorescence-activated cell cycle phase analysis (III, IV)

Cell cycle arrest is one of the crucial targets of anti-cancer agents. In this test, PI staining was carried out to investigate the phase arrest of the compounds. The PCa cancer cells were cultured in a 6-well plate as per Table 3. After 24 hrs, the cells were exposed to a vehicle control, HIC, AA, and MRS2365 for 48 hrs. Subsequently, the cells were washed with PBS and then soaked with an ice-cold 70% ethanol solution for 30 min. The collected pellets were re-suspended in a PI-Triton-RNase solution containing propidium for 15 min in the dark. RNase was used to minimize the RNA contamination in the samples in order to achieve optimal DNA resolution. The purpose of the PI was to bind to the DNA by intercalating between the base pairs. A nuclear and chromosome counterstain was executed and detected under a fluorescent microscope at the excitation/emission maxima of 493/636 nm. The red fluorescence images were captured for further analysis using CellProfiller 4.0 (Broad Institute, MA, USA) to detect and measure the biological features. The distribution of cell phases was determined using MATLAB R2018b (MathWorks Ltd., MA, USA).

4.9 Extraction to data analysis from RNA-sequencing (III)

The establishment of an *in vitro* cell model is an important step in studying the mechanisms of disease and in analyzing gene expression profiles and how individual cells respond to drug treatment. The changes in gene expression patterns point to the need for an explanation of both the desirable and undesirable aspects of drug therapy. RNA-seq is regarded as the next-generation sequencing technology for determining the number and identities of RNA molecules in various samples under

different conditions. In addition, RNA-seq analyses both the coding and non-coding RNA, in both the splicing and allele-specific expressions.

4.9.1 mRNA extraction and quantification (III)

In this experiment, the PCa cells were cultured in 6-well plates until they reached up to 70% cell confluency. After 24 hrs, the cells were treated with DMSO and HIC for 48 hrs. The cells were then collected in order to extract mRNA using a GeneJet RNA purification kit (Cat no. K0731, ThermoFisher Scientific, Waltham, MA, USA).

The procedure was to lyse the cells with a lysis buffer containing 400 mM β-mercaptoethanol, which is included in the kit (Cat no. M6250, Sigma-Aldrich, St.Louis, MO, USA). The lysates were purified using purification columns, and then washed with a wash buffer (also in the kit). The mRNA was collected in nuclease-free water and quantified using a Magellan™ microplate reader. There is a more detailed description of the mRNA purification process in Publication III. The whole transcriptome sequencing of the mRNA extraction was performed using Illumina NextSeq 500 at the University of Helsinki (Helsinki, Finland). The bcl data was collected in the FASTQ file format.

4.9.2 RNA-seq data analysis (III)

The readings were from a demultiplexed FASTA file and gene annotation, and GT Files mapped to FastQC using Ensembl gene annotation. Spliced-transcript alignment was used as a reference to calculate the number of reads and to detect the differential levels of genes between the 2 sample groups, also compared to the human genome. Pairwise comparisons between the various conditions were run using SAMtools and the "union" mode of high-throughput sequencing data (HTSeq). The SAMtools helped in dealing with the complex gapped sequences and the alignments with multiple or paired data. This method provides outputs such as a pair of alignment records. HTSeq supports processing the data on the level of sequenced fragments rather than reads in SAMtools. Analysis of the changes in the gene expression levels (DGE) between the experimental groups was normalized under reading count data and statistical analysis. There are various tools for DGE analysis such as Cuffdiff, edgeR, limma-voom, DESeq, and baySeq. The adjusted p-values were calculated according to the Benjamini-Hochberg procedure.

4.9.3 Regulated cell signal pathways (III)

GO annotations and the ClusterProfiler package enable the identification of the functional properties of the genes themselves, and any biological processes in which the genes are involved. The Kyoto encyclopedia of genes and genomes (KEGG) is a tool to build up general genomic information, along with higher-order functional information that is collected through bioinformatics analysis and standardized gene annotations. A combination of GO and KEGG was used in this study to test the gene signaling obtained from the DEGs analysis with a cut-off p-value < 0.05.

4.10 The identification of inhibitory effects in cancer formulation (III, IV)

4.10.1 The colony formation assay (III, IV)

To investigate the anti-cancer effects of different compounds on PCa cells, a colony formulation assay was performed as per (Franken et al., 2006). The cancer cells were seeded in 6-well plates for overnight incubation. Then the cancer cells were explored with DMSO, HIC, AA, and MRS2365. A MEME medium supplied with 10% FBS was changed every 3 days in the presence of the drugs. After 9 days of incubation, the plates were washed with PBS to remove any floating cells. Then the colonies were dyed with a 0.05% crystal violet dye for 10 min in RT. Images of the stained cell colonies were captured and the colonies were counted manually using an Axiovert 200 M microscope (Carl Zeiss, Germany). The inhibitory fraction of the drugs was calculated based on the number of colonies in the cancer cells treated with drugs compared to the number of colonies in the vehicle groups.

4.10.2 The MTS invasion assay (III)

To further explore the anti-cancer activity of the compounds, a cancer MTS assay was performed to study the cancer cell proliferation in the test compounds as per (Ha et al., 2021). In this study, the MTS assay was done to determine the anti-cancer effect of the compound in a time- and dose-dependent manner. The PCa cells were seeded in 12 well plates coated with 0.1% Matrigel for 48 hrs. The spheroids were treated with DMSO, HIC, and MRS2365.

To determine the anti-cancer activity of HIC in a dose-dependent manner, the cancer cells were treated with various concentrations of HIC (5 μM, 10 μM, and 20 μM) for 8 days. Images of the colonized areas were taken using a Nikon TE 2000-U microscope (Nikon Inc., Japan). The areas of the colonies were analyzed using ImageJ software 1.52 (National Institute of Health, USA) using Equation 7. All the data were presented as mean ± SEM, n = 3, scale bar = 100 μm.

$$\text{Colony area \%} = \frac{\text{Colony area of the drug-treated samples}}{\text{Colony area of the control groups}} \times 100\% \quad \text{Eq.(7)}$$

To investigate the inhibitory effects of HIC on cancer colonies in a time-dependent manner, the cells were treated with an IC_{50} concentration of HIC, MRS2365 and a vehicle control. Images of the colonies were collected on the first, third, and eighth days of the experiment. These images were captured and then quantified using ImageJ software version 1.52 using Equation 7.

4.11 Determination of the anti-metastatic activity of ligands (III, IV)

Metastatic cancer, a common phenomenon of stage IV cancers, exhibits genetic changes in the cancer cells, unlike in primary tumors. The PC3 cells for this experiment were taken from bone metastasis in a PCa, while the DU145 cells were obtained from the central nervous system metastasis of a PCa patient. Obviously, the PC3 and DU145 cells had metastasis activity, so the anti-metastatic effects of the compounds in the cancer cells could be reliably evaluated.

4.11.1 The wound-healing assay (III, IV)

A wound-healing assay, also known as a scratching assay, is a standard *in vitro* experiment for collecting evidence about migrated cancer cells. A cell-free area in the cell culture is created, either by physical exclusion, chemicals, or temperature. Evidence about the migrated cells is measured by the rate of gap closure compared to the size/rate of the scratches. In this experiment, the PCa cells were cultured in 6-well plates until they reached up to 80-90% cell confluence. Then, a 'wound' was created by scratching the plate membrane with 200 μL pipette tips. The floating cells were washed out with a warm PBS. Then the cells were treated for 24 hrs with a vehicle control, HIC, MRS2365, and AA in a MEME medium supplied with 1%

FBS. At each specified time interval, cell images were captured using an EVOS microscope in order to measure the gap areas. The gap closures were analyzed using ImageJ software 1.52. The fold change of the migrated cells was calculated using Equation 8.

$$W_{change} = \frac{W_{0-D} - W_{24-D}}{W_{0-C} - W_{24-C}} \times 100\% \quad \text{Eq.(8)}$$

The starting points of the scratch areas in the samples in the presence of either the drug or the vehicle control are $W_{0\text{-}D}$ and $W_{0\text{-}C}$, respectively. After 24 hrs incubation, the scratch areas in the drug-treated samples and the vehicles were $W_{24\text{-}D}$ and $W_{24\text{-}C}$, respectively.

4.11.2 The transwell migration assay (III, IV)

The transwell migration assay is used to measure the chemo-attractive properties of a chemical agent. It can also be used to measure the effect on the metastatic behavior of cancer cells by measuring the number of migrated cells through the transwell membrane. In our assay, the PCa cells were plated in the upper chamber (6-well type, pore size 8 μm) in the presence of either the DMSO or the drugs with a 1% serum medium. The lower chamber was plated with a 10% serum medium. After 24 hrs of incubation, the cancer cells tended to move from the lower nutrients to the higher nutrients for cell growth and metastasis. Here, the membranes of the chambers were fixed with solutions containing 3.7% paraformaldehyde (Cat no. 158127-5G; Sigma-Aldrich, St.Louis, MO, USA). The migrated cells were then dyed with 0.5% crystal violet (Cat no. 548629; Sigma-Aldrich, St.Louis, MO, USA). The membranes were further washed with warm PBS and dried at RT for 3 or 4 hrs. Random fields of the transwell membranes were captured using EVOS imaging systems so that the migrated cells could be counted manually under a microscope. The data were shown as a percentage of the number of migrated cells in the treated groups divided by the number of migrated cells in the vehicle groups. The vehicle control was the DMSO.

4.11.3 The invasion assay (III, IV)

A migrated cell is a cell which has moved from one area to another, whereas an invaded cell is one that penetrates an extracellular matrix (ECM) barrier through enzymatic degradation. To assess the inhibitory effects of the compound on cell

invasion, the transwells were coated and incubated with Corning® Matraigel® Basement Membrane Matrix (Corning, NY, USA) for 2 hrs. The PCa cells were plated in transwell and processed to detect any invaded cells, as outlined in the transwell migration assay.

4.12 Regulated cell signaling in PCa cells by ligands (III)

The activation of P2Y1R regulates PLC activity and has a critical role in changes to the levels of Ca^{2+}, IP3, and PKC (Delekate et al., 2014; Wan et al., 2016). It is known that activation of the PKC isoform stimulates the ERK, a member of Mitogen-activated protein kinases (MAPKs). In addition, it has been reported that P2Y1R can be regulated with IL-1 and TNFα production. To investigate the association of P2Y1R activation with MAPK and NF-κB signaling, the human phosphor MAPK array (Cat no. ARY002B; R&D systems, Boston, USA) and the human NF-κB pathway array (Cat no. ARY029; R&D systems, Boston, USA) were performed in a model PCa cancer.

The procedure for this assay was as shown in Figure 10. Briefly, the PCa cells were incubated with an IC_{50} concentration of HIC for 48 hrs. Next, the cancer cells were washed with PBS and then lysed with a cell lysis buffer contained 8.3 μg/mL Aprotinin (Cat no. 78432; ThermoFisher), 4.2 μg/mL Pepstatin (Cat no. 78436; ThermoFisher), and 1 mM Trypsin inhibitor (Cat no. T97767; Sigma-Aldrich, St.Louis, MO, USA). The protein concentrations of the samples were measured using an AccuOrange™ protein quantification kit (Cat no. 30071.T; Biotium, CA, USA) in approximate working concentrations. 200 μg of cell lysates were added to the micro-array membranes in the presence of an antibody cocktail at 4°C for 24 hrs. Representative membranes of protein array were shown in Figure 11. The next day the membranes were washed 3 to 5 times with a washing buffer and stained with a second antibody (included in the kit) for 2 hrs at RT. Images of the membranes were captured using ECL systems (GE Healthcare) with a Xenogen IVIS 200 imaging machine (PerkinElmer Inc., MA, USA). The density of the protein expression was measured using ImageJ software version 1.52. Protein contained in protein array membranes were listed in Table 4 and Table 5.

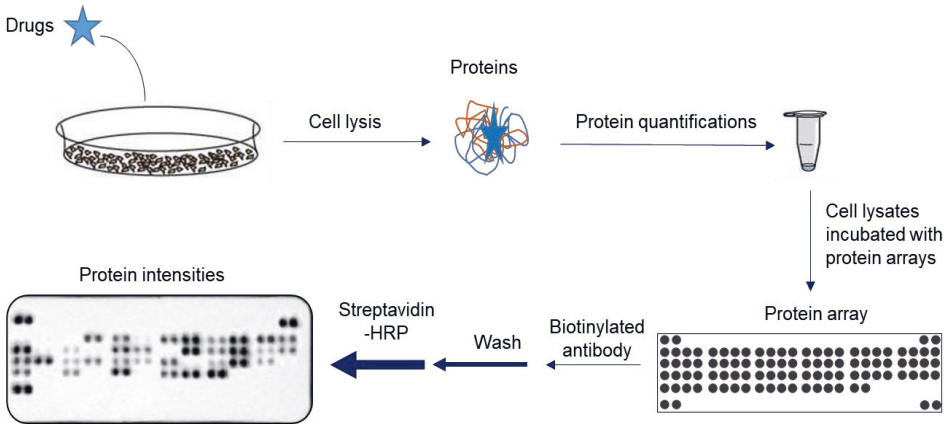

Figure 10. Representative procedure of protein array detection. Images of the protein array membranes were photographed using ECL systems. The densities of the protein expression were analyzed using ImageJ software for detecting the fold change levels (Li et al., 2018).

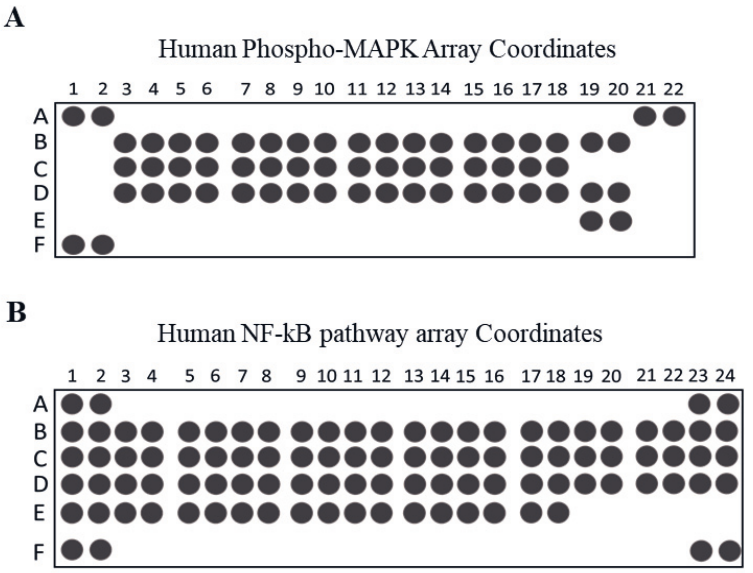

Figure 11. Representative membranes of protein array. (A) A membrane of the human phospho-MAPK array contains 26 different capture antibodies printed in duplicate. (B) A membrane of the human NF-κB array is used to detect the relative levels of 41 proteins and 4 serine or tyrosine phosphorylation sites in the NF-κB signal transduction. Each capture antibody was carefully selected using cell lysates prepared from cell lines known to express the target protein. Numerous immunoprecipitations and Western blots experiments are reduced by using protein array assay.

Table 4. List of proteins contained in the human phospho-MAPK array. The list of 21 proteins contained in the Human Phospho-MAPK array coordinates as shown in Figure 11A is indicated in the table below. All three major families of MAPK, ERK1/2, JNK1/2, and different p38 isoforms, are essential in investigating the roles these signaling molecules play in the mechanism underlying cell function and disease. Other intracellular proteins are included in the protein array membranes.

Human Phospho-MAPK Array			
Coordinate	**Target protein**	**Phosphorylation site detected**	**Protein name**
A1, A2	Reference spots	-	-
A21, A22	Reference spots	-	-
B3, B4	Akt1	S473	RAC-alpha serine/threonine-protein kinase
B5, B6	Akt2	S474	RAC-beta serine/threonine-protein kinase
B7, B8	Akt3	S472	RAC-gamma serine/threonine-protein kinase
B9, B10	Akt pan	S473, S474, S472	Protein kinase
B11, B12	CREB	S133	cAMP response element-binding protein
B13, B14	ERK1	T202/Y204	Extracellular signal-regulated kinase 1
B15, B16	ERK2	T185/Y187	Extracellular signal-regulated kinase 2
B17, B18	GSK-3α/β	S21/S9	Glycogen synthase kinase-3 alpha/beta
B19, B20	GSK-3β	S9	Glycogen synthase kinase-3 beta
C3, C4	HSP27	S78/S82	Heat shock protein 27
C5, C6	JNK1	T183/Y185	c-Jun N-terminal kinase 1
C7, C8	JNK2	T183/Y185	c_jun N-terminal kinase 2
C9, C10	JNK3	T221/Y223	c-jun N-terminal kinase 3
C11, C12	JNK pan	T183/Y185, T221/Y223	c-Jun N-terminal kinase
C13, C14	MKK3	S218/T222	Mitogen-activated protein kinase kinase 3
C15, C16	MKK6	S207/T211	Mitogen-activated protein kinase kinase 6
C17, C18	MSK2	S360	Ribosomal protein S6 kinase
D3, D4	p38α	T180/Y182	Mitogen-activated protein kinase 14
D5, D6	p38β	T180/Y182	Mitogen-activated protein kinase 11
D7, D8	p38δ	T183/Y185	Mitogen-activated protein kinase 13
D9, D10	p38γ	S46	Mitogen-activated protein kinase 12
D11, D12	p53	T421/S424	Tumor protein p53
D13, D14	p70 S6 kinase	S380	Ribosomal protein S6 kinase beta-1
D15, D16	RSK1	S386	Ribosomal s6 kinase 1
D17, D18	RSK2	S2448	Ribosomal s6 kinase 2
D19, D20	TOR	-	Serin/threonine-protein kinase
E19, E20	PBS	-	-
F1, F2	Reference spots	-	-

Table 5. List of proteins contained in the human NF-κB pathway array. Forty-one proteins and four serine or tyrosine phosphorylation sites involved in the NF-κB pathway array coordinated as shown in Figure 11B are listed in the table below. The levels of these proteins are simultaneously detected in a single sample.

Human NFκB Pathway array		
Coordinate	**Target protein**	**Protein name**
A1, A2, A23, A24	Reference spots	-
B1, B2	ASC	Apoptosis-associated speck-like protein containing a CARD
B3, B4	BCL10	B-cell lymphoma 10
B5, B6	CARD6	Caspase recruitment domain family member 6
B7, B8	CD40	Cluster of differentiation 40
B9, B10	cIAP1	Cellular inhibitor of apoptosis protein 1
B11, B12	cIAP2	Cellular inhibitor of apoptosis protein 2
B13, B14	FADD	Fas-associated death domain
B15, B16	Fas	Fas cell surface death receptor
B17, B18	IκBα	Inhibitor of Kappa B alpha
B19, B20	IκBε	Inhibitor of Kappa B epsilon
B21, B22	IKK1/IKKα/CHUK	IkappaB kinase 1
B23, B24	IKK2/IKKβ	Ikappa B kinase 2
C1, C2	IKKγ/NEMO	Ikappa B kinase gamma
C3, C4	IL-1 RI	Interleukin 1
C5, C6	IL-17 RA	Interleukin 17
C7, C8	IL-18 Rα	Interleukin 18
C9, C10	IRAK1	Interleukin-1 receptor-associated kinase 1
C11, C12	IRF5	Interferon regulatory factor 5
C13, C14	IRF8	Interferon regulatory factor 8
C15, C16	JNK 1/2	c-Jun N-terminal kinase 1/2
C17, C18	JNK2	c-Jun N-terminal kinase 2
C19, C20	TNFRSF3	Tumor necrosis factor receptor superfamily member 3
C21, C22	AEG-1	Astrocyte elevated gene 1
C23, C24	MYD88	Myeloid differentiation primary response 88
D1, D2	NFκB1	Nuclear factor NF-kappa B p105 subunit
D3, D4	NFκB2	Nuclear factor NF-kappa B p49 subunit
D5, D6	TNFRSF16	Tumor necrosis factor receptor superfamily member 16
D7, D8	p53	Tumor protein p53
D9, D10	p53 (pS46)	Tumor protein p53
D11, D12	RelA/p65	Transcription factor p65
D13, D14	RelA7p65 (pS529)	transcription factor p65
D15, D16	c-Rel	Proto-oncogene c-Rel
D17, D18	SHARPIN	Sharpin protein
D19, D20	SOCS6	Suppressor of cytokine signaling 6
D21, D22	STAT1p91	Signal transducer and activator of transcription 1

D23, D24	STAT1 (pY701)	Signal transducer and activator of transcription 1
E1, E2	STAT2	Signal transducer and activator of transcription 2
E3, E4	STAT2 (pY689)	Signal transducer and activator of transcription 2
E5, E6	STING	Stimulator of interferon genes
E7, E8	TLR2	Toll-like receptor 2
E9, E10	TNF RI/TNFRSF1A	Tumor necrosis factor receptor 1
E11, E12	TNF RII/TNFRSF1B	Tumor necrosis factor receptor 2
E13, E14	TRAF2	TNF receptor-associated factor 2
E15, E16	DR4	Death receptor 4
E17, E18	DR5	Death receptor 5
F1, F2	Reference spots	-
F23, F24	Negative control	Control (-)

4.13 Combination therapy assays (IV)

The mechanism of two drugs in a combination model was evaluated using the combination index (CI) (Foucquier and Guedj, 2015). CompuSyn Software version 4.0, Equation 7 was used to measure the values of CI. (ComboSyn Inc., Paramus, NJ, USA) (Chou and Talalay, 1984). The concentrations of drug 1 and drug 2 are (Dx)1 and (Dx)2. These are the concentrations required to exert the same inhibition on cell survival as the effect measured by concentrations D1 and D2 in the combinatorial model [(D1) + (D2)]. The values of CI below 0.9, in the range of 0.9 to 1.1, and above 1.1, are indicated for the synergistic, additive, and antagonistic interactions of the two drugs, respectively.

$$\mathrm{CI} = \frac{(\mathrm{D1})}{(\mathrm{Dx})1} + \frac{(\mathrm{D2})}{(\mathrm{Dx})2} \qquad \text{Eq.(9)}$$

4.14 Statistical analysis (I-IV)

All the experiments were conducted 3 to 5 times under the same conditions. The results were presented as ± means of the standard error of the mean (SEM) and analyzed using SPSS software version 26.0 (IBM SPSS statistics version, NY, USA). Any statistically significant differences between the two groups were analyzed using a t-test. An ANOVA test was used for calculating the differences between two or more samples. All tests with $*p < 0.05$ were regarded as statistically significant.

5 RESULTS

This chapter consists of five main sections covering the results obtained using the above methods in the four publications (I, II, III, and IV). In the first and second sections, the results are from an investigation of the novel ligands HIC and MB targeted at P2Y1R in PC3 and DU145 cell models. The top compound, HIC, was selected for further analysis of its apoptotic and mitochondrial activity in cancer cells, and this is described in the third section of this chapter. The anti-cancer capabilities of HIC were then intensely scrutinized in more detail with several biological experiments, and that is the focus of the fourth section. The final section is focused on the combinatorial therapy model of HIC and AA. This is a known AR inhibitor and is a crucial inhibitory factor against PCa proliferation and metastasis.

5.1 Determination of the novel P2Y1R-targeted ligands (I, II)

5.1.1 Analysis of P2Y1R protein structure (I, II)

Earlier studies of sequence analyses have confirmed that P2YRs are a subtype of GPCRs and belong to the Class A family, which is activated by both adenine and uracil ligands (Neumann et al., 2020). According to SWISS-PORT and TrEMBL, an analysis of 68 subset proteins of the homo sapiens database reveals a high structural similarity to eight members of the P2Y receptor family. In contrast, rhodopsin showed low sequential identification with the P2Y receptor. Therefore, one avenue of exploration in this study focused on the multiple sequence alignment of retrieved proteins in the presence of rhodopsin.

Additionally, the 8 P2YRs are divided into two distinct subgroups, the Gq- and Gi-couple subtypes (Lee et al., 2003). According to a sequence-structure analysis of the P2YRs, the endogenous ligand CysLT with P2YRs presents a highly conserved structural topology with seven transmembrane helices. The eighth amphipathic helix presents an extracellular amino-terminal region and a cytoplasmic carboxyl-terminal tail. The crystal structure of the CysLT receptor in a human has not yet been

experimentally resolved. In fact, it has only been extensively studied in cell lines and tissues. Furthermore, the available 3D structure has little structural similarity with the known structure of bovine Rhodopsin. Some efforts have been made to clone the human CysLT receptor (Jin et al., 1998). About 337 amino acids have been identified that present seven transmembrane domains for P2YRs and have the closest homology to the purinergic family of receptors. The absence of a crystal structure in the CysLT receptor is a bottleneck to identifying novel ligands. However, the structure of P2Y receptors has been solved and has been used to conduct various comparative structural analyses of the organisms.

The seven transmembrane helices of the P2Y1 protein structure contain two disulfide bonds whose N-terminal is linked together, while helix III is linked to the second extracellular loop, which increases stabilization of the extracellular loop 2 (ECLs) conformations. The ECL2 of P2Y1R appears as a hairpin structure. It is often detected in the bound GPCRs of most known peptides. Previous studies have investigated the crystal structure of the P2Y1R targeted at high resolution by two ligands, MRS2500 and BPTU (Yuan et al., 2016). MRS2500, a nucleotide-like antagonist, binds to the seven transmembrane bundles of P2Y1R whereas BPTU, a non-nucleotide-like antagonist, links to the external interface (Hechler et al., 2006). At a sub-atomic level, the models reveal that the atomic details of the two distinct ligands that are targeted at the binding sites of the receptor have contrasting chemical and structural characteristics.

Yet more designer ligands of P2Y1R may reveal more specific efficacies. In our experiments, the ligand binding site of P2Y1R was identified using a sitemap program with a site score of 1.064 in the interaction with CysLT and UDP. The volume of the ligand binding site was found to be 369.7 $Å^3$ with a surface exposure of about 0.555. Most of the geometrical features in the binding site of the P2Y1R protein structure were explored. The availability of a crystallographic structure of P2Y1R demonstrates the potential benefits of further drug discovery using computational models.

5.1.2 Docking analysis (I)

Previous reports have shown the inhibitory effects of 1-indolinoalkyl 2-phenolic compounds on cancer cell growth. In the light of these reports on the anti-cancer effects of phenolic compounds, this study has examined 923 compounds based on 1-indolinoalkyl 2-phenolic structure through molecular docking. The efficiency of the docking was determined by measuring the number of hydrogens, halogen bonds,

π-cation, salt bridges, aromatic bonds, and π- π interactions for the stability of compound synthesis. The glide score (gscore) values were the criterion used to select the best-docked compounds for virtual screening. Two compounds, HIC (**1**) and MB (**2**), were identified as the ligands with the highest binding affinity towards P2Y1R in terms of the highest docking score and Lipinski's rule. These compounds were selected for synthesis.

5.1.3 Model interaction of P2Y1R with ligands (I)

Two-dimensional interaction diagrams of the protein-ligand combination were used to identify the interactions of HIC and MB with P2Y1R. The diagrams indicated that P2Y1-HIC had the residues from 16 amino acid interactions, whereas P2Y1-MB had 19. Interestingly, the MRS2500-known ligand showed only 15 amino-acid interactions with P2Y1R (Houston et al., 2006). The interaction between P2Y1R and both compounds HIC and MB exhibited at least 6 hydrophobic bonds. These are recognized as the strongest interactions between protein-ligand bindings. Notably, the hbond energy of P2Y1R with the 2 compounds was over -0.902 Kcal/mol, whereas the score of hbond energy of P2Y1-MRS2500 was -0.920 Kcal/mol. Furthermore, the combination of P2Y1-HIC and P2Y1-MB also showed interactions at Arg287, Arg310, Arg195 (charged), Tyr303, Cys42, Cys202 (hydrophobic), and Leu44. The appearance of cysteine residues plays a crucial role in maintaining the precise pocket formation for the interaction of ligands and P2Y1R. These results clearly indicate that HIC and MB could be used as potential ligands targeted at P2Y1R.

5.1.4 The evaluation of ligand activity in intracellular Ca^{2+} (I)

Up until now, Ca^{2+} has been regarded as a direct messenger that is generated by P2Y1R activation through the activation of the Gαq subtype (Werry et al., 2002). More specifically, the activity of P2Y1R triggers the activation of PLC and then hydrolyses IP3, which increases the cytosolic Ca^{2+} mobilization. Changes in the downstream effector Ca^{2+} were used as a yardstick to determine whether HIC and MB have agonistic activity. Here, the intracellular Ca^{2+} level increased in both the PC3 and the DU145 cells after receiving serial concentrations of HIC and MB in a time-dependent manner. In addition, the cancer cells treated with 100 μM HIC

resulted in more than 2 times higher Ca^{2+} levels in both the PC3 and DU145 cells. Similarly, MB at 50 μM also induced a 2.5-fold increase in the Ca^{2+} levels in two PCa cell lines compared to the untreated cancer cells. Taken together, these results suggest that HIC and MB could act as agonists of P2Y1R and can be used to activate the Gαq signaling pathway. The characterization of HIC and MB on PCa cells was then evaluated through the siRNA of P2Y1R in PCa cells. In the presence of the siRNA of P2Y1R transfection, the fold changes of the Ca^{2+} levels were lower under HIC and MB treatment than they were in the groups which did not exhibit any siRNA. Thus, the results suggest that HIC and MB could act as selective agonists for P2Y1R.

5.1.5 The inhibitory effect of ligands on cell proliferation (I)

The ability to inhibit a cancer cell's survival is a primary factor in evaluating the biological activity of novel ligands in cancer research. Previous studies have shown that the agonists of P2Y1R can hamper cell growth and cell proliferation (Wei et al., 2011). In the present study, HIC and MB were identified as agonists that bind and interact with P2Y1R. To further explore the inhibitory effects of HIC and MB on PCa cell survival, the number of cells death was measured using an MTT assay. The results showed that HIC and MB increased the cell death rate when compared with the untreated groups. The IC_{50} values for a PC3 cell treated with HIC and MB were found to be around 15.98 μM and 33.57 μM, respectively. For comparison, the IC_{50} values were about around 15.64 μM and 25.64 μM in DU145 cells treated with HIC and MB, respectively.

Regarding the IC_{50} values, HIC can exert a greater inhibitory effect on PCa cells than MB. In contrast, the non-cancerous cells HEK293 and MEF were less sensitive to HIC, MB, and MRS2365 than the PCa cells. It has been reported that less than 20% cell death was observed in HEK293 at 100 μM of HIC and MB, and 1 μM of MRS2365 treatment. HIC induced more than 22% cell death in MEF cells, whereas less than 15% cell death was observed in the MB- and MRS2365-treated groups. These observations suggested that HIC and MB had specific cytotoxic effects in PCa cells. Therefore, further study on the dynamic cytotoxicity of the compounds was conducted using IC_{50} concentrations of these compounds on PCa cells. The percentage of cell proliferation decreased more in a time-dependent manner in the presence of HIC and MB than it did in cells treated with the DMSO after 24 hrs, 48

hrs, and 72 hrs of treatment. These findings suggest that HIC and MB could suppress PCa cell growth in both a time- and dose-dependent manner.

5.1.6 The activation of ligands in an apoptotic response (I)

Apoptosis is a common response of cells under stress, essential during their developmental stage and for tissue homeostasis. The activation of P2Y1R-MRS2365 in PC3 induces increased apoptosis (Wei et al., 2011). Here, the effect of our novel ligands on apoptotic cells was evaluated under a fluorescent microscope looking for any changes in the externalization of phosphatidylserine on a plasma membrane. HIC and MB respectively shifted nearly 23% and 29% of the viable PC3 cells into apoptotic ones (Figure 12). A similar trend was observed in the DU145 cells with a 20% increase in apoptosis in both the HIC- and MB-treated samples when compared with the untreated samples. Similarly, the positive control Na_3VO_4 showed 25.6% and 21.2% apoptosis in PC3 and DU145 cells, respectively. Taken together, the data were consistent with previous studies of the activation of P2Y1R in an apoptotic response.

ROS production has a dual function in cells, acting as both a stimulant of cell proliferation and metastasis on the one hand, and as an inductor of cell cycle checkpoints and cell death, on the other (Fiaschi and Chiarugi, 2012; Liou and Storz, 2010; Simon et al., 2000). A test was devised to evaluate the effect our compound had on PCa cells through ROS production. The cancer cells were labeled with H2DCFDA in the presence of HIC and MB, ROS production was found to have increased in both the cancer cells and in the positive control, H_2O_2. In PC3 cells, ROS showed a 1.41-fold change in the presence of HIC and a 1.22-fold change in the presence of MB. The same pattern was seen in the DU145 cells with a 1.36- and 1.01-fold increase after HIC and MB treatment, respectively. As a point of comparison, hydrogen peroxide expressed a 2.1- and 1.78-fold change in the PC3 and DU145 cells, respectively.

Caspase 3 and caspase 7 are both known inducers of the apoptotic process, which they do by cleaving to a diverse array of protein substrates (Li and Yuan, 2008). Since the activity of caspase 3/7 plays a crucial role in apoptosis, the anti-cancer effects of these two ligands were determined by evaluating their increased activity of caspase 3/7. In the treated cells, HIC increased 1.22- and 1.15-fold, reflecting the change of caspase 3/7 activity in the PC3 and DU145 cells, respectively. Similarly, the proportional change of caspase 3/7 activity was found to be 0.8 and 1.15 respectively

in the PC3 and DU145 cells in the presence of MB. In summary, the results showed that the novel agonists HIC and MB could induce ROS and caspase 3/7-dependent apoptosis.

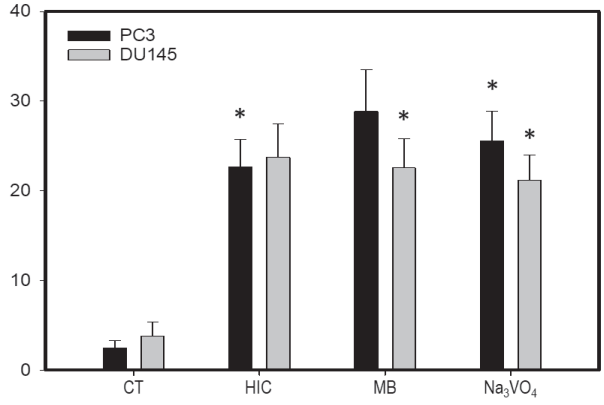

Figure 12. Activation of ligands on apoptotic response. Percentage of apoptosis cells in PC3 cells and DU145 cells in the corresponding condition. The values are considered as ± means SD, *p < 0.05, and n = 3.

5.2 HIC's inhibition on mitochondrial membrane activity (II)

Based on the above results, the evidence indicates that HIC is better than MB in increasing the number of apoptotic cells and the caspase 3/7 activity in PCa cells. Additionally, the IC_{50} values of HIC in PC3 and DU145 are lower than the IC_{50} values of MB. Therefore, HIC was selected for further evaluation in this study.

Mitochondrial membrane activity plays a crucial role in all mitochondrial activity due to the effects the ATP activity has on electron transport and ROS production (Mori et al., 2019). In addition, the top row of results indicated that after 48 hours that ROS production is one of the potential targets of HIC in PCa cells as the above results. Nevertheless, to further determine the anti-cancer effects of HIC on mitochondria, an MtMP assay in HIC-treated PCa cells with BITC-a positive control was performed. The fold change of the MtMP levels decreased under HIC and BITC treatment in both types of PCa cells when compared with the vehicle group (Figure 13A). Specifically, the decrease in the MtMP fold change was 0.14 and 0.74 in the HIC- and BITC-treated PC3 cells, respectively. In the DU145 cells, the fold change of MTMP decreased to 0.28- and 0.71 after HIC and BITC treatment, respectively.

Another consideration is that ROS production has dual functions in cell survival, depending on whether it is under normal or abnormal physiological conditions. One study showed that ROS production is an essential stimulator for cell proliferation and metastasis (Liou and Storz, 2010). However, this is in contrast to other studies which have shown that ROS production helps fight cancer by inducing cell cycle arrest and apoptosis (Feher et al., 2008). One of the most common metabolites of ROS production is GSH, which acts as an antioxidant in cells (Mori et al., 2019). To examine the anti-cancer capability of HIC in PC3 and DU145 cells, a glutathione assay was performed. As shown in Figure 13B, in the presence of HIC, the GSH level remained unchanged in the PC3 cells whereas it decreased to about 14.6% in the DU145 cells, when compared with the DMSO-treated groups. On the other hand, BITC induced a decrease of 28.7% and 34.6% in GSH levels in both the PC3 and DU145 cells respectively. Collectively, the findings suggest that HIC might well have an inhibitory effect on mitochondrial activity in PCa cells.

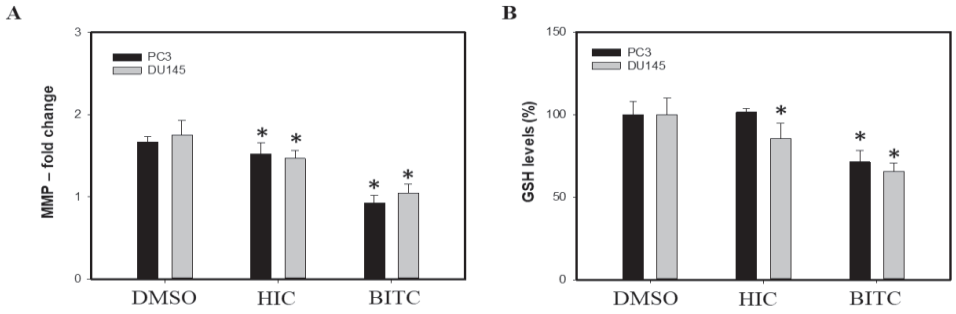

Figure 13. Inhibition of HIC on mitochondrial activity. (A) The fold change of MTMP activity in PC3 and DU145 cells treated with DMSO, HIC and BITC were determined by measuring the intensity of the fluorescence. (B) Percentage of GSH production was measured from the absorbance intensities of the samples. The change of GSH production was measured according to Equation 6. The experiments were repeated three times with the same biological and technical conditions to observe the statistical significance with the mean ± SD, * $p < 0.05$.

5.3 Evaluation of the inhibitory effects of HIC in PCa cells (III)

5.3.1 Investigation of the anti-cancer activity of HIC (III)

To investigate the potential cytotoxicity of HIC in PCa cells, a clonogenicity assay was performed. Upon treatment, PCa cells become more resistant to HIC than the DMSO group although there are variations in the number and size of the colonies. HIC significantly reduced the formation of the colonies by 50% in both PCa cells, whereas the positive control MRS2365 caused a reduction in the number of colonies of about ~53%. Notably, MRS2365 showed a lower percentage of inhibition in PCa colonies than HIC. In order to validate the inhibitory effect of HIC on cell viability, an MTS assay was examined using HIC in a dose- and time-dependent manner. Over half of the colony's area was suppressed after treatment with 5 μM, 10 μM, and 20 μM of HIC in the PC3 and DU145 cells. Additionally, the anti-cancer activity of the HIC was also evaluated by investigating the change in the spheroid area at various time-points for the PC3 cells and the DU145 cells on the 3rd and 8th days of treatment, respectively. Interestingly, the decrease of the spheroid area was noticeably less in the MRS2365 than in the DMSO control on the 3rd day of treatment. More than 50% inhibition was detected after 8 days of MRS2365 treatment in both PCa cells. Taken together, the results suggest that HIC was able to suppress the model colonies in both a dose- and time-dependent manner.

Another target for drug discovery is DNA damage. In this approach, the aim is to suppress the proliferation of PCa cells and thus inhibit the progression of the disease. Clinical trials have shown positive results for the new drugs targeted at DNA damage in cancer therapy (Bono et al., 2020). Detailed RNA-seq data analysis was carried out to explore the effect of HIC on transcriptomics. The results identified 19623 genes, including 3321 DEGs (16.4%), in both PCa cells with $*p < 0.05$. The top DEGs involved in DNA damage are listed in Figures 11E and 11F. Up-regulation of *CDKNLA*, *UVSSA, CCNB3*, and *NBR2* was detected in the PC3 cells, while the top down-regulated genes were *SOX4*, *MDM2*, *MDM3*, *TP73*, *CDK1*, *TUBA1A*, and *TUBA1B,* all of which were involved in DNA damage after 48-hour incubations with HIC (Figure 14A). Similarly, the top up-regulated genes in the DU145 cells treated with HIC include *TEP1*, *UVSSA*, and *NBR2*. In contrast, the down-regulated genes include *TUBA 1A*, *CDK2*, *SOX4*, *TUB 1B*, *TP73*, *CDK1*, *MDM2*, and *MDM4* (Figure 14B). *CDK1* and *CDK2* have crucial roles in DNA repair and G1 phase progression due to their p21 signaling. The down-regulated expression

of these genes not only promotes DNA damage related to cell phase arrest but also impedes DNA recovery (Poole et al., 2004). Furthermore, down-regulation of *MDM4* and *MDM2* enhances the stability and activity of p53 tumor suppression, thereby inhibiting cell survival and DNA repair (Carr and Jones, 2016). In addition, coding for p21 proteins was observed in the up-regulation of *CDKN1A*. This induces DNA damage and also activates G2-phase cyclin/CDKs proteins (Kreis et al., 2019). As a consequence, these genes are responsible for DNA damage, and they induce more G1 checkpoint arrests. Additionally, down-regulated expression of TP73 and SOX4 activates the p53 signaling pathway, which induces cell stress signaling, including cell death, DNA damage, and oxidative stress (Hur et al., 2010; E et al., 2014).

Many physiological processes, including tissue development and homeostasis, are dependent upon finding a balance between apoptosis and cell proliferation. Several of the studies cited here have shown that agonists of P2Y1R, such as ADP and MRS2365, promote cell apoptosis and inhibit cell proliferation (López et al., 2017; Muscella et al., 2018). This study has, additionally, validated the key differentially expressed genes involved in apoptosis-mediated cell death using micro-array analysis (Figure 14C and 14D). Upon HIC treatment, there was an increase in the expression of the pro-apoptotic genes *BAX* and *CDKN1A* in both types of PCa cells. An increase in *BAX* decreases a cell's resistance to apoptosis stimulation and is linked to cancer cell death, in addition to which, *CDKN1A* is a known inhibitor of DNA damage (Pearson et al., 2000; Kreis et al., 2019). The MYD88 protein is a crucial inhibitor of TLR3 signaling, which is essential in cancer therapy. It protects the host cells from unwanted immuno-pathologies linked to excessive production of IFN-β (Siednienko et al., 2011). Notably, the down-regulation of *PARPs* was noticed in both cell lines under HIC treatment. Specifically, the mRNA levels of *PARP10* and *PARP12* were inhibited in both the PC3 and the DU145 cells. The down-expressed levels of *PARP1* and *PARP4* were more noticeable in the PC3 cells, whereas the inhibitory expression of *PARP9* was more noticeable in the DU145 cells.

It is 50 years since the first report about the inhibitory activity of the PARP family created a revolution in cancer therapy (Chen, 2011; Rose et al., 2020). PARPs have several crucial functions in cancer therapy. They can support a DNA repair pathway, and other cellular processes such as transcription and modulation of the chromatin structure. These observations suggest that HIC's inhibition of cell proliferation might be related to DNA damage and the apoptotic response. In fact, the effects induced by HIC could be linked to p53, p21, and PARP signaling in both PC3 and DU145 cells.

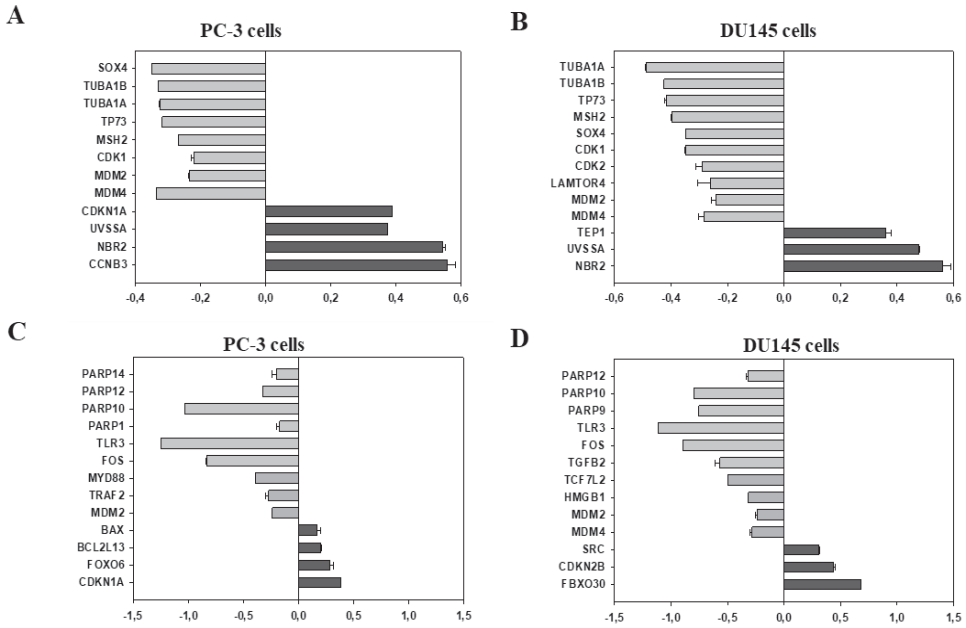

Figure 14. Investigation of anti-cancer activity of HIC. (A, B) List of top genes regulated by HIC with DNA damage in PC3 cells (A) and DU145 cells (B) via RNA-seq sequencing analysis. The top difference-expressed genes associated with apoptosis in PC3 cells (C) and DU145 cells (D). The graph presents means ± SD.

5.3.2 HIC suppression on the G1/S phase (III)

To determine the ability of HIC to arrest cell division at different cell phases, the distribution of cells in each phase was analyzed according to the DNA content in the different cell cycles. Following HIC treatment, a significantly higher percentage of arrested PC3 cells was observed in the G1 phase, but there was little change, still less a decrease, in the distribution of the PCa cells in the S and G2/M phases as shown in Figure 15. Specifically, over 45% of the HIC-treated PC3 and DU145 cells were arrested in the G1 phase, whereas the transitions to the S and G2/M phases were almost the same as for the DMSO control.

Based on the above observations, the genes regulated by HIC treatment and linked to the G1/S phases are analyzed. Notably, down-regulation of the *MCM*s was observed in both the PC3 and the DU145 cells, indicating its pivotal role in cell cycle suppression. The down-regulated expressions of *MDM4* in the PC3 cells and *MCM3-6* in the DU145 cells have been reported as crucial components for

restricting DNA elongation and inhibiting cell proliferation in the G1 phase (Siednienko et al., 2011). The down-expression of *CCNE2* and *CCNA2* by HIC was only observed in the DU145 cells. Cyclin E (*CCNE2*) and Cyclin A (*CCNA2*) are crucial stimulators for G1/S phase initiation and induced the activation of Cdk2 for the inception of DNA replication (Trovesi et al., 2013). The down-regulated expression of Cdk2 triggers G1/S phase arrest through the downstream activity of p53-p21 signaling. Furthermore, the *CDKN2A* and *CDKN2B* tumor expression genes in the G1/S checkpoint were inhibited in the DU145 cells when treated with HIC. Taken together, these findings suggest that the arrest of the G1 phase by HIC could regulate the inhibitory effect of HIC against PCa cell proliferation.

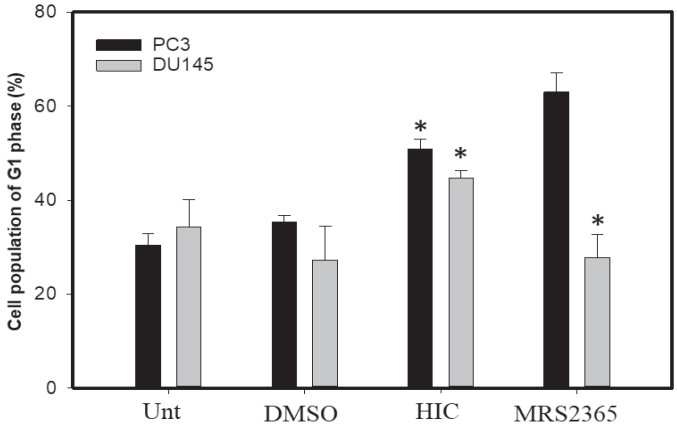

Figure 15. HIC suppression on the G1 phase in PCa cells. Propidium iodide-stained images of PC3 cells and DU145 cells were analyzed to calculate the percentage of cells in G1 phase of division after drug treatment. Data presented is the mean ± SD with *p < 0.05, n=3, t-test.

5.3.3 Identification of the anti-metastasis activity of HIC (III)

The activation of P2Y1R has dual functions in cell proliferation and cell metastasis in different cell lines. In this study, *in vitro* cell migration and invasion assays were conducted on a PCa model to determine the anti-metastasis effects of HIC. The results of a wound-healing assay indicated that HIC reduced the scratched areas of cancer cells in comparison with the DMSO group. After 12 hrs of incubation, a decrease in the wound closure capability was observed in PC3 cells treated with HIC and MRS2365. After 24 hrs of incubation, HIC still suppressed more migrated cells

in the wound area than the MRS2365 did. A similar pattern was documented in the DU145 cells treated with HIC and MRS2365 in a time-dependent manner.

To support the above findings, a transwell migration assay was also performed to assess whether the percentage of cell migration had effectively declined in the drug-treated groups, i.e., the number of cancer cells which had migrated from the lower-nutrient locations to the higher-nutrient ones through the membranes of the transwell. The migrated cells were stained with crystal violet dye for visualization and counted manually under a microscope. Compared to the vehicle group, there was a decrease in the cell migration of ~45 % in both types of PCa cells when treated with HIC.

To further explore the anti-metastasis ability of HIC in invaded cells, the PCa cells were examined in a Matrigel-coated transwell for 24 hrs in an invasion assay. A similar pattern of the inhibitory effects of HIC on the invaded cells was documented for both the PC3 and the DU145 cells. Collectively, these results also suggest that HIC could well have a strong anti-metastasis capability in PCa cell models.

Gene expression analysis was carried out to address the role of the genes involved in the cell migration and invasion that occurs in HIC treatment. The top DEGs are listed in Figure 16. Note that down-regulated expressions of *TGFB2*, *TGFB3*, *MEF2C*, *ANXA3*, *SCG2*, and *HMGB1* upon HIC treatments were observed in both PCa cells. Among these genes, it has been shown that the down-regulation of *TGF2* and *TGF3*, members of the multifunctional cytokine family, effectively diminished tumor invasion and angiogenesis (Padua and Massagué, 2008). Suppression of the invasion, and metastasis, was consistently observed through the activity of the TGF-β signaling that resulted from the down-regulation of *MEF2C* (Liu et al., 2004). The down-regulation of ANXA3 and BMP4 inhibits cancer metastasis and cell proliferation by decreasing the power of the matrix metalloproteinases (MTMPs) (Ampuja et al., 2013; Du et al., 2018). Furthermore, *SCG2*, the secretogranin II gene, promotes cell migration whereas *HMGB1*, (high mobility group box 1), which regulates migrated and invaded cells, was noted to be highly expressed (Wang et al., 2022). Thus, the downregulation of *SCG2* and *HMGB1* observed in the HIC-treated group has a negative effect on a migrated prostate tumor. Collectively, the findings

suggest that HIC may inhibit cell migration and the number of invaded cells through the down-regulation of the TGF-β signaling pathways.

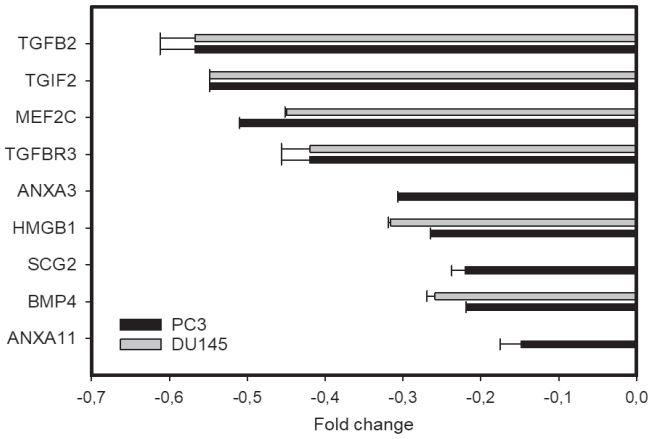

Figure 16. Lists of DEGs regulated by HIC in PCa cells. PC3 cells and DU145 cells show the lists of the top DEGs associated with the activity of HIC after 48 hrs treatment.

5.3.4 Regulation of HIC to p53 stabilization (III)

An association between P2Y1R and the MAPK-NFκB signaling pathways has been indicated in a number of research articles (Kuboyama et al., 2011; Kudirka et al., 2007; Zerr et al., 2011). This prompted us to evaluate the effects of HIC with protein expression profiling. The DU145 cells were selected to perform these mechanistic studies because HIC suppressed more cell proliferation and arrested both cell types in the G1/S phase in cell cycle progression.

To investigate any potential molecules targeted by HIC, a MAPK protein assay was carried out. Nitrocellulose membranes spotted with twenty-four differentially phosphorylated kinases were captured to analyze the fold change of the protein expression. The differential expressions of protein kinases upon the HIC-treated groups are shown in Figure 17, where $*p < 0.05$. The phosphorylation levels of ERK1/2, JNK1/2, and AKT were slightly increased after the HIC treatment. The fold changes in the signal intensity of the phosphorylated proteins were reported as over 1.09-fold-changes for ERK1, ERK2, JNK1, and JNK2. These results were in line with the previously observed capabilities of P2Y1R (Muscella et al., 2018). In our study, the activation of ERK1/2 was known to contribute to the regulation

between p53 and G1 phase arrest, which induces cell death in the ZL55 cell model. The absence or inhibition of the JNK1/2 protein suppresses the ADP-mediated growth of the ZL55 cells through the inhibitory expression of the p53 protein. The p53 pathway aids tumor suppression in its apoptotic response, leading to G1 arrest and cell death.

To further investigate the capabilities of P2Y1R in cell signaling, an NF-κB protein array was examined in HIC-treated DU145 cells. The fold change of the different proteins is presented in Figure 16 in the HIC- and DMSO-treated groups with $*p < 0.05$. Interestingly, an increase in the fold changes of protein p53 and phosphorylated protein p53-Ser45 was observed after HIC treatment. The activation of p53 induces apoptosis in transcription-dependent and -independent pathways, whereas the phosphorylated protein, p53-Ser46, contributes to apoptosis by the activation of pro-apoptosis targeted genes (Ozaki and Nakagawara, 2011). There was no observable change in the protein expressions of I-κB and NF-κB after HIC treatment. Taken together, the results suggest that the anti-cancer capability of HIC might be linked to the activation of the tumor suppression protein p53 via transcription-dependent or -independent mechanisms.

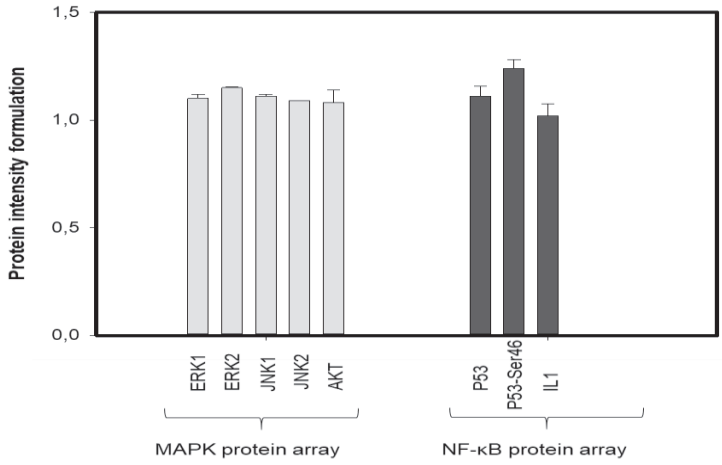

Figure 17. Analysis of protein arrays under HIC treatment. The images of MAPK and NF-κB protein arrays were photographed using a Xenogen IVIS 200 imaging system and evaluated via ImageJ analysis. The bar charts of MAPK array and NF-κB array present the fold change in protein expression after HIC- and DMSO-treatments.

5.4 Combinatorial therapy of HIC and AA in cancer models (IV)

5.4.1 The increased cytotoxicity of HIC plus AA in PCa cell survival (IV)

Current cancer chemotherapy research is looking for novel drugs with fewer side effects to attack cancer cells that are resistant to drug treatment. It seems clear that combinatorial drug treatments can be regarded as a potentially fruitful method for cancer therapy. For example, since drugs inhibit cell growth at different phases of the cell cycle, using a combination of drugs expands the arena in the fight to eliminate cancer cells.

Our research included MTT assays on the effects of HIC and AA on cell growth. In these experiments, cancerous and non-cancerous cells were dosed with varying concentrations of the two drugs for 48 hrs. In comparison with the vehicle group, HIC suppressed the growth of the PCa cells in increasing concentrations as per the testing method described above. The PC3 and DU145 cells' growth declined by up to ~80%. At the same time, the decrease in the growth of the non-cancerous cells HEK293 and MEF was observed to be ~15% at a concentration of 40 μM HIC. Meanwhile, the cell death of PC3 and DU145 cells was less than 50% when treated with 40 μM of AA. Statistically, the PC3 cells had 34.6% cell death whereas the DU145 cells had about 43.6% cell death at the same AA concentration, (40 μM). In the same experiment, after AA treatment the non-cancerous cell death rate was less than 15%. It is clear from the above values that HIC is more inhibitory to PCa cells than AA is. These findings are not new. They confirm the results of previous studies which have shown that PCa cells with a low expression of AR exhibit less suppression than the cancer cells which have a high expression of AA (Grossebrummel et al., 2016). In the light of these results, in the subsequent experiments to investigate the inhibitory effect of HIC and AA on cancer cell survival, the drugs were always administered at a ratio of 1:3, respectively.

After 48 hrs treatment, the percentage of cell survival in the PCa cells decreased noticeably as the concentrations of HIC and AA were increased (Figure 18A). Both the PC3 and DU145 cells lost almost half of their cell viability when treated with 15 μM HIC and 45 μM AA (1:3). Even with a slightly weaker concentration, 10 μM HIC to 30 μM AA, the percentage of cell death rose to over 50% in both types of PCa cells. It was clear from these tests that HIC and AA together induced more cell death than they did when used separately. The synergistic effects of the interaction between the two drugs were determined by assigning CI values for the

concentrations of the drugs and cell survival. Half of the PCa cells died under a combination of 10 μM HIC and 30 μM AA, whereas the survival of the non-cancerous cells was only reduced by less than ~20% under the same conditions. Therefore, it was these concentrations of HIC and AA that were selected for further experiments.

The next task was to conduct a clonogenic assay. In order to evaluate the efficacy of HIC plus AA in promoting cell reproductive death by DNA damage, colonies of cancerous cells were captured (Figure 18B). The resulting analysis showed that the PC3 cells' ability to form colonies was reduced 1.5-times more under a combined HIC+AA treatment than it was when the drugs were used separately. Furthermore, although treatment with HIC and AA separately (monotherapy) did decrease the colonization efficiency of the DU145 cells, when administered in combination, HIC and AA decreased this value by a further 25%. A similar result was obtained with a combination of HIC and AA, which decreased the cancer's colonization by about 60.1% in DU145 cells. These results show that treating PCa with a combination of HIC and AA causes more cancer cell death than single drug treatment.

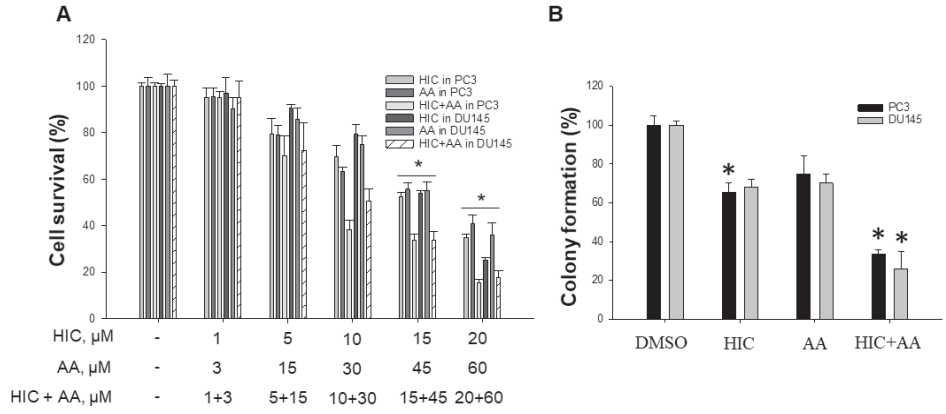

Figure 18. The sensitivity of cancerous and non-cancerous cells to HIC and AA. (A) Percentage of cell survival in PC3 cells and DU145 cells with serial concentrations of HIC and AA. (B) Evaluation of colony formation in PC3 and DU145 cells when compared with the drugs-treated groups and DMSO-groups. The data are presented as mean ± standard errors, *p < 0.05.

5.4.2 An evaluation of HIC and AA in apoptosis, caspase 3/7 activity and ROS production in PCa (IV)

Assays of apoptosis, caspase 3/7 activity, and ROS production were performed to further explore the inhibitory effects of HIC plus AA in PC3 and DU145 cells. The production of apoptotic cells was measured using Annexin V fluorescent staining. In general, the highest apoptotic populations in the PC3 and DU145 cells were observed under combinatorial treatment with HIC and AA together, which outperformed any treatments with the two drugs separately. The results showed that the number of apoptosis cells was ~1.3 times higher in the presence of HIC+AA together than it was in treatments with HIC or AA alone (Figure 19A). Clearly, AA in combination with HIC induced larger apoptotic populations in both cell lines, which is consistent with what is known about the drugs' inhibitory effects on cell proliferation.

Caspase 3/7 also plays a crucial executioner role in stimulating the intrinsic/extrinsic pathways needed for apoptosis. Thus, a Caspase 3/7 assay was carried out in the PC3 and DU145 cells to examine the anti-cancer effects of our two drugs. Under a mono-therapeutic treatment regimen, the activity of Caspase 3/7 increased ~0.19-fold under HIC alone and ~0.12-fold under AA when compared with the DMSO group in PC3 cells. The Caspase 3/7 in the DU145 cells increased ~0.1-fold in the presence of HIC and AA separately. As expected, the highest induction of Caspase 3/7 was observed with a combination of HIC plus AA for both the PC3 and the DU145 cells. This treatment induced a ~0.25-fold increase. The results showed that HIC plus AA increased the caspase activity in PCa cells more than a single dose of either drug did.

An increase in ROS production is known to be a capable stimulator for apoptosis and cell cycle checkpoints. It was evident from the above results that HIC + AA effectively inhibit cell survival. This prompted us to evaluate the impact of combinatorial treatment on a PCa model through the production of ROS. As the results of caspase 3/7 assay, HIC and AA raised the ROS production in both the PC3 and the DU145 cells. ROS production led to a 1.2-fold increase in both types of PCa cells when treated with HIC or AA separately, in comparison with the vehicle group. However, the combinatorial treatment increased the ROS production by over 1.4 times, which is more than the monotherapy treatment did, in both cell types. These findings are consistent with the earlier findings in this study. They show that a combination of HIC and AA is more efficient in inducing an apoptotic response,

Caspase 3/7 activity, and ROS production in cancer cells than single drug treatment regimens are.

5.4.3 Suppression of HIC and AA on G1 phase arrest (IV)

One of the main challenges in cancer therapy is uncontrolled cell division in cancer. The ability to arrest this cell division at a crucial phase is a critical mechanism for anti-cancer drugs. Therefore, a cell cycle assay was conducted to evaluate the effect of using the combinatorial drugs HIC + AA to arrest the cell phase distribution. The assay captured representative images of PCa cells, which were then used to analyze the cell-phase distribution. The images were examined by segmentation in order to detect the distribution of the cells in each phase under drug treatment.

The results of this assay are interesting. After HIC + AA treatment, there was no discernible difference in the percentage of cells at the G2 and M phases in either of the cell lines. After a single treatment with the drugs, the highest cell phase percentage in both types of PCa cells was observed in the G1 phase. In numbers, the proportion of G1 phase cells in the PC3 cells rose to 55.7% after separating single doses of HIC and AA when compared to the vehicle group. The results for the combinatorial approach are even more impressive. When the HIC plus AA were given in combination, the percentage of PC3 cells at the G1 phase was 75.1%. It was the same story with the DU145 cells. When they were given separate single doses of HIC and AA, 44.5% and 52.5% of the cells respectively were determined to be in the G1 phase (Figure 19B). When the HIC plus AA were given in combination, the percentage of DU145 cells at the G1 phase was measured at 77.1%. Taken together, the results show that a combination of HIC and AA induced more cell distribution in the G1 phase than separate HIC and AA treatments.

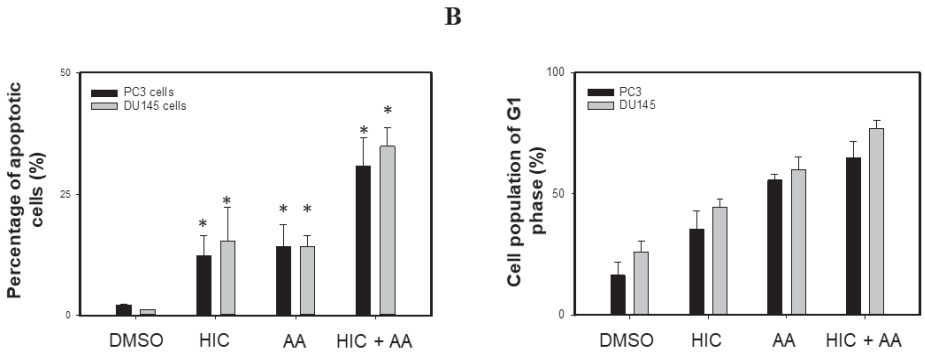

Figure 19. Combinatorial effects of HIC plus AA in apoptotic response and cell phase arrest. (A) The percentage of the cell population that presented apoptosis cells in the corresponding conditions of PC3 cells and DU145 cells. (B) Fluorescent images were captured and analyzed in ImageProfiler software to assess the distribution of cells in different cell phases. The experiments were performed using biological and technical repeats, with the mean ± SD, *p < 0.05.

5.4.4 Evaluation of the anti-metastasis activity of HIC and AA in PCa cells (IV)

Migrated and invaded cells are known to be a crucial factor in the development of a malignant tumor. Hence, novel anti-cancer drugs that can reduce the number of migrated and invaded cells are a potential target for research. Previous research has shown the anti-metastasis activity of HIC in PC3 and DU145 cells. However, nothing much is known about how AA inhibits the progression of such PCa cells, which prompted us to determine AA's effect on the migration and invasion of PCa cells.

After 24 hrs of combinatorial treatment with HIC plus AA, the invaded area of both PCa cells decreased steadily when compared with the DMSO. The decreases in the invaded areas were 23.5%, 27.15, and 46.4% respectively when treated with HIC alone, AA alone, and HIC + AA together. Similarly, encouraging results were also achieved with the DU145 cells, which had reductions of 29.5%, 35.2%, and 55.5% respectively when treated with HIC alone, AA alone, and HIC + AA together.

On the back of these findings, a more detailed analysis of the anti-metastasis activity of HIC plus AA was conducted in the form of an invasion assay, conducted after 24 hrs exposure with the chambers coated in matrigel. In comparison to the DMSO group, the invaded PC3 cells were inhibited by 66.4%, 60.4%, and 84.9% respectively when treated with HIC alone, AA alone, and HIC + AA together. In

the DU145 cells, the decreases in cell invasion were 21.5%, 24.3%, and 47.6% in the presence of HIC, AA, and HIC plus AA, respectively. Taken together, these results demonstrate that the combinational model of HIC and AA treatment suppresses more migrated and invaded cancer cells than exposure to the drugs separately would do.

6 DISCUSSION

This discussion will summarize the above findings and their theoretical implications in the light of previous studies. It will also present the significant achievements of this study and will outline the potential anti-cancer effects of HIC and AA when used as an anti-PCa drug with a number of different targets.

6.1 The associations of P2Y1R with apoptosis, mitochondrial activity and cell death

A fundamental understanding of the molecular details of ligands and P2Y1R interactions has always been integral to cancer research and therapy. A multitude of ligands has been investigated with *in vitro* models for use with P2Y1R in order to explore their clinical features (Delekate et al., 2014; Ecke et al., 2008; Fang et al., 1992; Hechler et al., 2006; Muscella et al., 2018; White and Burnstock, 2006). However, there is still some controversy over the roles of novel antagonists or agonists in the expression of P2Y1R in cancer models.

With computer-designed drug discovery, it is now possible to design novel small molecules for P2Y1R. The molecular docking models designed for this study were able to identify the interactions of a chemical library consisting of 923 compounds derived from a 1-indonoalkyl 2-phenolic structure with P2Y1R. The docking analysis indicated that HIC and MB had the potential to act as novel ligands for P2Y1R as they had the highest docking scores, and they satisfied the Lipinski rule. In addition, among the interactions between P2Y1R and the two ligands, some crucial amino acid interactions were observed which have a significant effect on folding and stability.

Furthermore, this study has investigated the function of P2Y1R in PC3 and DU145 cells and presented a detailed pharmacological model for the negative or low expression of AR. The synthesized phenolic compound derivatives HIC and MB were used to examine the activation of P2Y1R, targeted to increase Ca^{2+} levels. The activity of the two compounds in intracellular Ca^{2+} levels was observed in a dose and time-dependent manner, suggesting that these two compounds might work as

agonists for P2Y1R. A recent experiment has shown that calcium elevation can be induced with an extract of green tea that inhibited cell survival in PC3 and DU145 cells. However, the same pattern could not be induced in high-AR expression cells (Marchetti, 2022). Nevertheless, it seems probable that the levels of Ca^{2+} in PC3 and DU145 could play a critical role in inducing apoptosis and cell death.

Another finding of this study is the increase of caspase 3/7 activity and ROS production in PC3 and DU145 cells after 48 hrs of HIC treatment. Although no final conclusion about the ROS role in cancers has been reached, the promising effects of ROS production were noticed in terms of cell death and the cell cycle checkpoints (Feher et al., 2008). The results obtained from the cancer cells show that high levels of ROS production do contribute to an apoptotic response, as this triggers the collapse of MtMP and leads to the release of Cyt C into the cytosol (Hamanaka and Chandel, 2010). The increase in Cyt C in the cytoplasm initiates a caspase cascade reaction. Our research found that HIC inhibited meager levels of MtMP and promoted ROS production in both the PC3 and the DU145 cells. These findings are consistent with the hypothesis underlying this study about the link between Cyt C and the increase in Caspase 3/7 activity under the influence of HIC.

Interestingly, much attention has been focused on novel MtMP inhibitors as a new class of anti-cancer drugs (Lin et al., 2019; Zhang and Ye, 2012). Rotenone, an MtMP inhibitor, is one of the more promising of these drugs and has the same pattern on mitochondrial activity and ROS levels as HIC (Swarnkar et al., 2012). A study of Neuro-2a cells indicated that rotenone diminished the activity of the mitochondrial membrane and provoked ROS production. In addition, it is indicated that rotenone is linked to an increase in intracellular Ca^{2+}, caspase 3, and the expression of the calmodulin-dependent protein, kinase II (CaMKIIα). This induces apoptosis and cell death in neuronal cells. In addition, in PC3 cells, oxidase stress resulted in the activation of CaMKII signaling, which is also involved in the induction of intracellular calcium and ROS production. This in turn leads to the inhibitory activity of the mitochondrial membrane and cell death with an apoptotic response (Wang et al., 2017). All in all, the findings suggest that HIC could either be a potential MTMP inhibitor or a novel anti-cancer agent for further investigation in cancer therapy.

Clearly, there is a connection between the activity of HIC and the induction of apoptotic cells in PC3 and DU145 cells (after 48 hrs treatment). It is now 30 years since it was reported that agonists of P2YRs diminished the growth of negative-AR expression PCa cells, namely the PC3 and DU145 cells (Fang et al., 1992). Later, the reported apoptosis induced by the activity of P2Y1R endogenously expressed in PCa

cells is in line with previous reports about the functional effect of P2Y1R activation in PC3 cells, 1321N1 astrocytoma cells, and ZL55 cells (A et al., 2018; Dorota Wypych and Pawel Pomorski, 2012). In PC3 cells, after MRS2365 treatment, the P2Y1R mediates apoptosis. This is somehow related to ERK1/2 phosphorylation, caspase 3 activation, and LDH inhibition. In Wei et al.'s study, their chosen P2Y1R agonist, MRS2365, triggered an increase in the phosphorylation of ERK1/2, while a MAP kinase inhibitor, PD98059, significantly blocked cell apoptosis by P2Y1R activation (Wei et al., 2011). The rate of PC3 cell proliferation had already started to decline after 24 hrs incubation with MRS2365, and by the third day it had declined significantly.

In addition to the above, the activation of P2Y1R induced by ADP in ZL55 cells is known to regulate the stabilization of the p53 protein via the activation of either ERK1/2 or JNK1/2 phosphorylation (Muscella et al., 2018). The consequent effects are linked to the inhibition of cell proliferation, G1 phase checkpoints, and cell death. Recently, the anti-proliferation effect of P2Y1R was determined in 1321N1 astrocytoma cells transfected with human recombinant P2Y1. The study reported that the activation of P2Y1R in 1321N1 cells upon the agonist 2-MeSADP induced apoptosis by activating ERK1/2 and inhibiting the cell growth rate (Dorota Wypych and Pawel Pomorski, 2012). In the light of this, our study further investigated the possible involvement of P2Y1R activation in MAP kinase signaling and apoptosis.

Cancer therapy's exploration of apoptotic responses has had a significant effect on some basic scientific concepts. This is due to the fact that the anti-cancer effects of the therapies can be detected almost immediately by measuring the decrease in cancer cell growth and proliferation (Fesik, 2005). Notably, the genes involved in HIC treatment in this study were apoptotic genes regulated in PC3 and DU145 cells. Down-regulated expression of *MYD88*, *FOS*, *MDM4*, and TLR3 was observed, as was the up-regulated expression of *BAX* and *CDK1A*. The proteins MDM2 and MDM4 interact with the p53 protein and induce its degradation. BAX is an essential mediator for pro-apoptotic activation via the stabilization of p53. This p53 has a crucial role in the inhibition of cancer cell proliferation through its stability and its ability to recruit various signaling pathways (Carr and Jones, 2016; Rivlin et al., 2011). Recently, it has been proposed that an increase in genes regulated to p53 stabilization is involved in apoptotic responses, consisting of *BAX*, *SOX4*, *FOX*, *MDM2*, and *MDM4* (Carr and Jones, 2016; Pan et al., 2009; Rivlin et al., 2011). One of the most crucial functions of p53 is to affect an apoptotic response and interrupt the cancer's progression. A number of recent hypotheses have suggested that p53 is a marker in PCa progression (Ozaki and Nakagawara, 2011; Wan et al., 2018). In preclinical and

clinical trials, the evaluation of novel drugs targeted at apoptosis has long been regarded as a priority target in cancer treatment (Hickman, 1992). This thesis has addressed the function of HIC-targeted P2Y1R in the induction of apoptosis and p53 stabilization through up-regulated pro-apoptotic genes. Therefore, HIC supports these new hypotheses for investigating successful therapies for PCa.

Notably, this work has also shown that *PARPs* were inhibited due to the presence of HIC in PC3 and DU145 cells. The inhibition of PARPs is also a crucial target for pharmacological agents targeted at the enzyme poly ADP in DNA repair (Chen, 2011). PARPs' inhibition or knock-down cancer cells are reportedly linked to the activation of caspase 3 and apoptotic induction. Several studies have indicated novel, clinical drugs based on the inhibition of PARP expression in cancer therapy (Gong et al., 2021; Jang et al., 2020; Rose et al., 2020). Among the PARP inhibitors currently approved for clinical treatment by the FDA are olaparib, rucaparib, niraparib, and talaroparib (Litton et al., 2018; Bono et al., 2020; Anscher et al., 2021; Smith et al., 2022). Two of those drugs, olaparib and rucaparib, have already been commercially produced. They are now marketed as Lymparza and Rubrace and have been used in PCa to treat mCRPC patients, with dramatically promising results (Bono et al., 2020; Anscher et al., 2021). Niraparib has had promising results in patients with mCRPC in a phase-2 clinical trial (Smith et al., 2022). As for the potential uses of HIC in PCa therapy, this study has not only shown that it helps in the regulation of p53 signaling but also that it has inhibitory effects on PARPs.

There remains the need to clarify exactly how HIC-P2Y1 purinergic agonist inhibits cell survival and induces apoptosis, as well as its use with multiple signaling targets and its ability to induce p53 stabilization and inhibit PARP activity. Therefore, the study of p53-/- and PARP-/- models of PCa upon HIC should be further examined in the future.

6.2 The involvement of P2Y1R in DNA damage and cell cycle checkpoints

In order to better understand the relationship between HIC and cell death in PCa models, several experiments were carried out to demonstrate some essential aspects of the mechanisms and the anti-cancer effects of HIC in PCa cells.

HIC had inhibitory effects on colony formation and cell morphology. Moreover, the findings of this study suggest that HIC induces anti-tumor activity by inhibiting the spheroid areas in a time- and dose-dependent manner. A GO enrichment analysis

of a list of the genes that are up- and down-regulated by HIC treatment showed the involvement of DNA damage, replication, p53 signaling, p21 signaling, and G1/S phase arrest.

DNA damage was observed in both types of PCa cells after HIC treatment, which indicates regulation of the p53 signaling. The most promising of the up- and down-regulated genes were listed, such as the up-regulation of *CDKN1A*, *CCNB2*, *NBR2*, *UVSSAI*, and the down-regulation of *SOX4*, *MDM2*, *MDM3*, *TP73*, *CDK1* involved in DNA damage (Carr and Jones, 2016; Kyng et al., 2005; Trovesi et al., 2013). The down-regulated expression of *CDK1* and *CDK2* has been observed in DNA damage and G1 progression arrest (Bertoli et al., 2013; Trovesi et al., 2013). MDM2 and MDM4 also have crucial roles in suppressing the stability and activity of p53 proteins, thus enhancing cell growth and DNA recovery. In addition to the function of HIC on DNA damage, TP73 and SOX4 both activate p53 signaling, which induces cell death, DNA damage, and the increase in ROS production (Candi et al., 2014; Pan et al., 2009). The up-regulated expression of CDKN1A coded for the p21 protein plays a crucial role in DNA damage and further stimulates cell arrest in the G1 phase of the cell cycle (Abbas and Dutta, 2009). The tumor suppressor function of p21 has been reported in both *in vivo* and *in vitro* models. In the *in vivo* model, mice in which the expression of p21 was inhibited seemed to be more susceptible to hematopoietic, epithelial, and endothelial tumor progression than normal mice. In the same vein, other research has shown that in mice with colon carcinogen, p21 promotes more putative premalignant cells (Poole et al., 2004). It seems clear that the over-expression of p21 induces an apoptotic response and suppresses tumor volume in *in vivo* tests on mice. Thus, the results of gene analysis clearly suggest that HIC has a novel function in activating p53 and p21 signaling pathways in PCa therapy.

Several studies have reported the association between DNA damage and apoptotic response in cell cycle arrest (Carr and Jones, 2016; Kyng et al., 2005; Mateo et al., 2015; Pan et al., 2009; Trovesi et al., 2013). With reference to the lists of genes involved in the GO biological process and KEGG pathways regulated by HIC treatment, G1/S phase arrest was selected as a potential target for HIC in a PCa model. Based on the results of the DEGs regulated to the cell cycle, HIC induced cell population in the G1 phase of both the PC3 and the DU145 cells. It also caused S phase arrest in the DU145 cells through the down-regulation of the crucial mediator *Cdks*. The down-regulation of *CDK1*, *TP73*, *MCM4*, and *MCM6* induced cell proliferation throughout the G1 progression phase, this being due to the presence of HIC. The *MCM2-7* complex involves the creation of a pre-replication

complex of DNA and promotes the recruitment process of DNA polymerase for DNA replication (Issac et al., 2019). Increases in MCM4 and MCM6 expression are known as potential markers for tumor progression and prognosis through the driving force of G1 progression (Engeland, 2017). In addition, *Cyclin E* and *Cyclin A*, which are only inhibited by HIC in the DU145 cells, are essential stimulators for the G1/S phase (Trovesi et al., 2013).

All the findings from the gene analysis were consistent with the cell imaging analysis regarding the percentage of cell phase arrest by HIC. In pharmacology, there is a strong correlation between DNA damage and cell cycle arrest which makes HIC a very strong candidate for investigation as a new chemotherapy drug in cancer treatment (Lane and Hupp, 2003; Matthews et al., 2021; Trovesi et al., 2013; Vermeulen et al., 2003). The FDA has approved several drugs targeted at DNA damage in different cancers, including platinum drugs, cisplatin, oxaliplatin, rucaparib, chlorambucil, and temozolomide. Of these, rucaparib was approved for patients with mCRPC who have pre-indicated with AR drugs. This has shown promising effects on DNA damage (Adashek et al., 2019; Jang et al., 2020). There are several more drugs which target the cell phase checkpoints. These have been used in clinical trials in various types of cancers. According to Clinicaltrial.gov, these include flavopiridol, indisulam, bryostatin-1, PD 0332991, and AZD5438. According to the results of a number of phase-I trials, in general, it is safe to use these drugs on patients with PCa. In *in vitro* PCa models, bryostatin-1, PD0332991, and AZD5438 have been shown to have strong inhibitory effects on cell proliferation and survival via CDKs signaling (Von Burstin et al., 2010; Kaukoniemi et al., 2015; Raghavan et al., 2012).

Clearly, the results of our experiments indicate that HIC is a potential CDK inhibitor through its ability to control the down-regulated expressions of *CDKs* in gene analysis. Notably, DNA damage is also one of the HIC targets in *in vitro* PCa models. Therefore, HIC might have more potential to inhibit PCa with multi-molecule targets through DNA damage and G1/S phase arrest.

6.3 Evidence of the anti-metastasis activity of HIC in cancer

The findings of an *in vitro* assay using transwell chambers after 24 hrs treatment suggest that HIC could inhibit migrated and invaded cells. To better understand the anti-metastasis activity of HIC in cancer, a gene expression analysis was conducted. Its purpose was to show that the repression of metastatic genes in PC3 and DU145

cells declined in the presence of HIC after 48 hrs. The gene expression analysis also showed that the down-regulated expression of *TGFB2*, *TGFB3*, *ANXA3*, *HMGB1*, and *BMP4* was evident in both cell lines after HIC treatment. Earlier research had reported that a P2Y1R agonist inhibits the activity of cardiac fibroblasts in combination with TGF-β1 (Tian et al., 2021). However, no direct link between a P2Y1R agonist and a TGF receptor has yet been established. In our study, the HIC attenuated the expression of the TGFs in both cell lines. The TGFβ superfamily has a diverse set of growth factors including BMPs, MEFs, and differentiation factors. The activation of TFGβ signaling triggers the up-regulation of TGFβs, MEF2C, ANXA3, and BMP4, which accelerates cell progression and metastasis (Karlsson et al., 2005; Padua and Massagué, 2008; Yan et al., 2010). Interestingly, *BMP4* is directly linked to the migration and invasion of drug-resistant cancer cells, and is necessary for prostate tumor growth in bone metastasis (Karlsson et al., 2005). In the present study, *ANXA3* was down-regulated, which led to the conclusion that *ANXA3* may inhibit PCa proliferation through the inhibition of matrix metalloproteinases. There has been a report about how *ANXA3* inhibited the proliferation of cancer cells and evidently induced cell cycle G0/1 phase arrest and apoptotic response (Wang et al., 2019). Together, these results suggest that HIC negatively affects migrated and invaded cells by inhibiting the TGFβ signaling.

In further support of the suggestion that HIC induces anti-metastasis effects on PCa models, the down-regulated expression of *SOX4, MDM2*, and *MDM4* was noted in PC3 and DU145 cells. These genes are essential for controlling cell growth through their regulation of p53 activity (Nag et al., 2013; Ozaki and Nakagawara, 2011). In mammals, MDM2 and MDM4 bind to the wild-type p53 protein and induce its degradation, which in turn leads to a decline in the p53 activity that controls cell death and apoptosis (Issac et al., 2019). Thus, inhibition of *MDM2* and *MDM4* expression could promote p53 stability and activity, thereby enhancing DNA damage and apoptosis (Issac et al., 2019). The records of ClinicalTrials.gov indicate that MDM2 has received a lot of attention as a model for designing anti-cancer drugs. To date, over ten molecular drugs have been used in preclinical and clinical evaluations aimed at collecting data about the primary potential target, MDM2 (Konopleva et al., 2020). Our findings confirm that HIC could as also be a potential drug for use in PCa therapy because of its ability to inhibit MDMs.

6.4 Regulation between P2Y1R and p53 stabilization

The activity of P2Y1R has been investigated in various cell lines and the hypothesis related to its activation of cell death and apoptosis is clearly dependent on the particular cellular context and the cancer model (Barańska et al., 2017; Pfefferkorn et al., 2008; Tian et al., 2021; Tominaga et al., 2001; Wei et al., 2011; Wypych and Pomorski, 2012). Many earlier studies have indicated that activation of P2Y1R induced cell death and apoptotic population in PC3 cells (A et al., 2018; Dorota Wypych and Pawel Pomorski, 2012). Recently, another research group has reported the inhibition of ZL55 cell proliferation by an agonist of P2Y1R. This is ADP, which improved p53 stability and activated a PKC-dependent signaling pathway (A et al., 2018). Cellosaurus ZL55 cells with transfected siP2Y1 showed a lower expression of the p53 protein than the cells without transfected siRNA under ADP treatment. Thus, the activity of P2Y1R could have a positive connection with the stability and activity of p53. In many cell lines, p53 could promote various cellular responses involving cell growth arrest, which is necessary to induce the up-regulation of genes for p21 and p27 signaling (Engeland, 2017).

P21 caused a decrease in cyclin E, cyclin A, and cyclin B for inducing G1 phase arrest. Moreover, the expression of *CDKN1A* was noted under HIC treatment, whereas this gene is coded for p21 in controlling DNA damage. In addition, the activation of P2Y1R also provokes a slight increase in the phosphorylation of ERK1/2 and JNK1/2 in ZL55 cancer cells and contributes to the phosphorylation of RelA under transient ischemic conditions (Muscella et al., 2018). In the ZL55 cell model, ERK1/2 activation involves p53-dependent G1 arrest. However, other studies have indicated that ERK1/2 activity triggers the subsequent phosphorylation and stability of p53 for apoptosis. The activation of P2Y1R also promotes the phosphorylation of JNK1/2, which is linked to the modulation of p53 stability (Chen et al., 2010, 1996; Meiyun Fan et al., 2001). Our research also showed that HIC could induce a slight increase in the phosphorylation of ERK1/2 and JNK1/2 in DU145 cells.

These results all seem to support the hypothesis that ADP, an agonist of P2Y1R, could contribute to p53 stability and activity through the activation of MAPKs phosphorylation. However, the evaluation of p53 in patient samples is limited due to the protein's instability. One study has indicated that due to the ease with which the p53 protein mutates in cancer models, its mutations reinforce the growth of cancer cells (Lane and Hupp, 2003; Okuda et al., 2003). Nevertheless, most of the literature demonstrates the positive effects of p53 stabilization, which are that it has

the ability to inhibit cancer cell proliferation through the induction of apoptosis and DNA damage.

The last few decades' progress to stabilize wild-type p53 has raised the prospect of drug discoveries that can be applied to combinatorial models to inhibit cancer progression in clinical applications (Lane and Hupp, 2003). If there is only one thing to be concluded from this exhaustive study, it is that HIC can inhibit PCa growth through its ability to regulate P2Y1R with p53 signaling.

6.5 The revolution of combinatorial drugs in PCa therapy

It is well-known that anti-androgen therapy is one of the main targets for PCa treatment and drug development. In the early stages of PCa, medical or surgical castration are the most common methods for treating the patients and improving their quality of life (Armstrong, 2018; Sandhu et al., 2021). Abiraterone acetate, or AA, is an androgen biosynthesis inhibitor targeting the CYP17A1 enzyme (Alex et al., 2016). In the presence of AA, AR is blocked from interfering with the enzymes C17α hydroxylase and C17-C20 lyase. These inhibit PCa cell proliferation and survival. Recent clinical trials have investigated the promising inhibitory effects of AA in patients with either mCRPC or with CRPC (Cindolo et al., 2017). The FDA has now approved the combinatorial use of orally taken AA and prednisone in patients with PCa castration. This approval is based on the significant inhibitory effects AA has shown in clinical research (Auchus et al., 2014).

There has been little evidence of AA inhibitor activity in PCa cells with a low expression of AR. For instance, Martinal et al only showed that AA at 2 μM was unable to induce cell death in PC3 and DU145 cells after 96 hrs of incubation (Fragni et al., 2019). However, another group reported the first sign of AA activity at 30 μM can induce apoptotic response, cell death, and p21 protein expression in PC3 cells (Grossebrummel et al., 2016). In addition, proof of principle has been given that HIC acts as a p53 stabilizer to inhibit cell proliferation in PCa cells. The detailed molecular mechanism of HIC in combination with any clinical drugs has not yet been investigated.

This study aimed to investigate the combinatorial effects of HIC and AA in AR-low expression PC3 and DU145 cells. With the applied AA concentration of 40 μM, around 50% of cell death in both cell lines was observed after 48 hrs. Moreover, the data presented here provide evidence that AA at lower concentrations is even more

effective in killing cancer cells in the presence of HIC than AA as a single dose (monotherapy).

The combination of both drugs was thoroughly evaluated for their synergistic effects. Notably, in the same concentrations, the non-cancerous cells HEK and MEF were less sensitive to combinatorial drugs than the cancerous cells. Since apoptosis was the potential target of single HIC and AA in PC3 cells, Caspase 3/7 activity and ROS formulation were found to increase due to the synergic effects of the two drugs. Notably, the number of apoptotic cells increased more when treated with HIC plus AA in combination, than it did with the same drug concentrations given as single-drug (mono-therapeutic) treatments. And finally, combination treatment also inhibits cell proliferation via the suppression of the G1 phase in PC3 and DU145 cells.

Although AR activity is a mandatory target in controlling PCa cells, it is known that there are several proliferative signaling cascades which are targeted and activated in PCa growth, such as p53 signaling, TGFβ, epidermal growth factor, and estrogen receptor pathways (Bonkhoff, 2018; Lee et al., 2008). In the metastatic stages of PCa cells, TGFβ acts as a tumor promoter through suppression of the immune system, degradation of the cell matrix, and cancer angiogenesis (Shiota et al., 2021). The results of our gene analysis showed that HIC could inhibit cell metastasis through down-regulated expression in *TGB2*, *TGFB3*, *ANXA3*, *HMGB1*, and *BMP4* in both PC3 and DU145 cells. Additionally, abiraterone inhibits both type II and type III of the TGFβ receptors as well as the downstream signaling molecules Smad 3 and Smad 4 (Grossebrummel et al., 2016). Thus, it can be hypothesized that a strong reduction in the TGFβ signaling pathway is dependent on either abiraterone or HIC treatment in AR-negative or low-expression cells. Unfortunately, TGFβ signaling could not be investigated in this study, but it is clearly a likely candidate for investigation with HIC plus AA in future studies.

Finally, the tumor suppressors p53 and p21, which induce cell cycle arrest, genomic stability, DNA damage, and apoptotic population, are primary regulators of the apoptotic response in prostate tumors (Abbas and Dutta, 2009; Al Bitar and Gali-Muhtasib, 2019; Gordon et al., 2018). Increased DNA degradation in cancer cells, as well as the down-regulated expression of the key genes involved, i.e. *CDKs*, *Cyclin E*, and *Cycline A,* could contribute to the apoptotic mechanisms. In this study, HIC was able to induce stabilization of the p53 protein in DU145 cells and was also able to regulate the p21 signaling in both the PC3 and the DU145 cells. Those genes listed as having the potential to regulate cell death include the down-regulated

expression of *CDK2*, *Cyclin E*, *Cyclin A*, and *CDK4* and increased levels of *CDKN1A, BAX*, and *FOX*.

DNA damage was also identified as a target for a HIC down-regulated mechanism in the cytosol. Moreover, an increase in mRNA levels was observed in *BAX*, *Caspase3*, *p21*, and *Survivin* in PC3 cells treated with AA at 30 μM for 48 hrs (Grossebrummel et al., 2016). Our findings with the combined model of HIC and AA have also shown an increase in Caspase 3/7 activity and ROS production. Therefore, these findings suggest that HIC plus AA could be linked to cell death in PCa cells with a low expression of AR through p53 and p21. Furthermore, AA could inhibit cell survival in AR low- or negative-expressed cell lines with an increase in the dose and/or the time of treatment. What can safely be concluded is that combinatorial therapies, e.g. the combination of HIC and AA, have better inhibitory effects at lower concentrations in the treatment of PCa than monotherapy.

6.6 Strength and limitations

Here, the study has confirmed the anticancer activities of P2Y1R activation in PCa cells which have low expression levels of AR. The findings are more reliable because the experiments were carried out in different cell lines including cancer and non-cancerous cells. The methodologies contain multiple perspectives such as computational analysis, programmed cell death assay, microscope evaluation, gene expressions analysis, protein expression levels, and metastasis cancer assessment. In addition, the novel agonist of P2Y1R, HIC, could inhibit cancer cell growth through the inhibition of multiple biological targets including PARPs, CDKs, and TGF-β, and the activation of tumor suppressors such as p53 and p21. Therefore, HIC could be considered as an advanced drug for PCa therapy. However, the main limitation of the study is that the research was performed only in the culture cells. In addition, more evaluations of HIC's anticancer activities and the direct regulation between P2Y1R and PARPs and CDKs have not been executed through the knock-out of its crucial targets such as PARPs, CDKs, p53, and p21.

7 CONCLUSIONS

A prostate tumor is one of the most common and aggressive cancers in men. It requires extensive therapy with a combinatorial approach to drug administration in order to improve the patient's life quality. The long-term effects of the disease result in lower resistance to cancer metastasis. Like most cancers, PCa is a complex disease. It is induced by alterations in the intrinsic and extrinsic cellular processes. However, worldwide clinical research into GPCR-targeted drugs and the discovery of cancer therapies that utilize novel receptors on cancer cell membranes mean that the prognosis for PCa survival has improved to over 80%.

This thesis has shed light on the benefits of using a P2Y1R agonist as a pharmacological target for drug discovery against PCa. The main findings are summarized below:

1. Out of 923 chemicals, the top two compounds were HIC and MB. They had the highest docking scores and exhibited a stable hydrogen interaction with the P2Y1R protein. These compounds induced changes in intracellular Ca^{2+}, apoptosis, caspase 3/7 activity, and ROS production in *in vitro* models in AR-low expression PC3 and DU145 cells. HIC and MB were both found to induce cancer cell death and suppress cancer cell proliferation.
2. In comparison with MB, it was found that HIC causes more cell death at a lower IC_{50} concentration. Thus, HIC was chosen for further biological studies. Notably, HIC has been shown to have a potential inhibitory effect on mitochondrial activity and can thus be considered as an MtMP inhibitor worthy of further investigation.
3. The activation of P2Y1R is the prime target of HIC as this induces the stabilization and activation of the p53 protein in DU145 cells. The inhibitory effects on cancer cells were demonstrated through the apoptosis response, the G1/S phase arrest, reduced colony formation, and the prevention of metastasis. Gene analysis revealed that HIC could negatively regulate PCa cells through multiple molecular targets, such as the PARP and TGFβ inhibitors.
4. Combinatorial drug treatment with HIC and AA has the potential to improve the inhibition of PC3 and DU145 cells by arresting the G1 phase

and triggering cell death via apoptosis, mediated by ROS and caspase activation. Combinatorial drug treatment inhibits both the growth of migrated and invaded cells and also limits colony formation of the PCa cells. The results clearly suggest that HIC and AA have great potential as a combinatorial drug treatment for PCa cells.

.

8 REFERENCES

Abbas, T., and Dutta, A. (2009). P21 in Cancer: Intricate Networks and Multiple Activities. Nat. Rev. Cancer *9*, 400–414.

Adashek, J.J., Jain, R.K., and Zhang, J. (2019). Clinical Development of PARP Inhibitors in Treating Metastatic Castration-Resistant Prostate Cancer. Cells *8*, 1–12.

Ahmed, A., Ali, S., and Sarkar, F.H. (2014). Advances in Androgen Receptor Targeted Therapy for Prostate Cancer. J. Cell. Physiol. *229*, 271–276.

Alex, A.B., Pal, S.K., and Agarwal, N. (2016). CYP17 Inhibitors in Prostate Cancer: Latest Evidence and Clinical Potential. Ther. Adv. Med. Oncol. *8*, 267–275.

Alford, A. V, Brito Iii, J.M., Yadav, K.K., Yadav, S.S., Tewari, A.K., and Renzulli, J. (2017). The Use of Biomarkers in Prostate Cancer Screening and Treatment. Rev. Urol. *19*, 221–234.

Ampuja, M., Jokimäki, R., Juuti-Uusitalo, K., Rodriguez-Martinez, A., Alarmo, E.L., and Kallioniemi, A. (2013). BMP4 Inhibits the Proliferation of Breast Cancer Cells and Induces an MMP-dependent Migratory Phenotype in MDA-MB-231 Cells in 3D Environment. BMC Cancer *13*, 2–13.

Anantharaju, P.G., Gowda, P.C., Vimalambike, M.G., and Madhunapantula, S. V. (2016). An Overview on the Role of Dietary Phenolics for the Treatment of Cancers. Nutr. J. *15*, 1–16.

Antonarakis, E.S., Lu, C., Wang, H., Luber, B., Nakazawa, M., Roeser, J.C., Chen, Y., Mohammad, T.A., Chen, Y., Fedor, H.L., et al. (2014). AR-V7 and Resistance to Enzalutamide and Abiraterone in Prostate Cancer. N. Engl. J. Med. *371*, 1028–1038.

Antonarakis, E.S., Lu, C., Luber, B., Wang, H., Chen, Y., Nakazawa, M., Nadal, R., Paller, C.J., Denmeade, S.R., Carducci, M.A., et al. (2015). Androgen Receptor Splice Variant 7 and Efficacy of Taxane Chemotherapy in Patients With Metastatic Castration-Resistant Prostate Cancer. JAMA Oncol. *1*, 582–591.

Antonarakis, E.S., Lu, C., Luber, B., Wang, H., Chen, Y., Zhu, Y., Silberstein, J.L., Taylor, M., Maughan, B.L., Denmeade, S.R., et al. (2017). Clinical Significance of Androgen Receptor Splice Variant-7 mRNA Detection in Circulating Tumor Cells of Men With Metastatic Castration-Resistant Prostate Cancer Treated With First- and Second-Line Abiraterone and Enzalutamide. J. Clin. Oncol. *35*, 2149–2156.

Armstrong, A.J. (2018). Updates in Advanced Prostate Cancer 2018. Prostate Cancer Prostatic Dis. *121*, 449–450.

As, N.J. va., Norman, A.R., Thomas, K., Khoo, V.S., Thompson, A., Huddart, R.A., Horwich, A., Dearnaley, D.P., and Parker, C.C. (2008). Predicting the Probability of Deferred Radical Treatment for Localised Prostate Cancer Managed by Active Surveillance. Eur. Urol. *54*, 1297–1305.

Auchus, R.J., Yu, M.K., Nguyen, S., and Mundle, S.D. (2014). Use of prednisone with abiraterone acetate in metastatic castration-resistant prostate cancer. Oncologist *19*, 1231–1240.

Badani, K.K., Kemeter, M.J., Febbo, P.G., Lawrence, H.J., Denes, B.S., Rothney, M.P., Rothberg, M.B., and Brown, G.A. (2015). The Impact of a Biopsy Based 17-Gene Genomic Prostate Score on Treatment Recommendations in Men with Newly Diagnosed Clinically Prostate Cancer Who are Candidates for Active Surveillance. Urol. Pract. *2*, 181–189.

Bai, S., Zhang, B.Y., and Dong, Y. (2019). Impact of Taxanes on Androgen Receptor Signaling. Asian J. Androl. *21*, 249–253.

Barańska, J., Czajkowski, R., and Pomorski, P. (2017). P2Y1 receptors – Properties and Functional activities. In Advances in Experimental Medicine and Biology, pp. 71–89.

Bauman, G., Breau, R.H., Suzanne, K.-R., Louie, A. V., and Pautlere, S. (2017). Ontario Health Technology Assessment Series: Prolaris Cell Cycle Progression Test for Localized Prostate Cancer: A Health Technology Assessment. Ont. Health Technol. Assess. Ser. *17*, 1–75.

Beltran, H., Antonarakis, E.S., Morris, M.J., and Attard, G. (2016). Emerging Molecular Biomarkers in Advanced Prostate Cancer: Translation to the Clinic. Am. Soc. Clin. Oncol. Educ. B. *36*, 131–141.

Bergh, R.C.N. van den, Roemeling, S., Roobol, M.J., Aus, G., Hugosson, J., Rannikko, A.S., Tammela, T.L., Bangma, C.H., and Schröder, F.H. (2009). Outcomes of Men with Screen-Detected Prostate Cancer Eligible for Active Surveillance Who were Managed Expectantly. Eur. Urol. *55*, 1–8.

Berridge, M.J. (2016). The Inositol Trisphosphate/Calcium Signaling Pathway in Health and Disease. Physiol. Rev. *96*, 1261–1296.

Berthold, D.R., Pond, G.R., Roessner, M., Wit, R. de, Eisenberger, M., and Tannock, and I.F. (2008). Treatment of Hormone-Refractory Prostate Cancer with Docetaxel or Mitoxantrone: Relationships between Prostate-Specific Antigen, Pain, and Quality of Life Response and Survival in the TAX-327 Study. Clin. Cancer Res. *14*, 2763–2767.

Bertoli, C., Skotheim, J.M., and De Bruin, R.A.M. (2013). Control of Cell Cycle Transcription during G1 and S Phases. Nat. Rev. Mol. Cell Biol. *14*, 518–528.

Bhat, F.A., Sharmila, G., Balakrishnan, S., Singh, P.R., Srinivasan, N., and Arunakaran, J. (2014). Epidermal Growth Factor-Induced Prostate Cancer (PC3) Cell Survival and Proliferation is Inhibited by Quercetin, a Plant Flavonoid through Apoptotic Machinery. Biomed. Prev. Nutr. *4*, 459–468.

Bill-Axelson, A., Holmberg, L., Filén, F., Ruutu, M., Garmo, H., Busch, C., Nordling, S., Häggman, M., Andersson, S.O., Bratell, S., et al. (2008a). Radical Prostatectomy versus Watchful Waiting in Localized Prostate Cancer: the Scandinavian Prostate Cancer Group-4 Randomized Trial. J. Natl. Cancer Inst. *100*, 1144–1154.

Bill-Axelson, A., Holmberg, L., Filén, F., Ruutu, M., Garmo, H., Busch, C., Nordling, S., Häggman, M., Andersson, S.O., Bratell, S., et al. (2008b). Radical Prostatectomy Versus Watchful Waiting in Localized Prostate Cancer: The Scandinavian Prostate Cancer Group-4 Randomized Trial. J. Natl. Cancer Inst. *100*, 1144–1154.

Al Bitar, S., and Gali-Muhtasib, H. (2019). The Role of the Cyclin Dependent Kinase Inhibitor p21cip1/waf1 in Targeting Cancer: Molecular Mechanisms and Novel Therapeutics. Cancers (Basel). *11*, 2–21.

Blume-Jensen, P., Berman, D.M., Rimm, D.L., Shipitsin, M., Putzi, M., Nifong, T.P., Small, C., Choudhury, S., Capela, T., Coupal, L., et al. (2015). Biology of Human Tumors Development and Clinical Validation of an in situ Biopsy-Based Multimarker Assay for Risk Stratification in Prostate Cancer. Clin. Cancer Res. *21*, 2591–2600.

Bonkhoff, H. (2018). Estrogen Receptor Signaling in Prostate Cancer: Implications for Carcinogenesis and Tumor Progression. Prostate *78*, 2–10.

Bono, J. de, Mateo, J., Fizazi, K., Saad, F., Shore, N., Sandhu, S., Chi, K.N., Sartor, O., Agarwal, N., Olmos, D., et al. (2020). Olaparib for Metastatic Castration-Resistant Prostate Cancer. N. Engl. J. Med. *382*, 2091–2102.

de Bono, J.S., Logothetis, C.J., Molina, A., Fizazi, K., North, S., Chu, L., Chi, K.N., Jones, R.J., Goodman, O.B.J., Saad, F., et al. (2011). Abiraterone and Increased Survival in Metastatic Prostate Cancer. N. Engl. J. Med. *364*, 1995–2005.

Brawer, M.K. (2006). Hormonal Therapy for Prostate Cancer. Rev. Urol. *8*, 35–47.

Briganti, A., Fossati, N., Catto, J.W.F., Cornford, P., Montorsi, F., Mottet, N., Wirth, M., and Van Poppel, H. (2018). Active Surveillance for Low-risk Prostate Cancer: The European Association of Urology Position in 2018. Eur. Urol. *74*, 357–368.

Burdak-Rothkamm, S., Mansour, W.Y., and Rothkamm, K. (2020). DNA Damage Repair

Deficiency in Prostate Cancer. Trends in Cancer *6*, 974–984.

Von Burstin, V.A., Xiao, L., and Kazanietz, M.G. (2010). Bryostatin 1 Inhibits Phorbol Ester-Induced Apoptosis in Prostate Cancer Cells by Differentially Modulating Protein Kinase C (PKC) δ Translocation and Preventing PKCδ-Mediated Release of Tumor Necrosis Factor-α. Mol. Pharmacol. *78*, 325–332.

Campos-Contreras, A. del R., Díaz-Muñoz, M., and Vázquez-Cuevas, F.G. (2020). Purinergic Signaling in the Hallmarks of Cancer. Cells *9*, 1–24.

Candi, E., Agostini, M., Melino, G., and Bernassola, F. (2014). How the TP53 Family Proteins TP63 and TP73 Contribute to Tumorigenesis: Regulators and Effectors. Hum. Mutat. *35*, 702–714.

Cao, W., Li, F., Yao, J., and Yu, J. (2015). Prostate Specific G Protein Coupled Receptor is Associated with Prostate Cancer Prognosis and Affects Cancer Cell Proliferation and Invasion. BMC Cancer *15*, 1–9.

Carr, M.I., and Jones, S.N. (2016). Regulation of the Mdm2-p53 Signaling Axis in the DNA Damage Response and Tumorigenesis. Transl. Cancer Res. *5*, 707–724.

Cháirez-Ramírez, M.H., de la Cruz-López, K.G., and García-Carrancá, A. (2021). Polyphenols as Antitumor Agents Targeting Key Players in Cancer-Driving Signaling Pathways. Front. Pharmacol. *12*, 1–25.

Chattopadhyay, I., Wang, J., Qin, M., Gao, L., Holtz, R., Vessella, R.L., Leach, R.W., and Gelman, I.H. (2017). Src Promotes Castration-Recurrent Prostate Cancer through Androgen Receptor-Dependent Canonical and Non-Canonical Transcriptional Signatures. Oncotarget *8*, 10324–10347.

Chen, A. (2011). PARP Inhibitors: Its Role in Treatment of Cancer. Chin. J. Cancer *30*, 463–471.

Chen, L., Wang, S., Zhou, Y., Wu, X., Entin, I., Epstein, J., Yaccoby, S., Xiong, W., Barlogie, B., Shaughnessy, J.D., et al. (2010). Identification of Early Growth Response Protein 1 (EGR-1) as a Novel Target for JUN-Induced Apoptosis in Multiple Myeloma. Blood *115*, 61–70.

Chen, Y.R., Wang, X., Templeton, D., Davis, R.J., and Tan, T.H. (1996). The Role of c-Jun N-terminal kinase (JNK) in Apoptosis Induced by Ultraviolet C and γ Radiation. Duration of JNK Activation may Determine Cell Death and Proliferation. J. Biol. Chem. *271*, 31929–31936.

Cheng, L., Montironi, R., Bostwick, D.G., Lopez-Beltran, A., and Berney, D.M. (2012). Staging of Prostate Cancer. Histopathology *60*, 87–117.

Chhatriwala, M., Ravi, R.G., Patel, R.I., Boyer, J.L., Jacobson, K.A., and Harden, T.K. (2004). Induction of Novel Agonist Selectivity for the ADP-Activated P2Y1 Receptor versus the ADP-Activated P2Y12 and P2Y13 Receptors by Conformational Constraint of an ADP Analog. J. Pharmacol. Exp. Ther. *311*, 1038–1043.

Chiyomaru, T., Yamamura, S., Fukuhara, S., Yoshino, H., Kinoshita, T., Majid, S., Saini, S., Chang, I., Tanaka, Y., Enokida, H., et al. (2013). Genistein Inhibits Prostate Cancer Cell Growth by Targeting miR-34a and Oncogenic HOTAIR. PLoS One *8*, 1–10.

Chou, T.C., and Talalay, P. (1984). Quantitative Analysis of Dose-Effect Relationships: the Combined Effects of Multiple Drugs or Enzyme Inhibitors. Adv. Enzyme Regul. *22*, 27–55.

Cindolo, L., Natoli, C., De Nunzio, C., De Tursi, M., Valeriani, M., Giacinti, S., Micali, S., Rizzo, M., Bianchi, G., Martorana, E., et al. (2017). Abiraterone Acetate for Treatment of Metastatic Castration-resistant Prostate Cancer in Chemotherapy-naive Patients: An Italian Analysis of Patients' Satisfaction. Clin. Genitourin. Cancer *15*, 520–525.

Cooperberg, M.R., Carroll, P.R., and Klotz, L. (2011). Active Surveillance for Prostate Cancer: Progress and Promise. J. Clin. Oncol. *29*, 3669–3676.

Costea, T., Nagy, P., Ganea, C., Szöllősi, J., and Mocanu, M.-M. (2019). Molecular Sciences Molecular Mechanisms and Bioavailability of Polyphenols in Prostate Cancer. Int. J. Mol. Sci. *20*, 1062–1089.

Culig, Z., and Santer, F.R. (2014). Androgen Receptor Signaling in Prostate Cancer. Cancer Metastasis Rev. *33*, 413–427.

Cullen, J., Rosner, I.L., Brand, T.C., Zhang, N., Tsiatis, A.C., Moncur, J., Ali, A., Chen, Y., Knezevic, D., Maddala, T., et al. (2015). A Biopsy-based 17-gene Genomic Prostate Score Predicts Recurrence After Radical Prostatectomy and Adverse Surgical Pathology in a Racially Diverse Population of Men with Clinically Low- and Intermediate-risk Prostate Cancer. Eur. Urol. *68*, 123–131.

Cuzick, J., Thorat, M.A., Andriole, G., Brawley, O.W., Brown, P.H., Culig, Z., Eeles, R.A., Ford, L.G., Hamdy, F.C., Holmberg, L., et al. (2014). Prevention and Early Detection of Prostate Cancer. Lancet Oncol. *15*, 484–492.

Dalela, D., Santiago-Jiménez, M., Yousefi, K., Karnes, R.J., Ross, A.E., Den, R.B., Freedland, S.J., Schaeffer, E.M., Dicker, A.P., Menon, M., et al. (2017). Genomic Classifier Augments the Role of Pathological Features in Identifying Optimal Candidates for Adjuvant Radiation Therapy in Patients With Prostate Cancer: Development and Internal Validation of a Multivariable Prognostic Model. J. Clin. Oncol. *35*, 1982–1990.

Davis, I.D., Martin, A.J., Stockler, M.R., Begbie, S., Chi, K.N., Chowdhury, S., Coskinas, X., Frydenberg, M., Hague, W.E., Horvath, L.G., et al. (2019). Enzalutamide with Standard

First-Line Therapy in Metastatic Prostate Cancer. N. Engl. J. Med. *381*, 121–131.

Delekate, A., Füchtemeier, M., Schumacher, T., Ulbrich, C., Foddis, M., and Petzold, G.C. (2014). Metabotropic P2Y1 Receptor Signalling Mediates Astrocytic Hyperactivity in vivo in an Alzheimer's Disease Mouse Model. Nat. Commun. *5*, 1–14.

Dhyani, V., Gare, S., Gupta, R.K., Swain, S., Venkatesh, K. V., and Giri, L. (2020). GPCR Mediated Control of Calcium Dynamics: A Systems Perspective. Cell. Signal. *74*, 109717–109732.

Dirimanov, S., and Högger, P. (2019). Screening of Inhibitory Effects of Polyphenols on AKT-Phosphorylation in Endothelial Cells and Determination of Structure-Activity Features. Biomolecules *9*, 219–235.

Dominguez-Valentin, M., Joost, P., Therkildsen, C., Jonsson, M., Rambech, E., and Nilbert, M. (2016). Frequent Mismatch-Repair Defects link Prostate Cancer to Lynch Syndrome. BMC Urol. *16*, 1–7.

Dumont, C., Baciarello, G., Bosset, P.O., Lavaud, P., Colomba, E., Massard, C., Loriot, Y., Albiges, L., Blanchard, P., Bossi, A., et al. (2020). Long-term Castration-related Outcomes in Patients With High-risk Localized Prostate Cancer Treated With Androgen Deprivation Therapy With or Without Docetaxel and Estramustine in the UNICANCER GETUG-12 Trial. Clin. Genitourin. Cancer *18*, 444–451.

Ecke, D., Hanck, T., Tulapurkar, M.E., Schäfer, R., Kassack, M., Stricker, R., and Reiser, G. (2008). Hetero-oligomerization of the P2Y11 receptor with the P2Y 1 receptor controls the internalization and ligand selectivity of the P2Y11 receptor. Biochem. J. *409*, 107–116.

Ecke, T.H., Schlechte, H.H., Schiemenz, K., Sachs, M.D., Lenk, S. V., Rudolph, B.D., and Loening, S.A. (2010). TP53 Gene Mutations in Prostate Cancer Progression. Anticancer Res. *30*, 1579–1586.

Egevad, L., Ahmad, A.S., Algaba, F., Berney, D.M., Boccon-Gibod, L., Compérat, E., Evans, A.J., Griffiths, D., Grobholz, R., Kristiansen, G., et al. (2013). Standardization of Gleason Grading among 337 European Pathologists. Histopathology *62*, 247–256.

Endo, S., Yamato, K., Hirai, S., Moriwaki, T., Fukuda, K., Suzuki, H., Abei, M., Nakagawa, I., and Hyodo, I. (2011). Potent in vitro and in vivo Antitumor Effects of MDM2 Inhibitor Nutlin-3 in Gastric Cancer Cells. Cancer Sci. *102*, 605–613.

Engeland, K. (2017). Cell Cycle Arrest through Indirect Transcriptional Repression by p53: I have a DREAM. Cell Death Differ. *25*, 114–132.

Ewing, C.M., Ray, A.M., Lange, E.M., Zuhlke, K.A., Robbins, C.M., Tembe, W.D., Wiley, K.E., Isaacs, S.D., Johng, D., Wang, Y., et al. (2012). Germline Mutations in HOXB13 and

Prostate-Cancer Risk. N. Engl. J. Med. *366*, 141–149.

Falzarano, S.M., Ferro, M., Bollito, E., Klein, E.A., Carrieri, G., and Magi-Galluzzi, C. (2015). Novel Biomarkers and Genomic Tests in Prostate Cancer: A Critical Analysis. Minerva Urol. Nephrol. *67*, 211–242.

Fang, W.-G., Pirnia, F., Bang, Y.-J., Myers, C.E., and Trepel, J.B. (1992). P2-Purinergic Receptor Agonists Inhibit the Growth of Androgen-Independent Prostate Carcinoma Cells. J. Clin. Invest. *89*, 191–196.

Feher, A., Ötvös, K., Pasternak, T.P., and Pettkó-Szandtner, A. (2008). The Involvement of Reactive Oxygen Species (ROS) in the Cell Cycle Activation (G0-to-G1 transition) of Plant Cells. Plant Signal. Behav. *3*, 823–826.

Ferraldeschi, R., Nava Rodrigues, D., Riisnaes, R., Miranda, S., Figueiredo, I., Rescigno, P., Ravi, P., Pezaro, C., Omlin, A., Lorente, D., et al. (2015). PTEN Protein Loss and Clinical outcome from Castration-resistant Prostate Cancer Treated with Abiraterone Acetate. Eur. Urol. *67*, 795–802.

Fesik, S.W. (2005). Promoting Apoptosis as a Strategy for Cancer Drug Discovery. Nat. Rev. Cancer *5*, 876–885.

Fiaschi, T., and Chiarugi, P. (2012). Oxidative stress, tumor microenvironment, and metabolic reprogramming: A diabolic liaison. Int. J. Cell Biol.

Fischer-Valuck, B.W., Rao, Y.J., and Michalski, J.M. (2018). Intensity-modulated Radiotherapy for Prostate Cancer. Transl. Androl. Urol. *7*, 297–307.

Fizari, K., Sher, H.I., Sternberg, C.N., Miller, K., Chi, K., Basch, E., Hirmand, M., and de Bono, J.S. (2012). Impact of Enzalutamide, An Androgen Receptor (AR) Signalling Inhibitor, on Time to first Skeletal Related Event (SRE) and Pain in the Phase 3 AFFIRM Study. Ann. Oncol. *23*, 295–296.

Fizazi, K., Scher, H.I., Molina, A., Logothetis, C.J., Chi, K.N., Jones, R.J., Staffurth, J.N., North, S., Vogelzang, N.J., Saad, F., et al. (2012). Abiraterone Acetate for Treatment of Metastatic Castration-Resistant Prostate Cancer: Final Overall Survival Analysis of the COU-AA-301 Randomised, Double-blind, Placebo-controlled Phase 3 Study. Lancet. Oncol. *13*, 983–992.

Foucquier, J., and Guedj, M. (2015). Analysis of Drug Combinations: Current Methodological Landscape. Pharmacol. Res. Perspect. *3*, 1–11.

Fragni, M., Gallo, D., Nardini, M., Rossini, E., Vezzoli, S., Zametta, M., Longhena, F., Bellucci, A., Roca, E., Memo, M., et al. (2019). Abiraterone Acetate Exerts a Cytotoxic Effect in Human Prostate Cancer Cell Lines. Naunyn. Schmiedebergs. Arch. Pharmacol. *392*, 729–

742.

Franken, N.A.P., Rodermond, H.M., Stap, J., Haveman, J., and van Bree, C. (2006). Clonogenic Assay of Cells in vitro. Nat. Protoc. *1*, 2315–2319.

Fujita, K., and Nonomura, N. (2019). Role of Androgen Receptor in Prostate Cancer: A Review. World J. Mens. Health *37*, 288–295.

Gilad, Y., Gellerman, G., Lonard, D.M., and O'Malley, B.W. (2021). Drug Combination in Cancer Treatment—From Cocktails to Conjugated Combinations. Cancers (Basel). *13*, 1–26.

Gong, J., Posadas, E.M., Neil, B., Kim, H.L., Daskivich, T.J., Gupta, A., Sandler, H.M., Kamrava, M., Zumsteg, Z.S., Freedland, S.J., et al. (2021). Integrating PARP Inhibitors Into Advanced Prostate Cancer Therapeutics. Oncology *35*, 119–125.

Gordon, E., Ravicz, J., Liu, S., Chawla, S., and Hall, F. (2018). Cell Cycle Checkpoint control: The Cyclin G1/Mdm2/p53 axis Emerges as a Strategic Target for Broad-spectrum Cancer Gene Therapy - A Review of Molecular Mechanisms for Oncologists. Mol. Clin. Oncol. *9*, 115–134.

Graff, J.N., and Chamberlain, E.D. (2014). Sipuleucel-T in the Treatment of Prostate Cancer: An Evidence-based Review of its Place in Therapy. Core Evid. *10*, 1–10.

Green, A.K., Corty, R.W., Wood, W.A., Meeneghan, M., Reeder-Hayes, K.E., Basch, E., Milowsky, M.I., and Dusetzina, S.B. (2015). Comparative Effectiveness of Mitoxantrone Plus Prednisone Versus Prednisone Alone in Metastatic Castrate-Resistant Prostate Cancer After Docetaxel Failure. Oncologist *20*, 516–522.

Grewal, K., Grewal, K., and Tabbara, I.A. (2021). PARP Inhibitors in Prostate Cancer. Anticancer Res. *41*, 551–556.

Grossebrummel, H., Peter, T., Mandelkow, R., Weiss, M., Muzzio, D., Zimmermann, U., Walther, R., Jensen, F., Knabbe, C., Zygmunt, M., et al. (2016). Cytochrome P450 17A1 Inhibitor Abiraterone Attenuates Cellular Growth of Prostate Cancer Cells Independently from Androgen Receptor Signaling by Modulation of Oncogenic and Apoptotic Pathways. Int. J. Oncol. *48*, 793–800.

Guo, W., Zhang, J., Zhou, Y., Zhou, C., Yang, Y., Cong, Z., Dong, J., Yang, D., Dai, B., and Wang, M.W. (2021). GPR160 is a Potential Biomarker Associated with Prostate Cancer. Signal Transduct. Target. Ther. *6*, 1–3.

Ha, J., Lee, S., Park, J., Seo, J., Kang, E., Yoon, H., Kim, B.R., Lee, H.K., Ryu, S.E., and Cho, S. (2021). Identification of a Novel Inhibitor of Liver Cancer Cell Invasion and Proliferation through Regulation of Akt and Twist1. Sci. Rep. *11*, 1–11.

Hamanaka, R.B., and Chandel, N.S. (2010). Mitochondrial Reactive Oxygen Species Regulate Cellular Signaling and Dictate Biological Outcomes. Trends Biochem. Sci. *35*, 505–513.

Hamid, A.A., Gray, K.P., Shaw, G., MacConaill, L.E., Evan, C., Bernard, B., Loda, M., Corcoran, N.M., Van Allen, E.M., Choudhury, A.D., et al. (2019). Compound Genomic Alterations of TP53, PTEN, and RB1 Tumor Suppressors in Localized and Metastatic Prostate Cancer. Eur. Urol. *76*, 89–97.

Handy, C.E., and Antonarakis, E.S. (2018). Sipuleucel-T for the Treatment of Prostate Cancer: Novel Insights and Future Directions. Futur. Oncol. *14*, 907–917.

Hatano, K., Tohyama, N., Kodama, T., Okabe, N., Sakai, M., and Konoeda, K. (2019). Current Status of Intensity-modulated Radiation Therapy for Prostate Cancer: History, Clinical Results and Future Directions. Int. J. Urol. *26*, 775–784.

Hechler, B., Nonne, C., Roh, E.J., Cattaneo, M., Cazenave, J.-P., Lanza, F., Jacobson, K.A., and Gachet, C. (2006). MRS2500 [2-iodo-N6-methyl-(N)-methanocarba-2'-deoxyadenosine-3',5'-bisphosphate], a Potent, Selective, and Stable Antagonist of the Platelet P2Y1 Receptor with Strong Antithrombotic Activity in Mice. J. Pharmacol. Exp. Ther. *316*, 556–563.

Helsen, C., Broeck, T. Van den, Voet, A., Prekovic, S., Poppel, H. Van, Joniau, S., and Claessens, F. (2014). Androgen Receptor Antagonists for Prostate Cancer Therapy. Endocr. Relat. Cancer *21*, 105–118.

Herlemann, A., Huang, H.-C., Alam, R., Tosoian, J.J., Kim, H.L., Klein, E.A., Simko, J.P., Chan, J.M., Lane, B.R., Davis, J.W., et al. (2020). Decipher Identifies Men with Otherwise Clinically Favorable-intermediate Risk Disease Who may not be Good Candidates for Active Surveillance. Prostate Cancer Prostatic Dis. *23*, 136–143.

Hickman, J.A. (1992). Apoptosis Induced by Anticancer Drugs. Cancer Metastasis Rev. *11*, 121–139.

Hocevar, B.A., and Howe, P.H. (1998). Mechanisms of TGF-beta-Induced Cell Cycle Arrest. Miner. Electrolyte Metab. *24*, 131–135.

Houston, D., Ohno, M., Nocholas, R.A., Jacobson, K.A., and Harden, T.K. (2006). [32P]2-Iodo-N6-Methyl-(N)-Methanocarba-2'-Deoxyadenosine-3',5'-Bisphosphate ([32P]MRS2500), a Novel Radioligand for Quantification of Native P2Y1 Receptors. Br. J. Pharmacol. *147*, 459–467.

Hur, W., Rhim, H., Jung, C.K., Kim, J.D., Bae, S.H., Jang, J.W., Yang, J.M., Oh, S.T., Kim, D.G., Wang, H.J., et al. (2010). SOX4 Overexpression Regulates the P53-mediated Apoptosis in Hepatocellular Carcinoma: Clinical Implication and Functional Analysis in vitro. Carcinogenesis *31*, 1298–1307.

Iacovelli, R., Ciccarese, C., Schinzari, G., Rossi, E., Maiorano, B.A., Astore, S., D'Angelo, T., Cannella, A., Pirozzoli, C., Teberino, M.A., et al. (2020). Biomarkers of Response to Advanced Prostate Cancer Therapy. Expert Rev. Mol. Diagn. *20*, 195–205.

Issac, M.S.M., Yousef, E., Tahir, M.R., and Gaboury, L.A. (2019). MCM2, MCM4, and MCM6 in Breast Cancer: Clinical Utility in Diagnosis and Prognosis. Neoplasia *21*, 1015–1035.

Jacobson, K.A., Delicado, E.G., Gachet, C., Kennedy, C., von Kügelgen, I., Li, B., Miras-Portugal, M.T., Novak, I., Schöneberg, T., Perez-Sen, R., et al. (2020). Update of P2Y receptor pharmacology: IUPHAR Review 27. Br. J. Pharmacol. *177*, 2413–2433.

James, N.D., Caty, A., Payne, H., Borre, M., Zonnenberg, B.A., Beuzeboc, P., McIntosh, S., Morris, T., Phung, D., and Dawson, N.A. (2010). Final Safety and Efficacy Analysis of the Specific Endothelin A Receptor Antagonist Zibotentan (ZD4054) in Patients with Metastatic Castration-Resistant Prostate Cancer and Bone Metastases who were Pain-free or Mildly Symptomatic for Pain: a Double-Blind,. BJU Int. *106*, 966–973.

Jang, A., Sartor, O., Barata, P.C., and Paller, C.J. (2020). Therapeutic Potential of PARP Inhibitors in the Treatment of Metastatic Castration-Resistant Prostate Cancer. Cancers (Basel). *12*, 1–14.

Janssens, R., Communi, D., Pirotton, S., Samson, M., Parmentier, M., and Boeynaems, J.M. (1996). Cloning and Tissue Distribution of the Human P2Y1 Receptor. Biochem. Biophys. Res. Commun. *221*, 588–593.

Jiang, L., and Zawacka-Pankau, J. (2020). The p53/MDM2/MDMX-Targeted Therapies—a Clinical Synopsis. Cell Death Dis. *11*, 1–4.

Jin, J., Daniel, J.L., and Kunapuli, S.P. (1998). Molecular Basis for ADP-Induced Platelet Activation. II. The P2Y1 Receptor Mediates ADP-Induced Intracellular Calcium Mobilization and Shape Change in Platelets. J. Biol. Chem. *273*, 2030–2034.

JL, G., M, du P., M, S.-J., K, Y., DJS, T., L, K., BR, L., M, F., DYT, C., M, B., et al. (2017). Decipher test impacts decision making among patients considering adjuvant and salvage treatment after radical prostatectomy: Interim results from the Multicenter Prospective PRO-IMPACT study. Cancer *123*, 2850–2859.

Joung, J.Y., Cho, I.C., and Lee, K.H. (2011). Role of Pelvic Lymph Node Dissection in Prostate Cancer Treatment. Korean J. Urol. *52*, 437–445.

Kälkner, K.M., Wahlgren, T., Ryberg, M., Cohn-Cedermark, G., Castellanos, E., Zimmerman, R., Nilsson, J., Lundell, M., Fowler, J., Levitt, S., et al. (2007). Clinical Outcome in Patients with Prostate Cancer Treated with External Beam Radiotherapy and High Dose-rate Iridium 192 Brachytherapy Boost: a 6-year Follow-up. Acta Oncol. (Madr). *46*, 909–917.

Karantanos, T., Corn, P.G., and Thompson, T.C. (2013). Prostate Cancer Progression after Androgen Deprivation Therapy: Mechanisms of Castrate-Resistance and Novel Therapeutic Approaches. Oncogene *32*, 5501–5511.

Karantanos, T., Evans, C.P., Tombal, B., Thompson, T.C., Montironi, R., and Isaacs, W.B. (2015). Understanding the mechanisms of androgen deprivation resistance in prostate cancer at the molecular level. Eur. Urol. *67*, 470–479.

Karlsson, G., Liu, Y., Larsson, J., Goumans, M.-J., Lee, J.-S., Thorgeirsson, S.S., Ringnér, M., and Karlsson, S. (2005). Gene expression Profiling Demonstrates that TGF-beta1 Signals Exclusively through Receptor Complexes Involving Alk5 and Identifies Targets of TGF-beta Signaling. Physiol. Genomics *21*, 396–403.

Karna, P., Chagani, S., Gundala, S.R., Rida, P.C.G., Asif, G., Sharma, V., Gupta, M. V., and Aneja, R. (2012). Benefits of Whole Ginger Extract in Prostate Cancer. Br. J. Nutr. *107*, 473–484.

Karnes, R.J., Bergstralh, E.J., Davicioni, E., Ghadessi, M., Buerki, C., Mitra, A.P., Crisan, A., Erho, N., Vergara, I.A., Lam, L.L., et al. (2013). Validation of a Genomic Classifier that Predicts Metastasis Following Radical Prostatectomy in an at Risk Patient Population. J. Urol. *190*, 2047–2053.

Kaukoniemi, K.M., Rauhala, H.E., Scaravilli, M., Latonen, L., Annala, M., Vessella, R.L., Nykter, M., Tammela, T.L.J., and Visakorpi, T. (2015). Epigenetically Altered miR-193b Targets Cyclin D1 in Prostate Cancer. Cancer Med. *4*, 1417–1425.

Khan, N., Adhami, V.M., and Mukhtar, H. (2010). Apoptosis by Dietary Agents for Prevention and Treatment of Prostate Cancer. Endocr. Relat. Cancer *17*, R39–R52.

Khurana, A., and Shafer, D.A. (2019). MDM2 Antagonists as a Novel Treatment Option for Acute Myeloid Leukemia: Perspectives on the Therapeutic Potential of Idasanutlin (RG7388). Onco. Targets. Ther. *12*, 2903–2903.

Kim, H.L., Li, P., Huang, H.-C., Deheshi, S., Marti, T., Knudsen, B., Abou-Ouf, H., Alam, R., Lotan, T.L., Lam, L.L.C., et al. (2019). Validation of the Decipher Test for predicting adverse pathology in candidates for prostate cancer active surveillance. Prostate Cancer Prostatic Dis. *22*, 399–405.

Kim, S.T., Xu, B., and Kastan, M.B. (2002). Involvement of the Cohesin Protein, Smc1, in Atm-Dependent and Independent Responses to DNA Damage. Genes Dev. *16*, 560–570.

Klein, E.A., Cooperberg, M.R., Magi-Galluzzi, C., Simko, J.P., Falzarano, S.M., Maddala, T., Chan, J.M., Li, J., Cowan, K.H., Tsiatis, A.C., et al. (2014). A 17-gene Assay to Predict Prostate Cancer Aggressiveness in the Context of Gleason Grade Heterogeneity, Tumor Multifocality, and Biopsy Undersampling. Eur. Urol. *66*, 550–560.

Klein, M.E., Dabbs, D.J., Shuai, Y., Brufsky, A.M., Jankowitz, R., Puhalla, S.L., and Bhargava, R. (2013). Prediction of the Oncotype DX Recurrence Score: Use of Pathology-Generated Equations Derived by Linear Regression Analysis. Mod. Pathol. *26*, 658–664.

Kohaar, I., Petrovics, G., and Srivastava, S. (2019). Molecular Sciences A Rich Array of Prostate Cancer Molecular Biomarkers: Opportunities and Challenges. Int. J. Mol. Sci. *20*, 1813–1832.

Konopleva, M., Martinelli, G., Daver, N., Papayannidis, C., Wei, A., Higgins, B., Ott, M., Mascarenhas, J., and Andreeff, M. (2020). MDM2 Inhibition: an Important Step forward in Cancer Therapy. Leukemia *34*, 2858–2874.

Kreis, N.N., Louwen, F., and Yuan, J. (2019). The Multifaceted p21 (Cip1/Waf1/CDKN1A) in Cell Differentiation, Migration and Cancer Therapy. Cancers (Basel). *11*, 1220–1230.

Kuboyama, K., Harada, H., Tozaki-Saitoh, H., Tsuda, M., Ushijima, K., and Inoue, K. (2011). Astrocytic P2Y 1 Receptor is Involved in The Regulation of Cytokine/Chemokine Transcription and Cerebral Damage in a Rat Model of Cerebral Ischemia. J. Cereb. Blood Flow Metab. *31*, 1930–1941.

Kudirka, J.C., Panupinthu, N., Tesseyman, M.A., Dixon, S.J., and Bernier, S.M. (2007). P2Y Nucleotide Receptor Signaling through MAPK/ERK is Regulated by Extracellular Matrix: Involvement of beta3 Integrins. J. Cell. Physiol. *213*, 54–64.

Kyng, K.J., May, A., Stevnsner, T., Becker, K.G., Kølvrå, S., and Bohr, V.A. (2005). Gene Expression Responses to DNA Damage are Altered in Human Aging and in Werner Syndrome. Oncogene *24*, 5026–5042.

Laere, B. De, Oeyen, S., Mayrhofer, M., Whitington, T., Dam, P.-J. van, Oyen, P. Van, Ghysel, C., Ampe, J., Ost, P., Demey, W., et al. (2019). TP53 Outperforms other Androgen Receptor Biomarkers to Predict Abiraterone or Enzalutamide Outcome in Metastatic Castration-resistant Prostate Cancer. Clin. Cancer Res. *25*, 1766–1773.

Lane, D.P., and Hupp, T.R. (2003). Drug Discovery and p53. Drug Discov. Today *8*, 347–355.

Lange, J.M., Laviana, A.A., Penson, D.F., Lin, D.W., Bill-Axelson, A., Carlsson, S. V., Newcomb, L.F., Trock, B.J., Carter, H.B., Carroll, P.R., et al. (2020). Prostate Cancer Mortality and Metastasis under Different Biopsy Frequencies in North American Active Surveillance Cohorts. Cancer *126*, 583–592.

Lappano, R., and Maggiolini, M. (2011). G protein-coupled receptors: Novel targets for drug discovery in cancer. Nat. Rev. Drug Discov.

Lee, J.T., Lehmann, B.D., Terrian, D.M., Chappell, W.H., Stivala, F., Libra, M., Martelli,

A.M., Steelman, L.S., and McCubrey, J.A. (2008). Targeting Prostate Cancer Based on Signal Transduction and Cell Cycle Pathways. Cell Cycle *7*, 1745–1762.

Lee, S.Y., Wolff, S.C., Nicholas, R.A., and O'Grady, S.M. (2003). P2Y receptors modulate ion channel function through interactions involving the C-terminal domain. Mol. Pharmacol.

Lehto, U.-S., Tenhola, H., Taari, K., and Aromaa, A. (2017). Patients' Perceptions of the Negative Effects Following Different Prostate Cancer Treatments and the Impact on Psychological Well-Being: A Nationwide Survey. Br. J. Cancer *116*, 864–873.

Lertsuwan, K., Peters, W., Johnson, L., Lertsuwan, J., Marwa, I., and Sikes, R.A. (2017). Purinergic Receptor Expression and Cellular Responses to Purinergic Agonists in Human Prostate Cancer Cells. Anticancer Res. *37*, 529–538.

Li, J., and Yuan, J. (2008). Caspases in Apoptosis and Beyond. Oncogene *27*, 6194–6206.

Li, R., Liu, X., Yang, B., and Qiu, J. (2021). External Beam Radiotherapy for Prostate Cancer: What are the Current Research Trends and Hotspots? Cancer Med. *10*, 772–782.

Li, W.-H., Qiu, Y., Zhang, H.-Q., Liu, Y., You, J.-F., Tian, X.-X., and Fang, W.-G. (2013). P2Y2 Receptor Promotes Cell Invasion and Metastasis in Prostate Cancer Cells. Br. J. Cancer *109*, 1666–1675.

Li, W., Chen, H., Deng, H., Kuang, Z., Long, M., Chen, D., Liao, X., Li, M., Rock, D.L., Luo, S., et al. (2018). ORF Virus Encoded Protein ORFV119 Induces Cell Apoptosis through the Extrinsic and Intrinsic Pathways. Front. Microbiol. *9*, 1056–1069.

Lin, L., Liu, Y., Fu, S., Qu, C., Li, H., and Ni, J. (2019). Inhibition of Mitochondrial Complex Function—The Hepatotoxicity Mechanism of Emodin Based on Quantitative Proteomic Analyses. Cells *8*, 1–17.

Liou, G.Y., and Storz, P. (2010). Reactive Oxygen Species in Cancer. Free Radic. Res. *44*, 479–496.

Litton, J.K., Rugo, H.S., Ettl, J., Hurvitz, S.A., Gonçalves, A., Lee, K.-H., Fehrenbacher, L., Yerushalmi, R., Mina, L.A., Martin, M., et al. (2018). Talazoparib in Patients with Advanced Breast Cancer and a Germline BRCA Mutation. N. Engl. J. Med. *379*, 753–763.

Liu, D., Kang, J.S., and Derynck, R. (2004). TGF-β-Activated Smad3 Represses MEF2-Dependent Transcription in Myogenic Differentiation. EMBO J. *23*, 1557–1566.

Liu, P., Barkley, L.R., Day, T., Bi, X., Slater, D.M., Alexandrow, M.G., Nasheuer, H.P., and Vaziri, C. (2006). The Chk1-mediated S-phase Checkpoint Targets Initiation Factor Cdc45 via a Cdc25A/Cdk2-independent Mechanism. J. Biol. Chem. *281*, 30631–30644.

Loeb, S., and Ross, A.E. (2017). Genomic Testing for Localized Prostate Cancer: Where do we go from here? Curr. Opin. Urol. *27*, 495–499.

Loeb, S., Zhou, Q., Siebert, U., Rochau, U., Jahn, B., Mühlberger, N., Carter, H.B., Lepor, H., and Braithwaite, R.S. (2017). Active Surveillance Versus Watchful Waiting for Localized Prostate Cancer: A Model to Inform Decisions. Eur. Urol. *72*, 899–907.

López, I.H., Parada, D., Gallardo, P., Gascón, M., Besora, A., Peña, K., Riu, F., Pianetta, M.A., Abuchaibe, O., Royò, L.T., et al. (2017). Prognostic Correlation of Cell Cycle Progression Score and Ki-67 as a Predictor of Aggressiveness, Biochemical Failure, and Mortality in Men with High-risk Prostate Cancer Treated with External Beam Radiation Therapy. Reports Pract. Oncol. Radiother. *22*, 251–257.

Mamedova, L.K., Gao, Z.-G., and Jacobson, K.A. (2006). Regulation of Death and Survival in Astrocytes by ADP Activating P2Y1 and P2Y12 Receptors. Biochem. Pharmacol. *72*, 1031–1041.

Marascio, J., Spratt, D.E., Zhang, J., Trabulsi, E.J., Le, T., Sedzorme, W.S., Beeler, W.H., Davicioni, E., Dabbas, B., Lin, D.W., et al. (2019). Prospective Study to Define the Clinical Utility and Benefit of Decipher Testing in Men Following Prostatectomy. Prostate Cancer Prostatic Dis. *23*, 295–302.

Marchetti, C. (2022). Calcium Signaling in Prostate Cancer Cells of Increasing Malignancy. Biomol. Concepts *13*, 156–163.

Mateo, J., Carreira, S., Sandhu, S., Miranda, S., Mossop, H., Perez-Lopez, R., Nava Rodrigues, D., Robinson, D., Omlin, A., Tunariu, N., et al. (2015). DNA-Repair Defects and Olaparib in Metastatic Prostate Cancer. N. Engl. J. Med. *373*, 1697–1708.

Matt, S., and Hofmann, T.G. (2016). The DNA damage-induced cell death response: a roadmap to kill cancer cells. Cell. Mol. Life Sci. *73*, 2829–2850.

Matthews, H.K., Bertoli, C., and de Bruin, R.A.M. (2021). Cell Cycle Control in Cancer. Nat. Rev. Mol. Cell Biol. *23*, 74–88.

McKenney, J.K., Simko, J., Bonham, M., True, L.D., Troyer, D., Hawley, S., Newcomb, L.F., Fazli, L., Kunju, L.P., Nicolas, M.M., et al. (2011). The Potential Impact of Reproducibility of Gleason Grading in Men with Early Stage Prostate Cancer Managed by Active Surveillance: A Multi-institutional Study. J. Urol. *186*, 465–469.

Meiyun Fan, Mary E.Goodwin, Machael J.Birrer, and Timothy C.Chamber (2001). The c-Jun NH2-terminal Protein Kinase/AP-1 Pathway Is Required for Efficient Apoptosis Induced by Vinblastine. Cancer Res. *61*, 4450–4458.

Mitsiogianni, M., Koutsidis, G., Mavroudis, N., Trafalis, D.T., Botaitis, S., Franco, R.,

Zoumpourlis, V., Amery, T., Galanis, A., Pappa, A., et al. (2019). The Role of Isothiocyanates as Cancer Chemo-Preventive, Chemo-Therapeutic and Anti-Melanoma Agents. Antioxidants *8*, 20–35.

Montané, X., Kowalczyk, O., Reig-Vano, B., Bajek, A., Roszkowski, K., Tomczyk, R., Pawliszak, W., Giamberini, M., Mocek-Płóciniak, A., and Tylkowski, B. (2020). Current Perspectives of the Applications of Polyphenols and Flavonoids in Cancer Therapy. Molecules *25*, 2–26.

Moore, D.J., Chambers, J.K., Wahlin, J.-P., Tan, K.B., Moore, G.B., Jenkins, O., Emson, P.C., and Murdock, P.R. (2001). Expression Pattern of human P2Y Receptor Subtypes: a Quantitative Reverse Transcription-Polymerase Chain Reaction Study. Biochim. Biophys. Acta *1521*, 107–119.

Morgan, S.C., Hoffman, K., Loblaw, D.A., Buyyounouski, M.K., Patton, C., Barocas, D., Bentzen, S., Chang, M., Efstathiou, J., Greany, P., et al. (2018). Hypofractionated Radiation Therapy for Localized Prostate Cancer: Executive Summary of an ASTRO, ASCO, and AUA Evidence-Based Guideline. Pract. Radiat. Oncol. *8*, 354–360.

Mori, K., Uchida, T., Yoshie, T., Mizote, Y., Ishikawa, F., Katsuyama, M., and Shibanuma, M. (2019). A mitochondrial <scp>ROS</scp> pathway controls matrix metalloproteinase 9 levels and invasive properties in <scp>RAS</scp> -activated cancer cells. FEBS J. *286*, 459–478.

Muscella, A., Cossa, L.G., Vetrugno, C., Antonaci, G., and Marsigliante, S. (2018). Inhibition of ZL55 Cell Proliferation by ADP via PKC-Dependent Signalling Pathway. J. Cell. Physiol. *233*, 2526–2536.

Nader, R., Amm, J. El, and Aragon-Ching, J.B. (2018). Role of Chemotherapy in Prostate Cancer. Asian J. Androl. *20*, 221–229.

Nag, S., Qin, J., Srivenugopal, K.S., Wang, M., and Zhang, R. (2013). The MDM2-p53 pathway revisited. J. Biomed. Res. *27*, 254–271.

Natarajan, U., Venkatesan, T., Radhakrishnan, V., Samuel, S., Rasappan, P., and Rathinavelu, A. (2019). medicina Cell Cycle Arrest and Cytotoxic Effects of SAHA and RG7388 Mediated through p21 WAF1/CIP1 and p27 KIP1 in Cancer Cells. Medicina (B. Aires). *55*, 2–15.

Neumann, A., Müller, C.E., and Namasivayam, V. (2020). P2Y1-like nucleotide receptors—Structures, molecular modeling, mutagenesis, and oligomerization. Wiley Interdiscip. Rev. Comput. Mol. Sci.

Okuda, T., Otsuka, J., Sekizawa, A., Saito, H., Makino, R., Kushima, M., Farina, A., Kuwano, Y., and Okai, T. (2003). P53 Mutations and Overexpression Affect Prognosis of Ovarian Endometrioid Cancer but not Clear Cell Cancer. Gynecol. Oncol. *88*, 318–325.

Ozaki, T., and Nakagawara, A. (2011). Role of p53 in cell death and human cancers. Cancers (Basel). *3*, 994–1013.

Padua, D., and Massagué, J. (2008). Roles of TGFβ in Metastasis. Cell Res. *19*, 89–102.

Paller, C.J., and Antonarakis, E.S. (2011). Cabazitaxel: A Novel Second-line Treatment for Metastatic Castration-resistant Prostate Cancer. Drug Des. Devel. Ther. *5*, 117–13.

Pan, X., Zhao, J., Zhang, W.-N., Li, H.-Y., Mu, R., Zhou, T., Zhang, H.-Y., Gong, W.-L., Yu, M., Man, J.-H., et al. (2009). Induction of SOX4 by DNA Damage is Critical for P53 Stabilization and Function. Proc. Natl. Acad. Sci. U. S. A. *106*, 3788–3793.

Park, G., Kim, Y.J., Ahn, H., Park, W., Lee, J. sung, and Kim, Y.S. (2021). Salvage Hypofractionated Accelerated versus Standard Radiotherapy for the Treatment of Biochemical Recurrence after Radical Prostatectomy (SHARE): The Protocol of a Prospective, Randomized, Open-label, Superiority, Multi-institutional Trial. Trials *22*, 1–9.

Paudyal, P., Xie, Q., Vaddi, P.K., Henry, M.D., and Chen, S. (2017). Inhibiting G Protein βγ Signaling Blocks Prostate Cancer Progression and Enhances the Eficacy of Paclitaxel. Oncotarget *8*, 36067–36081.

Pavese, J.M., Krishna, S.N., and Bergan, R.C. (2014). Genistein Inhibits Human Prostate Cancer Cell Detachment, Invasion, and Metastasis 1-4. Am. J. Clin. Nutr. *100*, 431–437.

Pearson, A.S., Spitz, F.R., Swisher, S.G., Kataoka, M., Sarkiss, M.G., Meyn, R.E., McDonnell, T.J., Cristiano, R.J., and Roth, J.A. (2000). Up-regulation of the Proapoptotic Mediators Bax and Bak after Adenovirus-mediated p53 Gene Transfer in Lung Cancer Cells. Clin. Cancer Res. *6*, 887–890.

Petrylak, D.P. (2003). Docetaxel for the Treatment of Hormone-Refractory Prostate Cancer. Rev. Urol. *5*, 14–21.

Pfefferkorn, J.A., Choi, C., Winters, T., Kennedy, R., Chi, L., Perrin, L.A., Lu, G., Ping, Y.W., McClanahan, T., Schroeder, R., et al. (2008). P2Y1 Receptor Antagonists as Novel Antithrombotic Agents. Bioorg. Med. Chem. Lett. *18*, 3338–3343.

Phin, S., Moore, M.W., and Cotter, P.D. (2013). Genomic Rearrangements of PTEN in Prostate Cancer. Front. Oncol. *3*, 240–249.

Pi, M., and Quarles, L.D. (2012). GPRC6A Regulates Prostate Cancer Progression. Prostate *72*, 399–409.

Pizarro, J.G., Folch, J., de la Torre, A.V., Junyent, F., Verdaguer, E., Jordan, J., Pallas, M., and Camins, A. (2010). ATM is Involved in Cell-cycle Control through the Regulation of Retinoblastoma Protein Phosphorylation. J. Cell. Biochem. *110*, 210–218.

Poole, A.J., Heap, D., Carroll, R.E., and Tyner, A.L. (2004). Tumor Suppressor Functions for the Cdk Inhibitor P21 in the Mouse Colon. Oncogene *23*, 8128–8134.

Raghavan, P., Tumati, V., Yu, L., Chan, N., Tomimatsu, N., Burma, S., Bristow, R.G., and Saha, D. (2012). AZD5438, an Inhibitor of Cdk1, 2, and 9, Enhances the Radiosensitivity of Non-Small Cell Lung Carcinoma Cells. Int. J. Radiat. Oncol. Biol. Phys. *84*, 507–514.

Rapaport, E., and Fontaine, J. (1989). Generation of Extracellular ATP in Blood and its Mediated Inhibition of Host Weight Loss in Tumor-Bearing Mice. Biochem. Pharmacol. *38*, 4261–4266.

Ravery, V., Fizazi, K., Oudard, S., Drouet, L., Eymard, J.-C., Culine, S., Gravis, G., Hennequin, C., and Zerbib, M. (2011). The Use of Estramustine Phosphate in the Modern Management of Advanced Prostate Cancer. BJU Int. *108*, 1782–1786.

Rivlin, N., Brosh, R., Oren, M., and Rotter, V. (2011). Mutations in the p53 Tumor Suppressor Gene: Important Milestones at the Various Steps of Tumorigenesis. Genes Cancer *2*, 466–474.

Rose, M., Burgess, J.T., O'Byrne, K., Richard, D.J., and Bolderson, E. (2020). PARP Inhibitors: Clinical Relevance, Mechanisms of Action and Tumor Resistance. Front. Cell Dev. Biol. *8*, 879–901.

Rosenbaum, D.M., Rasmussen, S.G.F., and Kobilka, B.K. (2009). The Structure and Function of G-Protein-Coupled Receptors. Nature *459*, 356–363.

Rosenthal, S.A., Hu, C., Sartor, O., Gomella, L.G., Amin, M.B., Purdy, J., Michalski, J.M., Garzotto, M.G., Pervez, N., Balogh, A.G., et al. (2019). Effect of Chemotherapy With Docetaxel With Androgen Suppression and Radiotherapy for Localized High-Risk Prostate Cancer: The Randomized Phase III NRG Oncology RTOG 0521 Trial. J. Clin. Oncol. *37*, 1159–1168.

Ryan, C.J., Smith, M.R., Bono, J.S. De, Molina, A., Logothetis, C., Souza, P.L. De, Fizazi, K., Mainwaring, P.N., Rodriguez, J.M.P., Ng, S., et al. (2012). Interim Analysis (IA) results of COU-AA-302, a Randomized, Phase III Study of Abiraterone Acetate (AA) in Chemotherapy-Naive Patients (pts) with Metastatic Castration-Resistant Prostate Cancer (mCRPC). J. Clin. Oncol. *30*, LBA4518–LBA4518.

Sak, K., and Illes, P. (2005). Neuronal and Glial Cell Lines as Model Systems for Studying P2Y Receptor Pharmacology. Neurochem. Int. *47*, 401–412.

Sandhu, S., Moore, C.M., Chiong, E., Beltran, H., Bristow, R.G., and Williams, S.G. (2021). Prostate cancer. Lancet *398*, 1075–1090.

Sanford, M. (2013). Enzalutamide: A Review of Its Use in Metastatic, Castration-Resistant

Prostate Cancer. Drugs *73*, 1723–1732.

Scher, H.I., Graf, R.P., Schreiber, N.A., McLaughlin, B., Lu, D., Louw, J., Danila, D.C., Dugan, L., Johnson, A., Heller, G., et al. (2017). Nuclear-specific AR-V7 Protein Localization is Necessary to Guide Treatment Selection in Metastatic Castration-resistant Prostate Cancer. Eur. Urol. *71*, 874–882.

Shabbir, M., Ryten, M., Thompson, C., Mikhailidis, D., and Burnstock, G. (2008). Characterization of Calcium-independent Purinergic Receptor-mediated Apoptosis in Hormone-Refractory Prostate Cancer. BJU Int. *101*, 352–359.

Shadfan, M., Lopez-Pajares, V., and Yuan, Z.M. (2012). MDM2 and MDMX: Alone and Together in Regulation of p53. Transl. Cancer Res. *1*, 88–99.

Shamas-Din, A., Kale, J., Leber, B., and Andrews, D.W. (2013). Mechanisms of Action of Bcl-2 Family Proteins. Cold Spring Harb. Perspect. Biol. *5*, 1–21.

Shiota, M., Fujimoto, N., Matsumoto, T., Tsukahara, S., Nagakawa, S., Ueda, S., Ushijima, M., Kashiwagi, E., Takeuchi, A., Inokuchi, J., et al. (2021). Differential Impact of TGFB1 Variation by Metastatic Status in Androgen-Deprivation Therapy for Prostate Cancer. Front. Oncol. *11*, 1–7.

Shipitsin, M., Small, C., Choudhury, S., Giladi, E., Friedlander, S., Nardone, J., Hussain, S., Hurley, A.D., Ernst, C., Huang, Y.E., et al. (2014a). Identification of Proteomic Biomarkers Predicting Prostate Cancer Aggressiveness and Lethality Despite Biopsy-Sampling Error. Br. J. Cancer *111*, 1201–1212.

Shipitsin, M., Small, C., Giladi, E., Siddiqui, S., Choudhury, S., Hussain, S., Huang, Y.E., Chang, H., Rimm, D.L., Berman, D.M., et al. (2014b). Automated Quantitative Multiplex Immunofluorescence in situ Imaging Identifies Phospho-S6 and Phospho-PRAS40 as Predictive Protein Biomarkers for Prostate Cancer Lethality. Proteome Sci. *12*, 12–40.

Shukla, S., Bhaskaran, N., Babcook, M.A., Fu, P., MacLennan, G.T., and Gupta, S. (2014). Apigenin Inhibits Prostate Cancer Progression in TRAMP Mice via Targeting PI3K/Akt/FoxO Pathway. Carcinogenesis *35*, 452–460.

Siednienko, J., Gajanayake, T., Fitzgerald, K.A., Moynagh, P., and Miggin, S.M. (2011). Absence of MyD88 Results in Enhanced TLR3-Dependent Phosphorylation of IRF3 and Increased IFN-β and RANTES Production. J. Immunol. *186*, 2514–2522.

Simon, H.U., Haj-Yehia, A., and Levi-Schaffer, F. (2000). Role of reactive oxygen species (ROS) in apoptosis induction. Apoptosis.

Small, E.J., Schellhammer, P.F., Higano, C.S., Redfern, C.H., Nemunaitis, J.J., Valone, F.H., Verjee, S.S., Jones, L.A., and Hershberg, R.M. (2006). Placebo-controlled Phase III Trial of

Immunologic Therapy with Sipuleucel-T (APC8015) in Patients with Metastatic, Asymptomatic Hormone Refractory Prostate Cancer. J. Clin. Oncol. *24*, 3089–3094.

Smith, M.R., Scher, H.I., Sandhu, S., Efstathiou, E., Lara, P.N., Yu, E.Y., George, D.J., Chi, K.N., Saad, F., Ståhl, O., et al. (2022). Niraparib in Patients with Metastatic Castration-Resistant Prostate Cancer and DNA Repair Gene Defects (GALAHAD): a Multicentre, Open-label, Phase 2 trial. Lancet Oncol. *23*, 362–373.

Soloway, M.S., Soloway, C.T., Eldefrawy, A., Acosta, K., Kava, B., and Manoharan, M. (2010). Careful Selection and Close Monitoring of Low-risk Prostate Cancer Patients on Active Surveillance Minimizes the Need for Treatment. Eur. Urol. *58*, 831–835.

Spratt, D.E., Yousefi, K., Deheshi, S., Ross, A.E., Den, R.B., Schaeffer, E.M., Trock, B.J., Zhang, J., Glass, A.G., Dicker, A.P., et al. (2017). Individual Patient-Level Meta-Analysis of the Performance of the Decipher Genomic Classifier in High-Risk Men After Prostatectomy to Predict Development of Metastatic Disease. J. Clin. Oncol. *35*, 1991–1998.

Sriram, K., and Insel, P.A. (2018). G Protein-Coupled Receptors as Targets for Approved Drugs: How Many Targets and How Many Drugs? Mol. Pharmacol. *93*, 251–258.

Stangelberger, A., Waldert, M., and Djavan, B. (2008). Prostate Cancer in Elderly Men. Rev. Urol. *10*, 111–119.

Sun, G., Chen, X., Gong, U., Chen, Y., Li, G., Wei, F., Jiang, A., Niu, Y., and Shang, Z. (2019). Androgen Deprivation Therapy with Chemotherapy or Abiraterone for Patients with Metastatic Hormone-Naive Prostate Cancer: a Systematic Review and Meta-Analysis. Futur. Oncol. *15*, 1167–1179.

Suplat, D., Krzemiński, P., Pomorski, P., and Barańska, J. (2007). P2Y1 and P2Y12 Receptor Cross-talk in Calcium Signalling: Evidence from Nonstarved and Long-term Serum-deprived Glioma C6 cells. Purinergic Signal. *3*, 221–230.

Swarnkar, S., Goswami, P., Kamat, P.K., Gupta, S., Patro, I.K., Singh, S., and Nath, C. (2012). Rotenone-Induced Apoptosis and Role of Calcium: a Study on Neuro-2a Cells. Arch. Toxicol. *86*, 1387–1397.

Sweeney, C., Bracarda, S., Sternberg, C.N., Chi, K.N., Olmos, D., Sandhu, S., Massard, C., Matsubara, N., Alekseev, B., Parnis, F., et al. (2021). Ipatasertib plus Abiraterone and Prednisolone in Metastatic Castration-resistant Prostate Cancer (IPATential150): A Multicentre, Randomised, Double-blind, Phase 3 Trial. Lancet *398*, 131–142.

Tian, G., Zhou, J., Quan, Y., Kong, Q., Wu, W., and Liu, X. (2021). P2Y1 Receptor Agonist Attenuates Cardiac Fibroblasts Activation Triggered by TGF-β1. Front. Pharmacol. *12*, 88–98.

Tominaga, M., Wada, M., and Masu, M. (2001). Potentiation of capsaicin receptor activity by metabotropic ATP receptors as a possible mechanism for ATP-evoked pain and hyperalgesia. Proc. Natl. Acad. Sci. U. S. A. *98*, 6951–6956.

Tosoian, J.J., Trock, B.J., Landis, P., Feng, Z., Epstein, J.I., Partin, A.W., Walsh, P.C., and Carter, H.B. (2011). Active Surveillance Program for Prostate Cancer: An Update of the Johns Hopkins Experience. J. Clin. Oncol. *29*, 2185–2190.

Trovesi, C., Manfrini, N., Falcettoni, M., and Longhese, M.P. (2013). Regulation of the DNA Damage response by Cyclin-Dependent Kinases. J. Mol. Biol. *425*, 4756–4766.

Uemura, H., Ishiguro, H., Nagashima, Y., Sasaki, T., Nakaigawa, N., Hasumi, H., Kato, S., and Kubota, Y. (2005). Antiproliferative Activity of Angiotensin II Receptor Blocker through cross-talk between Stromal and Epithelial Prostate Cancer Cells. Mol. Cancer Ther. *4*, 1699–1709.

Usman, S., Khawer, M., Rafique, S., Naz, Z., and Saleem, K. (2020). The Current Status of Anti-GPCR Drugs Against Different Cancers. J. Pharm. Anal. *10*, 517–521.

Vermeulen, K., Van Bockstaele, D.R., and Berneman, Z.N. (2003). The Cell Cycle: A Review of Regulation, Deregulation and Therapeutic Targets in Cancer. Cell Prolif. *36*, 131–149.

Wahle, K.W.J., Brown, I., Rotondo, D., and Heys, S.D. (2010). Plant Phenolics in the Prevention and Treatment of Cancer. Adv. Exp. Med. Biol. *698*, 36–51.

Wan, H.-X., Hu, J.-H., Xie, R., Yang, S.-M., and Dong, H. (2016). Important Roles of P2Y Receptors in the Inflammation and Cancer of Digestive System. Oncotarget *7*, 28736–38747.

Wan, J., Zhang, J.U.N., and Zhang, J. (2018). Expression of p53 and its Mechanism in Prostate Cancer. Oncol. Lett. *16*, 378–385.

Wang, H., Yin, J., Hong, Y., Ren, A., Wang, H., Li, M., Zhao, Q., Jiang, C., and Liu, L. (2022). SCG2 is a Prognostic Biomarker Associated With Immune Infiltration and Macrophage Polarization in Colorectal Cancer. Front. Cell Dev. Biol. *9*, 3638–3651.

Wang, Q., Huang, L., and Yue, J. (2017). Oxidative Stress Activates the TRPM2-Ca 2+-CaMKII-ROS Signaling Loop to Induce Cell Death in Cancer Cells. Biochim. Biophys. Acta Mol. Cell Res. *1864*, 957–967.

Wang, W.G., Yan, D., Ye, H., Gustafson, G., Ghilezan, M., Martinez, A., and Krauss, D. (2018). Outcomes and Toxicity from a Prospective Study of Moderately Hypofractionated Radiation Therapy for Prostate Cancer. Adv. Radiat. Oncol. *3*, 163–169.

Wang, Y., Wang, C., Yang, Q., and Cheng, Y.-L. (2019). ANXA3 Silencing Ameliorates Intracranial Aneurysm via Inhibition of the JNK Signaling Pathway. Mol. Ther. Nucleic Acid

17, 540–550.

Warner, W.A., Sanchez, R., Dawoodian, A., Li, E., and Momand, J. (2012). Identification of FDA-Approved Drugs that Computationally Bind to MDM2. Chem. Biol. Drug Des. *80*, 631–637.

Warren, C.F.A., Wong-Brown, M.W., and Bowden, N.A. (2019). BCL-2 Family Isoforms in Apoptosis and Cancer. Cell Death Dis. *10*, 1–12.

Wasilenko, W.J., Cooper, J., Palad, A.J., Somers, K.D., Blackmore, P.F., Rhim, J.S., Wright, G.L., and Schellhammer, P.F. (1997). Calcium Signaling in Prostate Cancer Cells: Evidence for Multiple Receptors and Enhanced Sensitivity to Bombesin/GRP. Prostate *30*, 167–173.

Watson, P.A., Arora, V.K., and Sawyers, C.L. (2015). Emerging Mechanisms of Resistance to Androgen Receptor Inhibitors in Prostate Cancer. Nat. Rev. Cancer *15*, 701.

Wei, Q., Costanzi, S., Liu, Q.-Z., Gao, Z.-G., and Jacobson, K.A. (2011). Activation of the P2Y1 Receptor Induces Apoptosis and Inhibits Proliferation of Prostate Cancer Cells. Biochem. Pharmacol. *82*, 418–425.

Werry, T.D., Christie, M.I., Dainty, I.A., Wilkinson, G.F., and Willars, G.B. (2002). Ca2+ signalling by recombinant human CXCR2 chemokine receptors is potentiated by P2Y nucleotide receptors in HEK cells. Br. J. Pharmacol.

White, N., and Burnstock, G. (2006). P2 receptors and cancer. Trends Pharmacol. Sci. *27*, 211–217.

White, N., Ryten, M., Clayton, E., Butler, P., and Burnstock, G. (2005). P2Y Purinergic Receptors Regulate the Growth of Human Melanomas. Cancer Lett. *224*, 81–91.

Wisenbaugh, E.S., Andrews, P.E., Ferrigni, R.G., Schild, S.E., Keole, S.R., Wong, W.W., and Vora, S.A. (2014). Proton Beam Therapy for Localized Prostate Cancer 101: Basics, Controversies, and Facts. Rev. Urol. *16*, 67–76.

Wit, R. de, Bono, J. de, Sternberg, C.N., Fizazi, K., Tombal, B., Wülfing, C., Kramer, G., Eymard, J.-C., Bamias, A., Carles, J., et al. (2019). Cabazitaxel versus Abiraterone or Enzalutamide in Metastatic Prostate Cancer. N. Engl. J. Med. *381*, 2506–2518.

Wokołorczyk, D., Kluźniak, W., Stempa, K., Rusak, B., Huzarski, T., Gronwald, J., Gliniewicz, K., Kashyap, A., Morawska, S., Dębniak, T., et al. (2021). PALB2 Mutations and Prostate Cancer Risk and Survival. Br. J. Cancer *125*, 569–575.

Wolf, P. (2019). Tumor-Specific Induction of the Intrinsic Apoptotic Pathway—A New Therapeutic Option for Advanced Prostate Cancer? Front. Oncol. *9*, 1–5.

Wright, P.T., Schobesberger, S., and Gorelik, J. (2015). Studying GPCR/cAMP Pharmacology from the Perspective of Cellular Structure. Front. Pharmacol. *6*, 1–10.

Wypych, D., and Pomorski, P. (2012). P2Y1 Nucleotide Receptor Silencing and its Effect on Glioma C6 Calcium Signaling. Acta Biochim. Pol. *59*, 711–717.

Xia, C., Ma, W., Wang, F., Hua, S., and Liu, M. (2001). Identification of a Prostate-Specific G-Protein Coupled Receptor in Prostate Cancer. Oncogene *20*, 5903–5907.

Xu, G., and Shi, Y. (2007). Apoptosis Signaling Pathways and Lymphocyte Homeostasis. Cell Res. *17*, 759–771.

Yan, X., Yin, J., Yao, H., Mao, N., Yang, Y., and Pan, L. (2010). Increased Expression of Annexin A3 is a Mechanism of Platinum Resistance in Ovarian Cancer. Cancer Res. *70*, 1616–1624.

Yang, Y., Pan, X., Lei, W., Wang, J., and Song, J. (2006). Transforming Growth Factor-b1 Induces Epithelial-to-Mesenchymal Transition and Apoptosis via a Cell Cycle-Dependent Mechanism. Oncogene *25*, 7235–7244.

Yarden, R.I., Pardo-Reoyo, S., Sgagias, M., Cowan, K.H., and Brody, L.C. (2002). BRCA1 Regulates the G2/M Checkpoint by Activating Chk1 Kinase upon DNA Damage. Nat. Genet. *30*, 285–289.

Ye, R., Pi, M., Cox, J. V., Nishimoto, S.K., and Quarles, L.D. (2017). CRISPR/Cas9 Targeting of GPRC6A Suppresses Prostate Cancer Tumorigenesis in a Human Xenograft Model. J. Exp. Clin. Cancer Res. *36*, 1–13.

Ye, R., Pi, M., Nooh, M.M., Bahout, S.W., and Quarles, L.D. (2019). Human GPRC6A Mediates Testosterone-Induced Mitogen-Activated Protein Kinases and mTORC1 Signaling in Prostate Cancer Cells. Mol. Pharmacol. *95*, 563–572.

YK, J., W, H., L, J., JA, B., and DG, A. (2003). ATP modulates intracellular Ca2+ and firing rate through a P2Y1 purinoceptor in cane toad pacemaker cells. J. Physiol. *552*, 777–787.

Yonover, P., Steyaert, S., Cohen, J.J., Ruiz, C., Grafczynska, K., Garcia, E., DeHart, J., Brawer, M., Groskopf, J., and Criekinge, W. Van (2019). Clinical Utility Study of Confirms MDX for Prostate Cancer in a Community Urology Practice. Am. Soc. Clin. Oncol. *37*, 94–94.

Yuan, T.L., and Cantley, L.C. (2008). PI3K Pathway Alterations in Cancer: Variations on a Theme. Oncogene *27*, 5497–5510.

Yuan, S., Chan, H.C.S., Vogel, H., Filipek, S., Stevens, R.C., and Palczewski, K. (2016). The Molecular Mechanism of P2Y1 Receptor Activation. Angew. Chemie *55*, 10353.

Zerr, M., Hechler, B., Freund, M., Magnenat, S., Lanois, I., Cazenave, J.P., Léon, C., and Gachet, C. (2011). Major Contribution of the P2Y1 Receptor in Purinergic Regulation of TNFα-Induced Vascular Inflammation. Circulation *123*, 2404–2413.

Zhang, Y., and Ye, J. (2012). Mitochondrial Inhibitor as a New Class of Insulin Sensitizer. Acta Pharm. Sin. B *2*, 341–349.

Zhu, Y., Wu, J., Li, S., Wang, X., Liang, Z., Xu, X., Xu, X., Hu, Z., Lin, Y., Chen, H., et al. (2015). Apigenin Inhibits Migration and Invasion via Modulation of Epithelial Mesenchymal Transition in Prostate Cancer. Mol. Med. Rep. *11*, 1004–1008.

Zielinski, R.R., Eigl, B.J., and Chi, K.N. (2013). Targeting the Apoptosis Pathway in Prostate Cancer. Cancer J. *19*, 79–89.

De Zio, D., Cianfanelli, V., and Cecconi, F. (2013). New Insights into the Link Between DNA Damage and Apoptosis. Antioxid. Redox Signal. *19*, 559–571.

Overview | Prolaris gene expression assay for assessing long-term risk of prostate cancer progression | Advice | NICE.

PUBLICATIONS

PUBLICATION
I

Synthesis and preclinical validation of novel P2Y1 receptor ligands as a potent anti-prostate cancer agent

H. Le, T. Rimpiläinen, S. K. Mani, A. Murugesan, O. Yli-Harja, N. R. Candeias, and M. Kandhavelu

Scientific Reports (2019), 9, 18938
DOI: 10.1038/s41598-019-55194-8

SCIENTIFIC REPORTS
nature research

OPEN

Synthesis and preclinical validation of novel P2Y1 receptor ligands as a potent anti-prostate cancer agent

Hien Thi Thu Le[1], Tatu Rimpilainen[2], Saravanan Konda Mani[3], Akshaya Murugesan[1,4], Olli Yli-Harja[5,6], Nuno R. Candeias[2] & Meenakshisundaram Kandhavelu[1*]

Purinergic receptor is a potential drug target for neuropathic pain, Alzheimer disease, and prostate cancer. Focusing on the structure-based ligand discovery, docking analysis on the crystal structure of $P2Y_1$ receptor ($P2Y_1R$) with 923 derivatives of 1-indolinoalkyl 2-phenolic compound is performed to understand the molecular insights of the receptor. The structural model identified the top novel ligands, 426 (compound 1) and 636 (compound 2) having highest binding affinity with the docking score of −7.38 and −6.92. We have reported the interaction efficacy and the dynamics of $P2Y_1R$ protein with the ligands. The best hits synthesized were experimentally optimized as a potent $P2Y_1$ agonists. These ligands exhibits anti-proliferative effect against the PC-3 and DU-145 cells (IC_{50} = 15 µM – 33 µM) with significant increase in the calcium level in dose- and time-dependent manner. Moreover, the activation of $P2Y_1R$ induced the apoptosis via Capase3/7 and ROS signaling pathway. Thus it is evidenced that the newly synthesized ligands, as a $P2Y_1R$ agonists could potentially act as a therapeutic drug for treating prostate cancer.

Prostate cancer (PCa) is the most common cause of cancer deaths in men[1]. It has been characterized as a complex disease induced by the alteration in intrinsic and extrinsic cellular processes[2]. G-protein coupled receptors (GPCRs), the largest family of cell surface receptor plays a key role in metastatic cancer and hence considered as the promising targets for cancer treatment[3,4]. However, the substantial role of GPCRs in cancer progression and treatment remains questionable. Purinergic receptors (P2YRs), another member of GPCR family, found to be over-expressed in some types of cancer cells and tissues[5]. Based on the differences in gene sequence, protein structure, and functions, the P2YR family constitutes 8 homo-receptor subtypes, such as $P2Y_1$, $P2Y_2$, $P2Y_4$, $P2Y_6$, $P2Y_{11}$, $P2Y_{12}$, $P2Y_{13}$, and $P2Y_{14}$[6]. Of late, it has been identified that $P2Y_1$ expression is higher in PC-3[7–9] and DU-145 cells[9,10] both in normal and stimulation condition than in non-cancerous cells. Therefore, P2Y1R is considered as a noteworthy tumor cell marker and anticipated to be used as a target for inhibiting the PCa cell proliferation.

The stimulations of $P2Y_1R$ induce corresponding signal transduction pathways that varied for different cell types[11]. The selected P2Y1R-targeted agonist, MRS 2365 increases lactate dehydrogenase and intracellular calcium (Ca^{2+}) levels, in turn induces apoptosis and inhibits the PC-3 cells proliferation[8]. Furthermore, 2-MeSADP, a non-selective $P2Y_1$ agonist, stimulates intracellular Ca^{2+}, cell death and reduces cell aggression in 1321N1 astrocytoma cells transfected with the human $P2Y_1R$[12,13]. Still, in HUVEC cells, a $P2Y_1R$ antagonist MRS2179 leads to the formation of phosphatydilinositol, and phosphorylates the mitogen-activated protein kinases (MAPK)[14,15]. The activation of MAPK signaling possibly contributes to the re-endothelialization after vascular injury[14,15].

Other potential therapeutic applications for $P2Y_1R$ ligands includes, agonist as antidiabetic agents or antagonists as antithrombotic agents *in vitro* and *in vivo* models[16–18]. Although there is expression of $P2Y_1R$ in the human prostate, its role in the growth of PCa is yet to be characterized. In the present study, PC-3 and DU-145 PCa cells[19,20], were used to investigate the effect of $P2Y_1R$ and novel agonists in cell death and proliferation. Many

[1]Molecular Signaling Lab, Faculty of Medicine and Health Technology, Tampere University and BioMediTech, P.O.Box 553, 33101, Tampere, Finland. [2]Faculty of Engineering and Natural Sciences, Tampere University, Korkeakoulunkatu 8, 33101, Tampere, Finland. [3]Department of Crystallography & Biophysics, University of Madras, Guindy Campus, Chennai, 600025, India. [4]Department of Biotechnology, Lady Doak College, Thallakulam, Madurai, 625002, India. [5]Computational Systems Biology Research Group, Faculty of Medicine and Health Technology and BioMediTech, Tampere University, P.O.Box 553, 33101, Tampere, Finland. [6]Institute for Systems Biology, 1441 N 34th Street, Seattle, WA, 98103-8904, USA. *email: meenakshisundaram.kandhavelu@tuni.fi

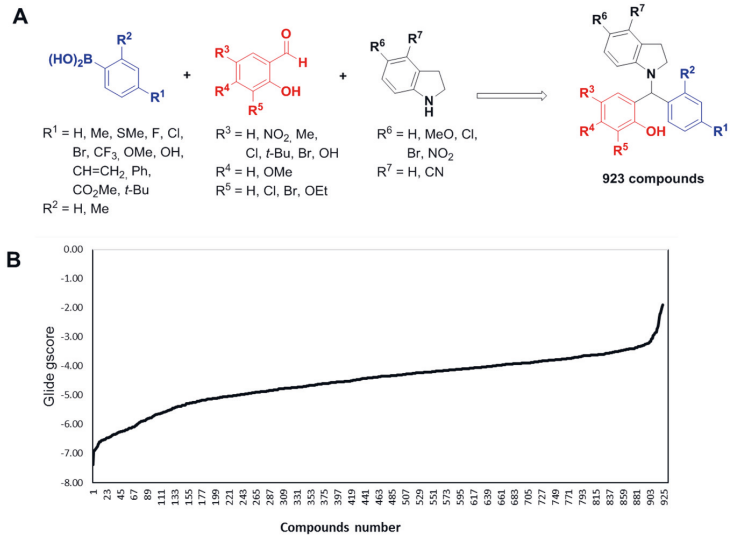

Figure 1. Hit identification based on docking score. (**A**) Library of 1-indolinoalkyl 2-phenols for $P2Y_1R$ docking screen. (**B**) Glide docking score (kcal/mol) of 923 compounds against $P2Y_1R$. Two ligand-like compounds **1** and **2** ranks top with high docking scores.

scaffolds such as 1,4-substituted triazoles, pyrimidines or pyrazoles are known for their antitumor activities[21–23]. Similarly, phenolic Mannich bases were recognized to possess anticancer and cytotoxic activity[24]. Derivatives of aminomethylated naphthols and 8-hydroxyquinoline induces apoptosis on activation of caspase-dependent pathways[24,25].

Our earlier reports have also demonstrated the ability of 1-indolinoalkyl 2-phenols to inhibit cancer cells growth[26]. Since phenolic compounds have profound role in inhibiting the cancer cell proliferation, a large variety of substituents of 1-indolinoalkyl 2-phenols is considered in the initial library for the docking studies. We synthesized a group of 1-indolinoalkyl 2-phenolic derivatives using 3-component Petasis borono-Mannich reaction (i.e., salicylaldehydes, indolines and boronic acids) and many potential hits are experimentally verified. Based on the probability of targeted $P2Y_1R$ signaling activation to inhibit PCa cell growth, a library of over 900 structures was built with single variation in the substituents from the different components along with their combinations. The best docking poses in the ligands interaction with $P2Y_1R$ was further analyzed. The detailed interaction of the three-dimensional structure of $P2Y_1R$ with the selective antagonist MRS2179 was performed for scrutinizing the newly synthesized ligands. The competence of new $P2Y_1$ ligand identified via molecular modeling, docking, and calcium kinetics is analyzed. The activation of $P2Y_1R$ down-stream signaling pathway and their effect in PCa is also explored through apoptosis, ROS and Caspase 3/7 assays. Our findings suggested that the identified ligands might potentially help in the treatment of the prostate cancer.

Results and Discussion

Novel ligands of $P2Y_1R$. The three – dimensional (3D) coordinates of $P2Y_1R$ was retrieved from Protein Data Bank with the code 4XNW (Resolution: 2.7 Å) comprising of 427 amino acid residues. The $P2Y_1$ protein model shares a canonical seven transmembrane helices each flanked by the topological domain like other known GPCR structures[27,28]. To study the binding mode of $P2Y_1R$, initially we performed the docking studies with the known antagonist MRS2500 (co-crystallized)[29], and an agonist MRS2365 (glide score −8.80 Kcal/mol) using Schrodinger. Over 900 compounds were designed using Java Molecular Editor (JME) and translated to structure data file which is compiled in the repository (Table S2 of SI) (Fig. 1A). $P2Y_1R$ model was docked with 923 compounds (Fig. 1B and Table S2 of SI). The docked results were analyzed based on the presence of hydrogen bonds, salt bridges, halogen bonds, aromatic bonds, π-cation and π-π interactions. All the conformers were scrutinized based on the binding mode and the stability of the protein-ligand complex. The library comprising 923 compounds was screened based on the docking score that are −7.0 and above (Fig. 1B and Table S2 of SI). The best two ligand like compounds 1 and 2 with the highest docking score, that satisfies Lipinski's rule were selected. The high glide score indicated a high binding affinity towards the $P2Y_1R$.

2D ligand interaction diagram showed the similar number of interaction of ligands with amino acid residues in the $P2Y_1R$, **1** with 16 interactions (Fig. 2A) and 2 with 19 interactions (Fig. 2B). Six hydrophobic interactions were found between **1** and $P2Y_1R$ while seven interactions between **2** and the receptor. Both ligands form interaction with cysteine, tyrosine and sulfur containing amino acid residues of the $P2Y_1R$. The Hydrophobic contact between the protein and ligands are the key property for the protein folding and stability[30]. The charged residue interactions were also observed between ligands and $P2Y_1R$ molecule at Arg287. Cation-pi stabilizing

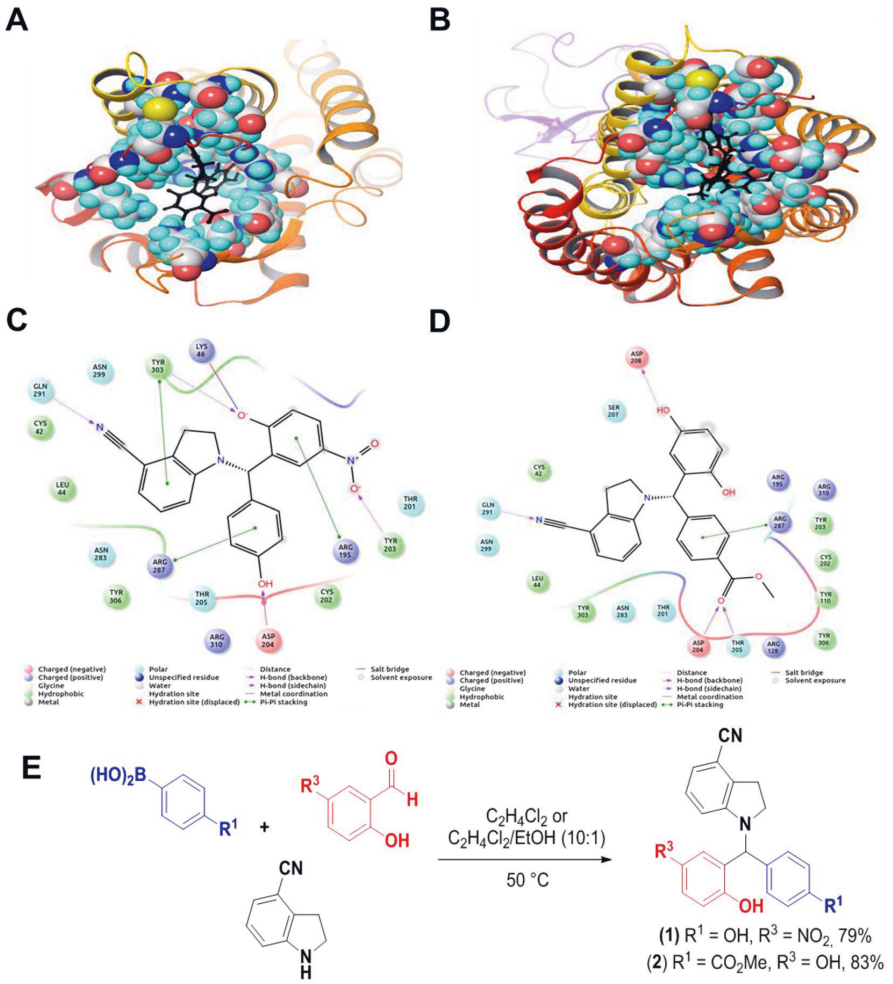

Figure 2. The ligand binding residues of the receptor is shown as the surface model and the ligand is shown in black colored ball and stick model (**A**) compound 1 and P2Y1 (**B**) compound 2 and P2Y1. The non-ligand interacting regions of receptor is shown as ribbon model. (**C**) Two-dimensional ligand interaction diagram of compound **1** and (**D**) compound **2**. The color coding and interactions are described in the ligand key. (**E**) Synthesis scheme of 1-indolinoalkyl 2-phenols **1** and **2**.

electrostatic interactions were found in similar number in both the ligands (Fig. 2C,D). There are a few interactions found to be conserved on both $P2Y_1R$-ligand **1** and **2** complexes at the amino acid residues such as Arg287, Arg310, Arg195 (Charged[38]), Tyr303, Cys42, Cys202 (Hydrophobic), and Leu44. The presence of cysteine residues at the interface is also essential for maintaining the precise pocket formation that allows the receptor to bind with the ligands[30]. These observations suggest that both ligands have the potentiality to bind with $P2Y_1R$.

The identified promising hits were organized through the abovementioned Petasis borono-Mannich reaction (Fig. 2E). Indoline-4-carbonitrile was prepared with 68% yield on reducing the corresponding indole with triethylsilane in TFA[31]. Both 1-indolinoalkyl 2-phenols was obtained in good yields upon reaction at 50 °C, while preparation of **2** requires longer reaction time (20 h vs 70 min for **1**) due to the lower reactivity of the boronic acid partner.

Novel ligand-P2Y1R interaction and signaling activation affects intracellular calcium. The activation of phospholipase C (PLC) is the common signal transduction pathway triggered by the $P2Y_1R$-G_q[32]. Phosphatatidylinositol-4,5-bisphosphatase is hydrolyzed by the PLC activation, which increases the cytosolic Ca^{2+} mobilization through the generated IP3 and diacylglycerol[33]. To elucidate the agonistic activity of these two compounds, we analyzed the changes in the downstream effector, Ca^{2+} in PCa cells[34]. As shown in Fig. 3,

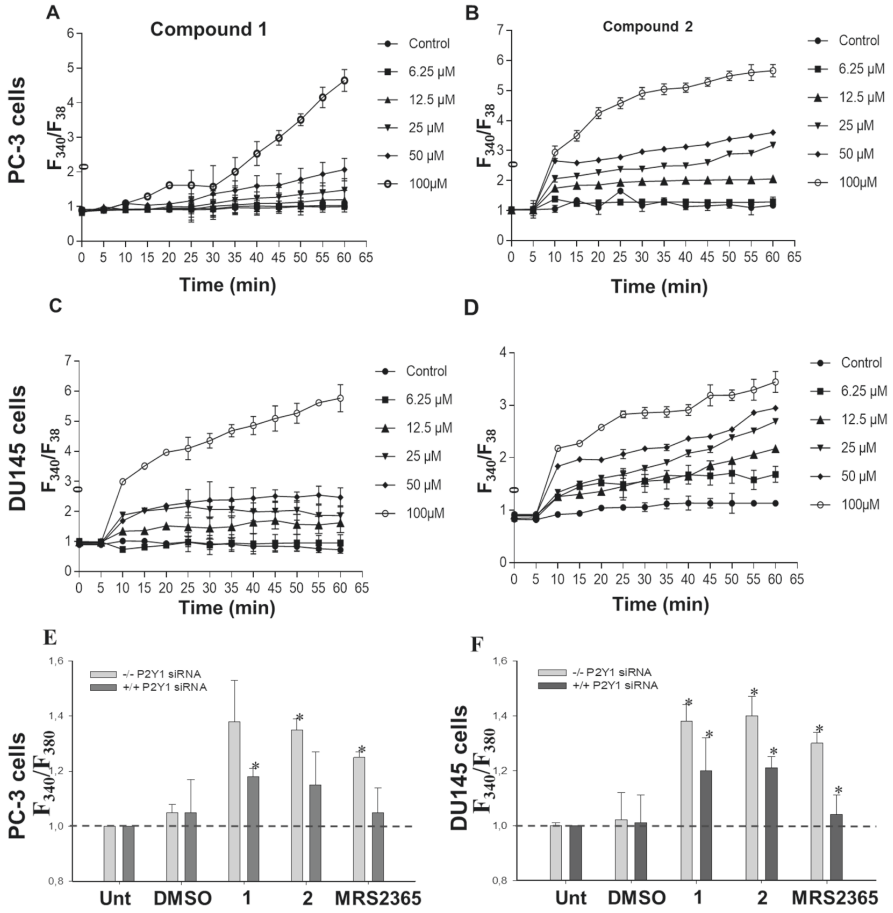

Figure 3. Measurement of intracellular calcium with Fura 2-AM on activation of P2Y1R by compound **1** and **2**. The fluorescence was measured using Magelan^{TM} microplate plate reader at every 5 min. The ratiometric Ca^{2+} fold change was analyzed based on the emitted fluorescence intensities of the samples. PC-3 cells were treated with (**A**) compound **1**, (**B**) compound **2** and DU-145 cells with (**C**) compound **1** and (**D**) compound **2**. (**E**) P2Y1R silencing by siRNA and and its effect on Ca^{2+} signaling activation by compound **1**, **2** and MRS2365 in PC-3 cells (**F**) same condition as "E" in DU-145 cells. The experiments were repeated 3 independent times, $^{*}p < 0.05$ by one-way ANOVA.

intracellular Ca^{2+} concentration increases in PC-3 (Fig. 3A,B) and DU-145 (Fig. 3C,D) cells over the concentration of compound **1** and **2** in a time dependent manner. As evident from Fig. 3A,C, compound **1** at 100 μM concentration increased the Ca^{2+} level in PC-3 and DU-145 cells which is 5 fold higher than the untreated condition after 60 min. Similarly, compound **2** at 25 μM also increased the Ca^{2+} by 3 fold higher than the untreated condition after 60 min. siRNA assay was also performed to confirm the $P2Y_1R$ targeted binding of the compound **1** and **2**. In the absence of $P2Y_1$ siRNA, there was 1.3 fold higher level of Ca^{2+} upon the activation of $P2Y_1R$ signal by MRS2365, compound **1** and **2**, whereas the presence of $P2Y_1$ siRNA showed 0.2 fold decrease in the level of Ca^{2+} in PC-3 cells (Fig. 3E) and DU- 145 cells (Fig. 3F). These results shows the $P2Y_1R$ specific interaction of the novel ligands that can act as an agonist which is congruent with the virtual screening results.

Growth inhibitory effects of compound 1 and 2 on PC-3 and DU-145 cells. $P2Y_1R$ has been used as a biomarker for the therapeutic treatments of PCa cells[35,36] and its agonists acting as an cell death inducer[9,12]. In the present study, compound **1** and **2** were chosen as an ideal ligand based on its potentiality to bind and interact with the $P2Y_1R$. Further to explore the cytotoxicity effect of these two ligands against the growth of PCa cells, MTT assay was performed. PC-3 and DU-145 cells were treated with varying concentrations of compound **1** and **2**. As given in the Fig. 4A, the compounds decreased the cell viability when relatively compared with the untreated control group. Dose-dependent experiment on PC-3 cells revealed the IC_{50} values as 15.98 μM for compound **1**

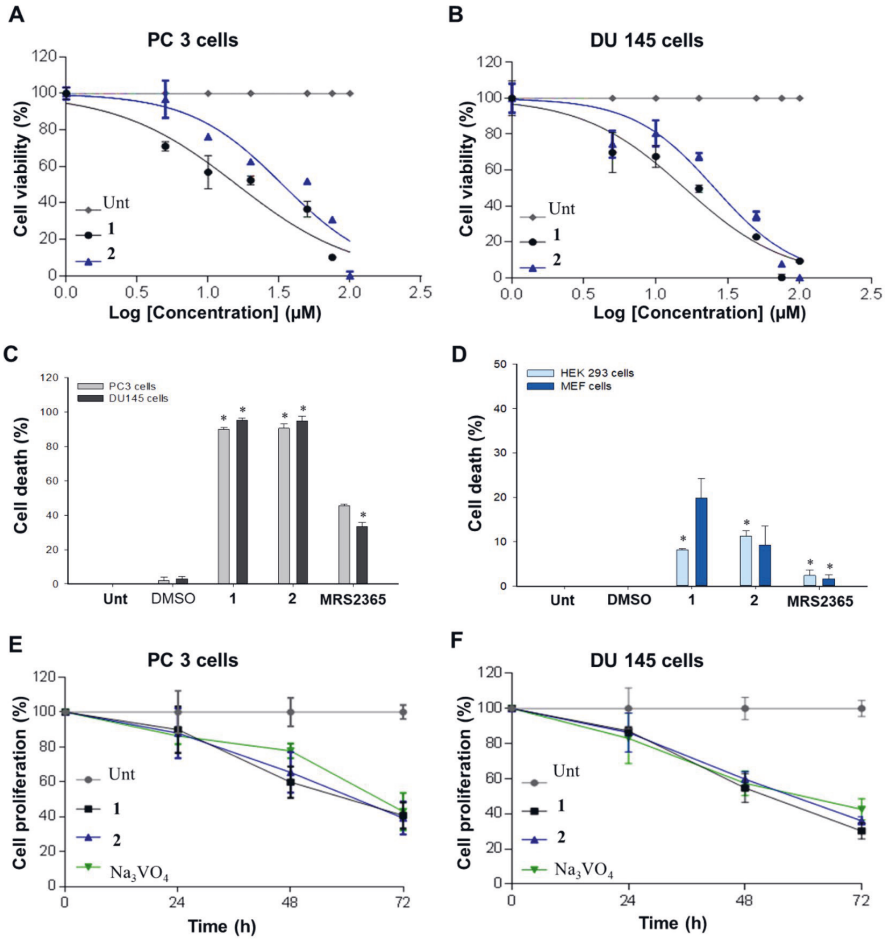

Figure 4. Effect of compound **1** and **2** on the cell viability. (**A**) PC-3 cells and (**B**) DU-145 cells were treated with the varying concentrations of compound **1** and **2**. IC_{50} of the untreated cells along with the respective compounds were determined by Prism 7.0. (**C**) PC3 and DU-145 cells and (**D**) HEK293 and MEF cells were treated with 100 μM of compound **1** and **2**, MRS2365 for 48 h with DMSO as negative control. (**E**) PC-3 and (**F**) DU-145 cells were incubated with the IC_{50} concentration of compound **1** and **2** and 50 μM Na_3VO_4 for 24 h, 48 h, and 72 h. The experiment was performed with replicates of biological and technical repeats. Statistical significance was considered at $^*p < 0.05$.

and 33.57 μM for compound **2**. Apparently, IC_{50} values for DU-145 cells was found to be 15.64 μM for compound **1** and 25.64 μM for compound **2** (Fig. 4B). Based on the IC_{50} values, compound **1** exerted a better cytotoxic effect on PCa cells than compound **2**. Notably, compound **1** and **2** induced ~96% of cell death in PCa cells whereas MRS2365, the positive control of $P2Y_1R$ agonist, induced about 38% of cell death (Fig. 4C). In contrast, HEK293 and MEF, non-cancerous cells, were significantly less sensitive when treated with compound **1**, **2**, and MRS365 than the PCa cells (Fig. 4D). The cell death of non-cancerous cells was observed to be less than 20% with 100 μM concentration of compound **1** and **2** treatment. These observation concluded that the compound **1** and **2** have cytotoxic effect specific for PCa cells.

To detect the effect of the compounds, the PC-3 and DU-145 cells were treated at different time points with IC_{50} concentration of **1** and **2**. Figure 4E,F have shown that the cell proliferation in the treated cells were significantly lower than the control group over the time. The effect of compound **1** and **2** on PC-3 reduced the cell proliferation to about 89%, 67%, and 42% and 90%, 69%, 40% respectively at 24 h, 48 h, and 72 h. Similarly, the impact of Na_3VO_4 on PC-3 cells have shown the reduced proliferation of about 92%, 81%, and 45% at 24 h, 48 h, and 72 h, respectively. The inhibition of cell proliferation of the compound **1** and **2** was higher than the positive control Na_3VO_4 at 48 h (Fig. 4E). In contrast, DU-145 cells, the cell growth was reduced from ~85% to ~60% progressively from 24 h to 48 h on treatment with compound **1**, **2** and Na_3VO_4 (Fig. 4F). However, at 72 h, the

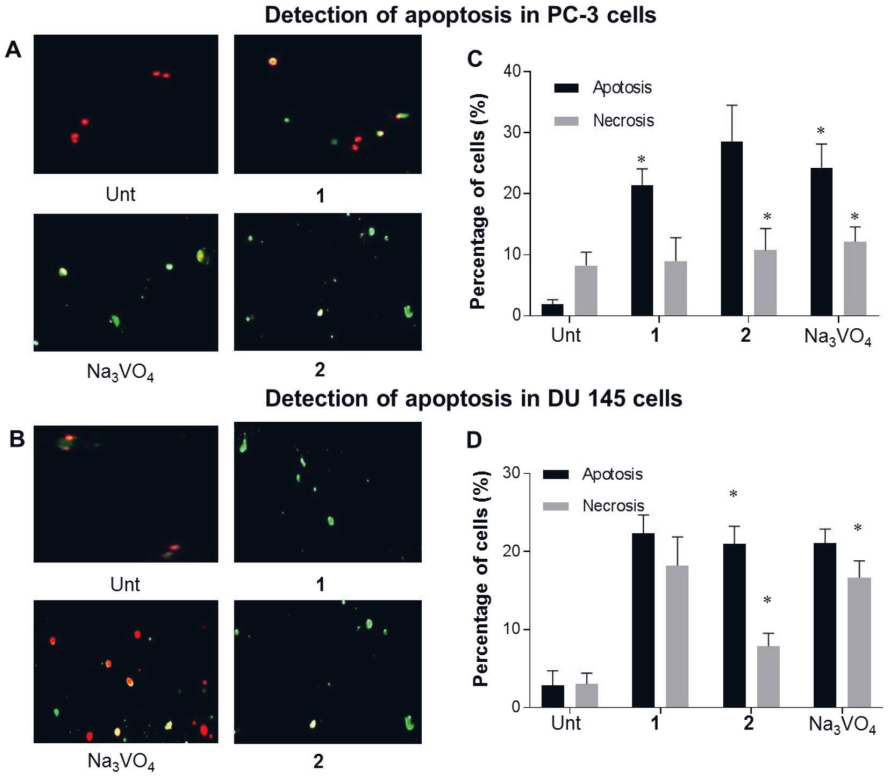

Figure 5. Induction of apoptosis by compound **1** and **2** on PCa cells. (**A**) Representative images of PC-3 cells stained with Annexin-V/PI in untreated, compound **1**, **2**, and Na_3VO_4 treated condition. (**B**) percentage of apoptotic and necrotic cell death in the corresponding condition as in A. (**C**) The representative images of DU-145 cells stained with Annexin-V/PI (**D**) the percentage of apoptosis and necrosis in DU-145 cells. Results are represented as mean of three independent experiments, mean ± S.D. *$P < 0.05$, versus control, $n = 3$.

proliferation was inhibited to 43% on treatment with compound **1** and **2**, which was higher than Na_3VO_4 treatment. These findings supports the hypothesis that compound **1** and **2** could inhibit the cancer cell proliferation on increasing the treatment time.

Effects of compound 1 and 2 on PCa apoptosis. Apoptosis is a common response to cell stress during the process of cell death[37] which can happen through the increase of intracellular Ca^{2+}, ROS and the activation of caspase[38]. We sought to determine the efficacy of the novel agonists **1** and **2** on PCa cell lines, Annexin V-affinity assay was performed. After 48 h of treatment, the fluorescent microscope images of PC-3 (Fig. 5A) and DU-145 cells (Fig. 5B) exposed the presence of apoptotic and necrotic cells. PC-3 cells on treatment with compound **1** and **2** caused apoptosis of 23.2% and 29.6% whereas the positive control Na_3VO_4 caused 25.6% apoptosis (Fig. 5C). DU-145 cells after 48 h treatment with compound **1**, **2** and Na_3VO_4 is marked with 20% increase in apoptotic cell fraction when compared to the untreated cells (Fig. 5D). Taken together, we conclude that the activation of $P2Y_1R$ by the compound **1** and **2** increases the cell death through apoptosis.

Production of ROS by compound 1 and 2 in PCa cells. ROS production exists under normal and abnormal physiological conditions of the cell[39]. The production of ROS affects several signaling pathways such as cell survival, phosphatase and kinase activities, and muscle plasticity[40]. ROS promotes many events of tumor progression like cell proliferation, metastasis, and angiogenesis[41]. ROS is also capable of inducing cell cycle arrest and cell death in cancer treatment[42]. In order to explore the effect of $P2Y_1R$ activation on prostate cancer via ROS, PC-3 and DU-145 cells were incubated with compound **1**, **2**, and H_2O_2. As shown in Fig. 6, the production of ROS increased in the presence of H_2O_2, compound **1** and **2** in PC-3 and DU-145 cells (Fig. 6A). We noticed an increase in the fold change of ROS to 1.41 and 1.22 in the compound **1** and **2** treated PC-3 cells respectively, when compared to the untreated condition. The positive control H_2O_2 expressed 2.1 fold change in ROS level which is greater than the compound **1** and **2** treatment. Likewise, ROS level in DU-145 cells also increased to 1.36 and 1.01 fold change on treatment with compound **1** and **2** whereas H_2O_2 showed 1.78 ROS fold change. The difference in

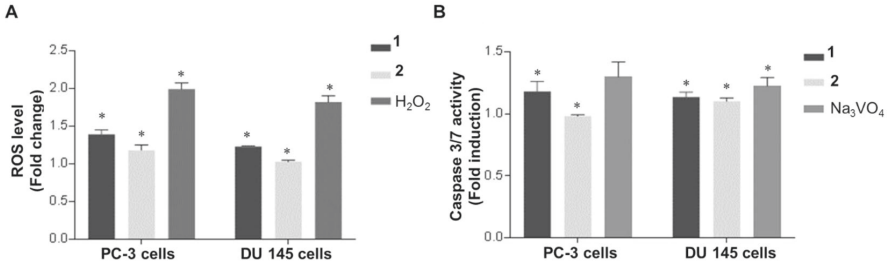

Figure 6. Production of ROS and activation of Caspase3/7 by compound **1** and **2** in PCa cells. (**A**) The fold change in ROS in PC-3 and DU-145 cells treated with compound **1**, **2** and H_2O_2. H2DCFDA labelled cells was used to measure the ROS production and its fluorescence signal was recorded using 96 well plate reader. The fold change of ROS was calculated using fluorescence intensities of the untreated control. (**B**) The fold change in Caspase 3/7 in PC-3 and DU-145 cells treated with compound **1**, **2**, and Na_3VO_4. Biological and the technical replicates were maintained to assess the significance of the results, with mean ± S.D. $*P < 0.05$, versus control, n = 3.

the fold change was proven to be statistically significant by ANOVA test with the P-*value* < 0.05 (Table S1 of SI). These results indicates that the agonists **1** and **2** enhanced the production of ROS in both PCa cells.

Activation of Caspase 3/7 by compound 1 and 2 on PCa. Apoptosis is induced through the activation of intracellular caspases and lead to the modification of protein substrate within the nucleus and cytoplasm[43]. Currently more than 14 caspases were cloned and partially their functions were determinuteed to be in programmed cell death[44]. Among them, caspases 3 and 7 have been identified as an executioner caspases that directly lead to the intrinsic/extrinsic pathways in apoptosis process[45,46]. Since the caspase plays an essential role in cell death, the anti-cancer effect of agonist **1** and **2** were explored by determinuteing the changes in the caspase 3/7 activity. As described in the Caspase-Glo® 3/7 assay, PC-3 and DU-145 cells were treated with compounds **1**, **2**, and Na_3VO_4. Interestingly, PC-3 cells treated with compound **1** exhibited an increase of caspase 3/7, showing 1.22 fold induction when compared to the untreated cells (Fig. 6B). Besides, compound **2** and positive control exhibited 0.8 and 1.26 fold induction, respectively. However, Caspase 3/7 activity increased similarly around 1.15-fold change in DU-145 cells on treatment with compound **1** and **2** than the untreated condition. The difference in the fold change of treated and untreated conditions were statistically significant as per ANOVA test (P-value < 0.05; Table S1 of SI). Collectively, the results demonstrated that the novel agonist **1** and **2** could induce apoptosis through Caspase 3/7 dependent signaling pathway.

Conclusion

$P2Y_1R$, a purinergic G_q protein, has been reported as the pharmacological target for the therapeutic treatment of PCa[20,47,48]. In the present research, molecular docking experiments was performed to investigate the interaction of a library of 923 1-indolinoalkyl 2-phenolic derivatives with $P2Y_1R$ protein. Docking analysis revealed that the compound **1** and **2** as the novel ligands. Furthermore, interactions of $P2Y_1R$ between these two ligands demonstrated the crucial aminuteo acid interactions responsible for the folding and stability. The synthesized 1-indolinoalkyl 2-phenolic derivatives **1** and **2** were purified and used for the activation of $P2Y_1R$, resulted in the increase of intracellular Ca^{2+} in PCa cell. The compound **1** and **2** induced Ca^{2+} level in a dose/time-dependent manner suggesting that these compounds are agonists for $P2Y_1R$. In addition, the activation of $P2Y_1R$ induced the cell death with IC_{50} concentration of 15–33 μM. The compound **1** and **2** promoted apoptosis and necrosis which increased ROS production and caspase 3/7 signaling. These results demonstrated that the findings are consistent with the earlier reports on the functional effect of $P2Y_1R$ activation in PCa cells[8,49]. We suggest that $P2Y_1R$ might be an attractive target for the treatment of prostate cancer. Thus it is concluded that the synthesized 1-indolinoalkyl 2-phenolic derivatives **1** and **2** could provide the new opportunity to develop $P2Y_1$-signaling mediated drugs for the treatment of PCa.

Materials and Methods

Structure model. Structure of the P2Y1R was retrieved from PDB with the identification code 4XNW[49]. The crystal structure of the human P2Y1R ~~in~~ complexed with the nucleotide antagonist MRS2500 at 2.7 Å resolution is used as a reference compound. Protein Preparation Wizard in Maestro[50] is used for the preparation of the 3D structure of the protein. Protein structure was stabilized by adding and optimizing the hydrogen atoms and bonds, removing atomic clashes, adding formal charges to the hetero groups and then optimizing at neutral pH. Finally, the structure was minuteimized with optimized potential for liquid simulations force field (OPLS-2005). The ligand binding site observed in the crystal structure is used as the control binding site whereas, docked complex with the known agonist, MRS2365 is used as the positive control. This is used to perform the further docking of 923 conformers.

Ligand library. The two-dimensional structures of 923 aminuteobenzylated phenols were generated using RD Kit library for Python and exported to Structure Data File (SDF). The ligand molecules were subjected to

LigPrep module of Schrödinger suite[51]. This module is used to generate the possible low energy stereoisomers with standard physical conditions. The prepared 923 ligands were subjected to high throughput virtual screening using the GLIDE (Grid based Ligand and Docking with Energetics) module of Schrödinger suite[52].

Docking screening. Receptor grid box for the 923 compounds were generated using the ligand binding site of the crystal structure (P2Y1R complexed with MRS2500). Ligands were docked to the protein using Glide software. Docking was performed in a "Standard Precision" (SP) mode and then by "Extra precision" mode (XP). The docked conformers were evaluated using Glide (G) Score[53].

Design and synthesis of $P2Y_1$ ligands with general remarks. The reactions were performed using the reagents from Sigma-Aldrich or TCI, and the experiment was performed under argon atmosphere. Thin-layer chromatography was done on pre-coated (Merck TLC silica gel 60 F254) aluminuteium plates, developed using cerium molybdate solution and visualized under UV light. Flash column chromatography was done on silica gel 60 (Merck, 0.040–0.063 mm). NMR spectra were recorded (Jeol ECZR 500) using $CDCl_3$ as solvent and calibration was done using tetramethylsilane as internal standard. Chemical shifts in ppm (δ) are specified to the $CDCl_3$ residual peak (δ 7.26) or TMS peak (δ 0.00) for ^{1}H NMR, to $CDCl_3$ (δ 77.16) for ^{13}C NMR. The peak splitting patterns were designated as; s = singlet, d = doublet, t = triplet, m = multiplet. Coupling constants, *J*, is represented in Hertz (Hz). High-resolution mass spectra was recorded on the Waters ESI-TOF MS spectrometer. Elemental analysis to detect C, N and H was determinuteed on Elementar vario EL III. Tested compounds shows purity > 95% upon elemental analysis. Indoline-4-carbonitrile was prepared as the earlier method for reducing the corresponding indole with triethylsilane[31] with the same spectral characterization[54] (Fig. S1 of SI).

1-(2-Hydroxy-5-nitrophenyl)(4-hydroxyphenyl)methyl)indoline-4-carbonitrile (1). Indoline-4-carbonitrile (71 mg, 0.5 mmol) was added to 2-hydroxy-5-nitrobenzaldehyde (84 mg, 0.5 mmol, 1 equiv) and (4-hydroxyphenyl) boronic acid (69 mg, 0.5 mmol, 1 equiv) in 5.0 mL DCE and 0.5 mL EtOH at 50 °C. The reaction was stirred for 70 minuteutes and the solvents were evaporated under reduced pressure. The gradient column chromatography was to purify the residue (DCM to DCM/EtOAc 85:15) to give compound **1** (152.7 mg, 0.39 mmol, 79% yield) as a light yellow solid. ^{1}H NMR (500 MHz, $CDCl_3$) δ 10.42 (br. s, 1 H), 8.12 (dd, *J* = 9.2, 2.9 Hz, 1 H), 7.98 (d, *J* = 2.9 Hz, 1 H), 7.24 (d, *J* = 8.6 Hz, 2 H), 7.12–7.06 (m, 2 H), 6.97 (d, *J* = 9.2 Hz, 1 H), 6.84 (d, *J* = 8.6 Hz, 2 H), 6.60 (d, *J* = 8.0 Hz, 1 H), 5.55 (br. s, 1 H), 5.38 (s, 1 H), 3.33 (td, *J* = 8.7, 3.8 Hz, 1 H), 3.25–3.07 (m, 3 H). ^{13}C NMR (126 MHz, $CDCl_3$) δ 161.9, 156.4, 151.1, 141.2, 136.9, 130.3, 129.3, 128.8, 126.6, 125.5, 125.0, 124.5, 117.8, 117.3, 116.3, 115.6, 109.2, 68.3, 52.9, 28.1. Elemental analysis: Calcd for $C_{22}H_{17}N_3O_4$: C, 68.21; H, 4.42; N, 10.85. Found: C, 65.03; H, 4.47; N, 9.81. HRMS (ESI/TOF): m/z calcd for $C_{22}H_{16}N_3O_4^-$ $[M-H]^-$, 386.1146; found 386.1129 (Fig. S2 and S3 of SI).

Methyl 4-((4-cyanoindolin-1-yl)(2,5-dihydroxyphenyl)methyl)benzoate (2). Indoline-4-carbonitrile (71 mg, 0.5 mmol) was added to a solution of 2,5-dihydroxybenzaldehyde (69 mg, 0.5 mmol, 1 equiv) and (4-(methoxycarbonyl)phenyl)boronic acid (90 mg, 0.5 mmol, 1 equiv) in 5.0 mL DCE at 50 °C. The reaction was agitated continuously for 20 h and the solvent were evaporated under reduced pressure. The residue was purified (gradient column chromatography, hexane/iPrOH 85:15 to hexane/iPrOH 80:20) to produce compound **2** (165.3 mg, 0.41 mmol, 83% yield) as an off-white solid. ^{1}H NMR (500 MHz, $CDCl_3$) δ 7.94 (d, *J* = 8.0 Hz, 2 H), 7.40 (d, *J* = 8.6 Hz, 2 H), 7.31 (br. s, 1 H), 6.95 (t, *J* = 7.7 Hz, 1 H), 6.90 (d, *J* = 7.4 Hz, 1 H), 6.73 (d, *J* = 8.6 Hz, 1 H), 6.66 (dd, *J* = 8.6, 2.9 Hz, 1 H), 6.52 (d, *J* = 2.9 Hz, 1 H), 6.43 (d, *J* = 8.0 Hz, 1 H), 5.89 (br. s, 1 H), 5.62 (s, 1 H), 3.87 (s, 3 H), 3.27 (t, *J* = 8.3 Hz, 2 H), 3.13–3.01 (m, 2 H). ^{13}C NMR (126 MHz, $CDCl_3$) δ 167.2, 151.7, 149.6, 148.3, 144.6, 135.7, 130.2, 129.5, 128.5, 128.5, 126.1, 121.8, 117.7, 117.5, 116.2, 115.7, 113.4, 108.4, 63.9, 52.5, 51.9, 27.9. Elemental analysis: Calcd for $C_{24}H_{20}N_2O_4 \bullet 1.05H_2O$: C, 68.74; H, 5.61; N, 6.68. Found: C, 68.42; H, 4.87; N, 6.60. HRMS (ESI/TOF): m/z calcd for $C_{24}H_{20}N_2O_4Cl^-$ $[M+Cl]^-$, 435.1117; found 435.1079 (Fig. S4 and S5 of SI).

Cell culture. PC-3 and DU-145 cells were maintained in Minuteimal Essential Medium Eagle (MEM; Sigma-Aldrich, St. Loius, MO, USA). HEK 293 and MEF cells were maintained in Dulbecco's modified eagle's medium. Mediums were supplemented with 10% fetal bovine serum (FBS; Biowest, France) and 1% penicillin/streptomycin (Sigma-Aldrich). Cells were cultured at 37 °C in humidified atmosphere of 5% CO_2. The media was changed once every 2 days. The culture was passaged using trypsin-EDTA (Sigma-Aldrich). Newly synthesized compounds **1** and **2** were diluted in dimethyl sulfoxide (DMSO, Sigma -Aldrich).

Cell viability measurement. PC-3, DU-145, HEK 293 and MEF cells were seeded with 1×10^4 cells/well in 96-well plates. At 70–80% confluence, cells were exposed to compound **1**, **2**, DMSO, and MRS2365 for 48 h. MTT and cytotoxicity assay (Bosterbio, CA, USA) was done to check the cell viability, as instructed by the manufacturer and the absorbance was measured at 570 nm using Magellan™ microplate reader (Tecan Group Ltd., Switzerland). Briefly, the cytotoxicity index was determinuteed using the untreated cells as control. DMSO was used as the vehicle control against compound **1** and **2**. The inhibition percentage of each compound, was calculated using the equation given below[55].

$$\%\ inhibition = \frac{A_c - A_{tr}}{A_c} \times 100$$

A_c, cell number of untreated cells; A_t, cell number of treated cells. A half maximal inhibitory concentration (IC_{50}) was determinuteed using the curve fitting program Prism 7.0 (GraphPad Software Inc., La Jolla, CA, USA).

Cell proliferation assay. 96-well plates was seeded with 1×10^4 cells/well concentration of PC-3 and DU-145. The overnight cultured cells were treated with compound **1** and **2** with the IC_{50} concentration or 2 mM sodium orthovanadate (Na_3VO_4; positive control)[56], and maintained in the 5% CO_2 incubator for 24 h, 48 h, and 72 h. MTT cell proliferation and cytotoxicity assay was performed to measure the cell survival following the manufacturer's instruction and the absorbance was measured at 570 nm using Magellan™ microplate reader. The cell viability was calculated as the percentage of cell number of treated cells relative to cell number of untreated cells at 24 h, 48 h, and 72 h.

Calcium kinetic assay. To carry out calcium kinetic assay, PC-3 and DU-145 cells 96-well black plate was plated with 1×10^4 cells/well as previously described[57]. After overnight incubation, the cells were washed with warm 1X phosphate buffered saline (PBS) (pH 7.2). The cells were further incubated with 2 µM Fura 2-AM (Sigma-Aldrich) and 0.01% Pluronic® F-127 (Sigma-Aldrich) in PBS for 30 minute at RT in dark condition. Compound **1** and **2** were prepared in PBS with varying concentration of 6.25 µM, 12.5 µM, 25 µM, 50 µM, and 100 µM. The reaction was started on adding the compounds to the dye and the fluorescence intensity was measured using Magelan™ microplate reader at 37 °C at every 5 minute. The excitation was calculated in two different alternative wavelength 340 nm and 380 nm and the emission of fluorescence was measured at 510 nm. The fold change of intracellular calcium was calculated following the equation below[58].

$$F_{340/380} = \frac{F_{340}^{tr} - F_{340}^{bg}}{F_{380}^{tr} - F_{380}^{bg}}$$

$F_{340/380}$, fold change of intracellular calcium; F_{340}^{tr} Emitted fluorescence intensities of samples with compound at 340/510 nm; F_{380}^{tr} Emitted fluorescence intensities of samples with compound at 380/510 nm; F_{340}^{bg} Background corrected emitted fluorescence intensities of samples without compound at 340/510 nm; F_{380}^{bg} Background corrected emitted fluorescence intensities of samples without compound at 380/510 nm. siRNA assay was also performed to check the specificity of the ligand binding with $P2Y_1R$. Predesigned siRNA against human $P2Y_1R$ was commercially synthesized (cat no. AM16708; Thermo Fisher Scientific, Waltham, MA, USA). PCa cells with the confluence of 60–70% were transfected with 20 nM of siRNA by Lipofectamine RNAiMAX Transfection Reagents (cat no. 13778030; Thermo Fisher Scientific). After 48 h of transfection, cells were measured to quantify the changes in the intracellular calcium level.

Detection of reactive oxygen species (ROS) formation. 12-well plates was seeded with 1×10^5 cells/well of PC-3 and DU-145 cells. After incubation overnight, the cells were treated with compound **1** and **2** for 5 h with their respective IC_{50} concentration or 10 mM hydrogen peroxide (H_2O_2), as positive control for ROS[59,60]. The cells were centrifuged at 3,000 rpm for 10 minute and the cell pellets were harvested. Cells were stained with 2 µM molecular probe 2',7'-dichlorodihydroflurescein diacetate (H_2DCFDA) for 10 minute in the dark. Subsequently, the stained cells were washed with warm PBS and incubated in the medium for 20 minute. Florescence of ROS was measured at 485 nm and 538 nm using Magelan™ microplate reader. The fold change of ROS product was determinuteed using the equation mentioned below[61].

$$Fold\ increase = \frac{F_{test} - F_{blank}}{F_{control} - F_{blank}}$$

F_{test} - fluorescence of the treated wells; $F_{control}$ - fluorescence of the untreated wells; F_{blank}- fluorescence of the unstained wells.

Apoptosis detection. To determinutee the ability of the compounds to induce cellular apoptosis, PC-3 and DU-145 cells were plated with 5×10^5 cells/well in 6 well plate. Cells were treated with compound **1** or **2** at IC_{50} concentration of each compound for 48 h. The cells were washed twice with PBS, and resuspended in 50 µl binding buffer, 2.5 ml Annexin V-FITC and 0.5 µl 7-aminuteoactinomycin D (7-AAD, labels GC-rich regions of DNA in permeabilized cells). The above mix of cells were incubated for 15 minute in the dark, followed by the addition of 200 µl binding buffer. Approximately 300 cells were analyzed by epifluorescence microscope (Nikon-Eclipse Ti-E inverted fluorescence microscope) under 20X objective for each analysis. Three biological repeats and two technical were used for each condition.

Caspase 3/7 assay. PC-3 and DU-145 cells were plated in 96-well white plate at a density of 1×10^4 cells/well 100 µl of cell culture medium. After 24 h of incubation, the cells were treated with IC_{50} concentration of the compound **1** and **2** for 5 h. Caspase 3/7 activity of cells was measured using Caspase-Glo® 3/7 Assay kit (Promega, Madison USA). Cells were equilibrated at room temperature (RT) for 30 minute. 100 µl of Caspase-Glo reagent was added to cells and incubated for 1 h at RT in dark condition. Luminuteescence of the sample was measured using Magellan™ microplate reader. The fold increase of caspase 3/7 activity was calculated by applying the equation used for ROS.

Statistical analysis. All the experiments were performed with three biological and technical repeats. The data was presented as the mean ± SEM. Statistical analysis was carried out by Student's t-test using GraphPad Prism 7.0 software. The differences among the experimental samples were analysed with one-way ANOVA. Statistical significance was considered with the P-value of <0.05.

Received: 28 May 2019; Accepted: 25 November 2019;
Published online: 12 December 2019

References

1. Van Hemelrijck, M. *et al.* Causes of death in men with localized prostate cancer: a nationwide, population-based study. *BJU Int* **117**, 507–514, https://doi.org/10.1111/bju.13059 (2016).
2. McKenzie, S. & Kyprianou, N. Apoptosis evasion: the role of survival pathways in prostate cancer progression and therapeutic resistance. *J Cell Biochem* **97**, 18–32, https://doi.org/10.1002/jcb.20634 (2006).
3. Lappano, R. & Maggiolini, M. GPCRs and cancer. *Acta Pharmacol Sin* **33**, 351–362, https://doi.org/10.1038/aps.2011.183 (2012).
4. van Jaarsveld, M. T., Houthuijzen, J. M. & Voest, E. E. Molecular mechanisms of target recognition by lipid GPCRs: relevance for cancer. *Oncogene* **35**, 4021–4035, https://doi.org/10.1038/onc.2015.467 (2016).
5. Jacobson, K. A., Balasubramanian, R., Deflorian, F. & Gao, Z. G. G protein-coupled adenosine (P1) and P2Y receptors: ligand design and receptor interactions. *Purinergic Signal* **8**, 419–436, https://doi.org/10.1007/s11302-012-9294-7 (2012).
6. Wang, X. & Chen, D. Purinergic Regulation of Neutrophil Function. *Front Immunol* **9**, 399, https://doi.org/10.3389/fimmu.2018.00399 (2018).
7. Janssens, R. *et al.* Cloning and tissue distribution of the human P2Y1 receptor. *Biochem Biophys Res Commun* **221**, 588–593, https://doi.org/10.1006/bbrc.1996.0640 (1996).
8. Wei, Q., Costanzi, S., Liu, Q. Z., Gao, Z. G. & Jacobson, K. A. Activation of the P2Y1 receptor induces apoptosis and inhibits proliferation of prostate cancer cells. *Biochem Pharmacol* **82**, 418–425, https://doi.org/10.1016/j.bcp.2011.05.013 (2011).
9. Shabbir, M., Ryten, M., Thompson, C., Mikhailidis, D. & Burnstock, G. Characterization of calcium-independent purinergic receptor-mediated apoptosis in hormone-refractory prostate cancer. *BJU Int* **101**, 352–359, https://doi.org/10.1111/j.1464-410X.2007.07293.x (2008).
10. Li, W. H. *et al.* P2Y2 receptor promotes cell invasion and metastasis in prostate cancer cells. *Br J Cancer* **109**, 1666–1675, https://doi.org/10.1038/bjc.2013.484 (2013).
11. Wan, H. X., Hu, J. H., Xie, R., Yang, S. M. & Dong, H. Important roles of P2Y receptors in the inflammation and cancer of digestive system. *Oncotarget* **7**, 28736–28747, https://doi.org/10.18632/oncotarget.7518 (2016).
12. Mamedova, L. K., Gao, Z. G. & Jacobson, K. A. Regulation of death and survival in astrocytes by ADP activating P2Y1 and P2Y12 receptors. *Biochem Pharmacol* **72**, 1031–1041, https://doi.org/10.1016/j.bcp.2006.07.017 (2006).
13. Bilbao, P. S., Katz, S. & Boland, R. Interaction of purinergic receptors with GPCRs, ion channels, tyrosine kinase and steroid hormone receptors orchestrates cell function. *Purinergic Signal* **8**, 91–103, https://doi.org/10.1007/s11302-011-9260-9 (2012).
14. Shen, J. & DiCorleto, P. E. ADP stimulates human endothelial cell migration via P2Y1 nucleotide receptor-mediated mitogen-activated protein kinase pathways. *Circ Res* **102**, 448–456, https://doi.org/10.1161/CIRCRESAHA.107.165795 (2008).
15. Corriden, R. & Insel, P. A. New insights regarding the regulation of chemotaxis by nucleotides, adenosine, and their receptors. *Purinerg Signal* **8**, 587–598, https://doi.org/10.1007/s11302-012-9311-x (2012).
16. Yelovitch, S. *et al.* Identification of a promising drug candidate for the treatment of type 2 diabetes based on a P2Y(1) receptor agonist. *J Med Chem* **55**, 7623–7635, https://doi.org/10.1021/jm3006355 (2012).
17. Pfefferkorn, J. A. *et al.* P2Y1 receptor antagonists as novel antithrombotic agents. *Bioorg Med Chem Lett* **18**, 3338–3343, https://doi.org/10.1016/j.bmcl.2008.04.028 (2008).
18. Delekate, A. *et al.* Metabotropic P2Y1 receptor signalling mediates astrocytic hyperactivity *in vivo* in an Alzheimer's disease mouse model. *Nat Commun* **5**, 5422, https://doi.org/10.1038/ncomms6422 (2014).
19. Burnstock, G. & Di Virgilio, F. Purinergic signalling and cancer. *Purinergic Signal* **9**, 491–540, https://doi.org/10.1007/s11302-013-9372-5 (2013).
20. Janssens, R. & Boeynaems, J. M. Effects of extracellular nucleotides and nucleosides on prostate carcinoma cells. *Br J Pharmacol* **132**, 536–546, https://doi.org/10.1038/sj.bjp.0703833 (2001).
21. Ferroni, C. *et al.* 1,4-Substituted Triazoles as Nonsteroidal Anti-Androgens for Prostate Cancer Treatment. *J Med Chem* **60**, 3082–3093, https://doi.org/10.1021/acs.jmedchem.7b00105 (2017).
22. Wang, M. *et al.* Design, synthesis and antitumor activity of Novel Sorafenib derivatives bearing pyrazole scaffold. *Bioorg Med Chem* **25**, 5754–5763, https://doi.org/10.1016/j.bmc.2017.09.003 (2017).
23. Kaur, R. *et al.* Anti-cancer pyrimidines in diverse scaffolds: a review of patent literature. *Recent Pat Anticancer Drug Discov* **10**, 23–71 (2015).
24. Roman, G. Mannich bases in medicinal chemistry and drug design. *Eur J Med Chem* **89**, 743–816, https://doi.org/10.1016/j.ejmech.2014.10.076 (2015).
25. Yadav, Y. *et al.* Design, synthesis and bioevaluation of novel candidate selective estrogen receptor modulators. *Eur J Med Chem* **46**, 3858–3866, https://doi.org/10.1016/j.ejmech.2011.05.054 (2011).
26. Doan, P., Nguyen, T., Yli-Harja, O., Candeias, N. R. & Kandhavelu, M. Effect of alkylaminophenols on growth inhibition and apoptosis of bone cancer cells. *Eur J Pharm Sci* **107**, 208–216, https://doi.org/10.1016/j.ejps.2017.07.016 (2017).
27. Latorraca, N. R., Venkatakrishnan, A. J. & Dror, R. O. GPCR Dynamics: Structures in Motion. *Chem Rev* **117**, 139–155, https://doi.org/10.1021/acs.chemrev.6b00177 (2017).
28. Kontoyianni, M. Docking and Virtual Screening in Drug Discovery. *Methods Mol Biol* **1647**, 255–266, https://doi.org/10.1007/978-1-4939-7201-2_18 (2017).
29. Wong, P. C., Watson, C. & Crain, E. J. The P2Y1 receptor antagonist MRS2500 prevents carotid artery thrombosis in cynomolgus monkeys. *J Thromb Thrombolysis* **41**, 514–521, https://doi.org/10.1007/s11239-015-1302-7 (2016).
30. Zhou, H. X. & Pang, X. Electrostatic Interactions in Protein Structure, Folding, Binding, and Condensation. *Chem Rev* **118**, 1691–1741, https://doi.org/10.1021/acs.chemrev.7b00305 (2018).
31. Yao, C. H. *et al.* Discovery of novel N-beta-D-xylosylindole derivatives as sodium-dependent glucose cotransporter 2 (SGLT2) inhibitors for the management of hyperglycemia in diabetes. *J Med Chem* **54**, 166–178, https://doi.org/10.1021/jm101072y (2011).
32. Li, Z., Delaney, M. K., O'Brien, K. A. & Du, X. Signaling during platelet adhesion and activation. *Arterioscler Thromb Vasc Biol* **30**, 2341–2349, https://doi.org/10.1161/ATVBAHA.110.207522 (2010).
33. Putney, J. W. & Tomita, T. Phospholipase C signaling and calcium influx. *Adv Biol Regul* **52**, 152–164, https://doi.org/10.1016/j.advenzreg.2011.09.005 (2012).
34. Guzman, S. J. & Gerevich, Z. P2Y Receptors in Synaptic Transmission and Plasticity: Therapeutic Potential in Cognitive Dysfunction. *Neural Plast* **2016**, 1207393, https://doi.org/10.1155/2016/1207393 (2016).
35. Tapia-Vieyra, J. V. & Mas-Oliva, J. Apoptosis and cell death channels in prostate cancer. *Arch Med Res* **32**, 175–185 (2001).
36. Bellezza, I., Tucci, A. & Minelli, A. 2-Chloroadenosine and human prostate cancer cells. *Anticancer Agents Med Chem* **8**, 783–789 (2008).
37. Fulda, S., Gorman, A. M., Hori, O. & Samali, A. Cellular stress responses: cell survival and cell death. *Int J Cell Biol* **2010**, 214074, https://doi.org/10.1155/2010/214074 (2010).
38. Ouyang, L. *et al.* Programmed cell death pathways in cancer: a review of apoptosis, autophagy and programmed necrosis. *Cell Prolif* **45**, 487–498, https://doi.org/10.1111/j.1365-2184.2012.00845.x (2012).
39. Zorov, D. B., Juhaszova, M. & Sollott, S. J. Mitochondrial reactive oxygen species (ROS) and ROS-induced ROS release. *Physiol Rev* **94**, 909–950, https://doi.org/10.1152/physrev.00026.2013 (2014).
40. Zorov, D. B., Filburn, C. R., Klotz, L. O., Zweier, J. L. & Sollott, S. J. Reactive oxygen species (ROS)-induced ROS release: a new phenomenon accompanying induction of the mitochondrial permeability transition in cardiac myocytes. *J Exp Med* **192**, 1001–1014 (2000).

41. Fiaschi, T. & Chiarugi, P. Oxidative stress, tumor microenvironment, and metabolic reprogramming: a diabolic liaison. *Int J Cell Biol* **2012**, 762825, https://doi.org/10.1155/2012/762825 (2012).
42. Masgras, I. *et al*. Reactive oxygen species and mitochondrial sensitivity to oxidative stress determine induction of cancer cell death by p21. *J Biol Chem* **287**, 9845–9854, https://doi.org/10.1074/jbc.M111.250357 (2012).
43. Parrish, A. B., Freel, C. D. & Kornbluth, S. Cellular mechanisms controlling caspase activation and function. *Cold Spring Harb Perspect Biol* **5**, https://doi.org/10.1101/cshperspect.a008672 (2013).
44. Man, S. M., Karki, R. & Kanneganti, T. D. Molecular mechanisms and functions of pyroptosis, inflammatory caspases and inflammasomes in infectious diseases. *Immunol Rev* **277**, 61–75, https://doi.org/10.1111/imr.12534 (2017).
45. Lamkanfi, M. & Kanneganti, T. D. Caspase-7: a protease involved in apoptosis and inflammation. *Int J Biochem Cell Biol* **42**, 21–24, https://doi.org/10.1016/j.biocel.2009.09.013 (2010).
46. Boland, K., Flanagan, L. & Prehn, J. H. Paracrine control of tissue regeneration and cell proliferation by Caspase-3. *Cell Death Dis.* **4**, e725, https://doi.org/10.1038/cddis.2013.250 (2013).
47. Calvert, R. C. *et al*. Immunocytochemical and pharmacological characterisation of P2-purinoceptor-mediated cell growth and death in PC-3 hormone refractory prostate cancer cells. *Anticancer Res* **24**, 2853–2859 (2004).
48. Hechler, B. & Gachet, C. Purinergic Receptors in Thrombosis and Inflammation. *Arterioscler Thromb Vasc Biol* **35**, 2307–2315, https://doi.org/10.1161/ATVBAHA.115.303395 (2015).
49. Zhang, D. *et al*. Two disparate ligand-binding sites in the human P2Y1 receptor. *Nature* **520**, 317–321, https://doi.org/10.1038/nature14287 (2015).
50. Sastry, G. M., Adzhigirey, M., Day, T., Annabhimoju, R. & Sherman, W. Protein and ligand preparation: parameters, protocols, and influence on virtual screening enrichments. *J Comput Aided Mol Des* **27**, 221–234, https://doi.org/10.1007/s10822-013-9644-8 (2013).
51. Friesner, R. A. *et al*. Glide: a new approach for rapid, accurate docking and scoring. 1. Method and assessment of docking accuracy. *J Med Chem* **47**, 1739–1749, https://doi.org/10.1021/jm0306430 (2004).
52. Friesner, R. A. *et al*. Extra precision glide: docking and scoring incorporating a model of hydrophobic enclosure for protein-ligand complexes. *J Med Chem* **49**, 6177–6196, https://doi.org/10.1021/jm051256o (2006).
53. Kitchen, D. B., Decornez, H., Furr, J. R. & Bajorath, J. Docking and scoring in virtual screening for drug discovery: methods and applications. *Nat Rev Drug Discov* **3**, 935–949, https://doi.org/10.1038/nrd1549 (2004).
54. Piatnitski Chekler, E. L. *et al*. 1-(2-Hydroxy-2-methyl-3-phenoxypropanoyl)indoline-4-carbonitrile derivatives as potent and tissue selective androgen receptor modulators. *J Med Chem* **57**, 2462–2471, https://doi.org/10.1021/jm401625b (2014).
55. Le, H. T. T., Cho, Y. C. & Cho, S. Methanol extract of Guettarda speciosa Linn. inhibits the production of inflammatory mediators through the inactivation of Syk and JNK in macrophages. *Int J Mol Med* **41**, 1783–1791, https://doi.org/10.3892/ijmm.2018.3377 (2018).
56. Khalil, A. A. & Jameson, M. J. Sodium Orthovanadate Inhibits Proliferation and Triggers Apoptosis in Oral Squamous Cell Carcinoma *in vitro*. *Biochemistry (Mosc)* **82**, 149–155, https://doi.org/10.1134/S0006297917020067 (2017).
57. Liu, K. *et al*. A multiplex calcium assay for identification of GPCR agonists and antagonists. *Assay Drug Dev Technol* **8**, 367–379, https://doi.org/10.1089/adt.2009.0245 (2010).
58. Kumon, R. E. *et al*. Spatiotemporal effects of sonoporation measured by real-time calcium imaging. *Ultrasound Med Biol* **35**, 494–506, https://doi.org/10.1016/j.ultrasmedbio.2008.09.003 (2009).
59. Rudzka, D. A., Cameron, J. M. & Olson, M. F. Reactive oxygen species and hydrogen peroxide generation in cell migration. *Commun Integr Biol* **8**, e1074360, https://doi.org/10.1080/19420889.2015.1074360 (2015).
60. Ogawa, Y. *et al*. Reactive oxygen species-producing site in hydrogen peroxide-induced apoptosis of human peripheral T cells: involvement of lysosomal membrane destabilization. *Int J Mol Med* **13**, 383–388 (2004).
61. Barzegar, A. & Moosavi-Movahedi, A. A. Intracellular ROS protection efficiency and free radical-scavenging activity of curcumin. *PLoS One* **6**, e26012, https://doi.org/10.1371/journal.pone.0026012 (2011).

Acknowledgements

H.L. acknowledge the TUT-RAE for the project grant support and Tampere University of Technology for Instrumental facility grant support. N.R.C acknowledge the JAES for the project support and publication.

Author contributions

T.R. and N.R.C. synthesized and characterized the compounds; H.L. executed the experiments and data analysis. K.M.S. executed the docking and virtual screening O.Y., N.R.C. and M.K. conceived and managed all studies. H.L., A.M. and M.K. revised the manuscript. All the authors contributed to writing the manuscript.

Competing interests

The authors declare no competing interests.

Additional information

Supplementary information is available for this paper at https://doi.org/10.1038/s41598-019-55194-8.

Correspondence and requests for materials should be addressed to M.K.

Reprints and permissions information is available at www.nature.com/reprints.

Publisher's note Springer Nature remains neutral with regard to jurisdictional claims in published maps and institutional affiliations.

PUBLICATION II

Molecular interaction of HIC, an agonist of P2Y1 receptor, and its role in prostate cancer apoptosis

H. Le, A. Murugesan, T. Ramesh, O. Yli-Harja, K. M. Saravanan, and M. Kandhavelu

International Journal of Biological Macromolecules (2021), 198

DOI: 10.1016/j.ijbiomac.2021.08.103

International Journal of Biological Macromolecules 189 (2021) 142–150

Contents lists available at ScienceDirect

International Journal of Biological Macromolecules

journal homepage: www.elsevier.com/locate/ijbiomac

Molecular interaction of HIC, an agonist of P2Y1 receptor, and its role in prostate cancer apoptosis

Hien Thi Thu Le [a], Akshaya Murugesan [a,b], Thiyagarajan Ramesh [c], Olli Yli-Harja [d,e], Konda Mani Saravanan [f,1], Meenakshisundaram Kandhavelu [a,*,1]

[a] Molecular Signaling Lab, Faculty of Medicine and Health Technology, Tampere University, P.O. Box 553, 33101 Tampere, Finland
[b] Department of Biotechnology, Lady Doak College, Thallakulam, Madurai 625002, India
[c] Department of Basic Medical Sciences, College of Medicine, Prince Sattam Bin Abdulaziz University, Al-Kharj 11942, Saudi Arabia
[d] Computational Systems Biology Group, Faculty of Medicine and Health Technology, Tampere University, P.O. Box 553, 33101 Tampere, Finland
[e] Institute for Systems Biology, 1441N 34th Street, Seattle, WA 98103-8904, USA
[f] Scigen Research and Innovation Pvt Ltd, Periyar Technology Business Incubator, Thanjavur 613403, Tamil Nadu, India

ARTICLE INFO

Keywords:
Purinergic receptor
Indoline derivative
Drug design
Molecular simulation
Prostate cancer

ABSTRACT

Prostate cancer is a heterogeneous, slow growing asymptomatic cancer that predominantly affects man. A purinergic G-protein coupled receptor, P2Y1R, is targeted for its therapeutic value since it plays a crucial role in many key molecular events of cancer progression and invasion. Our previous study demonstrated that indoline derivative, 1 ((1-(2-Hydroxy-5-nitrophenyl) (4-hydroxyphenyl) methyl)indoline-4-carbonitrile; HIC), stimulates prostate cancer cell (PCa) growth inhibition *via* P2Y1R. However, the mode of interaction of P2Y1R with HIC involved in this process remains unclear. Here, we have reported the molecular interactions of HIC with P2Y1R. Molecular dynamics simulation was performed that revealed the stable specific binding of the protein-ligand complex. *In vitro* analysis has shown increased apoptosis of PCa-cells, PC3, and DU145, upon specific interaction of P2Y1R-HIC. This was further validated using siRNA analysis that showed a higher percentage of apoptotic cells in PCa-cells transfected with P2Y-siRNA-MRS2365 than P2Y-siRNA-HIC treatment. Decreased mitochondrial membrane potential (MMP) activity and reduced glutathione (GSH) level show their role in P2Y1R-HIC mediated apoptosis. These *in silico* and *in vitro* results confirmed that HIC could induce mitochondrial apoptotic signaling through the P2Y1R activation. Thus, HIC being a potential ligand upon interaction with P2Y1R might have therapeutic value for the treatment of prostate cancer.

1. Introduction

Prostate cancer (PCa) is the second leading cause of death in men and the rate of incidence of metastasis PCa has increased significantly in recent years. The treatment for PCa is grounded on surgical removal, radiotherapy, and hormone therapy. Promising molecule(s) or ligands with clinical value have to be yet explored to reduce the PCa associated deaths. The primary goal of drug discovery is to critically investigate the potential ligands responsible for signaling processes controlling various cellular behaviors [1,2]. To identify such ligands with desired clinical outcomes, computational approaches play a promising role.

Gunaine-Protein Coupled Receptors (GPCRs) are the largest and most important integral membrane receptors [3,4] that serve as attractive targets due to their therapeutic relevance in various diseases, especially cancer. It is estimated that more than 800 GPCRs are encoded in the human proteome [5]. Most of these are seven helical transmembrane signaling proteins and are found as the target for about approximately 700 approved drugs [6]. The GPCRs exhibit an extracellular amino terminus and an intracellular carboxy-terminus to perform important physiological roles in the cell by interacting with a diverse set of ligands [7–9].

GPCRs are divided into six classes, namely Class A (rhodopsin-like

Abbreviations: HIC, 1 ((1-(2-hydroxy-5-nitrophenyl) (4-hydroxyphenyl) methyl)indoline-4-carbonitrile); P2Y1R, purinergic G-protein coupled receptor; MMP, mitochondrial membrane potential; GSH, tripeptide, γ-L-glutamyl-L-cysteinyl-glycine; PCa, prostate cancer; GPCRs, Gunaine-Protein Coupled Receptors; PBS, phosphate buffered saline; DMSO, diluted in dimethyl sulfoxide.

* Corresponding author.
E-mail address: Meenakshisundaram.kandhavelu@tuni.fi (M. Kandhavelu).

[1] Equal contribution.

https://doi.org/10.1016/j.ijbiomac.2021.08.103
Received 30 June 2021; Received in revised form 11 August 2021; Accepted 12 August 2021
Available online 20 August 2021

receptors), Class B (secretin family), Class C (metabotropic glutamate receptors), Class D (fungal mating pheromone receptors), Class E (cAMP receptors), and Class F (frizzled FZD), and smoothened (SMO) receptors [10,11]. These different classes of GPCRs located on the cell surfaces can bind to specific ligands to transmit a signal into the cell in order to perform important diverse cellular functions [12–14]. Thus, the conformational dynamics of GPCRs is extremely important for the cellular signaling process [15,16].

P2Y receptors are purinergic GPCRs, believed as a common biological target that is activated by the extracellular signaling molecules like nucleotides such as Adenosine Tri Phosphate (ATP) and Uridine Diphosphate (UDP) [17,18]. The use of P2Y receptor as a potential therapeutic target for the treatment of acute diseases such as different types of cancer, inflammation, and digestive diseases could have far-reached the clinical consequences [19,20]. Recently, it has been suggested that the platelet aggregation aided by the P2Y1 receptor (P2Y1R), makes it as an important antithrombotic drug target [21,22].

The availability of crystallographic structure of GPCR in protein data bank has advanced the structural data analysis on GPCR through computer-aided drug discovery. The crystal structures of the human P2Y1R in complex with a nucleotide antagonist MRS2500 and a non-nucleotide antagonist BPTU were reported [23] with the resolution of 2.7 Å and 2.2 Å, respectively. The atomic crystal structures of the human P2Y1R bound to MRS2500 and BPTU help us in understanding the mechanism of these anti-thrombotic ligands identifying their purinoreceptor target, allowing for new drug discovery. Interestingly, the structures show two different ligand binding sites, revealing the atomic details of P2Y1R's ligand binding modes [23]. P2Y1R's seven transmembrane bundles contain a binding site that could be recognised by MRS2500, where BPTU binds to an allosteric pocket on the lipid bilayer's external receptor interface. The overall architecture of P2Y1R and ligand binding modes were detailed by Zhang et al. [23].

In our previous research, to better understand the molecular insights of P2Y1R's in PCa drug discovery, 923 derivatives of 1-indolinoalkyl 2-phenolic compound were tested by molecular docking [20]. The docking resulted in the identification of two compounds that are further chemically synthesized and experimentally optimized as potent P2Y1 agonists. Moreover, we have shown that P2Y1R as a potential onco-target and its activation caused apoptosis in PCa cells through the Capase3/7 and ROS signaling pathways [20]. In the present work, we have explored the protein-ligand interactions of the identified phenolic compound with P2Y1R. Also, we have performed a 100 ns atomic molecular dynamics simulation to understand the binding and stability of the protein-ligand complex (P2Y1-HIC) with reference to the crystal complex (P2Y1-MRS2500). The action of P2Y1R and the anti-cancer effects of novel ligand in PC3 and DU145 cells also have been explored through various assays like apoptosis, mitochondrial membrane potential (MMP), and glutathione (GSH). The above findings provided an insight into the identified ligand as a novel therapeutic agent for prostate cancer treatment.

2. Materials and methods

2.1. Structural models

The sequence of P2Y1R (Uniprot ID: P47900, 373 amino acids; PDB ID: 4XNW at 2.70 Å resolution) was obtained from Protein Data Bank [24]. The P2Y1 protein model shares a canonical seven transmembrane helices each flanked by the topological domain like other known GPCR structures. In our earlier studies, to better comprehend the molecular insights of the P2Y1 receptor (P2Y1R), a docking study with 923 compounds was done on the crystal structure of the receptor [20]. The RD Kit library for Python was used to generate the two-dimensional structures of 923 ligands, which were then exported to a Structure Data File (SDF). The ligand molecules were subjected to the Schrödinger suite's LigPrep module [25]. The ligand-binding region of the crystal structure (P2Y1R complexed with MRS2500) was used to build the receptor grid box for the 923 molecules. Using the GLIDE (Grid-based Ligand and Docking with Energetics) module of the Schrödinger suite, the produced 923 ligands were subjected to high throughput virtual screening [26,27]. Glide software was used to dock ligands to the protein. Docking was done in two modes: "Standard Precision" (SP) and "Extra Precision" (XP). Glide (G) Score was used to evaluate the docked conformers. The best ligand-like compound 1((1-(2-Hydroxy-5-nitrophenyl)(4-hydroxyphenyl) methyl)indoline-4-carbonitrile; HIC) with the highest docking score, that satisfies Lipinski's rule was selected for further analysis. The high glide score of HIC was considered in the present study indicates its high binding affinity towards the P2Y1R.

2.2. Molecular dynamics simulations

The crystal structure of P2Y1-MRS2500 and P2Y1-HIC obtained through molecular docking was subjected to molecular dynamics simulations in the lipid environment. The purpose of these simulations was to analyze the protein conformational dynamics in a membrane environment and to check its stability [28,29]. GROMACS 4.6 software was used to perform the molecular dynamics simulations with GROMOS force field parameter which is the commonly used lipid force field [30]. The protein was oriented by aligning its principal axis along the *Z*-axis by using la101psx module in the VMD [31] and the periodic boundary conditions were applied to the xyz dimension. The topology of the ligand was generated using ACPYPE antechamber [32]. The protein was inserted in the lipid bilayer made up of DOPC molecules and each lipid was complemented by water molecules. A 1 ns isothermal-isovolumetric ensemble (NVT- Constant Number Volume and Temperature & NPT-Constant Number Pressure and Temperature) simulation was performed to equilibrate the water box at position restrain of protein heavy atom with force constant 1000 kJ/(mol*Å) in x, y, z dimension. Subsequently, another 100 ns NPT ensemble MD simulation was used for the production simulation. The Nosé–Hoover thermostat and Parrinello-Rahman barostat were used for the simulation with a fixed temperature of 300 K and a pressure of 1 atm. The plots were generated by using Gnuplot program (http://www.gnuplot.info/).

2.3. Chemicals

Compound HIC was synthesized as previous mentioned (Le et al., 2019). MRS2365 (Cat no. 2157) was purchased from Tocris Bioscience (Bristol, England) and benzyl isothiocyanate (BITC; cat no. 252492-5g) from Sigma-Aldrich (St. Louis, MO; USA). HIC diluted in dimethyl sulfoxide (DMSO; cat no. D2650-100ML, Sigma-Aldrich) was used as working solution.

2.4. Cell culture

Human PCa cell lines PC3 and DU145 cells were maintained in Minimum essential medium eagle (MEME; cat no. M4655-6X500ML, Sigma-Aldrich) supplemented with 10% Fetal bovine serum (FBS; cat no. S181H-500, Biowest, Nuaille, France), 0.1 mg/mL Streptomycin, 100 U/mL Penicillin (Cat no. P4333, Sigma-Aldrich), and 0.025 mg/mL Amphotericin B (Cat no. A9528-50MG, Sigma-Aldrich). The cells were cultured periodically using 1× trypsin (Cat no. 25-3000-054, ThermoFisher Scientific, Waltham, MA, USA) and maintained at 37 °C in a humidified incubator supplied with 5% CO_2.

2.5. siRNA P2Y1R ASSAY

siRNA P2Y1R was designed and purchased from Thermo Fisher Scientific Inc. (Cat no. AM16708). The sequence for the synthesis of siRNA was mentioned as follow: sense, 5′GCCCUGAUCUUCUACUACUTT 3′; antisense, 5′ AGUAGUAGAAGAUCAGGGCTG 3′. PC3 and DU145 were seed in 6 well-plate at a

density of 3×10^5 cells/well. The cells at a confluence of 60%–70% were transfected with siRNA at a concentration of 1 μM using Lipofectamine RNAiMAX Transfection Reagent (Cat no. 13778030, Thermo Fisher Scientific, Waltham, MA, USA). The transfected cells were maintained in the appropriate cell culture condition until they reach a confluence of 80% to 90% which was subjected for apoptosis assay.

2.6. Apoptotic staining assay

To determine the selective agonist potential of HIC on PCa cells, apoptotic assay was performed using Dead cell apoptosis kit (Cat no. V13241, ThermoFisher Scientific, Waltham, MA, USA) and 4′,6-Diamidion-2-Phenylindeole, dihydrochloride (DAPI) (Cat no. D3571, Thermo Fisher Scientific). PC3 and DU145 cells transfected with siRNA were plated in 6-well plate at a density of 5×10^5 cells/well. After 24 h, cells were treated with vehicle control, DMSO (0.1%), positive control-MRS2365 (1 μM), and IC_{50} concentration of HIC (*i.e.*, 15.98 μM for PC3 cells and 15.64 μM for DU145 cells) for 48 h. The cells were collected and washed twice with warm phosphate buffered saline (PBS). Sequentially, cells were incubated with 1× Annexin-binding buffer supplied with the kit for 15 min in the dark condition. Further, FITC conjugated Annexin V, propidium iodide (PI), and DAPI were added to the cell suspension and incubated for 15 min in CO_2 incubator. The fluorescence images of cells were captured using EVOS FL (ThermoFisher Scientific, Waltham, MA, USA) under 20× objective for each analysis.

2.7. Mitochondrial membrane potential assay

To measure the mitochondrial membrane potential (MMP) levels of PCa, MMP assay (Cat no. MAK159-1KT, Sigma-Aldrich) was performed. PC3 and DU145 cells were seeded in 96-well black plate with clear bottom at a density of 1×10^4 cells/well. After 24 h of incubation, cells were treated with vehicle control DMSO (0.1%), IC_{50} concentration of HIC (*i.e.*, 15.98 μM for PC3 cells and 15.64 μM for DU145 cells), and benzyl isothiocyanate (BITC, as a positive control at a concentration of 20 μM) [33,34]. After 48 h of treatment, 50 μl of JC-10 dye in buffer A was added to the cells and incubated for 1 h. Further, the cells were treated with 50 μl of buffer B for 5 min before subjecting in a Magellan™ microplate reader (Tecan Group Ltd., Switzerland). The plates were measured at a bottom-read using dual fluorescence with the excitation/emission of red/green (*red*: excitation 540 nm, emission 590 nm and *green*: excitation 490 nm, emission 525 nm). The ratio of red/green fluorescence intensity was used to determine the MMP using the Eq. (1)

$$\text{Fold change} = \frac{F_{RT} - F_{RB}}{F_{GT} - F_{GB}} \quad (1)$$

where, F_{RT} is red fluorescence of samples treated with drugs; F_{RB} is red fluorescence of untreated samples; F_{GT} is green fluorescence of samples treated with drugs; F_{GB} is green fluorescence of untreated samples.

2.8. Glutathione assay

Glutathione (GSH: tripeptide, γ-l-glutamyl-l-cysteinyl-glycine) in PC3 and DU145 cells were determined using Glutathione colorimetric detection kit (Cat no. EIAGSHC, ThermoFisher Scientific Waltham, MA, USA) following the manufactures' protocol. Briefly, cells were treated with vehicle control, DMSO (0.1%), IC_{50} concentration of HIC (*i.e.*, 15.98 μM for PC3 cells and 15.64 μM for DU145 cells), and positive control, BITC at a concentration of 20 μM for 48 h. Sequentially, the cells were washed with ice cold PBS and resuspended in 5% aqueous 5-sulfosalicylic acid dehydrate (SSA). The cells were then lysed using cold lysate buffer (PBS buffer containing 1 mM ethylenediaminetetraacetic acid (EDTA)). The supernatant was collected by centrifugation of the cell lysates at 12,000 rpm for 10 min at 4 °C. Approximately a volume of 50 μl collected supernatant was added in 96-well back plate which is suspended with 25 μl of colorimetric detection reagent and 25 μl of reaction mixture provided in the kit. The absorbance of samples was read at 405 nm using a Magellan™ microplate reader. The percentage of GSH production was calculated using the absorption of samples as the mention in the kit.

2.9. Statistical analysis

All the experiments were performed three or five times with the same biological and technical repeats. The results are presented as means ± standard error of the mean (SEM) based on IBM SPSS Statistics version 26 (IBM APSS Statistics version, NY, USA). Statistical analysis was analysed using *t*-test. Differences between two more samples and experiments were calculated using one-way ANOVA. The data were considered as statistically significant results with $*p < 0.05$.

3. Results

3.1. Sequence analysis

Human P2Y receptors comprise eight subtypes of GPCRs that belong to the Class-A family, respond to both adenine and/or uracil nucleotides [35]. Homology search using SWISS-PROT and TrEMBL databases against the subsets of *Homo sapiens*, revealed 68 proteins with high similarity to P2Y receptors. Low sequence identity was observed between rhodopsin and the P2Y receptors and hence multiple-sequence alignment of the retrieved proteins using rhodopsin as the template was performed. Thus, the phylogenetic tree was constructed that clearly delineated two distinct subgroups of P2Y receptors, such as Gq-coupled subtypes (*e.g.*, P2Y1) and Gi couple subtypes (*e.g.*, P2Y12). Fig. 1 obtained from the sequence features page of Protein Data Bank (PDB) schematically represents the sequence-structure-binding of P2Y receptor that evidenced the similar structural arrangements of both P2Y and CysLT receptors targeted by the endogenous ligands like CysLT and UDP. In the figure, a scale at the top represents the P2Y amino acid residue's position in the sequence. The red and yellow color bars at different positions indicate the secondary structural elements such as helix and strand respectively. The binding site residue's position is shown as blue and red balls whereas glycosylation and metal-binding sites are indicated as green balls. In the end, transmembrane helices and topological domain regions are shown as green and blue color bars.

These families of receptors (CysLT and P2Y) shows a highly conserved structural topology with seven transmembrane helices connected by three extracellular and intracellular loops, of which the eighth amphipathic helix act as an extracellular amino-terminal region and a cytoplasmic carboxyl-terminal tail [23]. Both P2Y and CysLT receptors that belong to the purine receptor cluster, share a typical seven-transmembrane spanning topology activated by nucleotides. However, this cluster has several "orphan receptors" responding to multiple unidentified endogenous ligands, of which GPR17 was found to be a common ancestral progenitor evolved from P2Y and CysLT receptors [36]. The availability of the P2Y family of receptor's atomic structure solved at high resolution made us to perform various structural analyses to gain insights about ligand-binding aspects.

3.2. Structure analysis

A typical P2Y1R was found to be targeted by two endogenous ligands like CysLT and UDP. The P2Y1R structure is solved experimentally in complex with MRS2500 and detailed receptor-ligand interactions are reported earlier [23]. The reported crystal structure of P2Y1R reveals the presence of two distinct ligand binding sites binding with nucleotide antagonist (MRS2500 binding within seven transmembrane bundles) and non-nucleotide antagonist (BPTU binding to external receptor interface with the lipid bilayer) at high resolution. The binding sites in

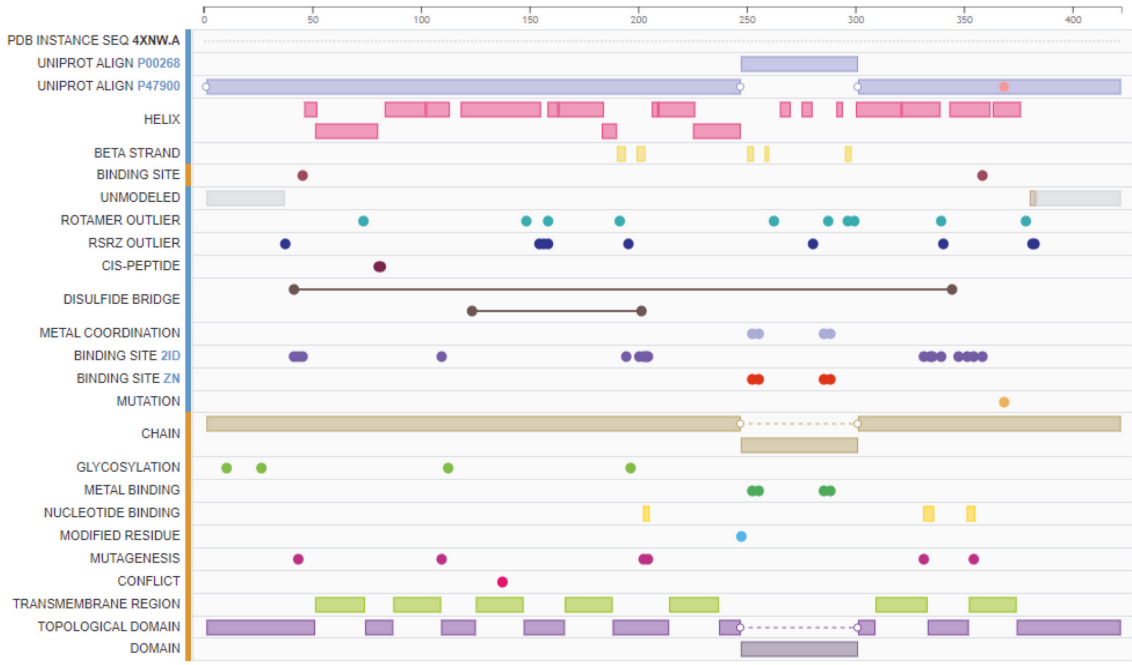

Fig. 1. Sequence-structure-binding information about P2Y1 receptor is presented schematically.

the crystal structure of P2Y1R are mainly made up of helices and have distinct geometrical features. The three-dimensional representation of P2Y1-MRS2500 complex (used as a control to make comparisons) solved crystallographically (Fig. 2A) and P2Y1-HIC complex obtained by glide docking (Fig. 2B) was shown in Fig. 2. The glide docking score of P2Y1-HIC is −7.38. To make a comparison, we have docked the MRS2500 with P2Y1 which resulted in a −8.80 glide score. The two-dimensional ligand interaction profile and glide docking score of P2Y1-HIC (Fig. 2) revealed the relatively strong interaction as observed in the P2Y1-MRS2500 crystal structure. We have observed that 14 amino acid residues of HIC interact with P2Y1R whereas; the control compound MRS2500 has shown 20 amino acids interaction with P2Y1R. The P2Y1-HIC formed four conventional hydrogen bonds (203TYR, 204ASP, 205THR, and 208ASP), whereas P2Y1-MRS2500 formed five conventional hydrogen bonds (204ASP, 205THR, 283ASN, 303TYR, and 306TYR). The amino acid residues like 46LYS and 95ARG in P2Y1 form salt bridges with HIC as observed in the control structure. The van der Waals hydrophobic interaction between P2Y1-HIC is similar to that of P2Y1-MRS2500 which is evident from Fig. 2. We observed that the stabilising interactions between P2Y1-HIC and P2Y1-MRS2500 are quite comparable, including hydrogen bonds, salt bridges, and van der Waals hydrophobic interactions.

3.3. Molecular dynamics simulations

P2Y1R complexed with MRS2500 and HIC was prepared to perform all-atom molecular dynamics simulations in a lipid bilayer environment to understand the stability of the molecules. The average Root Mean Square Deviation (RMSD) of protein backbone in P2Y1-MRS2500 is about 0.5 Å (Fig. 3A) and P2Y1-HIC (Fig. 3B) is about 0.6 Å throughout the 100 ns simulation time. The P2Y1-HIC complex (P2Y1-MRS2500 as control) is found to be stable in terms of RMSD. To further explore the energetics of complexes, we have computed the total energy of the system and found that the energy of P2Y1-MRS2500 (Fig. 3C) and P2Y1-HIC (Fig. 3D) is relatively comparable throughout the simulation time. The average total energy of the system is −325,000 kJ/mol.

The largest values were found in the root mean square fluctuations (RMSFs) of movement by individual amino acid residues involved in ligand binding and catalysis throughout the sequence (Supplementary Fig. 1A and C). The distance (≥3.5 Å) and the hydrogen donor–hydrogen acceptor angle (30°) were used to compute hydrogen bond formation using Gromacs tools. Also, the number of hydrogen bonds formed by the amino acid residues of P2Y1R-HIC complex (Supplementary Fig. 1B) is comparable with P2Y1-MRS2500 (Supplementary Fig. 1D) crystal complex. Not surprisingly, it is evident from the results that the P2Y-MRS2500 crystal structure was found to be more stable when compared to the P2Y1- HIC complex.

3.4. Induction of apoptosis by HIC in prostate cancer cells

Our previous study has revealed the ability of HIC in inducing apoptosis in Pca cells, PC3 and DU145 [20]. Also, it was proven that the activation of P2Y1R inhibits cell proliferation and increases apoptotic responses in PC3 cells [37]. In the present study, in order to further investigate the selectivity of HIC towards P2Y1R, we have performed the apoptosis assay in PCa cells in the inhibition of P2Y1 protein expression. The fluorescent images of PC3 and DU145 cells transfected cells with and/or without P2Y1 siRNA showed the presence of apoptotic cells (Fig. 4A and B). HIC and MRS2365 induced apoptosis to about 25.32% and 24.7% respectively, in P2Y1-siRNA (−/−) transfected PC3 cells. Whereas, the P2Y1 siRNA (+/+) transfected PC3 cells showed 18.4% and 18.3% respectively, upon HIC and MRS2365 treatment (Fig. 4A). Similarly, in P2Y1-siRNA (−/−) transfected DU145 cells, the induction of apoptotic was observed to be 30.3% and 24.7%, whereas P2Y1 siRNA (+/+) showed 20.4% and 15.4% upon HIC and MRS2365 treatment, respectively (Fig. 4B). These data revealed the possibility of interaction between P2Y1 and HIC which can act as an agonist and induces apoptosis in PCa cells. Also, the efficient binding of HIC to P2Y1R was

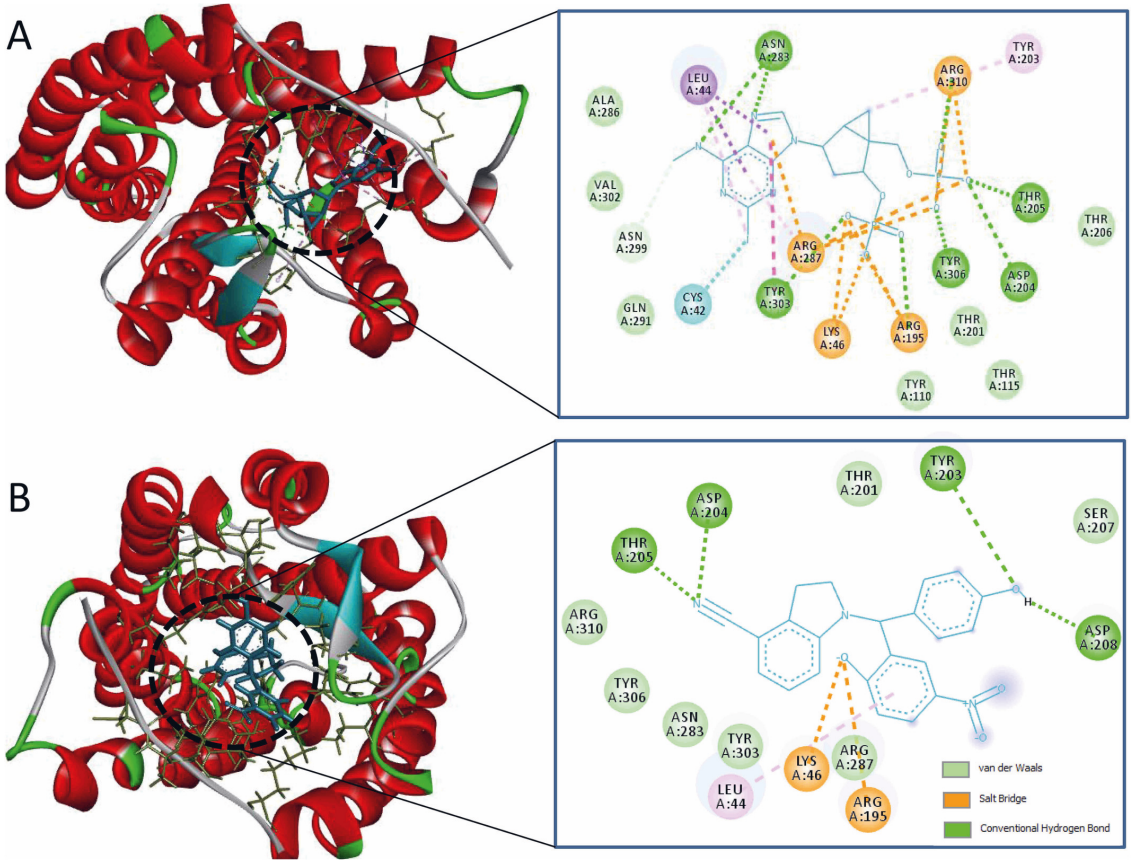

Fig. 2. Structure analysis.
A. Crystal structure of P2Y1-MRS2500 complex and its two-dimensional chemical interactions. B. The P2Y1-HIC complex obtained from glide docking and its two-dimensional chemical interactions. The figure is generated by using discovery studio visualizer's plotting option.

evident from the apoptosis data where higher percentage of apoptosis was observed in PCa cells transfected with P2Y-siRNA treated MRS2365 than the cells transfected with P2Y-siRNA treated HIC.

3.5. Role of HIC in inhibiting mitochondrial membrane activity

Mitochondria influences many cellular processes such as cell metabolism, cell growth, cell communication, and apoptosis. MMP plays a critical role in mitochondrial activity due to its reflections on the process of election transport *via* cell membranes and reactive oxygen species (ROS) generations under ATP activation [38–40]. Since high levels of ROS production can activate apoptosis process, injury cancer cells appear the collapse of MMP and lead to the release of cytochrome C into the cytosol [38]. One of the results of this mechanism is to trigger other downstream events in the apoptosis cascade by P2Y1 receptor signaling activation on binding of HIC ligand. The previous study has reported that HIC induces apoptotic cells and increases ROS production after 48 h incubation in PCa cells. In this study, in order to further investigate the anti-cancer activity of HIC through the influence of MMP production, we have performed MMP assay in PC3 and DU145 cells incubated with HIC and BITC (positive control). As shown in Fig. 5A, the level of MMP decreased in the presence of HIC and BITC in both the PC3 and DU145 cells than the vehicle control, DMSO. A fold change of 0.14- and 0.28- was observed in HIC treated PC3 and DU145 cells, respectively with 0.74- and 0.71-fold change in BITC treated PC3 and DU145 cells, respectively. These data demonstrated the efficiency of HIC in inhibiting the activity of MMPs through the activation of P2Y1 receptor downstream signaling, thereby regulating the crucial behaviors of the PCa disease progression.

3.6. Suppression of HIC in glutathione

ROS production exhibits in normal and abnormal physiological conditions of the cells [41]. Oxidative stress was necessary for an initial increase in cell growth, cell metastasis, and angiogenesis during which ROS production might induce cell cycle arrest and cell death during cancer treatment [42,43]. GSH is the most common metabolite detected during oxidative stress and ROS production [44,45] and acts as an antioxidant that scavenges the free radicals and detoxifies the cells [46]. Our earlier data by Le et al. [20], have shown the potential of HIC in increasing the production of ROS, which further prompted us in investigating the level of GSH. It was observed from the result that GSH level was not reduced upon HIC treated PC3 cells whereas significant reduction of about 14.6% of GSH observed in DU145 cells than the DMSO treated PC3 cells. On the other hand, BITC significantly reduced the GSH level to about 28.7% and 34.6% in both PC3 and DU145 cells, respectively (Fig. 5B). These data suggest that the HIC might have specific inhibitory ability of GSH production in PCa cells.

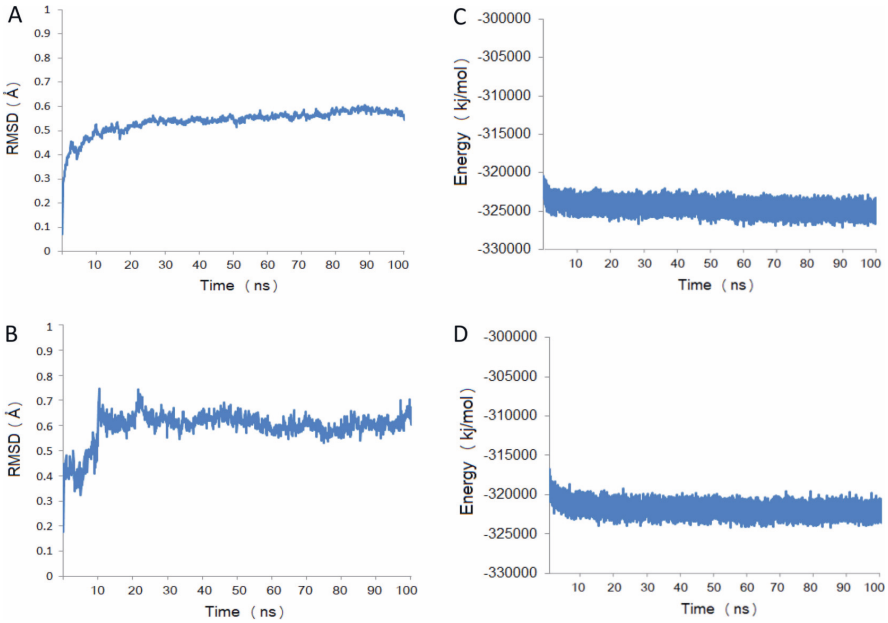

Fig. 3. Molecular dynamic simulations.
A. The backbone RMSD of P2Y1-MRS2500 for the 100 ns simulation time. B. The backbone RMSD of P2Y1-HIC for the 100 ns simulation time. C. The energy of the P2Y1-MRS2500 for the 100 ns simulation time. D. The energy of the P2Y1-HIC for the 100 ns simulation time.

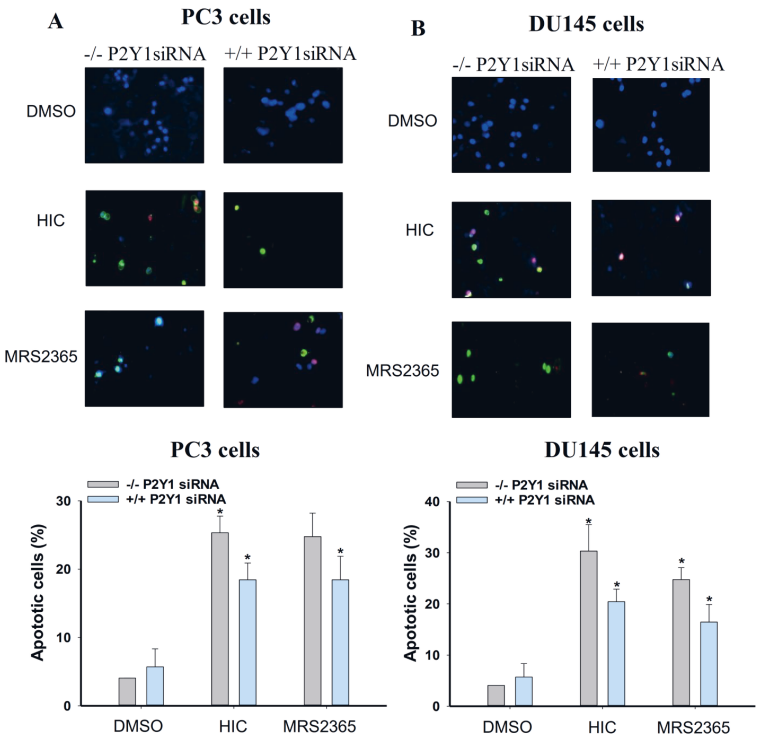

Fig. 4. Induction of apoptosis by HIC in prostate cancer cells.
Microscopic images of PC3 cells (A) and DU145 cells (B) stained with Annexin-V/PI/DAPI upon HIC treatments with DMSO as a vehicle group and MRS2365 as a positive control group. Percentage of apoptotic cells were presented in the corresponding condition. Results were showed as mean of three independent experiments, mean ± S·D, $^{*}p < 0.05$.

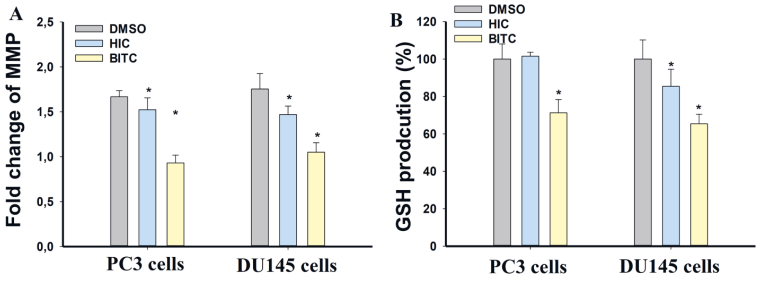

Fig. 5. Inhibition of HIC in mitochondrial membrane activity and glutathione in prostate cancer cells. (A) The fold change in MMP activity in prostate cancer cells treated with DMSO, HIC, and BITC was calculated based on fluorescence signaling measured using 96 well plate reader. (B) GSH production was determined following the absorbance of samples. The change of GSH levels was calculated using absorbance intensities of samples and untreated groups. Biological and technical replicates were remained to perform the significance of the results, with mean ± SD, *p < 0.05, $n = 3$.

4. Discussion

G protein-coupled receptors (GPCRs) are the most extensively researched therapeutic targets, owing to their importance in human pathology and pharmacological testability [47]. Various ligands are under investigation for the deorphanized GPCR to explore their clinical outcomes. Very limited GPCRs have been associated with cancer development and progression based on their differential expression. Through computer-aided drug discovery, designing small molecular ligands binding to the therapeutic membrane receptors is considered to be a challenging task. Our earlier studies on exploring the therapeutic potential of P2Y1R were done by docking the crystal structure of the receptor with 923 derivatives of 1-indolinoalkyl 2-phenolic compound. The best hits were synthesized and found to be an effective P2Y1 agonists. The protein-ligand interactions and the molecular dynamics simulation of P2Y1-HIC complex revealed the binding stability by forming hydrogen bonds throughout the simulation time and atomic interaction pattern of the defined receptor-ligand complex.

Further, the selectivity of HIC for P2Y1R and its anti-cancer effects against PC3 and DU145 cell models was analysed. HIC was found to induce apoptosis in PCa cells and induces ROS production based on the activation of P2Y1R after 48 h treatment [20]. P2Y1R siRNA analysis revealed that the HIC treated PCa cells showed less percentage of apoptosis than the cells in the absence of siRNA, revealing the binding specificity of HIC to P2Y1R. Similar data was also observed in computational model where HIC could act as a selective agonist of P2Y1R in PC3 and DU145 cells.

Consequently, much attention has been focused on developing MMP inhibitors (MMPIs) as a new class of anticancer drugs [48]. Several drugs have the ability to disrupt the mitochondrial machinery in various stages of clinical trials by raising oxidative stress, a process that enhances the production of ROS [49,50]. Accumulation of ROS can lead to loss of MMP and mPTP opening, thus allowing the release of *cytochrome C* into the cytoplasm and the initiation of a caspase cascade reaction [51]. Here, HIC was found to reduce to a meager level of MMP in both PC3 and DU145 cells. Notably, this finding is consisted with the previous study about the activation of caspase 3 by HIC treatment in PCa.

It is a well-known fact that the mitochondrial electron transport chain is a major source of cellular ROS, where the retention of GSH by mitochondria is an important mechanism for protection against ROS [52]. ROS production after HIC treatment was observed by an increased apoptotic response in both PC3 and DU145 cells [20]. In the present study, we found that HIC had a least inhibitory effect on GSH level only in DU145 cells. This might be due to the higher rate of ROS production only after the GSH levels declined below the baseline of ~20% in cancer cell condition [44].

It is also related that increased ROS production has been primarily related to the induction of apoptosis rather than being a direct and simple response to the GSH depletion alone [44]. As discussed above, computer aided drug discovery and experimental approaches have revealed the ability of HIC to be a selective agonist of P2Y1R, which might be further investigated for its therapeutic outcome against prostate cancer.

5. Conclusion

The structure based computer aided drug discovery along with *in vivo experiments* assisted in charting the effective ligands for various targets especially for prostate cancer. We used *in silico* and *in vivo* experiments to better understand the structural characteristics of P2Y1 receptors in this study. The glide docking model of P2Y1-HIC is considered for the study along with the crystal structure of P2Y1-MRS2500 as a control to make comparisons. Further, we performed 100 ns molecular dynamics simulations on the P2Y1-HIC and P2Y1-MRS2500 to study the crucial amino acid interactions responsible for binding and stability. The docking and molecular dynamics simulations reveal the binding of P2Y1-HIC with reference to the control structural complex. Our *in vivo* experimental findings explored the biological response of HIC on prostate cancer cells. Overall, we believe that the ligand and structure based drug pipelines along with experimental approaches have led to breakthroughs in understanding the pharmacological outcomes of the P2Y1-HIC complex.

Supplementary data to this article can be found online at https://doi.org/10.1016/j.ijbiomac.2021.08.103.

Author contributions

K.M.S involved in docking studies and H.L in biological studies. H.L, A.M, K.M.S contributed data analysis. H.L, A.M, K.M.S, R.T and M.K involved in interpretation of the scientific data. M.K and O.Y.H conceived and managed all studies. M.K and R.T performed quality check and edited the manuscript. M.K and K.M.S. developed the project. All the authors contributed for the manuscript writing.

Funding statement

H.L was supported by the University of Tampere (TUT-RAE fund) during the project.

Declaration of competing interest

The authors claim no conflicts of interest.

Acknowledgement

We would like to thank Faculty of Medicine and Health Technology, Tampere, Finland for providing instrumental facility for experimental work.

Ethical approval and consent to participate

Not applicable.

References

[1] A.J. Venkatakrishnan, Structure and activation mechanism of GPCRs, in: Top. Med. Chem, 2019, pp. 53–64, https://doi.org/10.1007/7355_2018_62.

[2] N.R. Latorraca, A.J. Venkatakrishnan, R.O. Dror, GPCR dynamics: structures in motion, Chem. Rev. 117 (2017) 139–155, https://doi.org/10.1021/acs.chemrev.6b00177.

[3] V. Katritch, V. Cherezov, R.C. Stevens, Structure-function of the G protein-coupled receptor superfamily, Annu. Rev. Pharmacol. Toxicol. 53 (2013) 531–556, https://doi.org/10.1146/annurev-pharmtox-032112-135923.

[4] M. Congreve, C. de Graaf, N.A. Swain, C.G. Tate, Impact of GPCR structures on drug discovery, Cell 181 (2020) 81–91, https://doi.org/10.1016/j.cell.2020.03.003.

[5] A.J. Kooistra, S. Mordalski, G. Pándy-Szekeres, M. Esguerra, A. Mamyrbekov, C. Munk, G.M. Keseru, D.E. Gloriam, GPCRdb in 2021: integrating GPCR sequence, structure and function, Nucleic Acids Res. (2021), https://doi.org/10.1093/nar/gkaa1080.

[6] K. Sriram, P.A. Insel, G protein-coupled receptors as targets for approved drugs: how many targets and how many drugs? Mol. Pharmacol. (2018) 251–258, https://doi.org/10.1124/mol.117.111062.

[7] J. Wang, T. Hua, Z.J. Liu, Structural features of activated GPCR signaling complexes, Curr. Opin. Struct. Biol. 63 (2020) 82–89, https://doi.org/10.1016/j.sbi.2020.04.008.

[8] P. Nguyen, P. Doan, T. Rimpilainen, S. Konda Mani, A. Murugesan, O. Yli-Harja, N. R. Candeias, M. Kandhavelu, Synthesis and preclinical validation of novel indole derivatives as a GPR17 agonist for glioblastoma treatment, J. Med. Chem. (2021), https://doi.org/10.1021/acs.jmedchem.1c00277.

[9] P. Doan, P. Nguyen, A. Murugesan, K. Subramanian, S. Konda Mani, V. Kalimuthu, B.G. Abraham, B.W. Stringer, K. Balamuthu, O. Yli-Harja, M. Kandhavelu, Targeting orphan G protein-coupled receptor 17 with T0 ligand impairs glioblastoma growth, Cancers. 13 (2021), https://doi.org/10.3390/cancers13153773.

[10] K.C. Chou, Prediction of G-protein-coupled receptor classes, J. Proteome Res. 4 (2005) 1413–1418, https://doi.org/10.1021/pr050087t.

[11] G.M. Hu, T.L. Mai, C.M. Chen, Visualizing the GPCR network: classification and evolution, Sci. Rep. 7 (2017), https://doi.org/10.1038/s41598-017-15707-9.

[12] C.D. Hanlon, D.J. Andrew, Outside-in signaling - a brief review of GPCR signaling with a focus on the drosophila GPCR family, J. Cell Sci. 128 (2015) 3533–3542, https://doi.org/10.1242/jcs.175158.

[13] T. Kenakin, Theoretical aspects of GPCR?ligand complex pharmacology, Chem. Rev. (2017), https://doi.org/10.1021/acs.chemrev.5b00561.

[14] A. Gusach, I. Maslov, A. Luginina, V. Borshchevskiy, A. Mishin, V. Cherezov, Beyond structure: emerging approaches to study GPCR dynamics, Curr. Opin. Struct. Biol. 63 (2020) 18–25, https://doi.org/10.1016/j.sbi.2020.03.004.

[15] Q. Zhou, D. Yang, M. Wu, Y. Guo, W. Guo, L. Zhong, X. Cai, A. Dai, W. Jang, E. Shakhnovich, Z.J. Liu, R.C. Stevens, N.A. Lambert, M.M. Babu, M.W. Wang, S. Zhao, Common activation mechanism of class a GPCRs, elife 8 (2019), https://doi.org/10.7554/eLife.50279.

[16] J. Shonberg, R.C. Kling, P. Gmeiner, S. Löber, GPCR crystal structures: medicinal chemistry in the pocket, Bioorganic Med. Chem. 23 (2015) 3880–3906, https://doi.org/10.1016/j.bmc.2014.12.034.

[17] W. Fischer, U. Krugel, P2Y receptors: focus on structural, pharmacological and functional aspects in the brain, Curr. Med. Chem. 14 (2007) 2429–2455, https://doi.org/10.2174/092986707782023695.

[18] I. Von Kügelgen, K. Hoffmann, Pharmacology and structure of P2Y receptors, Neuropharmacology 104 (2016) 50–61, https://doi.org/10.1016/j.neuropharm.2015.10.030.

[19] H.X. Wan, J.H. Hu, R. Xie, S.M. Yang, H. Dong, Important roles of P2Y receptors in the inflammation and cancer of digestive system, Oncotarget 7 (2016) 28736–28747, https://doi.org/10.18632/oncotarget.7518.

[20] H.T.T. Le, T. Rimpilainen, S. Konda Mani, A. Murugesan, O. Yli-Harja, N. R. Candeias, M. Kandhavelu, Synthesis and preclinical validation of novel P2Y1 receptor ligands as a potent anti-prostate cancer agent, Sci. Rep. (2019), https://doi.org/10.1038/s41598-019-55194-8.

[21] K.A. Jacobson, E.G. Delicado, C. Gachet, C. Kennedy, I. von Kügelgen, B. Li, M. T. Miras-Portugal, I. Novak, T. Schöneberg, R. Perez-Sen, D. Thor, B. Wu, Z. Yang, C.E. Müller, Update of P2Y receptor pharmacology: IUPHAR review 27, Br. J. Pharmacol. 177 (2020) 2413–2433, https://doi.org/10.1111/bph.15005.

[22] L.T. Woods, K.M. Forti, V.C. Shanbhag, J.M. Camden, G.A. Weisman, P2Y receptors for extracellular nucleotides: contributions to cancer progression and therapeutic implications, Biochem. Pharmacol. (2021), 114406, https://doi.org/10.1016/j.bcp.2021.114406.

[23] D. Zhang, Z.G. Gao, K. Zhang, E. Kiselev, S. Crane, J. Wang, S. Paoletta, C. Yi, L. Ma, W. Zhang, G.W. Han, H. Liu, V. Cherezov, V. Katritch, H. Jiang, R.C. Stevens, K.A. Jacobson, Q. Zhao, B. Wu, Two disparate ligand-binding sites in the human P2Y<inf>1</inf> receptor, Nature (2015), https://doi.org/10.1038/nature14287.

[24] H.M. Berman, T.N. Bhat, P.E. Bourne, Z. Feng, G. Gilliland, H. Weissig, J. Westbrook, The Protein Data Bank and the challenge of structural genomics, Suppl, Nat. Struct. Biol. 7 (2000) 957–959. doi:10.1038/80734.

[25] Schrödinger, LigPrep | Schrödinger, Schrödinger Release 2018-1. (2018).

[26] R.A. Friesner, R.B. Murphy, M.P. Repasky, L.L. Frye, J.R. Greenwood, T.A. Halgren, P.C. Sanschagrin, D.T. Mainz, Extra precision glide: docking and scoring incorporating a model of hydrophobic enclosure for protein-ligand complexes, J. Med. Chem. (2006), https://doi.org/10.1021/jm051256o.

[27] R.A. Friesner, J.L. Banks, R.B. Murphy, T.A. Halgren, J.J. Klicic, D.T. Mainz, M. P. Repasky, E.H. Knoll, M. Shelley, J.K. Perry, D.E. Shaw, P. Francis, P.S. Shenkin, Glide: a new approach for rapid, accurate docking and scoring. 1. Method and assessment of docking accuracy, J. Med. Chem. (2004), https://doi.org/10.1021/jm0306430.

[28] P. Marimuthu, K. Singaravelu, Prediction of hot spots at myeloid cell leukemia-1-inhibitor Interface using energy estimation and alanine scanning mutagenesis, Biochemistry (2018), https://doi.org/10.1021/acs.biochem.7b01048.

[29] P. Marimuthu, K. Singaravelu, Unraveling the molecular mechanism of benzothiophene and benzofuran scaffold-merged compounds binding to anti-apoptotic myeloid cell leukemia 1, J. Biomol. Struct. Dyn. (2019), https://doi.org/10.1080/07391102.2018.1474805.

[30] B. Hess, C. Kutzner, D.Van Der Spoel, GROMACS 4: algorithms for highly efficient, load-balanced, and scalable molecular simulation, J. Chem. 4 (3) (2008) 435–447.

[31] J. Eargle, D. Wright, Z. Luthey-Schulten, Multiple alignment of protein structures and sequences for VMD, Bioinformatics (2006), https://doi.org/10.1093/bioinformatics/bti825.

[32] A.W. Sousa Da Silva, W.F. Vranken, ACPYPE - AnteChamber PYthon Parser interfacE, BMC Res. Notes (2012), https://doi.org/10.1186/1756-0500-5-367.

[33] K.C. Lai, A.N.C. Huang, S.C. Hsu, C.L. Kuo, J.S. Yang, S.H. Wu, J.G. Chung, Benzyl lsothiocyanate (BITC) inhibits migration and invasion of human colon cancer HT29 cells by inhibiting matrix metalloproteinase-2/-9 and urokinase plasminogen (uPA) through PKC and MAPK signaling pathway, J. Agric. Food Chem. 58 (2010) 2935–2942, https://doi.org/10.1021/jf9036694.

[34] H.J. Cho, D.Y. Lim, G.T. Kwon, J.H. Kim, Z. Huang, H. Song, Y.S. Oh, Y.H. Kang, K. W. Lee, Z. Dong, J.H.Y. Park, Benzyl isothiocyanate inhibits prostate cancer development in the transgenic adenocarcinoma mouse prostate (TRAMP) model, which is associated with the induction of cell cycle G1 arrest, Int. J. Mol. Sci. 17 (2016) 264, https://doi.org/10.3390/ijms17020264.

[35] S. Costanzi, L. Mamedova, Z.G. Gao, K.A. Jacobson, Architecture of P2Y nucleotide receptors: structural comparison based on sequence analysis, mutagenesis, and homology modeling, J. Med. Chem. 47 (2004) 5393–5404, https://doi.org/10.1021/jm049914c.

[36] R. Fredriksson, M.C. Lagerström, L.G. Lundin, H.B. Schiöth, The G-protein-coupled receptors in the human genome form five main families. phylogenetic analysis, paralogon groups, and fingerprints, Mol. Pharmacol. (2003), https://doi.org/10.1124/mol.63.6.1256.

[37] Q. Wei, S. Costanzi, Q.Z. Liu, Z.G. Gao, K.A. Jacobson, Activation of the P2Y1 receptor induces apoptosis and inhibits proliferation of prostate cancer cells, Biochem. Pharmacol. (2011), https://doi.org/10.1016/j.bcp.2011.05.013.

[38] A.A. Starkov, The role of mitochondria in reactive oxygen species metabolism and signaling, in: Ann. N. Y. Acad. Sci, Blackwell Publishing Inc., 2008, pp. 37–52, https://doi.org/10.1196/annals.1427.015.

[39] P.S. Vaiyapuri, A.A. Ali, A.A. Mohammad, J. Kandhavelu, M. Kandhavelu, Time lapse microscopy observation of cellular structural changes and image analysis of drug treated cancer cells to characterize the cellular heterogeneity, Environ. Toxicol. (2015), https://doi.org/10.1002/tox.21950.

[40] A. Viswanathan, D. Kute, A. Musa, S. Konda Mani, V. Sipilä, F. Emmert-Streib, F. I. Zubkov, A.V. Gurbanov, O. Yli-Harja, M. Kandhavelu, 2-(2-(2,4-Dioxopentan-3-ylidene)hydrazineyl)benzonitrile as novel inhibitor of receptor tyrosine kinase and PI3K/AKT/mTOR signaling pathway in glioblastoma, Eur. J. Med. Chem. (2019), https://doi.org/10.1016/j.ejmech.2019.01.021.

[41] V. Aggarwal, H.S. Tuli, A. Varol, F. Thakral, M.B. Yerer, K. Sak, M. Varol, A. Jain, M.A. Khan, G. Sethi, Role of reactive oxygen species in cancer progression: molecular mechanisms and recent advancements, Biomolecules 9 (2019) 735, https://doi.org/10.3390/biom9110735.

[42] I. Masgras, S. Carrera, P.J. De Verdier, P. Brennan, A. Majid, W. Makhtar, E. Tulchinsky, G.D.D. Jones, I.B. Roninson, S. Macip, Reactive oxygen species and mitochondrial sensitivity to oxidative stress determine induction of cancer cell death by p21, J. Biol. Chem. 287 (2012) 9845–9854, https://doi.org/10.1074/jbc.M111.250357.

[43] T. Fiaschi, P. Chiarugi, Oxidative stress, tumor microenvironment, and metabolic reprogramming: a diabolic liaison, Int. J. Cell Biol. (2012), https://doi.org/10.1155/2012/762825.

[44] J.S. Armstrong, K.K. Steinauer, B. Hornung, J.M. Irish, P. Lecane, G.W. Birrell, D. M. Peehl, S.J. Knox, Role of glutathione depletion and reactive oxygen species generation in apoptotic signaling in a human B lymphoma cell line, Cell Death Differ. 9 (2002) 252–263, https://doi.org/10.1038/sj.cdd.4400959.

[45] A. Bansal, M. Celeste Simon, Glutathione metabolism in cancer progression and treatment resistance, J. Cell Biol. 217 (2018) 2291–2298, https://doi.org/10.1083/jcb.201804161.

[46] D.M. Townsend, K.D. Tew, H. Tapiero, The importance of glutathione in human disease, Biomed. Pharmacother. 57 (2003) 145–155, https://doi.org/10.1016/S0753-3322(03)00043-X.

[47] A.S. Hauser, M.M. Attwood, M. Rask-Andersen, H.B. Schiöth, D.E. Gloriam, Trends in GPCR drug discovery: new agents, targets and indications, Nat. Rev. Drug Discov. 16 (2017) 829–842, https://doi.org/10.1038/nrd.2017.178.

[48] F. Mannello, G. Tonti, S. Papa, Matrix metalloproteinase inhibitors as anticancer therapeutics, Curr. Cancer Drug Targets 5 (2005) 285–298, https://doi.org/10.2174/1568009054064615.

[49] K. Mori, T. Uchida, T. Yoshie, Y. Mizote, F. Ishikawa, M. Katsuyama, M. Shibanuma, A mitochondrial ROS pathway controls matrix metalloproteinase 9 levels and invasive properties in RAS-activated cancer cells, FEBS J. 286 (2019) 459–478, https://doi.org/10.1111/febs.14671.

[50] G. Sawicki, Synergistic effect of inhibitors of MMPs and ROS-dependent modifications of contractile proteins on protection hearts subjected to oxidative

stress, Curr. Pharm. Des. 20 (2014) 1345–1348, https://doi.org/10.2174/1381612811319990556.
[51] M. Redza-Dutordoir, D.A. Averill-Bates, Activation of apoptosis signalling pathways by reactive oxygen species, Biochim. Biophys. Acta - Mol. Cell Res. 1863 (2016) 2977–2992, https://doi.org/10.1016/j.bbamcr.2016.09.012.
[52] R.Z. Zhao, S. Jiang, L. Zhang, Z., Bin Yu, Mitochondrial electron transport chain, ROS generation and uncoupling (review), Int. J. Mol. Med. 44 (2019) 3–15, https://doi.org/10.3892/ijmm.2019.4188.

PUBLICATION III

Functional characterization of HIC, a P2Y1 agonist, as a p53 stabilizer for prostate cancer cell death induction

H. Le, A. Murugesan, N. R. Candeias, O. Yli-Harja, and M. Kandhavelu

Future Medicinal Chemistry (2021), 13, 21

DOI: 10.4155/fmc-2021-0159

Research Article

For reprint orders, please contact: reprints@future-science.com

Future Medicinal Chemistry

Functional characterization of HIC, a P2Y1 agonist, as a p53 stabilizer for prostate cancer cell death induction

Hien Thi Thu Le[1,2], Akshaya Murugesan[1,2,3], Nuno R Candeias[4,5], Olli Yli-Harja[6,7] & Meenakshisundaram Kandhavelu*[,1,2]

[1]Molecular Signaling Lab, Faculty of Medicine & Health Technology, Tampere University, Finland
[2]BioMeditech & Tays Cancer Center, Tampere University Hospital, PO Box 553, 33101, Tampere, Finland
[3]Department of Biotechnology, Lady Doak College, Thallakulam, Madurai, 625002, India
[4]Faculty of Engineering & Natural Sciences, Tampere University, 33101, Tampere, Finland
[5]LAQV-REQUIMTE, Department of Chemistry, University of Aveiro, 3810-193, Aveiro, Portugal
[6]Computational Systems Biology Group, Faculty of Medicine & Health Technology, Tampere University, PO Box 553, 33101, Tampere, Finland
[7]Institute for Systems Biology, 1441N 34th Street, Seattle, WA 98103-8904, USA
*Author for correspondence: meenakshisundaram.kandhavelu@tuni.fi

Background: (1-(2-hydroxy-5-nitrophenyl)(4-hydroxyphenyl)methyl)indoline-4-carbonitrile (HIC), an agonist of the P2Y1 receptor (P2Y1R), induces cell death in prostate cancer cells. However, the molecular mechanism behind the inhibition of HIC in prostate cancer remains elusive. **Methods and results:** Here, to outline the inhibitory role of HIC on prostate cancer cells, PC-3 and DU145 cell lines were treated with the respective IC_{50} concentrations, which reduced cell proliferation, adherence properties and spheroid formation. HIC was able to arrest the cell cycle at G1/S phase and also induced apoptosis and DNA damage, validated by gene expression profiling. HIC inhibited the prostate cancer cells´ migration and invasion, revealing its antimetastatic ability. P2Y1R-targeted HIC affects p53, MAPK and NF-κB protein expression, thereby improving the p53 stabilization essential for G1/S arrest and cell death. **Conclusion:** These findings provide an insight on the potential use of HIC, which remains the mainstay treatment for prostate cancer.

First draft submitted: 27 May 2021; Accepted for publication: 20 August 2021; Published online: 10 September 2021

Keywords: apoptosis • cell death • P2Y1 receptor • prostate cancer • signaling pathways

newlands press

Graphical abstract:

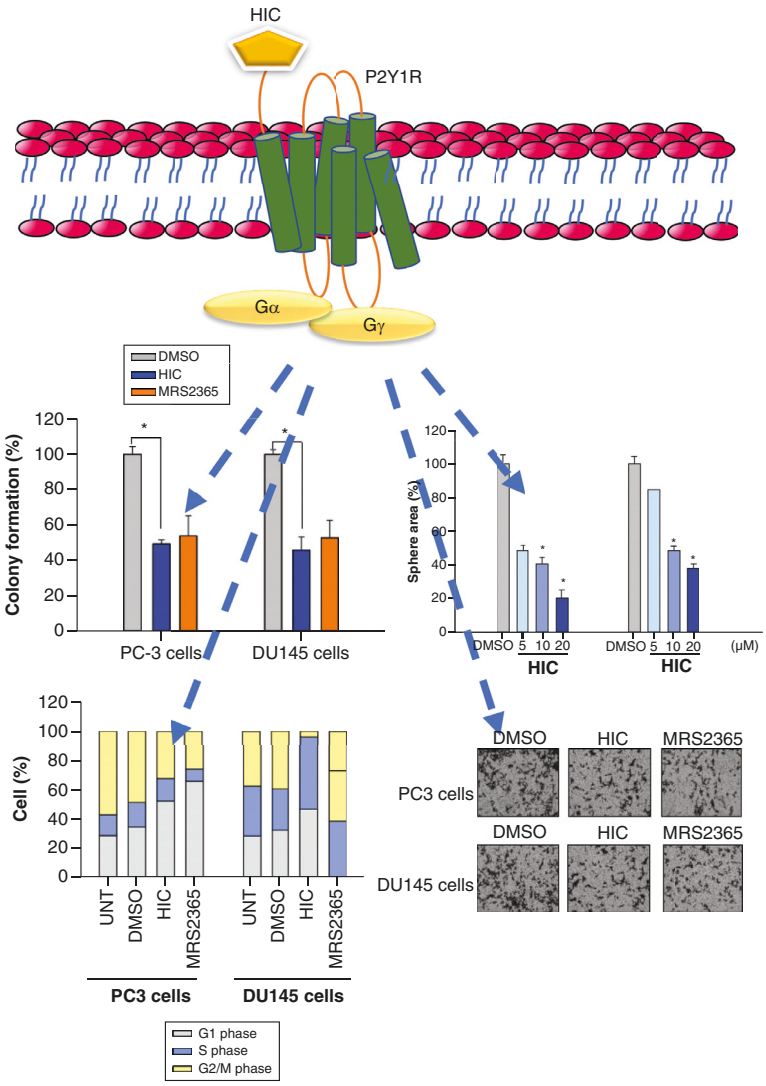

Prostate cancer (PCa) is the second leading cause of death in males worldwide [1,2], but the molecular mechanism behind PCa cell invasion and migration is very limited [2,3]. This has allowed the development of novel therapies with specific targets. The G-protein-coupled receptors (GPCRs) are a group of plasma membrane receptors whose signaling regulates a plethora of biological functions in tumorigenesis [4]. GPCR, when overexpressed by the circulating agonist, can contribute to tumor cell growth. Thus GPCR-targeted drugs are considered as a promising therapeutic strategy for treating a variety of cancers, including PCa [5]. At least one-third of all marketable drugs are GPCR-based agonists or antagonists [4,5], of which only a few are successfully exploited to inhibit cancer signaling pathways. Among GPCRs, purinergic receptors 1 (P2Y1R) are highly expressed in PC3 and DU145 cancer cells [6–9]. P2Y1R is also suggested as a therapeutic target for suppressing PCa cell growth [7,10]. The activity of P2Y1R has been investigated in different biological responses such as cell death and proliferation [10–12]. Signaling pathways regulated by P2Y1R are dependent on cellular context. For example, the activation of P2Y1R

in Madin-Darby canine kidney epithelial cells and lymphatic endothelial cells strongly promotes cell growth by inducing intracellular Ca^{2+} level [11,13]. On the other hand, the activation of P2Y1R is known to induce apoptosis and suppress proliferation in other cell types [10,14]. P2Y1R-Gq protein is linked to phospholipase C activation, which plays a crucial role in the transmission of astrocytic Ca^{2+} levels and inositol-trisphosphate and the activation of protein kinase C (PKC) [15,16]. It is known that activation of a PKC isoform by P2Y1R can stimulate ERK, a member of the MAPK signal transduction pathway [17,18]. This pathway is also associated with cell proliferation and differentiation [19]. ERK1/2 is known to increase p53 stabilization, required for G1 arrest, in the ZL55 cell cycle [20].

Several agonist-like or antagonist-like compounds of P2Y1R have been considered as potential cancer therapeutic drugs [14,21,22]. For example, MRS 2365, a selective agonist of P2Y1R, inhibits cell growth and induces cell apoptosis and caspase 3 activity of PC3 cells [7]. Furthermore, 2-methylthioadenosine diphosphate (2-MeSADP) and ADP, non-selective agonists of P2Y1R , induce intracellular transduction pathways involving intracellular Ca^{2+}, PKC, phosphorylation of ERK1/2 and JNK1/2 in ZL55 cells [20]. Thus ADP promotes P2Y1R activation and p53 stabilization-mediated G1 cell arrest and inhibits mesothelioma progression [20]. On the other hand, MRS2179, as an antagonist of P2Y1R , leads to phosphorylation of ERK1/2 and contributes to re-endothelialization after vascular injury [23]. Therefore focusing on the appropriate downstream signaling pathway of P2Y1R is considered as an important therapeutic target against PCa.

Earlier it was identified that (1-(2-hydroxy-5-nitrophenyl)(4-hydroxyphenyl)methyl)indoline-4-carbonitrile (HIC), a synthesized agonist of P2Y1R , induced cell death and apoptosis in a PCa model [10]. Also, HIC was found to induce the caspase 3/7 activity and reactive oxygen species (ROS) formation and thus inhibited cell proliferation with long-term treatment [10]. The anticancer effect of HIC was also observed through the analysis of apoptosis [10]. Although the activity of HIC in relation to P2Y1R was identified, the detailed mechanism in PCa cells remains elusive. Therefore the present study was aimed at evaluating and exploring the anticancer effect of HIC on PC3 and DU145 cells. Colony and spheroid assays were performed to determine the anticancer effect of HIC on PCa cells. High-throughput sequencing analysis was also performed to identify the regulated genes at the transcription level in cell cycle arrest and the apoptosis pathway. The antimetastatic effect of HIC was evaluated by wound healing, migration and invasion assays. Differential expression of proteins involved in the MAPK and NF-κB pathways was identified through protein array analysis to elucidate the role of HIC through P2Y1R activation in PCa cells. It was identified that HIC could inhibit cell proliferation and migration through the modulation of MAPK and p53 signaling pathways.

Materials & methods

Chemical synthesis

HIC was designed and synthesized as previously described [10]. Briefly, HIC was synthesized after adding indoline-4-carbonitrile to 2-hydroxy-5-nitrobenzaldehyde and (4-hydroxyphenyl) boronic acid in 5.0 ml dichloroethane (DCE) and 0.5 ml ethanol at 50°C. After stirring for 70 min at that temperature, solvents were evaporated under reduced pressure and the residue purified through gradient column chromatography. The compound was solubilized to a 100-mM stock solution in dimethyl sulfoxide (DMSO; Sigma-Aldrich, MO, USA).

Cell culture

PC3 and DU145 cells were cultured in minimum essential medium Eagle at 37°C (MEME, cat no. 4655; Sigma-Aldrich) containing 10% (v/v) fetal bovine serum (FBS, cat no. S181H; Biowest, Nuaillé, France), 50 U/ml penicillin and 50 U/ml streptomycin (Sigma-Aldrich). PCa cells were maintained at 37°C in a humidified incubator with 5% CO_2 and were passaged using 1× trypsin solution (Cat no. 59427C; Sigma-Aldrich) every 3–5 days. All the experiments were performed in triplicate and the cells were counted using Trypan blue staining (Cat no. T8154; Sigma-Aldrich) in a TC-10 automated cell counter (Bio-Rad, Hercules, CA).

Colony assay

The colony assay was performed using a previously reported method [24]. Briefly, the nontransfected and transfected cells were seeded in six-well culture plates at a density of 1.0×10^3 cells per well. After 24 h, the cells were treated with DMSO, HIC and MRS 2365. The cells were maintained in an appropriate cell culture environment; the medium was changed every 4 days and the cells were retreated with HIC after each medium change. After 9 days post-treatment, the colonies formed were washed with phosphate-buffered saline (PBS) and fixed with 75%

methanol and 25% acetic acid for 10 min. The plates were then stained with 0.5% crystal violet in ethanol for 15 min. Colonies were counted using an Axiovert 200 M microscope (Zeiss, Oberkochen, Germany). Survival fraction was calculated using Equation 1:

$$\textit{Inhibitory ratio}\ (\%) = \frac{\textit{No.of colonies treated with drugs}}{\textit{No.of cell treated with vehicle}} \times 100\% \quad \text{(Eq. 1)}$$

To investigate the anticancer effect of HIC on PC3 and DU145 cells, cells were plated in 12-well culture plates with a density of 1×10^5 cells/well. After 24 h, the cells were treated with DMSO and/or HIC at the IC_{50} concentration (15.98 μM for PC3 cells and 15.64 μM for DU145 cells). The cells were incubated for 48 h and then washed with warm PBS (pH 7.2) to remove the floating dead cells. Images was captured using a Nikon TE 2000-U microscope (Nikon, Inc., Tokyo, Japan) at 20× magnification.

Matrix preparation

Corning® Matrigel® Basement Membrane Matrix (Cat no. 354234; Corning, NY, USA) was used for coating the culture plates as per the manufacturer's datasheet. A Matrigel bottle was thawed and aliquoted to 500 μl and stored at -20°C until use. For the invasion assay, 1% Matrigel stock solution was prepared using RHB-A medium (Y40001, AH Diagnostics, Vantaa, Finland). The working solution was used to sufficiently cover the well surface for the spheroids assay. The Matrigel was kept in the incubator for 2 h.

MTS invasion assay

PC3 and DU145 cells were seeded in 12-well plates at a density of 1×10^3 cells per well for 48 h. Matrigel (0.1%) was added to the plates after the removal of media and the plates were subjected to overnight incubation. The spheroids were treated with 5, 10 and 20 μM of HIC for 8 days. The spheroid formation was captured using a Nikon TE 2000-U microscope at 40× magnification. Spheroid area was measured using ImageJ software 1.52 (NIH, MD, USA).

To determine the anticancer effect of HIC on spheroid development in a time-dependent manner, colonospheres were treated with the IC_{50} concentration of HIC, 1 μM MRS2365 and DMSO as the control. The effect was analyzed on days 1, 3 and 8. Images of spheroid formation were captured at the different time points. Spheroid area was quantified using ImageJ with Equation 2. All data shown were calculated as mean ± standard error of the mean (n = 6).

$$\text{Sphere area } \% = \frac{\text{Spheroid area of samples treated drug}}{\text{Spheroid area of control groups}} \times 100\% \quad \text{(Eq. 2)}$$

mRNA extraction

PC3 and DU145 cells were seeded in six-well plates at a density of 5×10^5 cells/well. After overnight incubation, cells were treated with the IC_{50} concentration of HIC, with DMSO as a control, at 37°C for 48 h. The cells were collected by centrifugation and total mRNA was collected using the GeneJET RNA Purification kit (cat no. K0731; Thermo Scientific, MA, USA) following the manufacturer's protocol. Briefly, cells were extracted in lysis buffer supplemented with 400 mM β-mercaptoethanol (Cat no. M6250, Sigma-Aldrich). The lysates were centrifuged at 10,000 rpm for 10 min. The supernatants were transferred into a new RNase-free microcentrifuge tube. Ethanol (96–100%) was added and mixed gently by pipetting. Lysates were transferred to the purification column inserted in the collection tube and washed twice with wash buffer. Purified RNA was dissolved in nuclease-free water. The concentration of mRNA was measured using Magellan™ microplate reader (Tecan, Männedorf, Switzerland).

Illumina sequencing & bioinformatics analysis

The 12 RNA samples extracted were transferred to the Biomedicum Functional Genomics Unit (FuGU, University of Helsinki, Helsinki, Finland) for whole-transcriptome sequencing using Illumina NextSeq 500 (Illumina, CA, USA) [25]. The .bcl file from the RNA sequencing was converted into FASTQ file format for further *in silico* analysis.

RNASeq data analysis

The human genome FASTA file and gene annotation GTF file were obtained from Ensembl [26] based on FasQC [27]. STAR, an open-source aligner, was used to calculate read counts, detect the differential level of genes and map the reads to the human genome [28]. Differential expression analysis was determined by SAMtools [29] and the

'union' mode of HTSeq [30] using the high-performance research computing resources provided by TUT TCSC Narvi Cluster (https://wiki.eduuni.fi/display/tutsgn/TUT+Narvi+Cluster). Differentially expressed genes (DEGs) with a q-value less than 0.05 were identified using DESeq2 [31] using R programming. The p-values were adjusted for multiple testing using the Benjamini–Hochberg procedure [32]. A false discovery rate-adjusted p-value (i.e., a q-value) <0.05 was set for the selection of DEGs.

Gene ontology & pathway analysis

A combination of gene ontology (GO) and the ClusterProfiler package was used for pathway analyses [33,34]. We performed GO biological process and Kyoto Encyclopedia of Genes and Genomes (KEGG) pathways over-representation tests using the gene signature obtained from the DEG analysis [35]. These packages support the analysis of the human genome. For multiple testing and correction, a combination of binomial test, Bonferroni correction and z-scores was created using the standard to check the regulated genes either inhibited or activated by HIC. In both the KEGG pathways and GO terms, the statistical analyses were used with a cutoff p-value < 0.05.

Annexin V–FITC apoptosis assay

To detect the effect of HIC on apoptosis, PC3 and DU145 cells were subjected to Annexin V–FITC apoptosis detection kit (Cat no. APOAF-20TST, Sigma-Aldrich). PCa cells were plated in six-well culture plate at a density of 2×10^5 cells/well. Cells were treated with DMSO (vehicle control) and/or 16 µM HIC for 48 h in the incubator. Cells were then washed with PBS, resuspended with the binding buffer and incubated for 15 min in the dark, according to the manufacturer's protocol. After adding additional binding buffer, cells were detected under an epifluorescence microscope (Nikon-Eclipse Ti-E inverted fluorescence microscope) using a 20× objective.

Cell cycle assay

The drug intervention at different cell cycle phases was identified using a propidium iodide kit (cat no. P4170, Sigma-Aldrich) following the manufacturer's protocol. Briefly, PC3 and DU145 cells were plated in six-well plates at a density of 3×10^5 cells/well and incubated overnight. PCa cells were incubated with DMSO, MRS2365 and HIC for 48 h, then collected and resuspended in cold PBS. Subsequently, the cells were fixed with cold 70% ethanol and incubated on ice for 30 min. The pellets were collected by centrifugation and resuspended in PI-Triton-RNase including propidium iodide, Triton™ X-100 and RNaseA for 15 min in the dark. Images were captured using an EVOS™ fluorescence microscope (Thermo Fisher Scientific, MA, USA) at 40× magnification. Around 300 cells of each condition were observed under the microscope. The photos were analyzed using CellProfiler 4.0 and the cell cycle phases were analyzed using MATLAB R2018b (MathWorks Ltd, MA, USA).

Wound-healing assay

PC3 and DU145 cells were seeded in six-well plates at a density of 1.5×10^6 cells/well and cultures were maintained until 90% confluence was reached. The plates were carefully scratched using 200-µl pipette tips to draw a linear 'wound' in the cell monolayer of each well. The plates were washed twice with warm PBS to remove the floating cells and incubated in MEME media containing 1% FBS in the presence and absence of HIC or MRS2365 for 24 h. The control well contained 0.1% DMSO as the vehicle control. Images of the cells that migrated into the wound surface were captured using a Nikon TE 2000-U microscope at 4× magnification at 0, 12 and 24 h after the drug treatment. The percentage of migrated cells was calculated using Equation 3

$$A_{migrated} = \frac{A_{0-D} - A_{24-D}}{A_{0-C} - A_{24-C}} \times 100\% \quad \text{(Eq. 3)}$$

where $A_{0\text{-}D}$ = the area of the scratch in samples treated with drugs at the starting time; $A_{24\text{-}D}$ = the area of the scratch in samples treated with drugs after 24 h treatment; $A_{0\text{-}C}$ = the area of the scratch in samples treated with DMSO at the starting time; $A_{24\text{-}C}$ = the area of the scratch in samples treated with DMSO after 24 h treatment. The change in the average wound closure is represented as the percentage of wound recovery. Three independent experiments were performed to verify statistical significance.

Transwell invasion & migration assay

The effect of HIC in inhibiting the migration of PCa cells was assessed using the Transwell invasion assay. PC3 and DU145 cells at a density of 5×10^5 cells/well were seeded in 500 µl of MEME supplemented with 1% FBS

and transferred into the top chamber of six-Transwell plates with 8-μm pore size (SPL, Gyeonggi-do, Korea) with or without the presence of HIC and/or MRS2365. The lower chamber was filled with 2 ml of MEME with 10% FBS. The plates were kept in the incubator.

For the Matrigel invasion assay, the upper surface of a filter membrane in the upper compartment of a Transwell (pore size 8 μm) was coated with 200 μl of Matrigel (0.5 mg/ml; Corning) and allowed to settle for 2 h. PCa cells were seeded into the chamber of six-Transwell plates in the absence or presence of the drugs.

After 24 h, the cells that migrated or invaded the membranes were fixed in 3.7% paraformaldehyde in PBS for 15 min. These migrative or invasive cells were dyed with 0.5% crystal violet in 2% ethanol for 30 min. The membranes were then washed thrice with PBS. Five or eight random fields of the membrane were observed under the microscope. Migrated or invaded cells were counted and calculated based on the average of a total number of cells. Data are expressed as the percentage of the number of migrated or invaded cells per field using Equation 4

$$\%\ of\ invaded\ cells = \frac{No.cells_{Drug}}{No.cells_{Control}} \times 100\% \qquad \text{(Eq. 4)}$$

where $No.cells_{Drug}$ is the number of cells migrated or invaded through the membranes of Transwell under drug treatment, and $No.cells_{Control}$ is the number of cells migrated or invaded through the membranes of Transwell under DMSO treatment.

Membrane-based antibody microarray analysis

Membrane-based antibody microarrays were done using Proteome Profiler Human phosphorylated kinase Array (cat no. ARY002B) and Proteome Profiler Human NF-κB pathway Array (cat no. ARY029) from R&D systems (MA, USA). The procedure was performed according to the manufacturer's protocol. Briefly, DU145 cells (5×10^6 cells/ml) were treated with 15.64 μM HIC at 37°C in 5% CO_2 for 48 h. After incubation, the cells were washed twice with cold PBS and collected by centrifugation. The cells were lysed using lysis buffer supplemented with 2 mM vanadate, 8.3 μg/ml aprotinin, 4.2 μg/ml pepstatin and 1 mM trypsin inhibitor (Sigma-Aldrich). Concentrations of soluble cell lysates were measured using the AccuOrange™ protein quantitation kit (cat no.30071-T; Biotium, CA, USA). Microarray membranes were blocked with a blocking buffer for 2 h at room temperature. Then the membranes were simultaneously treated with 200 μg of proteins in cell lysates and a biotinylated antibody cocktail overnight at 4°C. After washing five times with washing buffer, the membranes were incubated with streptavidin-conjugated horseradish peroxidase for 2 h at room temperature and washed with washing buffer before detection. The expressions of proteins were detected using ECL western blotting systems (GE Healthcare, IL, USA) with a Xenogen IVIS 200 imaging machine (PerkinElmer Inc., MA, USA). The density of protein expressions was analyzed using ImageJ. The relative level of protein expressions of treated to untreated groups was calculated based on the density of protein expression.

Statistical analysis

All experiments were performed in triplicate. The results are expressed as mean ± standard deviation. Student's *t*-test and one-way analysis of variance were done to prove the significance of the data. The results with $p < 0.05$ were considered statistically significant. Statistical analyses were performed using Sigma Plot 14 (Systat Software, Inc., Slough, UK).

Results

The anticancer effects of HIC on PCa cells

HIC was found to induce apoptosis in the PC3 and DU145 cell models. To assess the potential anticancer effects of HIC on PCa cell proliferation, the cells were treated for 48 h with the IC_{50} concentrations of HIC (Figure 1A): 15.98 μM for PC3 and 15.64 μM for DU145, respectively. As shown in Figure 1B, the cytotoxic effect of HIC reduced the cell density when compared with DMSO-treated cells. The PC3 and DU145 cells also lost their adherence properties and exhibited abnormal morphology upon HIC treatment.

To validate the cytotoxic effect of HIC, a clonogenicity assay was performed to identify its ability to reduce the percentage of colonies by inhibiting the proliferation of PCa cells. The PCa cells were treated with the IC_{50} concentration of HIC, using MRS2365 as positive control and DMSO as vehicle control (Figure 1B). The cells resistant to HIC were allowed to grow for 9 days post-treatment. Figure 1C shows the stained colonies having differences in the number and the size of the PCa cells. HIC significantly inhibited colony formation, with about

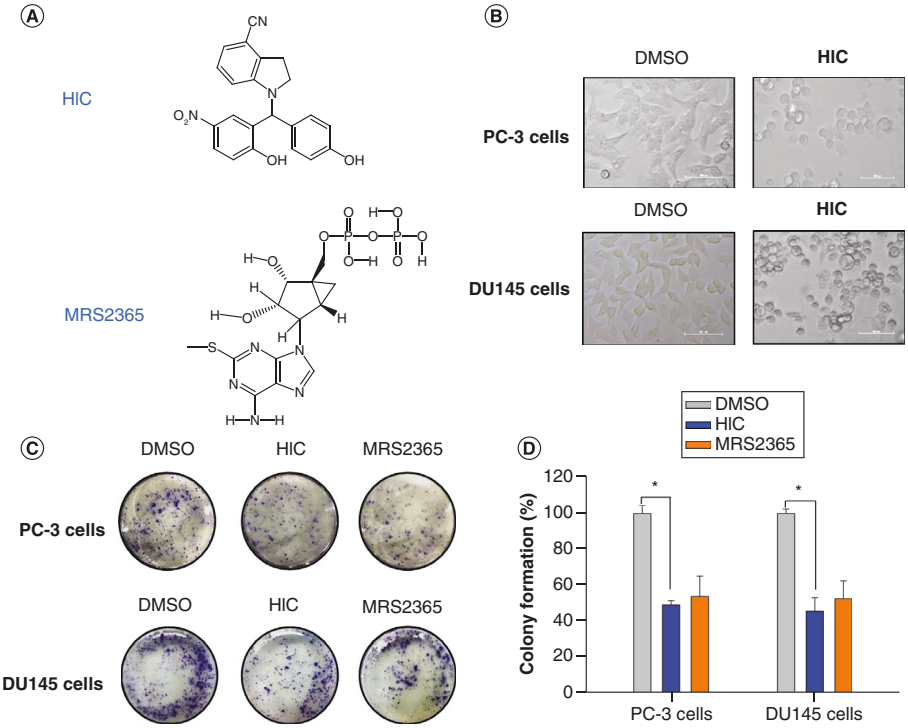

Figure 1. The anticancer effects of HIC on prostate cancer cells through P2Y1R activation. (A) Chemical structures of HIC and MRS2365. **(B)** Clonogenicity assay on prostate cancer (PCa) cells treated with the IC_{50} concentration of HIC, with MRS2365 used as the positive control and DMSO as the vehicle control. **(C)** The colony-forming ability of the PCa cells at 48 h. Cells were stained with crystal violet and imaged under fluorescent microscope at 20× magnification (scale bar = 100 μm). **(D)** Bar graph showing the percentage of colony formation in PCa cells treated with HIC and/or MRS2365 after 9 days, with DMSO control (vehicle control) (n = 6; *$p < 0.05$).

49.47 ± 2.3% for PC3 and 45.9 ± 7.4% for DU145 compared with the vehicle control (DMSO). MRS2365 showed comparatively less sensitivity and percentage of inhibition than HIC, with about 54.6 ± 11.3% and 52.8 ± 9.9% in PC3 and DU145 cells, respectively (Figure 1D).

Dose- & time-dependent cytotoxicity analysis of HIC in PCa spheroids

A tumor spheroid model generated from PC3 and DU145 was used as an intermediate *in vitro* and *in vivo* system to study the anticancer activity of HIC. The dose-responsive effect of HIC on spheroid formation by PCa cells was evaluated by measuring the size of the spheroids after 96 h of treatment. The size of the spheroids was observed to be inversely proportional to the concentration of HIC. The area of the spheroids was measured using ImageJ and compared with the control group. The spheroid area was reduced by ~50% upon 20 μM HIC treatment in both PC3 (Figure 2A) and DU145 cells (Figure 2B). The PC3 spheroid area decreased to about 52.4 ± 3.3, 40.9 ± 3.66 and 20.76 ± 4.8%, while the DU145 spheroid area showed 84.6 ± 3.15, 48.8 ± 2.3 and 38.23 ± 2.6% reduction upon 5, 10 and 20 μM of HIC treatment, respectively (Figure 2C). Thus HIC significantly reduced the colonosphere formation in both cell lines, with a higher effect in PC3 spheroids than in DU145 spheroids.

Meanwhile, the time-dependent effect of HIC in the PCa spheroids was analyzed on days 1, 3 and 8 after treatment. MRS2365 was used as a positive control and DMSO as the vehicle control. The spheroid area was reduced in PCa cells after day 3 of HIC and MRS2365 treatment (Figure 2D & E). The size of spheroids was reduced to 52.3 ± 3.1% and 64.3 ± 2.3% for PC3 cells (Figure 2F) and 29.1 ± 2.9% and 57.8 ± 1.6% for DU145 cells on the third and eighth day of treatment, respectively (Figure 2G), compared with the DMSO-treated control. MRS2365 also significantly reduced the spheroid area to about 50% after 8 days' treatment in both PC3

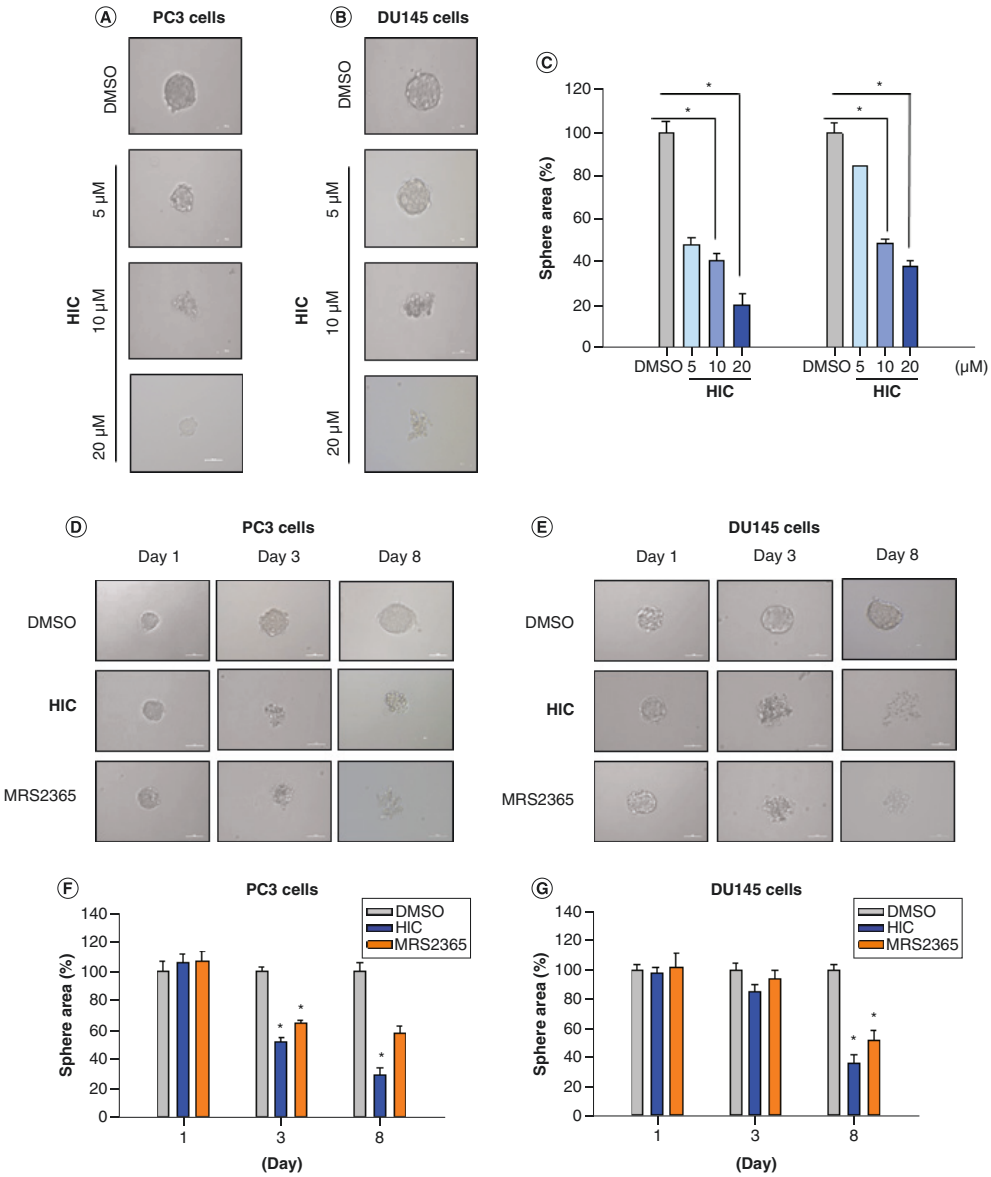

Figure 2. The inhibitory effects of HIC on spheroid growth in a dose- and time-dependent manner. (A & B) Effect of HIC on spheroid formation in **(A)** PC3 and **(B)** DU145 cells upon varying concentrations, with DMSO as the vehicle control. **(C)** Spheroid area (μm^2) upon concentration-dependent HIC treatment in both PCa cell lines, where there is significant difference when compared with DMSO. Time-dependent effect of HIC in the PCa spheroids was analyzed at days 1, 3 and 8, with DMSO as a vehicle control and MRS2365 as the positive control in **(D)** PC3 and **(E)** DU145 cells. **(F & G)** Spheroid area (μm^2) upon time-dependent HIC treatment in **(F)** PC3 and **(G)** DU145 cells. All experiments were performed in triplicate. Significant data are denoted by *$p < 0.05$ using Student's *t*-test.

and DU145 cells. In our previous study, we found that HIC inhibited cell proliferation and induced apoptosis through caspase 3/7 activity and increased ROS production in PCa cells [10]. Similar results were reported by Wei *et al.* [7], who suggested that MRS2365 increases apoptotic cells, caspase 3 activity and lactate dehydrogenase in PC3 cells and thereby inhibits their proliferation. MRS2365 was also able to induce ERK1/2 phosphorylation, suggesting its crucial role in the prostate cancer signaling pathway [7]. Collectively, our results suggest that HIC could inhibit tumor spheroid models in a time- and dose-dependent manner.

Induction of differential gene expression by HIC

RNAseq analysis was performed to compare the drug-withdrawn PCa cells with the HIC-treated PCa cells at the transcriptome level. Principal component analysis for 19,623 genes revealed 3221 DEGs (16.41%) sharing principal components for PC3 and DU145 cell lines, suggesting a diverse set of transcriptomic responses upon HIC treatment (Figure 3A & B). A total of 1913 DEGs (9.74%) were modulated in PC3 cells and 1290 DEGs (6.57%) in DU145 cells ($p < 0.05$, Supplementary Files 1 & 2). Heat maps were generated for PC3 and DU145 cells illustrating the differential expression data (Figure 3C & D). Out of 1919 DEGs in PC3 cells, 576 genes were upregulated and 391 were downregulated with significant fold change between the HIC and DMSO treated groups (Figure 3E). Likewise, DU145 showed 530 upregulated DEGs and 635 downregulated DEGs (Figure 3F).

Regulation of signaling pathways involved in cellular damage

The differentially expressed transcripts were categorized through the PANTHER annotation tool, whereby enrichment analysis of biological processes was performed to determine the potential GO and KEGG pathways regulated by HIC treatment. These included a few GO biological processes related to DNA replication, damage response in signal transduction by p53 class mediator, polymerase binding, G1/S phase DNA damage and DNA repair regulated under HIC treatment in PC3 and DU145 cells (Figure 4A & B). For a deeper insight, we also analyzed the key genes regulated in DNA damage process upon HIC treatment in both PCa cell lines. The top upregulated genes in treated PC3 cells included *CDKNIA*, *CCNB3*, *NBR2* and *UVSSA*, while the top downregulated genes were *SOX4*, *MDM2*, *MDM4*, *TP73*, *CDK1*, *TUBA1A* and *TUBA1B*, involved in DNA damage repair (Figure 4C). Similarly, DU145 cells treated with HIC revealed upregulation of *TEP1*, *UVSSA* and *NBR2*, while downregulated genes included *TUBA1A*, *TUBA1B*, *TP73*, *SOX4*, *CDK1*, *CDK2*, *MDM2* and *MDM4* (Figure 4D). *CDK1* [36] and *CDK2* [37] downregulation play a central role in DNA damage-induced cell cycle arrest and DNA repair. Also, downregulation of *SOX4* expression contributes to the inhibition of cell apoptosis, increases cell invasion and metastasis and maintains cancer-initiating cells, and the functions of *TP73* and *SOX4* are related to the p53 signaling pathway [38]. Based on the activation of p53, HIC can induce cell stress signals such as cell death, DNA damage and oxidative stress [38,39].

Downregulation of *MDM4* and *MDM2* regulates p53 activity and stability, thus enhancing DNA damage and reducing cell survival [40,41]. Furthermore, the upregulation of *CDKN1A* (coding for p21 protein) has been observed to be responsible for DNA damage and further activation of G1-phase cyclin/CDKs complexes [42]. Thus HIC was found to regulate genes involved in DNA damage through the activation of p52/p21 signaling in both the PCa cell lines.

Furthermore, we also analyzed KEGG data reflecting the functional pathways and GO annotation representing the molecular functions upon HIC treatment in both cell lines. Based on the lists of GO biological processes, the MAPK and NF-κB signaling pathways were noted as the potential targets of HIC action when the results of treatment were compared with those of the vehicle groups (Supplementary Files 3 & 4). KEGG pathways regulated by HIC treatment in both cell lines are listed in Figure 4E & F. HIC was deemed to be highly related to the p53 signaling pathway, cell cycle arrest and DNA damage. Taken together, these results suggest that p53 mediates DNA damage, whereas MAPK and NF-κB signaling pathways might potentially be regulated by HIC in PCa cells.

HIC induced apoptosis & G1/S cell cycle arrest in PCa cells

Several reports have shown that the activation of P2Y1R induces cell death in PCa cells [7,9,10]. The process of apoptosis is a double-edged sword; thus targeting defects or abnormalities in the apoptotic pathway might be an interesting approach to cancer treatment. The Annexin V–FITC apoptosis assay was performed to investigate the anticancer effect of HIC on PCa cells. Cells that fluoresce bright red represent necrotic cells, while cells in fluorescent bright green are positive for the apoptotic process. As shown in Figure 5A, PC3 and DU145 cells treated with HIC showed a greater number of cells entering apoptosis than the vehicle controls. In order to pursue

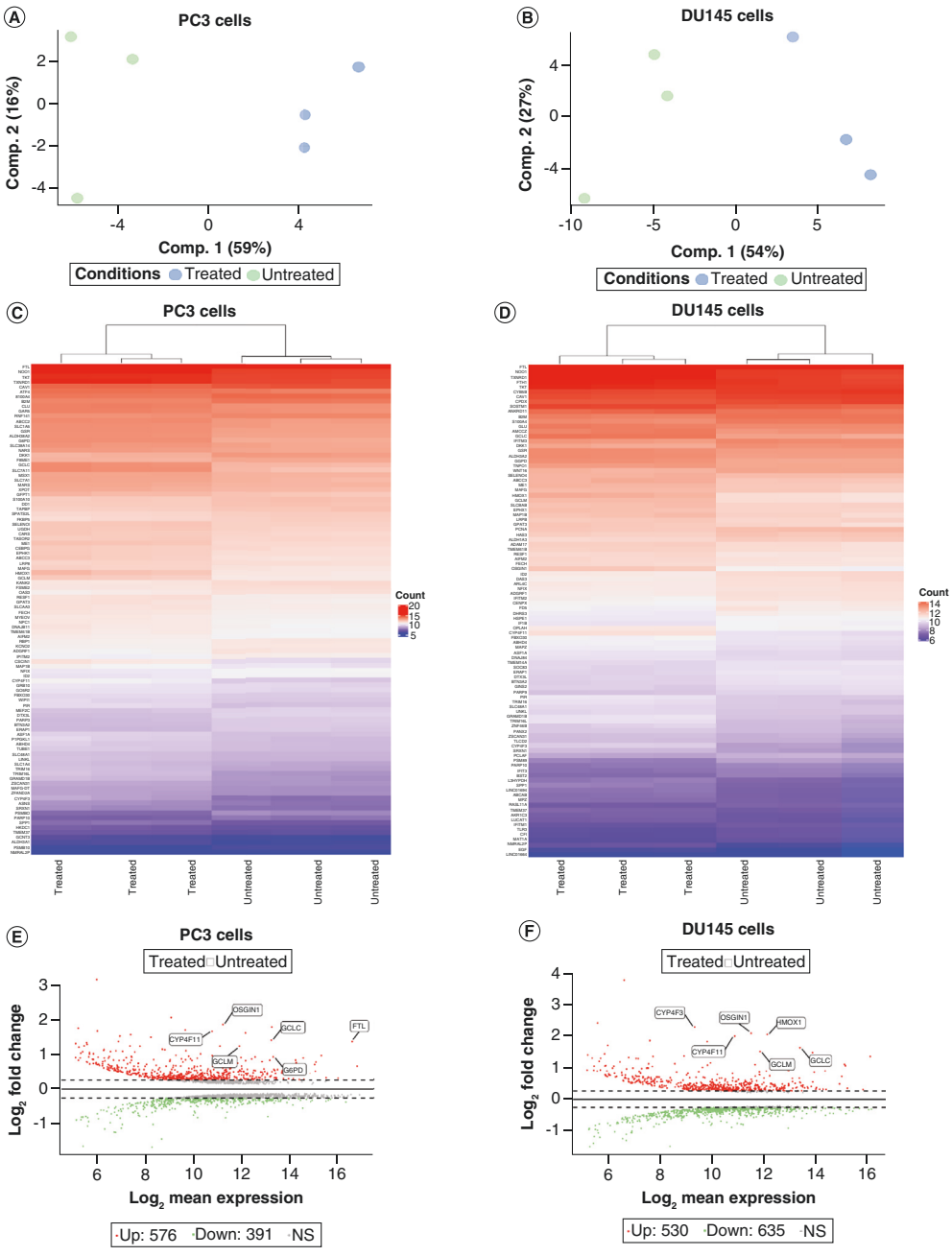

Figure 3. Analysis of gene expression in prostate cancer cells upon HIC treatment. (A & B) Gene expression modulation between the HIC-treated group and the DMSO-treated (vehicle) group in (A) PC3 cells and (B) DU145 cells. **(C & D)** Heat maps generated by the R program represent the difference in the expression levels of genes for (C) PC3 and (D) DU145 cells. Higher and lower levels of transcript accumulation are indicated by blue and red colors, respectively, while white stripes indicate the median level of expression. **(E & F)** The fold change of genes, represented by red dots for upregulated expression and green dots for downregulated expression in (E) PC3 and (F) DU145 cells. The data were normalized and *p < 0.05 considered significant.

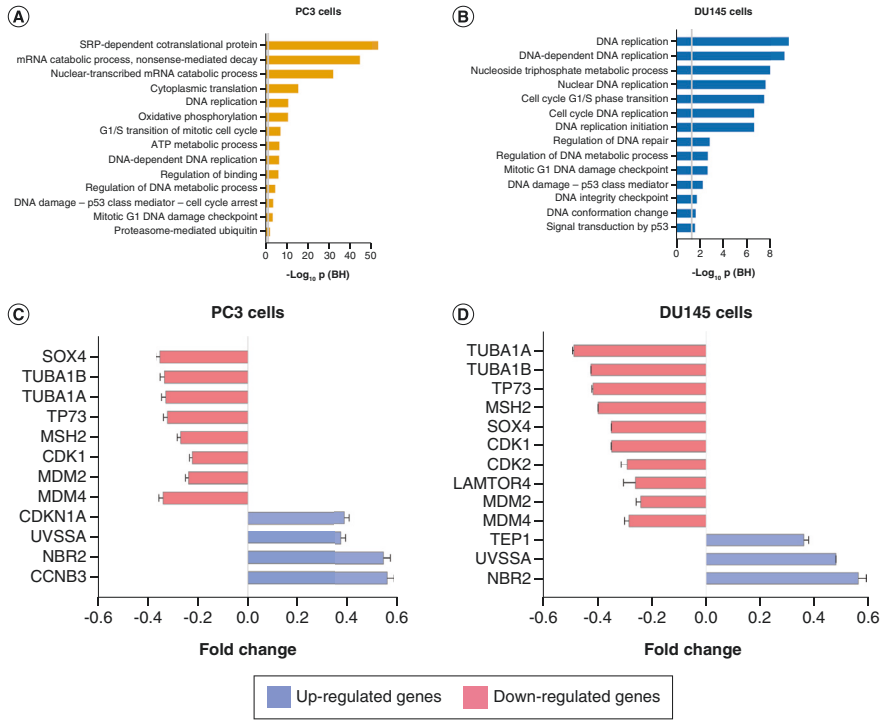

E

KEEG pathway	Value	p-value
DNA replication	1.78E-11	4.74326E-09
Oxidative phosphorylation	1.53908E-08	1.90762E-06
Cell cycle	158478E-07	1.05513E-05
p53 signaling pathway	0.003080914	0.038714185
Mismatch repair	0.001291764	0.02293448

F

KEEG pathway	Value	p-value
Oxidative phosphorylation	8.98472E-11	8.25964E-09
Protein processing in endoplasmic reticulum	5.66993E-09	3.90927E-07
DNA replication	1.71169E-07	5.24518E-06
Cell cycle	0.00058,759	0.011575,074
Ribosome	9.63442E-35	2.65707E-32

Figure 4. Inhibition of HIC on dynamic cellular damage. (A & B) Genome annotation using PANTHER was done in (A) PC3 and (B) DU145 cells. **(C & D)** The top differentially expressed genes involved in DNA damage upon HIC treatment in (C) PC3 and (D) DU145 cells are represented as a color-coded graph with red for downregulated genes and blue for upregulated genes. **(E & F)** Kyoto Encyclopedia of Genes and Genomes pathway regulated by HIC treatment in (E) PC3 and (F) DU145 cells. The expression of differentially expressed genes was considered significant when *$p < 0.05$.

more insights on the apoptotic effect of HIC, we also performed microarray analysis; key DEGs involved in the apoptotic process are listed in Figure 5B. Upon HIC treatment, key DEGs involved in the apoptotic process, such as *BAX* and *CDKN1A*, were found to be upregulated in both the PCa cell lines. *BAX* is known as a mediator of the tumor suppressor p53 in cancer [43]. Downregulation of several survival genes, such as *MYD88*, *MDM2*, *MDM4* and *TLR3*, was also noticed in both the cell lines. MYD88 protein functions as a negative regulator of TLR3, which is essential in restricting TLR3 signaling associated with the over expression of IFN-β [44]. MDM2 and MDM4 proteins negatively correlate with the expression of CDK inhibitor and directly interact with p21 and p53, hence promoting the degradation [40,41]. These observations suggest that the apoptotic phenomena induced by HIC in PCa cells might relate not only to p53 signaling but also to p21 pathways in both PC3 and DU145 cells. DNA damage and apoptosis response have been known to regulate cell cycle arrest and cell proliferation [45]. In this study, cell cycle analysis was done to identify the effect of HIC arresting the cells at different phases of cell division. As shown in Figure 5C & D, microscopic images revealed the percentage of PC3 cells in G1 phase significantly increased to 52.3 and 65.9% when treated with HIC and MRS2365, respectively, with 34.5% for

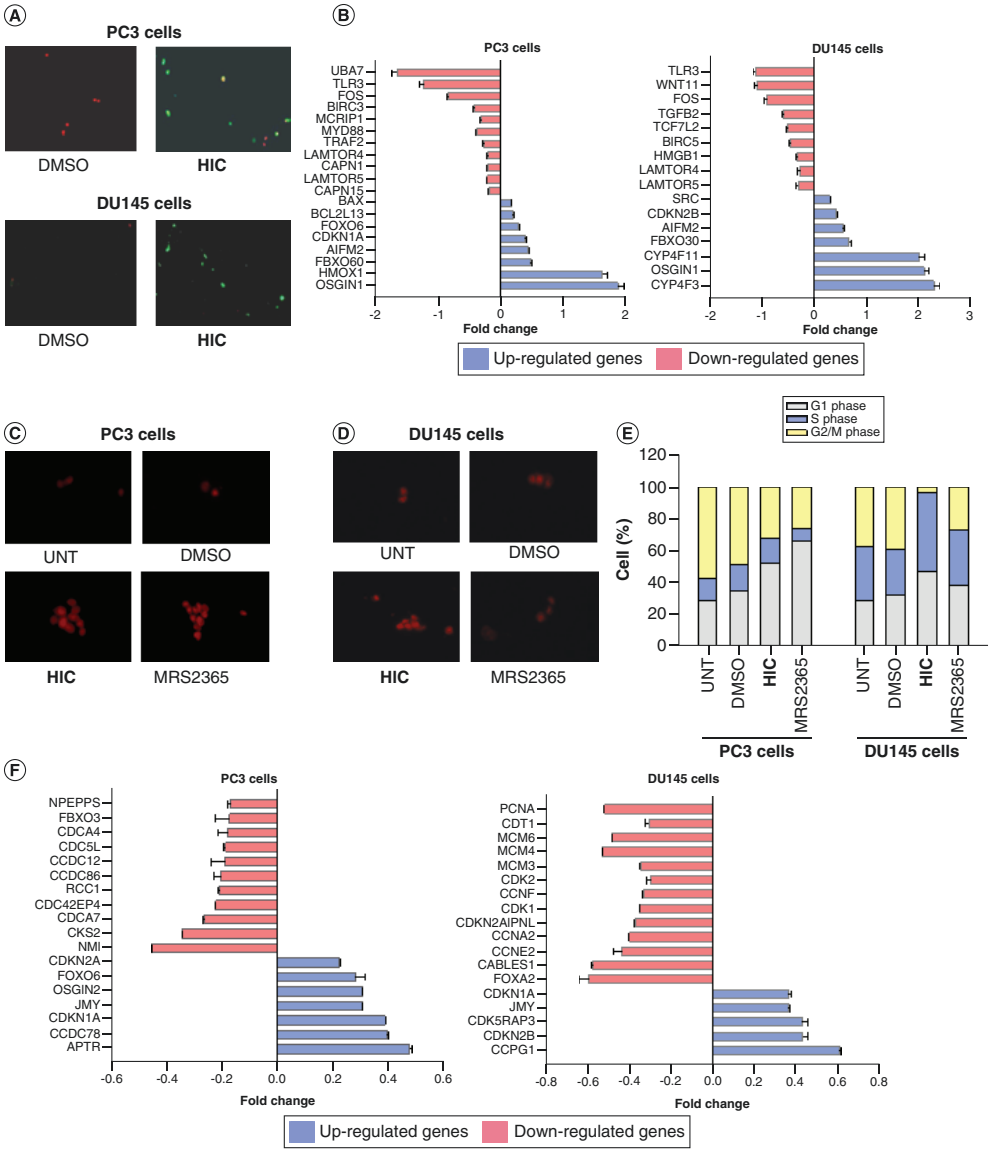

Figure 5. The activity of HIC through apoptotic response and G1/S cell cycle arrest in prostate cancer cells. (A) Microscopic images of PC3 and DU145 cells stained with Annexin-V/propidium iodide upon HIC treatment, with DMSO as vehicle control. **(B)** Top differentially expressed genes associated with apoptosis regulated by HIC treatment for PC3 and DU145 cells, represented as a color-coded graph. **(C & D)** Propidium iodide staining of **(C)** PC3 and **(D)** DU145 cells upon HIC treatment, with MRS2365 and DMSO as control. **(E)** Percentage of dividing cells in each phase of the cell cycle determined by MATLAB R2013b (*t*-tests; n = 6). **(F)** Key genes involved in cell cycle arrest and their fold changes, shown as a color-coded graph.

vehicle control (Figure 5E). The transition of PC3 cells to S phase was not significant among the samples (16.9, 15.4 and 8.2% upon DMSO, HIC and MRS2365 treatment, respectively). Likewise, the percentage of DU145 cells in G1 phase was about 46.7, 38.5 and 32.4% upon HIC, MRS2365 and DMSO treatment, respectively. Additionally, 49.7, 34.5 and 28.2% of DU145 cells in S phase was observed when treated with HIC, MRS2365

and DMSO, respectively (Figure 5E). It was observed that a higher fraction of cells was arrested at the proliferative G1 phase in PC3 cells and at G1/S phase in DU145 cells upon HIC treatment.

There are several biological processes involved in cell cycle pathways that were either inhibited or enhanced by HIC treatment in PC3 and DU145 cells (Supplementary Files 3 & 4). Based on the above data, the genes involved in G1/S phase were selectively analyzed (Figure 5F). In both PC3 and DU145 cells, *MCM*s, *CDKN1A* and *CDK2* expression were reduced by HIC. Downregulation of *MCM*s (*MCM2* and *MCM4* in PC3 cells; *MCM3*, *MCM4* and *MCM6* in DU145 cells) is known as a crucial component which restricts DNA elongation and thus inhibits the proliferation at G1 phase [46]. In addition, HIC reduced the expression of *CCNE2* and *CCNA2* in DU145 cells. Cyclins E (*CCNE2*) and A (*CCNA2*) are known as essential stimulators for G1/S phase initiation and activate CDK2 for initiation of DNA replication [47]. The downregulation of *CDK2* triggers the G1/S checkpoint through the activation of the p53-p21 pathways [48]. Also, HIC increased the expression of *CDKN2A* and *CDKN2B* which are involved in G1/S phase arrest [49]. Based on the gene expression data, p53 activation and the downregulation of cyclins and cyclin-dependent kinase were determined under HIC treatment in both cell lines. Collectively, the results suggest that HIC suppresses G1 progression in PC3 cells and G1/S transition in DU145 cells. The induction of G1/S phase arrest may be associated with the inhibitory effects of HIC on cancer cell growth and the activation of P2Y1R on cell apoptosis.

The antimetastatic effects of HIC on PCa cells

Several studies have reported that P2Y1R mediates cell growth and/or decreases cell proliferation in different cell lines [12,14,21]. Here we performed a cell migration and invasion assay to investigate the effect of HIC on PCa cell metastasis. The ability of HIC in inhibiting the migration of PC3 and DU145 cells was examined by a wound healing assay [50]. The cells were treated with the IC_{50} concentration of HIC on each cell line; the drug reduced the wound closure ability in a time-dependent manner when compared with the vehicle (Figure 6A & B). After 12 h of treatment, a similar pattern of inhibition of migration was observed in both cell lines upon HIC and MRS2365 treatment. However, after 24 h, HIC inhibited more cell migration than MRS2365 in both PC3 and DU145 cells. The wound area recovery was calculated for both PC3 and DU145 cells to compare the efficiency of HIC and MRS2365 as anti-metastasis agents. For HIC and MRS2365, respectively, the PC3 cell line showed $20.19 \pm 9.03\%$ and $21.05 \pm 9.2\%$ of recovery area at 12 h, and $37.15 \pm 7.32\%$ and $50.31 \pm 7.18\%$ at 24 h (Figure 6C). Similarly, in DU145 cells, the wound recovery rates of HIC- and MRS2365-treated cells after 12 h were $20.08 \pm 11.75\%$ and $24.76 \pm 12.21\%$, respectively. After 24 h, HIC showed $39.78 \pm 7.68\%$ migrated area, while MRS2365 presented a higher migrated area of about $64.23 \pm 6.77\%$ (Figure 6D).

The Transwell migration assay confirmed the above observations in which migrated cells were effectively reduced in the presence of HIC. The PCa cells were plated in 1% FBS medium in the upper chambers with or without drugs for 24 h. The Transwells along with migrated cells were stained with crystal violet (Figure 6E). Compared with the vehicle group, reductions of about $45.1 \pm 5.52\%$ and $55.7 \pm 5.95\%$, respectively, in the migration of PC3 and DU145 cells were observed when the cells were treated with HIC (Figure 6F). Thus the results indicate that HIC effectively reduced the movement of PC3 and DU145 cells. To further determine the inhibitory effect of HIC on the invaded cells, PCa cells were treated with the drug and allowed to invade in Matrigel-coated Transwells for 24 h (Figure 6G). HIC suppressed the invasion by $55.1 \pm 5.96\%$ and $50.8 \pm 8.81\%$ in PC3 and DU145 cells, respectively, when compared with the untreated group (Figure 6H). These data clearly showed that HIC could strongly suppress PCa cell invasion.

To explore the effect of HIC in detail, gene expression analysis was carried out simultaneously. Genes associated with cell migration and invasion are listed in Figure 6I & J. Here, the top 20 DEGs in PC3 and DU145 cells were reported upon HIC treatment. In both PCa cell lines, the expression of *TGFB2*, *TGFB3*, *MEF2C*, *ANXA3*, *SCG2, HMGB1* and *BMP4* was downregulated by HIC treatment. Among these genes, *TGFB2* and *TGFB3* belong to the TGF-β multifunctional cytokines family that promotes invasiveness and angiogenesis in tumor cells [51]. MEF2C transcription factor is known to induce epithelial–mesenchymal transition and invasiveness of carcinoma through the activity of TGF-β [52]. In addition, the downregulation of ANXA3 and BMP4 proteins suppresses tumor metastasis and decreases the proliferation of cancer cells through the inhibition of matrix metalloproteinases [53,54]. *SCG2*, encoding the motility-related protein SGII, is highly expressed in cancer tissue and involved in cancer cell migration [55]. *HMGB1* is also upregulated in several types of cancers, while its downregulation inhibits cell proliferation, migration and invasion [56]. The downregulation of SCG2 and HMGB1 protein in PC3 cells was observed upon HIC treatment, suggesting the crucial effect of HIC on prostate cancer cell migration. Similarly, HIC

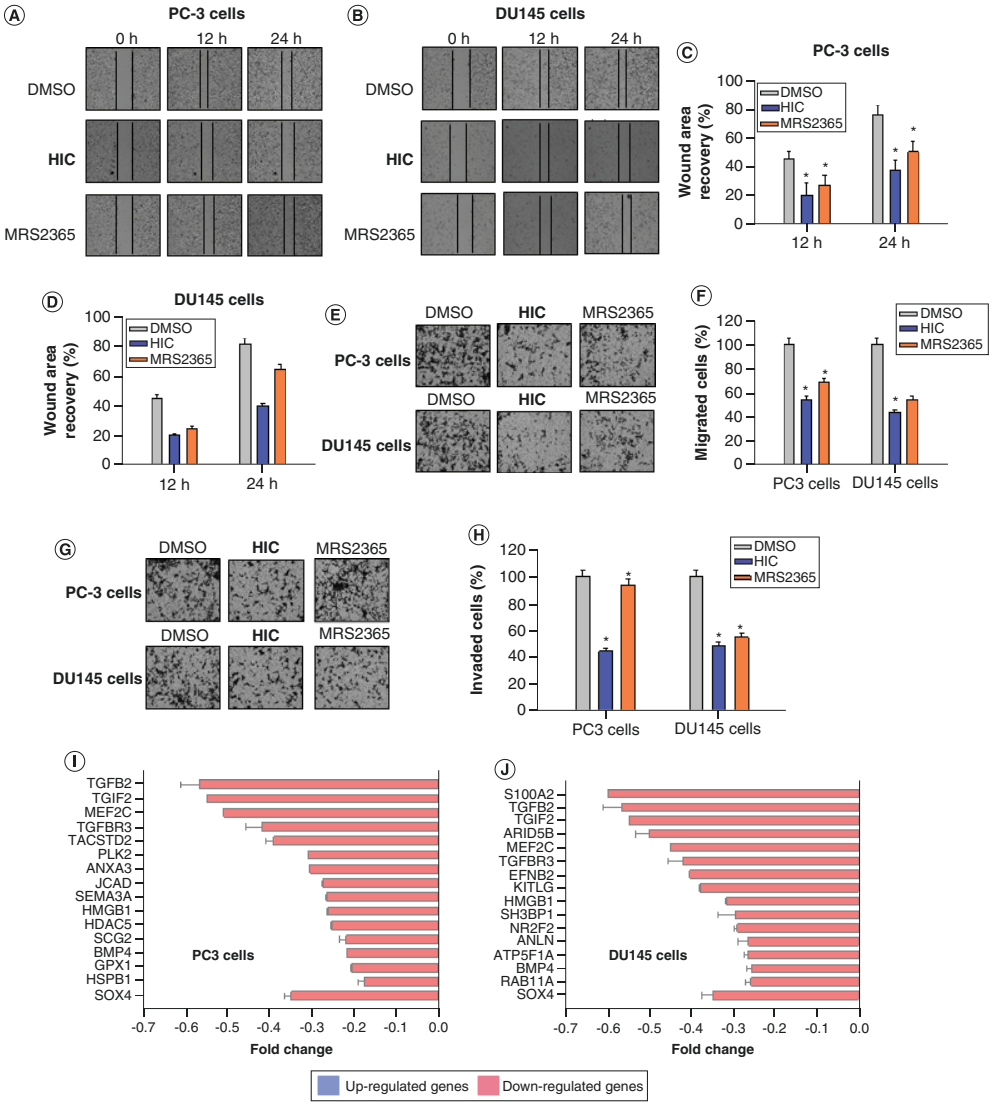

Figure 6. The antimetastatic effects of HIC on prostate cancer cells. (A & B) Wound healing assay showing the ability of HIC in inhibiting the migration of **(A)** PC3 and **(B)** DU145 cells at different time points (0, 12 and 24 h). **(C & D)** Percentage of wound area recovery was calculated for **(C)** PC3 and **(D)** DU145 cells upon HIC treatment, with MRS2365 as positive control and DMSO as vehicle control. **(E)** Microscopic images of HIC-treated prostate cancer (PCa) cells showing Transwell migration assay. **(F)** Percentage of inhibition of migration of PCa cells after HIC treatment. **(G)** Microscopic images of PCa cells in Matrigel-coated Transwell, representing the invaded cells. **(H)** Percentage of inhibition of invasion of PCa cells after HIC treatment. **(I & J)** Top differentially expressed genes associated with cell migration and invasion in **(I)** PC3 and **(J)** DU145 cell lines upon HIC treatment, represented as color-coded graphs.

downregulated the expression of *SOX4*, *MDM2* and *MDM4* in both cell lines; these could inhibit cell proliferation, migration and apoptosis induction, thus regulating p53 activity. Notably, in human cancers, downregulation of wild-type p53 function is inhibited by high levels of MDM2 and MDM4, which in turn lead to the downregulation of tumor-suppressive p53 pathways. The inhibition of MDM2 and MDM4–p53 interaction regulates p53 activity and stability, enhancing DNA damage and reducing cell survival; hence it presents an appealing therapeutic strategy

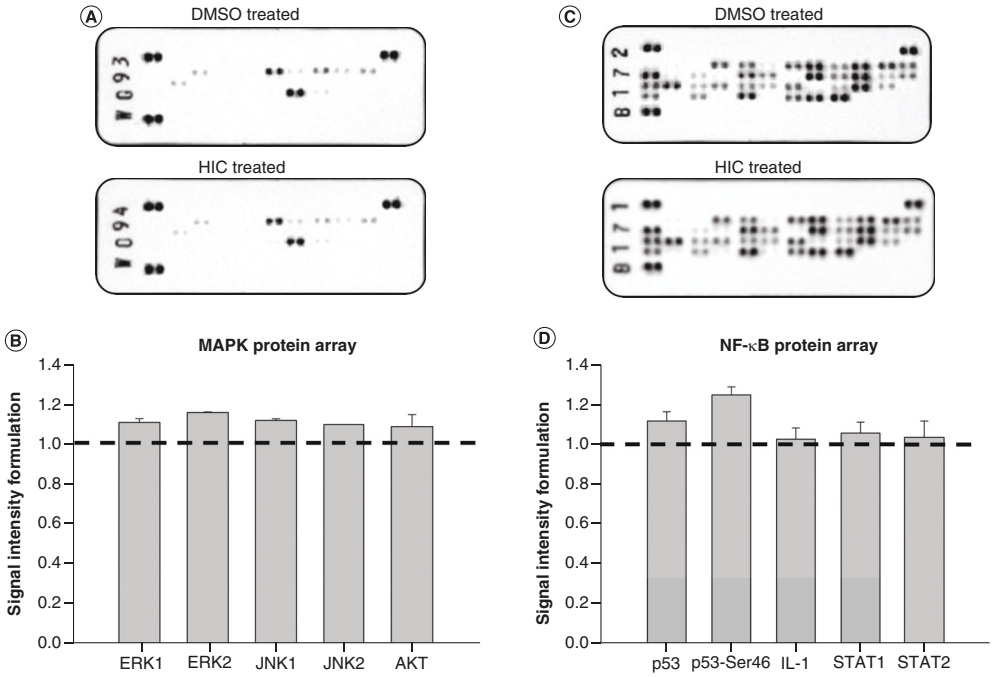

Figure 7. Regulation of HIC on MAPK and NF-κB signaling pathways. (A) Phospho-MAPK protein array analysis in DU145 cells treated with HIC after 48 h. **(B)** Bar chart showing the relative density of expression of proteins of MAPK between HIC- and DMSO-treated groups. **(C)** NF-κB protein array analysis in DU145 cells treated with HIC after 48 h. Images were captured using Xenogen IVIS 200 imaging system. **(D)** Bar diagram showing the relative expression of NF-κB protein with the percentage changes in luminescence intensity relative to DMSO control.

for the treatment of cancer [57]. Collectively, the results suggest that HIC negatively affects cell metastasis through the regulation of TGF-β and p53 pathways in PCa cells.

Regulation of MAPK & NF-κB signaling pathway

The association of P2Y1R with the activation of NF-κB and MAPK signaling prompted us to examine the effect of HIC on the respective protein expression. We selected DU145 cells for these mechanistic studies because HIC seemed to be more effective in suppressing their growth and inducing G1/S phase arrest. To identify which phosphorylated kinase was significantly stimulated by HIC, protein profiling of a human phospho-MAPK protein array using the DU145 cell line was done. DU145 cells were treated with HIC, with DMSO as vehicle control, then the samples were tested for the differential expression of phosphorylated kinases. Twenty-four differentially phosphorylated kinases were identified in the phospho-MAPK array. Changes in the expression of very few kinases were observed between HIC- and DMSO-treated groups (Figure 7A); the fold change of phosphorylation levels with p-value < 0.05 is presented in Figure 7B. Increased expression of ERK1/2, JNK1/2 and AKT phosphorylation was observed in HIC-treated cells. The fold changes in the signal intensity of phosphorylated proteins ERK1, ERK2, JNK1, JNK2 and AKT (Ser473) were found to be 1.1, 1.21, 1.11, 1.09 and 1.08, respectively. These results are consistent with the function of P2Y1R, which upregulates the activated forms of ERK1/2, JNK1/2 and AKT. Conversely, phosphorylation of p38 and MKK3/6 remained unchanged over basal levels by HIC treatment in comparison with the DMSO group. ERK1/2 activation is known to regulate p53 signaling-dependent G1 arrest, which mediates either cell growth or apoptotic response based on the downstream targets [58–60]. In addition, JNK1/2 has been demonstrated to stimulate p53 signaling and the downstream target of p53 [61–63]. The p53 pathway has been reported as the essential tumor suppressor for cell apoptosis, G1 cell cycle arrest and cell proliferation [64]. To get more insight into the modulatory effect of P2Y1R on the NF-κB pathway, we performed a proteome profiler array

to identify the differential expression of proteins of NF-κB signaling upon HIC treatment. Five out of 27 proteins were differentially expressed between the HIC- and DMSO-treated groups ($p < 0.05$; Figure 7C). Protein p53 and phosphorylated protein p53-Ser46 were increased, with fold changes of 1.11 and 1.24, respectively, for the HIC and DMSO groups (Figure 7D). One of the most important p53 functions is its ability to activate apoptosis through transcription-dependent and transcription-independent mechanisms. Moreover, the phosphorylated form of p53 at Ser46 enhances apoptosis by activating proapoptotic target gene transcription. The levels of IL-1, STAT1 and STAT2 proteins were slightly increased by HIC, with fold changes of 1.02, 1.05 and 1.03, respectively. Interestingly, the protein expression of I-κB, NF-κB remained unchanged on HIC treatment. Collectively, the results suggest that HIC could suppress the proliferation of cancer cells through ERK1/2, JNK and p53 signaling pathways.

Discussion

Several studies have shown that P2Y1R has a dual function in promoting or inhibiting cancer cell proliferation and metastasis [21,23,65]. Our previous report has shown that HIC, a selective agonist of P2Y1R, reduces PCa cell growth in a time- and dose-dependent manner [10]. In addition, HIC promotes cell apoptosis by increasing the activity of caspase 3/7 and ROS production.

In this study we performed several experiments to investigate the mechanism and anticancer effects of HIC in PC3 and DU145 cell models. HIC was found to inhibit colony formation and cell proliferation in PCa cells (Figure 1). Moreover, the results indicated that HIC exhibited antitumor activity by reducing spheroid areas in a time- and dose-dependent manner in a system that more closely resembles the *in vivo* setting (Figure 2). GO analysis revealed the list of genes upregulated and downregulated by HIC included genes involved in DNA replication, DNA damage in response to signal transduction by p53 tumor suppressor and p21, G1/S arrest phase DNA damage (Figures 3 & 4). Thus DNA damage was induced in both PC3 cells and DU145 cells by HIC treatment related to p53 signaling. Our data also showed the anticancer activity of HIC through the apoptosis, G1/S phase arrest and p53 upregulation effects in both PCa cell lines (Figure 5). Apoptotic response was then determined with the downregulated genes such as *MYD88*, *FOS*, *MDM2*, *MDM4* and *TLR3* and upregulated genes such as *BAX*, *CDK1A* and *FBXO*. MDM2 and MDM4 are known to increase p53 protein degradation, while BAX is the crucial mediator for proapoptotic signaling through the activation of p53 [40,66,67]. In addition, HIC induces cell cycle arrest at G1 phase of PC3 cells and G1/S phase of DU145 cells, through the downregulation of cyclin-dependent kinases. We found that HIC induced cell cycle arrest in both PCa cell lines at G1, which was associated with downregulation of *CDK1*, *TP73*, *MCM4* and *MCM6*. In addition, Cyclin E and Cyclin A, essential stimulators for G1/S cell cycle progression, were decreased by HIC in DU145 cells [68]. Additionally, the antimetastatic effect of HIC on PCa cells was observed through the inhibition of migrating and invading cells. Genes involved in the metastatic process (*TGB2*, *TGFB3*, *MEF2C*, *ANXA3* and *BMP4*) were found to be downregulated under HIC treatment. These genes regulate to TGF-β receptor and increase the metastatic process in cells [51–54]. Several studies have reported that the cross-talk between p53 and TGF-β signaling regulates cell growth and cell phase arrest [69,70]. Collectively, HIC might induce p53 signaling and promote cell death through its activation.

Multiple signaling pathways have an influence on p53 activation, such as MAPKs and NF-κB pathways [71]. P2Y1R activation also induces the phosphorylation of ERK1/2 and JNK1/2 and involves NF-κB pathways in cancer and inflammation [72,73]. MAPK signaling has been known to promote either cell growth or cell apoptosis depending on the cell types and catalysts [19]. Especially, ERK1/2 activation is linked with the subsequent phosphorylation and stabilization of p53 for apoptosis [23,58–60]. In addition, JNK1/2 has been reported to directly or indirectly modulate p53 and its downstream targets in cell death [20,61–63]. Here we found that the protein levels of ERK1/2 and JNK1/2 phosphorylation were increased by HIC in DU145 cells. These results were consistent with the hypothesis that P2Y1R could regulate p53 stabilization through the activation of ERK1/2 and JNK1/2 [20]. The stabilization of p53 protein inducing DNA damage and G1/S phase arrest could decrease the expression of cancer genes that are conducive to metastasis [74]. In addition, the protein expression of I-κB and NF-κB remained unchanged, whereas IL-1 expression was slightly increased with a fold change of about 1.03 in the NF-κB protein array. Therefore the regulation of NF-κB signaling through the activation of P2Y1R by HIC was not observed in PCa cells. However, the expression of p53 and p53-Ser46 proteins was increased by HIC treatment. These proteins promote apoptosis through the activation of proapoptotic target transcription [74]. In addition, our previous study showed that P2Y1R activation increased the Ca^{2+}, caspase 3/7 activity and ROS levels in PC3 and DU145 cells. Ca^{2+}, PKC-α and PKC-δ are important P2Y1R secondary messengers that help in MAPK activation [75–77]. Ca^{2+} levels directly increase the phosphorylation level of ERK1/2 in mammalian cell models [78]. Moreover, PKC-α is known as a

mediator for p53 activity, which plays a crucial role in preventing cell growth by ADP and 2-MeSADP, agonists of P2Y1R [20,75].

Overall, our results suggest new insights into the use of HIC in PCa treatment. HIC induces apoptosis and cell cycle arrest by modulating P2Y1R activation and the p53 signaling pathway. The anticancer effect of HIC on inhibiting PCa cells' growth and spheroid development implies HIC as a potential cancer therapeutic. It is likely that HIC can be developed as an anticancer agent against PCa proliferation.

Conclusion

Overall, our findings are consistent with the earlier studies on the anticancer effect of P2Y1 agonists in cancer cells and in PCa cells in particular. HIC regulates several genes involved in DNA damage, the major cell cycle checkpoints, apoptotic response and metastasis. Additionally, it inhibits cell proliferation and migration through the modulation of MAPKs and p53 signaling pathways. Thus HIC can be developed for the treatment of PCa.

Future perspective

PCa is the second leading cause of cancer-related death in men. Surgery in combination with radiation therapy, chemotherapy and hormonal therapy is the main mode of treatment for PCa. New treatment regimens are pursued to extend the survival of cancer patients with metastasis. The present research on P2Y1R and HIC-mediated cell death and apoptosis will provide therapeutic advances in PCa treatment. The regulation of P2Y1R activation and stabilization of p53 protein by HIC might improve the understanding of cell proliferation and DNA damage in PCa treatment. The evidence provided by the present research on cellular migration and invasion, gene expression analysis and cell cycle analysis might increase the therapeutic implications for advanced PCa treatment.

Summary points

- The functional activity of (1-(2-hydroxy-5-nitrophenyl)(4-hydroxyphenyl)methyl)indoline-4-carbonitrile (HIC), an agonist of the P2Y1 receptor, was evaluated.
- HIC reduced the cell proliferation, adherence property and spheroid formation of prostate cancer cells.
- HIC was able to arrest the cell cycle at G1/S phase and induced apoptosis.
- HIC regulates the downstream signaling pathways of prostate cancer cells.
- HIC affects p53, MAPK and NF-κB.
- HIC activated the phosphorylation of ERK1/2 and JNK1/2, p53 and p53-ser46 proteins.
- HIC functioned as a p53 stabilizer for prostate cancer cell death induction.

Supplementary data

To view the supplementary data that accompany this paper please visit the journal website at: www.future-science.com/doi/suppl/10.4155/fmc-2021-0159

Financial & competing interests disclosure

H Le acknowledges TUT-RAE for the project grant support and Tamper University for Instrumental facility grant support. N Candeias acknowledges the Janne and Aatos Erkko Foundation, Academy of Finland (Decision 326487) and Fundação para a Ciência e Tecnologia (CEE-CINST/2018) for financial support. The authors also thank A Musa, Tampere University for the technical support in gene expression analysis. The authors have no other relevant affiliations or financial involvement with any organization or entity with a financial interest in or financial conflict with the subject matter or materials discussed in the manuscript apart from those disclosed.

No writing assistance was utilized in the production of this manuscript.

References

1. Attard G, Parker C, Eeles RA *et al.* Prostate cancer. *Lancet* 387(10013), 70–82 (2016).
2. Litwin MS, Tan HJ. The diagnosis and treatment of prostate cancer: a review. *JAMA* 317(24), 2532–2542 (2017).
3. Marucci G, Santinelli C, Buccioni M *et al.* Anticancer activity study of A3 adenosine receptor agonists. *Life Sci.* 205, 155–163 (2018).
4. Yu S, Sun L, Jiao Y, Lee LTO. The role of G protein-coupled receptor kinases in cancer. *Int. J. Biol. Sci.* 14(2), 189–203 (2018).
5. Saengsawang W, Rasenick MM. G protein-coupled receptors. *Encycl. Cell Biol.* 3, 51–55 (2016).
6. Janssens R, Communi D, Pirotton S, Samson M, Parmentier M, Boeynaems JM. Cloning and tissue distribution of the human P2Y1 receptor. *Biochem. Biophys. Res. Commun.* 221(3), 588–593 (1996).

7. Wei Q, Costanzi S, Liu QZ, Gao ZG, Jacobson KA. Activation of the P2Y1 receptor induces apoptosis and inhibits proliferation of prostate cancer cells. *Biochem. Pharmacol.* 82(4), 418–425 (2011).
8. Li WH, Qiu Y, Zhang HQ *et al.* P2Y2 receptor promotes cell invasion and metastasis in prostate cancer cells. *Br. J. Cancer* 109(6), 1666–1675 (2013).
9. Shabbir M, Ryten M, Thompson C, Mikhailidis D, Burnstock G. Characterization of calcium-independent purinergic receptor-mediated apoptosis in hormone-refractory prostate cancer. *BJU Int.* 101(3), 352–359 (2008).
10. Le HTT, Rimpilainen T, Konda Mani S *et al.* Synthesis and preclinical validation of novel P2Y1 receptor ligands as a potent anti-prostate cancer agent. *Sci. Rep.* 9(1), 18938 (2019).
11. Buvinic S, Bravo-Zehnder M, Boyer JL, Huidobro-Toro JP, González A. Nucleotide P2Y1 receptor regulates EGF receptor mitogenic signaling and expression in epithelial cells. *J. Cell Sci.* 120(Pt 24), 4289–4301 (2007).
12. Woehrle T, Ledderose C, Rink J, Slubowski C, Junger WG. Autocrine stimulation of P2Y1 receptors is part of the purinergic signaling mechanism that regulates T cell activation. *Purinergic Signal.* 15(2), 127–137 (2019).
13. Niimi K, Ueda M, Fukumoto M *et al.* Transcription factor FOXO1 promotes cell migration toward exogenous ATP via controlling P2Y1 receptor expression in lymphatic endothelial cells. *Biochem. Biophys. Res. Commun.* 489(4), 413–419 (2017).
14. Mamedova LK, Gao ZG, Jacobson KA. Regulation of death and survival in astrocytes by ADP activating P2Y1 and P2Y12 receptors. *Biochem. Pharmacol.* 72(8), 1031–1041 (2006).
15. Harden TK, Waldo GL, Hicks SN, Sondek J. Mechanism of activation and inactivation of Gq/phospholipase C-β signaling nodes. *Chem. Rev.* 111(10), 6120–6129 (2011).
16. Mizuno N, Itoh H. Functions and regulatory mechanisms of Gq-signaling pathways. *NeuroSignals* 17(1), 42–54 (2009).
17. Xu KP, Dartt DA, Yu FSX. EGF-induced ERK phosphorylation independent of PKC isozymes in human corneal epithelial cells. *Investig. Ophthalmol. Vis. Sci.* 43(12), 3673–3679 (2002).
18. Yin J, Yu FSX. ERK1/2 mediate wounding- and G-protein-coupled receptor ligands-induced EGFR activation via regulating ADAM17 and HB-EGF shedding. *Investig. Ophthalmol. Vis. Sci.* 50(1), 132–139 (2009).
19. Sun Y, Liu WZ, Liu T, Feng X, Yang N, Zhou HF. Signaling pathway of MAPK/ERK in cell proliferation, differentiation, migration, senescence and apoptosis. *J. Recept. Signal Transduct.* 35(6), 600–604 (2015).
20. Muscella A, Cossa LG, Vetrugno C, Antonaci G, Marsigliante S. Inhibition of ZL55 cell proliferation by ADP via PKC-dependent signalling pathway. *J. Cell. Physiol.* 233(3), 2526–2536 (2018).
21. Wong PC, Watson C, Crain EJ. The P2Y1 receptor antagonist MRS2500 prevents carotid artery thrombosis in cynomolgus monkeys. *J. Thromb. Thrombolysis* 41(3), 514–521 (2016).
22. Li Y, Yin C, Liu P, Li D, Lin J. Identification of a different agonist-binding site and activation mechanism of the human P2Y1 receptor. *Sci. Rep.* 7(1), 13764 (2017).
23. Shen J, DiCorleto PE. ADP stimulates human endothelial cell migration via P2Y1 nucleotide receptor-mediated mitogen-activated protein kinase pathways. *Circ. Res.* 102(4), 448–456 (2008).
24. Borowicz S, Van Scoyk M, Avasarala S *et al.* The soft agar colony formation assay. *J. Vis. Exp.* (92), e51998 (2014).
25. Pehkonen H, Lento M, Von Nandelstadh P *et al.* Liprin-α1 modulates cancer cell signaling by transmembrane protein CD82 in adhesive membrane domains linked to cytoskeleton. *Cell Commun. Signal.* 16(1), 41 (2018).
26. Hubbard T, Barker D, Birney E *et al.* The Ensembl genome database project. *Nucleic Acids Res.* 30(1), 38–41 (2002).
27. Babraham Institute. FASTQC: a quality control tool for high throughput sequence data. www.bioinformatics.babraham.ac.uk/projects/fastqc/
28. Dobin A, Davis CA, Schlesinger F *et al.* STAR: ultrafast universal RNA-seq aligner. *Bioinformatics* 29(1), 15–21 (2013).
29. Li H, Handsaker B, Wysoker A *et al.* The Sequence Alignment/Map format and SAMtools. *Bioinformatics* 25(16), 2078–2079 (2009).
30. Anders S, Pyl PT, Huber W. HTSeq – a Python framework to work with high-throughput sequencing data. *Bioinformatics* 31(2), 166–169 (2015).
31. Love MI, Huber W, Anders S. Moderated estimation of fold change and dispersion for RNA-seq data with DESeq2. *Genome Biol.* 15(12), 550 (2014).
32. Benjamini Y, Hochberg Y. Controlling the false discovery rate: a practical and powerful approach to multiple testing. *J. R. Stat. Soc. Ser. B* 57(1), 289–300 (1995).
33. Ashburner M, Ball CA, Blake JA *et al.* Gene ontology: tool for the unification of biology. *Nat. Genet.* 25(1), 25–29 (2000).
34. Yu G, Wang LG, Han Y, He QY. ClusterProfiler: an R package for comparing biological themes among gene clusters. *OMICS* 16(5), 284–287 (2012).
35. Kanehisa M, Goto S. KEGG: Kyoto Encyclopedia of Genes and Genomes. *Nucleic Acids Res.* 28(1), 27–30 (2000).
36. Wang HY, Kim NH. CDK2 is required for the DNA damage response during porcine early embryonic development. *Biol. Reprod.* 95(2), 31 (2016).

37. Gao SY, Li J, Qu XY, Zhu N, Ji YB. Downregulation of Cdk1 and CyclinB1 expression contributes to oridonin-induced cell cycle arrest at G2/M phase and growth inhibition in SGC-7901 gastric cancer cells. *Asian Pacific J. Cancer Prev.* 15(15), 6437–6441 (2014).
38. Hur W, Rhim H, Jung CK *et al.* SOX4 overexpression regulates the p53-mediated apoptosis in hepatocellular carcinoma: clinical implication and functional analysis *in vitro*. *Carcinogenesis* 31(7), 1298–1307 (2010).
39. Urist M, Tanaka T, Poyurovsky MV, Prives C. p73 induction after DNA damage is regulated by checkpoint kinases Chk1 and Chk2. *Genes Dev.* 18(24), 3041–3054 (2004).
40. Mancini F, Pieroni L, Monteleone V *et al.* MDM4/HIPK2/p53 cytoplasmic assembly uncovers coordinated repression of molecules with anti-apoptotic activity during early DNA damage response. *Oncogene* 35(2), 228–240 (2016).
41. Toledo F, Wahl GM. MDM2 and MDM4: p53 regulators as targets in anticancer therapy. *Int. J. Biochem. Cell Biol.* 39(7–8), 1476–1482 (2007).
42. Hussain T, Saha D, Purohit G *et al.* Transcription regulation of *CDKN1A* (*p21/CIP1/WAF1*) by TRF2 is epigenetically controlled through the REST repressor complex. *Sci. Rep.* 7(1), 11541 (2017).
43. Nag S, Qin J, Srivenugopal KS, Wang M, Zhang R. The MDM2–p53 pathway revisited. *J. Biomed. Res.* 27(4), 254–271 (2013).
44. Siednienko J, Gajanayake T, Fitzgerald KA, Moynagh P, Miggin SM. Absence of MyD88 results in enhanced TLR3-dependent phosphorylation of IRF3 and increased IFN-β and RANTES production. *J. Immunol.* 186(4), 2514–2522 (2011).
45. Matt S, Hofmann TG. The DNA damage-induced cell death response: a roadmap to kill cancer cells. *Cell. Mol. Life Sci.* 73(15), 2829–2850 (2016).
46. Das SP, Borrman T, Liu VWT, Yang SCH, Bechhoefer J, Rhind N. Replication timing is regulated by the number of MCMs loaded at origins. *Genome Res.* 25(12), 1886–1892 (2015).
47. Gordon E, Ravicz J, Liu S, Chawla S, Hall F. Cell cycle checkpoint control: the cyclin G1/Mdm2/p53 axis emerges as a strategic target for broad-spectrum cancer gene therapy – a review of molecular mechanisms for oncologists. *Mol. Clin. Oncol.* 9(2), 115–134 (2018).
48. Neganova I, Vilella F, Atkinson SP *et al.* An important role for CDK2 in G1 to S checkpoint activation and DNA damage response in human embryonic stem cells. *Stem Cells* 29(4), 651–659 (2011).
49. Peyressatre M, Prével C, Pellerano M, Morris MC. Targeting cyclin-dependent kinases in human cancers: from small molecules to peptide inhibitors. *Cancers (Basel)* 7(1), 179–237 (2015).
50. Doan P, Nguyen T, Yli-Harja O *et al.* Effect of alkylaminophenols on growth inhibition and apoptosis of bone cancer cells. *Eur. J. Pharm. Sci.* 107, 208–216 (2017).
51. Haque S, Morris JC. Transforming growth factor-β: a therapeutic target for cancer. *Hum. Vaccines Immunother.* 13(8), 1741–1750 (2017).
52. Xu J, Lamouille S, Derynck R. TGF-β-induced epithelial to mesenchymal transition. *Cell Res.* 19(2), 156–172 (2009).
53. Ampuja M, Jokimäki R, Juuti-Uusitalo K, Rodriguez-Martinez A, Alarmo EL, Kallioniemi A. BMP4 inhibits the proliferation of breast cancer cells and induces an MMP-dependent migratory phenotype in MDA-MB-231 cells in 3D environment. *BMC Cancer* 13, 429 (2013).
54. Du R, Liu B, Zhou L *et al.* Downregulation of annexin A3 inhibits tumor metastasis and decreases drug resistance in breast cancer. *Cell Death Dis.* 9(2), 126 (2018).
55. Peitsch WK, Doerflinger Y, Fischer-Colbrie R *et al.* Desmoglein 2 depletion leads to increased migration and upregulation of the chemoattractant secretoneurin in melanoma cells. *PLoS ONE* 9(2), e89491 (2014).
56. Shen H, Xu L, You C *et al.* miR-665 is downregulated in glioma and inhibits tumor cell proliferation, migration and invasion by targeting high mobility group box 1. *Oncol. Lett.* 21(2), 156 (2021).
57. Woodfield SE, Shi Y, Patel RH *et al.* MDM4 inhibition: a novel therapeutic strategy to reactivate p53 in hepatoblastoma. *Sci. Rep.* 11(1), 2967 (2021).
58. Fukasawa K, Vande Woude GF. Synergy between the Mos/mitogen-activated protein kinase pathway and loss of p53 function in transformation and chromosome instability. *Mol. Cell. Biol.* 17(1), 506–518 (1997).
59. Mor O, Yaron P, Huszar M *et al.* Absence of *p53* mutations in malignant mesotheliomas. *Am. J. Respir. Cell Mol. Biol.* 16(1), 9–13 (1997).
60. Okuda T, Otsuka J, Sekizawa A *et al. p53* mutations and overexpression affect prognosis of ovarian endometrioid cancer but not clear cell cancer. *Gynecol. Oncol.* 88(3), 318–325 (2003).
61. Chen L, Wang S, Zhou Y *et al.* Identification of early growth response protein 1 (EGR-1) as a novel target for JUN-induced apoptosis in multiple myeloma. *Blood* 115(1), 61–70 (2010).
62. Fan M, Goodwin ME, Birrer MJ, Chambers TC. The c-Jun NH2-terminal protein kinase/AP-1 pathway is required for efficient apoptosis induced by vinblastine. *Cancer Res.* 61(11), 4450–4458 (2001).
63. Saha MN, Jiang H, Yang Y *et al.* Targeting p53 via JNK pathway: a novel role of RITA for apoptotic signaling in multiple myeloma. *PLoS ONE* 7(1), e30215 (2012).

64. Chen J. The cell-cycle arrest and apoptotic functions of p53 in tumor initiation and progression. *Cold Spring Harb. Perspect. Med.* 6(3), a026104 (2016).
65. Domercq M, Brambilla L, Pilati E, Marchaland J, Volterra A, Bezzi P. P2Y1 receptor-evoked glutamate exocytosis from astrocytes. *J. Biol. Chem.* 281(41), 30684–30696 (2006).
66. Shadfan M, Lopez-Pajares V, Yuan ZM. MDM2 and MDMX: alone and together in regulation of p53. *Transl. Cancer Res.* 1(2), 88–89 (2012).
67. Pearson AS, Spitz FR, Swisher SG *et al.* Up-regulation of the proapoptotic mediators Bax and Bak after adenovirus-mediated *p53* gene transfer in lung cancer cells. *Clin. Cancer Res.* 6(3), 887–890 (2000).
68. Zhu J, Chen M, Chen N *et al.* Glycyrrhetinic acid induces G1-phase cell cycle arrest in human non-small cell lung cancer cells through endoplasmic reticulum stress pathway. *Int. J. Oncol.* 46(3), 981–988 (2015).
69. Higgins SP, Tang Y, Higgins CE *et al.* TGF-β1/p53 signaling in renal fibrogenesis. *Cell. Signal.* 43, 1–10 (2018).
70. Oh IR, Raymundo B, Kim MJ, Kim CW. Mesenchymal stem cells co-cultured with colorectal cancer cells showed increased invasive and proliferative abilities due to its altered p53/TGF-β1 levels. *Biosci. Biotechnol. Biochem.* 84(2), 256–267 (2020).
71. Gen SW. The functional interactions between the p53 and MAPK signaling pathways. *Cancer Biol. Ther.* 3(2), 156–161 (2004).
72. van der Vorst EPC, Theodorou K, Wu Y *et al.* High-density lipoproteins exert pro-inflammatory effects on macrophages via passive cholesterol depletion and PKC-NF-κB/STAT1-IRF1 signaling. *Cell Metab.* 25(1), 197–207 (2017).
73. Chen L, He HY, Li HM *et al.* ERK1/2 and p38 pathways are required for P2Y receptor-mediated prostate cancer invasion. *Cancer Lett.* 215(2), 239–247 (2004).
74. Hafner A, Bulyk ML, Jambhekar A, Lahav G. The multiple mechanisms that regulate p53 activity and cell fate. *Nat. Rev. Mol. Cell Biol.* 20(4), 199–210 (2019).
75. Muscella A, Vetrugno C, Antonaci G, Cossa LG, Marsigliante S. PKC-δ/PKC-α activity balance regulates the lethal effects of cisplatin. *Biochem. Pharmacol.* 98(1), 29–40 (2015).
76. Basu A. Involvement of protein kinase C-δ in DNA damage-induced apoptosis. *J. Cell. Mol. Med.* 7(4), 341–350 (2003).
77. Chuderland D, Seger R. Calcium regulates ERK signaling by modulating its protein–protein interactions. *Commun. Integr. Biol.* 1(1), 4–5 (2008).
78. Liu Y, Song X, Shi Y *et al.* WNK1 activates large-conductance Ca2+-activated K+ channels through modulation of ERK1/2 signaling. *J. Am. Soc. Nephrol.* 26(4), 844–854 (2015).

PUBLICATION IV

P2Y1 agonist HIC in combination with androgen receptor inhibitor abiraterone acetate impairs cell growth of prostate cancer

H. Le, A. Murugesan, N. R. Candeias, T. Ramesh, O. Yli-Harja, and M. Kandhavelu

Apoptosis (2022), 27

DOI: 10.1007/s10495-022-01716-1

Apoptosis (2022) 27:283–295
https://doi.org/10.1007/s10495-022-01716-1

P2Y1 agonist HIC in combination with androgen receptor inhibitor abiraterone acetate impairs cell growth of prostate cancer

Hien Thi Thu Le[1] · Akshaya Murugesan[1,2] · Nuno R. Candeias[3,4] · Thiyagarajan Ramesh[5] · Olli Yli-Harja[6,7] · Meenakshisundaram Kandhavelu[1]

Accepted: 24 January 2022 / Published online: 7 February 2022

Abstract
P2Y receptors belong to the large superfamily of G-protein-coupled receptors and play a crucial role in cell death and survival. P2Y1 receptor has been identified as a marker for prostate cancer (PCa). A previously unveiled selective P2Y1 receptor agonist, the indoline-derived HIC (1-(1-((2-hydroxy-5-nitrophenyl)(4-hydroxyphenyl)methyl)indoline-4-carbonitrile), induces a series of molecular and biological responses in PCa cells PC3 and DU145, but minimal toxicity to normal cells. Here, we evaluated the combinatorial effect of HIC with abiraterone acetate (AA) targeted on androgen receptor (AR) on the inhibition of PCa cells. Here, the presence of HIC and AA significantly inhibited cell proliferation of PC3 and DU145 cells with time-dependent manner as a synerfistic combination. Moreover, it was also shown that the anticancer and antimetastasis effects of the combinratorial drugs were noticed through a decrease in colony-forming ability, cell migration, and cell invasion. In addition, the HIC + AA induced apoptotic population of PCa cells as well as cell cycle arrest in G1 progression phase. In summary, these studies show that the combination of P2Y1 receptor agonist, HIC and AR inhibitor, AA, effectively improved the antitumor activity of each drug. Thus, the combinatorial model of HIC and AA should be a novel and promising therapeutic strategy for treating prostate cancer.

Keywords Prostate cancer · Abiraterone acetate · Indoline · Apoptosis · Proliferation

✉ Meenakshisundaram Kandhavelu
Meenakshisundaram.kandhavelu@tuni.fi

[1] Molecular Signaling Group, Faculty of Medicine and Health Technology, Tampere University and BioMediTech, P.O.Box 553, 33101 Tampere, Finland

[2] Department of Biotechnology, Lady Doak College, Thallakulam, Madurai 625002, India

[3] Faculty of Engineering and Natural Sciences, Tampere University, Korkeakoulunkatu 8, 33101 Tampere, Finland

[4] LAQV-REQUIMTE, Department of Chemistry, University of Aveiro, 3810-193 Aveiro, Portugal

[5] Department of Basic Medical Sciences, College of Medicine, Prince Sattam Bin Abdulaziz University, Al-Kharj 11942, Kingdom of Saudi Arabia

[6] Computational Systems Biology Research Group, Faculty of Medicine and Health Technology and BioMediTech, Tampere University, P.O.Box 553, 33101 Tampere, Finland

[7] Institute for Systems Biology, 1441N 34th Street, Seattle, WA 98103-8904, USA

Abbreviations

HIC	1 (1-(2-Hydroxy-5-nitrophenyl) (4-hydroxyphenyl) methyl)indoline-4-carbonitrile)
P2Y1R	Purinergic G-protein coupled receptor
AR	Androgen receptor
PCa	Prostate cancer
GPCRs	G protein-coupled receptors
PBS	Phosphate-buffered saline
DMSO	Diluted in dimethyl sulfoxide
MTT	3-(4,5-Dimethylthiazol-2-yl)-2,5-Diphenyltetrazolium Bromide
DAPI	4′,6-Diamidino-2-phenylindole
AA	Abiraterone acetate
PI	Propidium iodide

Introduction

Prostate cancer (PCa) is the most common malignant tumour diagnosed in men around the world [1]. It is known as the third leading cancer causing death in males, estimated at around 0.3 million patients' death per year [2]. However,

metastatic PCa remains incurable due to its resistant characteristics against many chemotherapeutic drugs. Recently, second-generation anti-androgen therapy such as abiraterone acetate (AA), apalutamide, bicalutamide, etc. [3–7] is considered as a potential therapy for treating PCa. The research for novel strategies and regimens to treat PCa has being continued but reducing the doses of drugs and improving the patients' lives remains an open challenge.

Anti-androgen therapy is often utilized to treat PCa and increase the patients' survival [8, 9]. In the early stage of PCa, medical or surgical castration is the common method for patients treatment [10, 11]. However, the disease can still progress and be resistant to the primary treatment. Such a type of cancer is called castrate-resistant PCa (CRPC) [12]. In androgen receptor (AR)-positive cell line (LNCap cells), the anticancer effect of androgen biosynthesis inhibitor AA was observed to occur via the degradation of the CYP17A1 enzyme. This cytochrome P450, family 17, subfamily A, polypeptide 1 enzyme is crucial for androgen-dependent cancers and hyperplasia [13, 14]. AA inhibits the production of androgens by interfering with the enzymes C17α hydroxylase and C17-C20 lyase, which suppresses PCa cells growth and metastasis [15]. Based on the down-regulated mechanism of AA, the common hypothesis is that the drug reduces the expression of AR and inhibits AR signaling, which is the crucial antitumor activity of the drug [16]. The clinical studies reported promising results in Phase I and II trials of patients with metastatic CRPC tested [17, 18]. Thus, AA (Zytiga, Janssen Biotech Inc.) was accepted by the US Food and Drug Administration (FDA) for patients with metastatic CRPC who had received prior chemotherapy [19]. FDA later approved the use of AA tablets in combination with castration and prednisone for the treatment of metastatic high-risk castration sensitive PCa (CSPC) [20, 21]. We have previously found limited evidence of AA activity, at low concentrations of AA, in inhibiting the proliferation of AR-negative PC3 and DU145 cells [22, 23]. Martina et al. reported that 2 μM of AA did not show cell death in PC3 and DU145 after 96 h treatment [22]. Additionally, it is evident that treatment of 30 μM AA can induce apoptosis on PC3 cell death [23]. On the other hand, purinergic receptor 1 ($P2Y_1R$) is highly expressed in PC3 and DU145 cells in both normal and cancer cells [24–27]. The activation of $P2Y_1R$ is suggested as a therapeutic target for suppressing PCa cell growth [26]. For example, MRS 2365, a selective agonist of P2Y1R, decrease cell proliferation and increase apoptotic cells' and Caspase 3's activities in PC3 cells [26]. Recently, we designed and synthesized a $P2Y_1R$ agonist, 1-(1-((2-hydroxy-5-nitrophenyl)(4-hydroxyphenyl)methyl)indoline-4-carbonitrile (HIC) to activate the $P2Y_1R$ signaling [28–30]. HIC is a time- and dose-dependent selective inhibitor of PC3 and DU145 cell growth [28]. In addition, the activation of P2Y1R induces apoptosis, Caspase 3/7 activity, and ROS production in these cell lines [28]. Although the activity of HIC was identified as a potential drug-like compound again the growth of PC3 and DU145, the combinatorial effect of HIC along with any known clinical drug is yet to be investigated.

In this work, we aim to investigate the combinatorial effect of HIC and AA in the treatment of PC3 and DU145 cells. Here we measure the PCa cell death in a dose- and time-dependent manner, and colony formation. We have also measured the combinational index (CI) for the combinatorial activity of HIC and AA. Further, the anticancer and anti-metastasis effects were evaluated by apoptosis, caspase 3/7, ROS formulation, wound healing, and invasion assay. Finally, we have also measured the combinatorial effect of HIC and AA on PCa cell phase arrest. The comprehensive in vitro evaluation of combined HIC and AA of the present study will provide a basis for future clinical studies.

Materials and methods

Preparation of chemicals

Compound 1-(1-((2-hydroxy-5-nitrophenyl)(4-hydroxyphenyl)methyl)indoline-4-carbonitrile (HIC) was synthesized as described previously [28]. Abiraterone acetate (AA) was purchased from Sigma-Aldrich (St. Louis, MO, USA). HIC and AA compounds were diluted at 100 μM stocks in dimethyl sulphoxide (DMSO; Sigma-Aldrich).

Cell culture

PCa cell lines, PC3 and DU145, were cultured in Minimum essential medium eagle (MEME; Sigma-Aldrich). Noncancer cell lines HEK293 and MEF were maintained in Dulbecco's modified eagle medium–high glucose (DMEM; Sigma-Aldrich). Mediums were supplemented with 10% Fetal bovine serum (Biowest, Nuaille, France), 0.1 mg/mL streptomycin, 100 U/mL penicillin (Sigma-Aldrich), and 0.025 mg/mL amphotericin B (Sigma-Aldrich). Cells were grown at 37 °C in a humidified condition of 5% CO_2. Cells were passaged every 3–4 days using trypsin 1X (Sigma-Aldrich). To prepare cells for assays, cells were counted using trypan blue solution (Sigma-Aldrich) and countess II FL automated cell counter (ThermoFisher Scientific, Waltham, MA, USA).

Cell proliferation and cytotoxicity assay

To determine the sensitivity of PCa and noncancer cells to HIC and AA, cells were plated with a density of 1×10^4 cells/well in 96-well clear-bottom plates for 24 h. Cells were dosed with various concentrations of HIC (1.25, 2.5, 5, 7.5, 15, and 40 μM) and AA (5, 10, 20, 30, 40, and 50 μM) for

48 h. For the combinational drug model, PCa cell lines and noncancer cells were seeded in 96-well clear-bottom plates at a density of 1×10^4 cells/well for 24 h incubation. PC3 and DU145 cells were incubated with DMSO, HIC (1, 5, 10, 15, and 20 µM), AA (3, 15, 30, 45, and 60 µM), or combination of HIC and AA for 48 h. HEK293 and MEF cells were treated with HIC (1, 5, 10, and 15 µM) and AA (3, 15, 30, and 45 µM) together. After 48 h treatment, cell death was determined using MTT cell proliferation and cytotoxicity assay kit (Bosterbio, CA, USA) as described previously [28]. Briefly, the cells were labelled with MTT labelling reagent (0.5 mg/mL MTT reagent final concentration in phosphate-buffered saline, PBS) and incubated for 4 h in a humidified chamber. Then, formazan solubilization solution was added to each well and kept for 4 h in a dark condition. Treatments were carried out in triplicate. The optical densities (OD) of the supernatants were measured at 570 nm using a Magellan™ microplate reader (Tecan Group Ltd., Switzerland). The inhibitory effects of drugs were calculated using the equation given below,

$$\%inhibition = \frac{A_c - A_{tr}}{A_c} \times 100 \quad (1)$$

where A_c is the cell number of untreated cells, and A_{tr} is the cell number of drugs treated cells. DMSO treated groups was considered as the vehicle control.

Combination therapy assays

The mechanism of drug interaction was determined using the combination index (CI). CI values were calculated using the CompuSyn software (ComboSyn Inc., Paramus, NJ, USA) following the below equation [31, 32].

$$CI = \frac{(D1)}{(Dx)1} + \frac{(D2)}{(Dx)2} \quad (2)$$

(Dx)1 and (Dy)2 are the concentration of each drug required to produce the same effects as the effect produced by doses D1 and D2 in the combination [(D1) + (D2)]. CI values < 0.9, 0.9 < CI < 1.1, and 1.1 < CI indicate synergistic, additive, and antagonistic effect of two drugs, respectively [33].

Pharmacokinetic assay

PC3 and DU145 cells were seeded in a 96-well plate at 1×10^4 cells/well. After 24 h incubation, PCa cells were treated with DMSO, 10 µM HIC, 30 µM AA, and 10 µM HIC + 30 µM AA for 24, 48, and 72 h in an incubator. MTT cell proliferation and cytotoxicity assay kit were used to determine cell death. Inhibition percentage was analyzed using Eq. 1 for cell viability assay. DMSO sample was used as vehicle control.

Colony assay

PC3 and DU145 cells were seeded at 500 cells per well in six-well plates and incubated overnight. The cells were then treated with DMSO, 10 µM HIC, 30 µM AA, or with combinations of HIC and AA. The media with and without drugs were refreshed every 3 days. After incubation for 12 days, the plates were washed gently two times with PBS. Colonies were then treated with fixing solution (3.7% paraformaldehyde in PBS) for 10 min in RT. The colonies were washed two times with PBS and stained with a 0.05% crystal violet solution for 10 min at room temperature. Images were captured under a microscope. Colonies over 50 cells were counted directly using an Axiovert 200 M microscope (Carl Zeiss, Germany). Survival fraction was measured using Eq. 3. DMSO-treated samples were considered vehicle samples.

$$Inhibitory\ ratio(\%) = \frac{No.\ of\ colonies\ treated\ with\ drugs}{No.\ of\ cell\ treated\ with\ vehicle} \times 100\% \quad (3)$$

4′,6-Diamidino-2-Phenylindole, dihydrochloride (DAPI), Annexin V, and propidium iodide (PI) staining assay

To determine the induction of apoptotic and necrosis by that target drugs, we carried out the cell apoptosis assay using a dead cell apoptosis kit (Sigma-Aldrich) and DAPI staining (ThermoFisher Scientific). PC3 and DU145 cells were plated in a six-well plate with a density of 5×10^5 cells/well. After 24 h incubation, cells were incubated with DMSO, 10 µM HIC, and/or 30 µM AA for 48 h. The cells were collected with PBS and then incubated with 50 µL 1X Annexin-binding buffer from the kit for 15 min in the dark condition. Then 5 µL FITC conjugated Annexin V, 1 ng/mL PI, and 300 nM DAPI was added to the cell suspension for 15 min in an incubator. The fluorescence images of cells were captured using EVOS FL (ThermoFisher Scientific) under 20× objective for each analysis. The fluorescence microscopy image data was analyzed to find out the differences in the plasma membrane integrity and permeability using Annexin V/PI dual staining. We have integrated both the semi-automated image processing along with manual counting to extract the fluorescence intensity values and thus measured the percentage of apoptotic and necrotic cells.

Caspase 3/7 activity

To determine the caspase 3/7 activity, PC3 and DU145 cells were seeded in 96-well white plates at a density of 1×10^4 cells/well overnight. The cells were treated with DMSO, 10 µM HIC, 30 µM AA, and combinational 10 µM HIC and 30 µM AA for 5 h. AA is the suitable control which not only act as a anti-androgen therapy for treating prostate cancer, but also functions as a caspase-3 inhibitor. Caspase 3/7 was measured by using a Caspase-Glo®3/7 assay kit (Promega, Madison, WI, USA) following the manufactural protocol. Caspase-Glo reagent was added to the cells and then incubated in an incubator for 1 h. The luminescence of the samples was measured using a Magellan™ microplate reader. The fold change of Caspase 3/7 activity was determined using the below equation,

$$Fold\ increase = \frac{L_{test} - L_{blank}}{L_{control} - L_{blank}} \quad (4)$$

where: L_{test} is the luminescence of drugs treated wells; L_{blank} is the luminescence of untreated wells and; $L_{control}$ is the luminescence of the unstained wells.

ROS assay

PC3 and DU145 cells were plated in 12-well plates with a density of 1×10^5 cells/well overnight. The cells were treated with 10 µM HIC, 30 µM AA, 10 µM HIC + 30 µM AA, and 10 mM hydrogen peroxide (H_2O_2) as a positive control for ROS for 5 h. The cells were collected and then incubated with 20 µM 2',7'-dichlorodihydrofluorescein diacetate (H2DCFA) (Sigma-Aldrich) for 30 min in the dark condition. The stained cells were washed 2 times with PBS and incubated in the culture medium for 20 min in an incubator. The fluorescence of ROS products was measured at 485 nm (excitation) and 538 nm (emission) by a Magellan™ microplate reader. The fold change of ROS production was calculated according to Eq. 5.

$$Fold\ change = \frac{F_{test} - F_{blank}}{F_{control} - F_{blank}} \quad (5)$$

where: F_{test} is the fluorescence of drugs treated cells; $F_{control}$ is the fluorescence of untreated cells and; F_{blank} is the fluorescence of unstained cells.

Cell cycle analysis

PC3 and DU145 cells were plated in a 6-well plate at the density of 5×10^6 cells/well. After 24 h incubation, the cells were dosed with DMSO, 10 µM HIC, 30 µM AA, or the combination of HIC and AA for 48 h. Cell phases were determined using a propidium iodide kit (Sigma-Alrich). The cells were washed two times with cold PBS and then fixed in 70% ethanol on ice for 10 min. Subsequently, the cells were dyed in 200 µL of PI-Triton-RNase solution (20 µg/mL PI, 0.2 mg/mL RNase, and 0.1% Triton X-100 in PBS) for 15 min in the dark condition. Fluorescence images were captured using EVOS FL at 20 × magnification. The images were analyzed using CellProfiler software 4.0 [34] and cell cycle phases were calculated using MATLAB R2020a (MathWorks Ltd., MA, USA).

Wound-healing assay

PC3 and DU145 cells were seeded in six-well plates with a density of 1.5×10^6 cells/well for 24 h. At 80–90% confluence, the wound was made with 200 µL pipette tips. The floating cells were removed by washing the plates two times with warm PBS. The cells were then incubated with DMSO, 10 µM HIC, and/or 30 µM AA in 1% FBS media for 24 h. The images of the migrated cells into the wound surface were captured using EVOS imaging systems. The wound areas were measured using ImageJ software 1.52 (National Institutes of Health, USA). The wound closure was calculated using Eq. 6.

$$W_{change} = \frac{W_{0-D} - W_{24-D}}{W_{0-C} - W_{24-C}} \times 100\% \quad (6)$$

where: $W_{0\text{-}D}$ is the scratch area in samples treated with drugs at the starting point; $W_{24\text{-}D}$ is the scratch area in samples treated with drugs after 24 h incubation; $W_{0\text{-}C}$ is the scratch area in vehicle groups at the starting point and; $W_{24\text{-}C}$ is the scratch area in vehicle groups after 24 h incubation. DMSO treated groups were considered as the vehicle groups.

Invasion assay

Transwells (6-well type, pore size 8 µm) were coated with Corning® Matrigel® Basement Membrane Matrix (Corning, NY, USA) for 2 h in an incubator. PC3 and DU145 cells (5×10^5 cells/well) were seeded to the upper chamber in the absence or presence of HIC and AA in 1% FBS media. The lower chamber was completely filled with FBS medium. After 24 h incubation, the chambers' membranes were treated with Fixing solution (3.7% paraformaldehyde in PBS) for 10 min. Next, the chambers were washed gently with warm PBS. The membranes with invaded cells were stained with 0.5% crystal violet in 2% EtOH. After 5 min, the membranes were washed with PBS and kept dry at room temperature. Five random fields of the membranes were observed. Invaded cells were calculated based on the average number of cells from five random areas. Data were

presented as the percentage of the number of invaded cells based on the vehicle group.

Statistical analysis

All the experiments were repeated three or five times with the same biological and technical conditions. The results are represented as means ± standard error of the mean (SEM) using IBM SPSS Statistics version 26. Differences between samples groups and experimental conditions were analyzed using one-way ANOVA followed by GraphPad Prism 8.0 software. Statistical significance was considered with $*p < 0.05$.

Results

Sensitivity of PCa and noncancer cells to HIC and AA

To assess the effective concentrations of HIC and AA (Fig. 1A) on cell death, PCa and non-cancer cells were incubated with increasing concentrations of HIC and AA for 48 h and cell viability was determined by MTT assay. Results show that HIC decreased cellular growth in a concentration-dependent manner compared to vehicle-treated cells (Fig. 1B). At a dosage of 40 μM HIC, PC3 and DU145 cells were inhibited to ~ 80% after 48 h treatment. At the same concentrations of HIC, the cell growth of HEK293 and MEF cells was similar to DMSO control groups (Fig. 1B). The IC_{50} values of HIC for PC3 and DU145 cells were determined as 15.98 μM and 15.64 μM, respectively. Conversely, AA showed lower inhibitory effects on the growth of PCa cells than HIC at 40 μM after 48 h treatment (Fig. 1C). The cell death was observed at about 34.6 ± 1.8% and 43.6 ± 1.9% in PC3 and DU145 cells at 40 μM AA treatment. These results are consistent with prior findings that AA had slight inhibitory effects on cell proliferation of PC3 and DU145 cells which have low expression of AR [22, 23]. Therefore, our results suggest that PC3 and DU145 cells are more sensitive to HIC than AA.

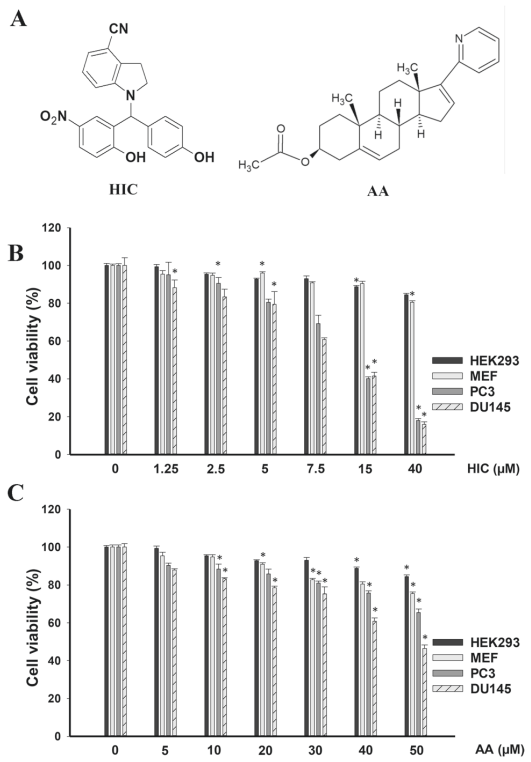

Fig. 1 Sensitivity of PCa and noncancer cells to HIC and AA. Structure of HIC and AA (**A**). Percentage of cell viability with HIC treatment (**B**) and AA treatment (**C**) were determined using MTT assay. PC3, DU145, HEK293, and MEF cells were treated with increasing doses of HIC and AA for 48 h. Values are presented as the means ± SD of three biological experiments. $*p < 0.05$ relatives to DMSO-treated group

HIC and AA cotreatment reduces cell growth in PCa cells

Next, to understand the effect of combined drugs treatment, PC3 and DU145 cells were treated with HIC and AA alone and the combination of HIC and AA (HIC + AA) at specific concentrations, as described in the methods section. Based on the sensitivity of HIC and AA on PC3 and DU145 cells, HIC and AA concentrations were adjusted to maintain a constant 1:3 ratio of HIC:AA for PC3 and DU145 cells. When HIC and AA were combined, a dramatic reduction in cell viability was observed (Fig. 2A, B). Cell death in both PC3 and DU145 cells ~ 50% was observed when in presence of 15 μM HIC or 45 μM AA (Fig. 2A, B). At an intermediate dosage of combined 10 μM HIC and 30 μM AA cell proliferation was inhibited more than 50% in both cell lines. These results identified that the co-treatment of HIC + AA induced stronger inhibitory effects on cell growth in PCa cells than using a single drug treatment. Subsequently, HEK 293 and MEF cells treated with the same concentrations of two drugs did not show a significant decrease in cell survival compared with vehicle groups (Fig. 2C). The synergistic effect of HIC and AA was analyzed based on CI values. Table 1 shows the CI values for DU145 and PC3 cells treated with the combination of HIC and AA. CI values less than 0.9, from 0.9 to 1.1, or more than 1.1 allow indicating the quantification of synergism, additive, or antagonism of two drugs, respectively. In addition, the combination of 10 μM HIC and 30 μM AA was less sensitive to the non-cancer cells

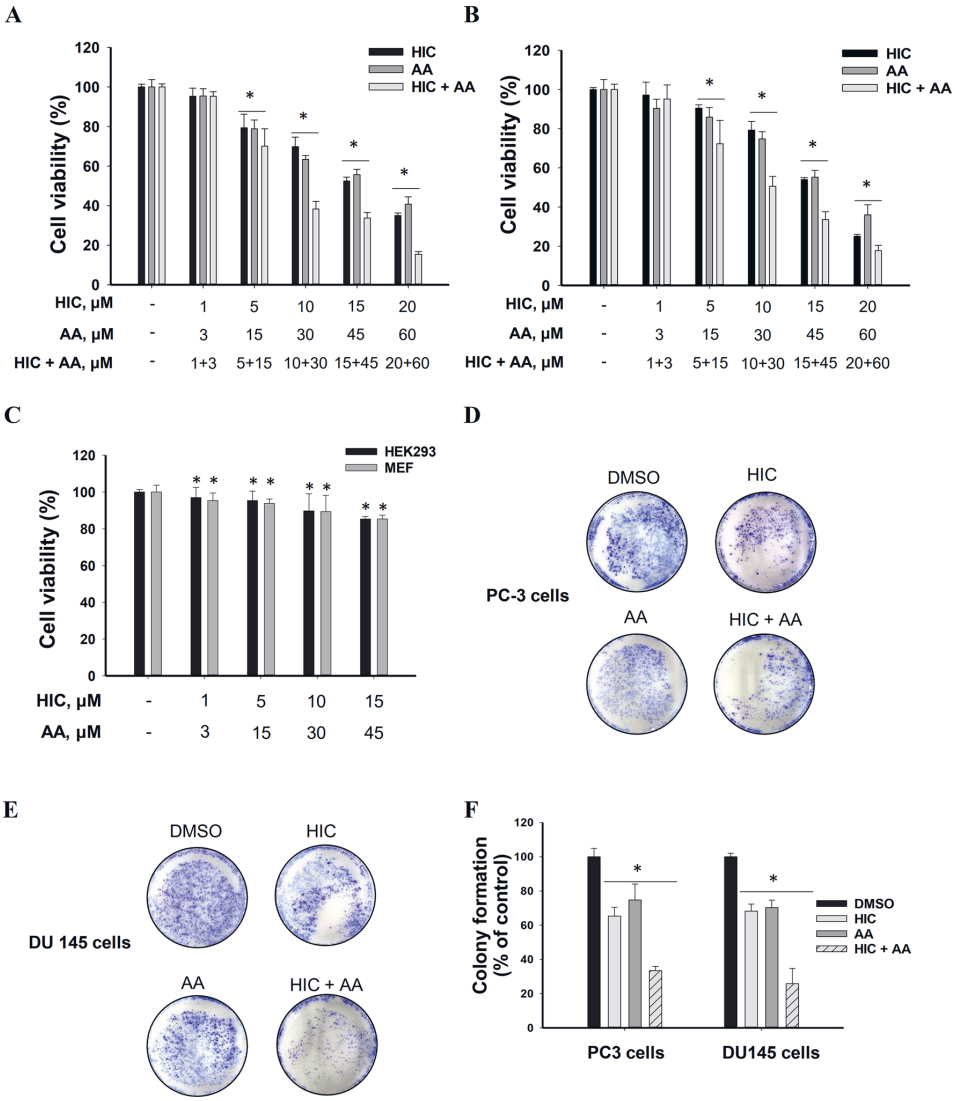

Fig. 2 HIC and AA co-treatment reduces cell growth in PCa cells. Percentage of PC3 (**A**) and DU145 (**B**) cells viability in the presence of HIC and AA, alone or in combination with indicated concentrations. Percentage of cell viability for HEK293 and MEF cells with co-treated HIC and AA (**C**). Representative images of PC3 (**D**) and DU145 (**E**) cells treated with HIC, AA, or a combination of both in Clonogenic survival assay. The bar graph presented the colony formulation of PCa cells with HIC and AA treatment based on the normalization with DMSO groups (**F**). Data were analyzed by one-way ANOVA; $*p < 0.05$ relatives to DMSO-treated group

Table 1 Combination index (CI) values for combined use of HIC and AA in PC3 and DU145 cells

Cell lines	HIC μM	AA μM	Effect %	CI	Cell lines	HIC μM	AA μM	Effect %	CI
PC3 cells	1	3	4.88	2.02	DU145 cells	1	3	6.71	1.89
	5	15	27.71	1.33		5	15	30.02	1.49
	10	30	49.43	1.11		10	30	61.63	0.85
	15	45	66.45	0.88		15	45	66.23	1.06
	20	60	82.23	0.57		20	60	84.69	0.53

survival (Fig. 2C) than for PCa cells (Fig. 2A, B). Therefore, these combinatorial concentrations were selected to perform further experiments.

To determine the anticancer effect of combined HIC and AA, the effects of both drugs on tumour cell clonogenicity in PC3 and DU145 cells were examined. Cells were treated with HIC and AA as described in the methods section. As shown in Fig. 2D, E, cotreatment with HIC and AA markedly inhibited PCa colony formation more than in single drugs treatment. In detail, PC3 colony formation was reduced by 34.7%, 25.3%, and 59.5% by HIC, AA, and HIC + AA combined treatments, respectively (Fig. 2F). The effect of HIC and AA cotreatment was 1.7 and 2.4 times more effective than HIC and AA alone. Similarly, the decrease of DU145 colonies was observed as 31.7%, 23.7%, and 60.1% by the presence of HIC, AA, and HIC + AA, respectively (Fig. 2F). The combined use of HIC and AA increased 1.5 to 2 times the effect of single AA in both PC3 and DU145 cells. These data purpose that the combinatorial treatment of HIC + AA can stop the colony formation. It is worth to suggest that the combinatorial treatment can stop the PCa cells division in vitro.

Combination of HIC and AA inhibits the proliferation of PCa cells in a time-dependent manner

Growth kinetics of cells treated with HIC, AA and HIC + AA were measured as described in the methods section to understand the effect of using combined drugs over time. As shown in Fig. 3A, the cell proliferation in treated PC3 cells was significantly lower in HIC and AA treatment than in the control group over time. The inhibition on the proliferation of PC3 cells was about 11.7%, 30.1%, and 54.4% by HIC, and about 4.6%, 20.1%, and 59.2% by AA treatments, at 24 h, 48 h, and 72 h respectively. However, a stronger inhibitory effect was observed in the combined use of HIC and AA groups after 24 h treatment. HIC and AA cotreatment induced 10.6%, 57.6%, and 74.4% of PC3 cell growth at 24 h, 48 h, and 72 h, respectively. Similarly, in DU145 cells, the cell proliferation was decreased from 50.5 to 97.3% progressively from 24 to 72 h on the treatment with HIC and AA. However, the impact of HIC and AA co-presence showed a reduced proliferation to 90.3%, 40.5%, and 17.5% at 24, 48, and 72 h, respectively. These findings suggest that the proliferation was inhibited on treatment with HIC + AA stronger than in single-drug treatments. In addition, HIC and AA could inhibit cancer cell proliferation by increasing the treatment time.

Combinatorial effect of HIC and AA induces apoptosis through caspase 3/7 activation and ROS production

To investigate whether synergistic loss of cell viability in PCa cells was related to the apoptotic process or not, we further examined the effect of drugs by Annexin V-affinity assay. Post 48 h of treatment, the fluorescent microscope images of PCa cells were captured to expose the presence of apoptotic (green) and necrotic (red) cells (Fig. 4). As shown in Fig. 4A, co-treatment of HIC and AA significantly increased the number of apoptotic cells (green) more than DMSO groups after 2 days of treatment. The increase of apoptotic cells in PC3 cells was observed ~ 12.2% and 14.2% by HIC and AA single treatment, respectively, whereas the combinatorial drugs induced 40.4% apoptotic population (Fig. 4A). Similarly, the induction of apoptotic responses in DU145 cells was 34.8% in the co-treatment of HIC and AA whereas 15.2% and 14.3% increases were determined in treatments with HIC and AA, respectively. These findings suggest that AA in combination with HIC induced apoptosis in PC3 and DU145 cells in agreement with the observed inhibitory effects on cell survival.

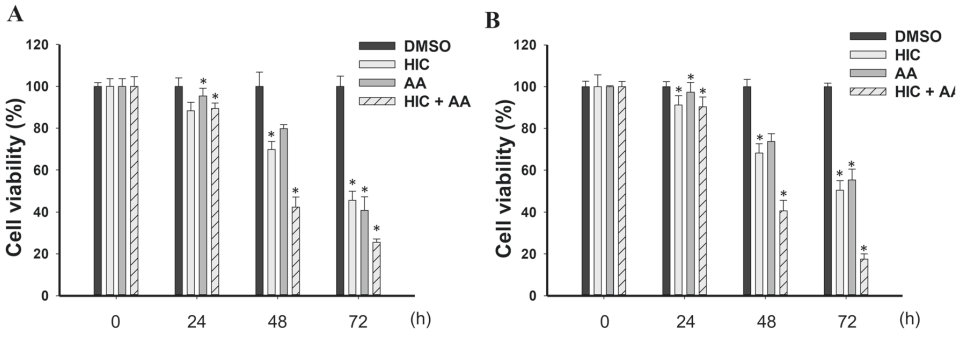

Fig. 3 Combination of HIC and AA inhibits the proliferation of PCa cells in a time-dependent manner. Percentage of cell viability in **A** PC3 and **B** DU145 cells treated with HIC, AA, and HIC + AA combination for 24, 48, and 72 h. The percentage of cell survival was normalized to DMSO groups. The experiment was performed with n = 6. Statistical significance was considered with *$*p < 0.05$*

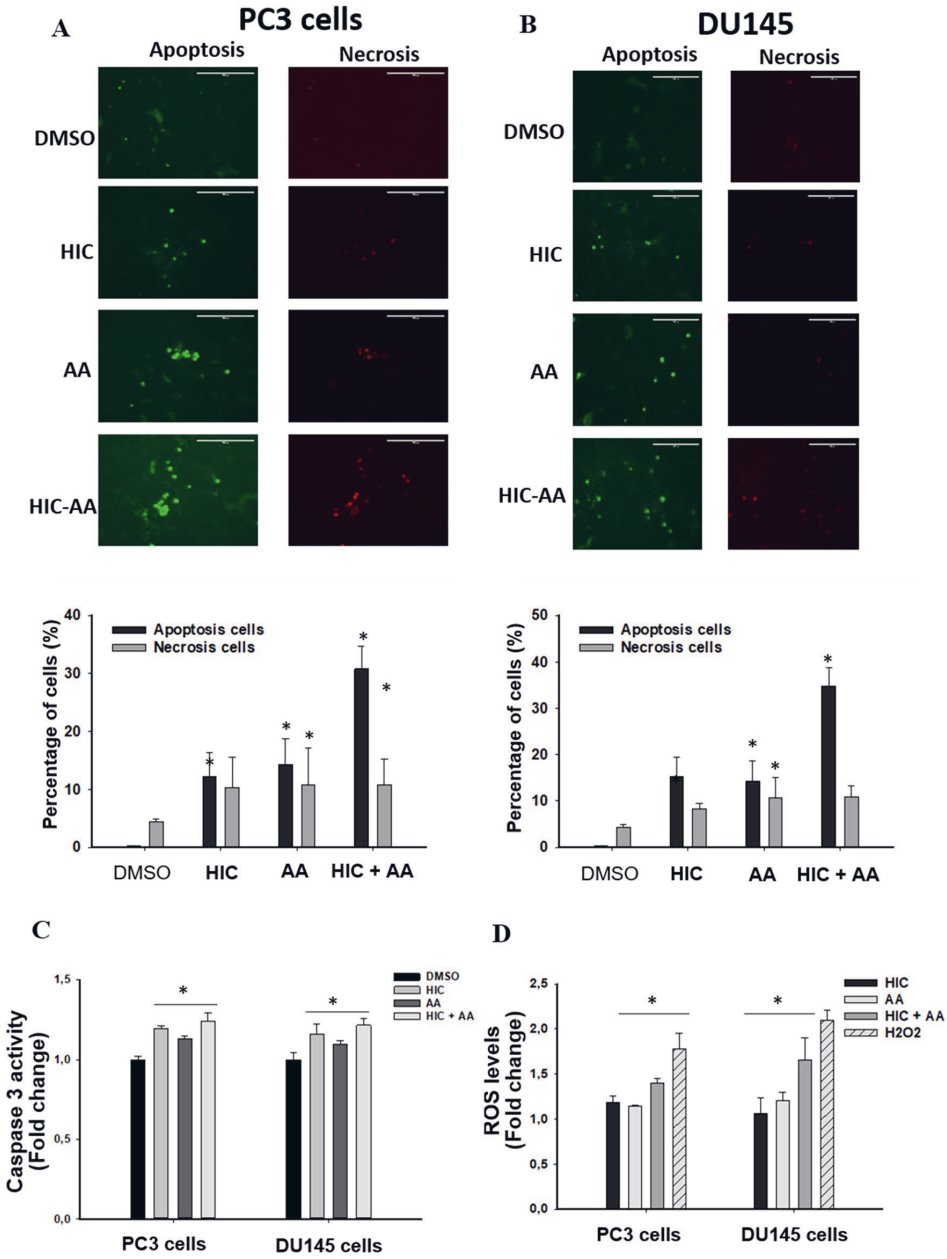

Fig. 4 Combinatorial effect of HIC and AA induces apoptosis, caspase 3/7 activation, and ROS production. Representative images of PC3 (**A**) and DU145 (**B**) cells stained with DAPI/Annexin-V/PI in DMSO, HIC, AA, and cotreated drugs condition. Percentage of apoptotic and necrotic cells were presented in the corresponding conditions. **C** Fold changes of caspases 3/7 activity in PC3 and DU145 cells compared to DMSO groups. **D** Fold change of ROS production in PC3 and DU145 cells were calculated using fluorescence intensities based normalized against DMSO control. Biological and technical replicates were performed to analyze the results, with mean ± SD, $*p < 0.05$, n = 6

The activation of Caspase 3/7 is known as the crucial player in cell death and apoptosis [35]. To investigate the anticancer effect of HIC and AA, a Caspase 3/7 assay was performed in PC3 and DU145 cells. On treatment with the combination of HIC and AA, PC3 and DU145 cells have shown increasing fold changes of Caspase 3/7 (Fig. 4C). We noticed an increase in fold change of caspase 3/7 activity to 1.19 and 1.12 in HIC- and AA-treated PC3 cells, respectively, when compared to the vehicle group. Interestingly, the increase of Caspase 3/7 activity was observed in HIC and AA-cotreated PC3 cells with a fold change of about 1.24. Likewise, the activation of Caspase 3/7 in DU145 cells also increased to 1.15- and 1.09-fold change on treatment with HIC and AA whereas HIC + AA showed 1.21 caspase 3/sevenfold change. The difference in the fold change of treated and untreated groups was considered as a statistical analysis through ANOVA test with $p < 0.05$. These findings showed that the combined treatment with HIC and AA, induced more caspase activity than treatment with one of the single compounds. Moreover, HIC and AA could induce apoptosis through the Caspase 3/7 dependent signaling pathway. It is noted that caspase-3 play a crucial role in the apoptosis process in various cell lines, which is primarily responsible for the cleavage of poly(ADP-ribose) polymerase (PARP) during cell death. In our previous study [36], we have reported the total gene expression profile of PC3 and DU145 cells treated with HIC compound. We found the downregulation of PARP10 and PARP12 expression in both the cell lines. Furthermore, PARP1 and PARP14 was also downregulated in PC3 cells, while PARP9 was downregulated in DU145 cells. These observations further support that caspase 3 is activated upon the treatment of HIC compound." The differential expression of PARP is plotted as graph and presented as a supplementary Fig. 1.

Accumulation of ROS at mitochondria is one of the apoptotic mechanisms in the intrinsic cell death pathway [37, 38]. A high level of ROS might damage proteins, nucleic acid, and result in oxidative stress and cellular dysfunctions [39]. In addition, ROS is known as a capable stimulator inducing cell cycle arrest and cell death in cancer therapeutics [40]. In order to investigate the effect of HIC and AA combination on PCa via ROS productivity, PC3 and DU145 cells were treated with HIC, AA, and H_2O_2 (positive control). As shown in Fig. 4D, the fold change of ROS production increased in the presence of HIC, AA, and H_2O_2 in both cell lines. The fold change of ROS was increased ~ 1.2 in both HIC- or AA-treated PCa cells. HIC and AA co-treatment increased the fold change of ROS with 1.4 and 1.6 in PC3 and DU145 cells, respectively. Therefore, ROS productivity was noticeably higher in HIC + AA-treated cells than in HIC- and AA-treated cells.

Combined use of HIC and AA suppresses the G1 phase of the PCa cell cycle

Apoptosis is the major cellular response that can regulate cell cycle arrest and induce cell death [41, 42]. To evaluate whether the combination of HIC and AA induces cell cycle distribution in PCa cells, cell cycle analysis was examined as described in the methods section. Fig. 5A, B exemplify fluorescence images of DNA content in each cell phase, treated by selected compounds. The cells were segmented to detect the distribution of each phase under different conditions. The proportion of the G1 phase of PC3 cells was increased after treatment with HIC and AA by 35.5% and 55.7%, respectively, compared to the vehicle group with 16.4% for the G1 phase. Interestingly the combined use of HIC with AA induced the highest G1 proportion to 75.1% (Fig. 5A). The transition of S phase of PC3 cells was not significantly different among vehicle, HIC, and AA treatment, about 34.0%, 40.1%, and 34.4%, respectively. Interestingly, the distribution of G1 phase in DU145 cells was observed as the same as in PC3 cells. A higher percentage of the G1 phase, 77.1%, was observed in the combinatorial treatment of HIC and AA. The proportion of G1 phase in DU145 cells treated with HIC and AA was calculated as 44.5% and 60.5%, respectively. Furthermore, in the S phase of DU145 cells, the percentage of the population in HIC, AA, and HIC + AA, and vehicle-treated cells was 30.0%, 15.0%, 9.0%, and 24.0%, respectively. Notably, a higher fraction of G1 phase arrest in both PC3 and DU145 cells was observed in HIC and AA co-treated groups. Taken together, the results suggested that the combined treatment of HIC and AA arrested the PCa cells at G1 proliferation phases, leading to higher suppression than the treatments with HIC and AA alone.

Metastatic activity of PCa cells was inhibited by treatment with HIC and AA

The cell migration and invasion are known as important characteristics of malignant tumour cells, thus inhibiting migration and invasion of cells are considered as crucial targets in developing new anticancer therapeutics [43, 44]. Here we performed the cell migration and invasion assay to investigate the effect of HIC and/or AA on PC3 and DU145 cells. As shown in Fig. 6A, the PCa cells were scratched and treated with drugs. The invaded areas of PCa cells after HIC + AA treatment decreased steadily after 12 h of incubation whilst it increased over time after DMSO treatment. 24 h of post-treatment, the invaded areas of PC3 cells decreased to 23.5%, 27.1%, and 46.4% by HIC, AA, and HIC + AA, respectively. Notably, a similar pattern was also observed in DU145 cells. The percentage of migrated cells in DU145 cells was reduced to 29.5% by HIC, 35.2% by AA, and 55.5% by HIC + AA treatment. In addition, to further

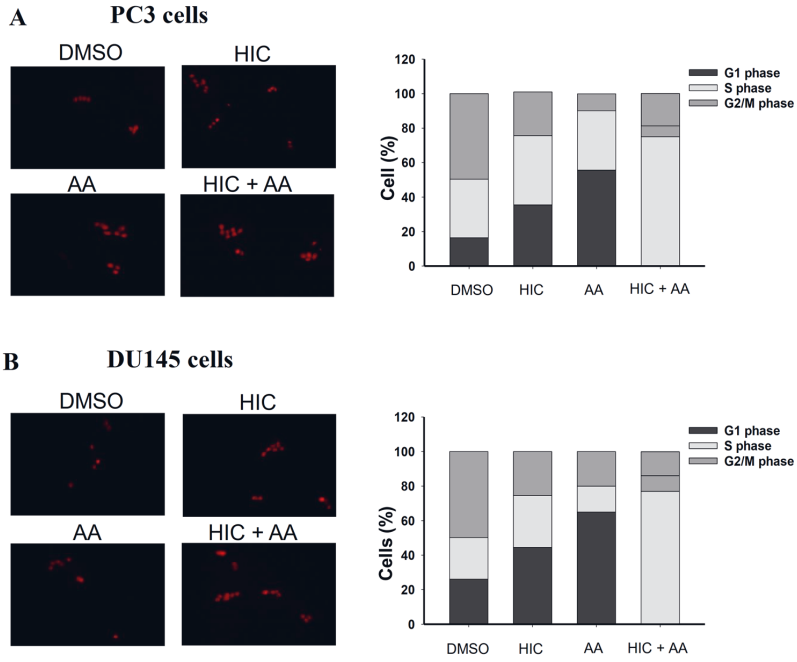

Fig. 5 Combination of HIC and AA suppresses the G1 phase of the PCa cell cycle. PC3 and DU145 cells were treated with HIC and AA alone or in combination for 48 h. Cells were fixed and stained with PI. Microscopic images of PC3- (**A**) and DU145- (**B**) treated cells were captured and analyzed to detect cell-cycle distribution. The percentage of cells in each phase was calculated and presented. Data is shown as mean ± SD, *$p < 0.05$, n = 6

explore the anti-metastasis effect on the invaded cells, we performed the invasion assay with HIC and AA co-treatment. PC3 and DU145 cells were treated with HIC and AA and then measured the invaded activity via Matrigel-coated transwell after 24 h treatment. As shown in Fig. 6B, cell invasion decreased in both cells when drugs were present. A significant decrease caused by HIC and AA co-treatment was observed in DU145 cells. In detail, the invaded cells in DU145 cells were inhibited to 78.5%, 75.7%, and 52.4% by HIC, AA, and HIC + AA treatments, respectively (Fig. 6B). These results demonstrate that the combination of both HIC and AA potentially inhibits cell migration and invasion of PCa cells.

Discussion

In the present study, we characterized the pharmacological activity of HIC, P2Y1 receptor agonist, in androgen-independent cancer cell lines models PC-3 and DU145. Former studies concerning HI, have served as proof of principle: PC-3 and DU145 cell growth inhibition was induced by HIC were the compound act as a p53 stabilizer in prostate cancer cells, however, the detailed molecular mechanism of HIC in combination with any clinical drugs are yet to be investigated [30]. Here, we investigated the potential mechanism involved in the inhibition of cell growth in AR-negative-cell lines, PC3 and DU145, by AA and HIC co-treatments. Our results suggest that these cell lines were sensitive to HIC at the IC_{50} range of 15–18 µM after 48 h treatment. The metastatic cell lines PC3 and DU145 which are both AR low and represent castrate-resistant metastatic disease, are equally responsive to HIC. AR-negative PC3 and DU145 cells exhibited comparably growth inhibition responses to the presence of AA.

The applied AA concentration of 40 µM induced ~ 50% cell death after 48 h treatment. AA was minimally effective in killing PC3 and DU145 cells at the concentration utilized, but the combination of both compounds results in synergistic-induced loss of cell viability. Moreover, normal cell lines are less sensitive to the combined effects of HIC and AA than PCa cells in the same conditions. Concerning the apoptosis produced by the combination of HIC and AA, we showed that Caspase 3/7 activity and ROS formulation increased due to the synergic effect of the two drugs. One possible mechanism of cell death is cell cycle arrest. The cell phases arrested by AA and HIC in these cells have not been reported. Here, we found that the combination between HIC and AA suppressed the G1 phase in both cell lines.

Besides the numerous AR signaling events in PCa cells, chemotherapy widely exerts its anticancer effect by triggering apoptotic mechanisms of tumour cells [45]. A primary regulator of apoptosis is the tumour suppressor p53, which plays a key role in cell cycle control, genomic stability, and apoptosis [46]. Increased DNA fragmentation as well as downregulation of the cell survival factor surviving also

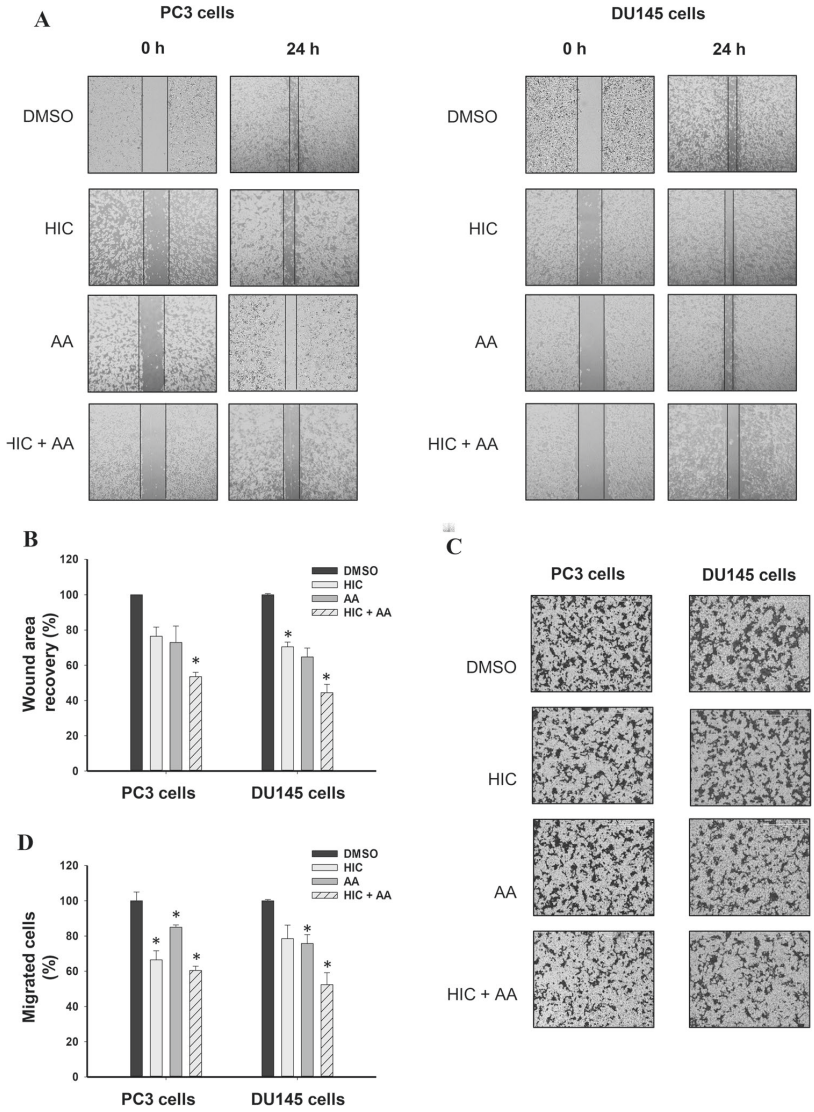

Fig. 6 Inhibition of metastatic properties of PCa cells. **A** The wounds of PC3 and DU145 cells were created using a scratcher, and then cells were incubated with HIC, AA, alone or a combination of both. Representative images were captured at 0 and 24 h. A mark in these images was placed to locate the same area on the scratch. Percentage of relative wound closure was shown as a bar graph. **B** Invaded cells were captured under the microscope. The bar graph presented is the percentage of cell invasion based on DMSO groups. Experiments were repeated three times with technical repeats, n = 6, *$p < 0.05$, ANOVA test

confirm the involment of execution of apoptotic mechanisms. Further, increased level of the cell cycle inhibitor p21 and the effector caspase3 also confirms the role of apoptosis ativation [47], 48. From our previous studies, HIC was known to induce the stability of p53 and regulate p21 signaling in PCa cells. The decrease of mRNA levels was observed in *CDK2*, *Cyclin E*, *Cyclin A*, *CDK4* in the incubation of HIC in PC3 and DU145 cells [30]. Interestingly, DNA fragment was determined as one factor in the HIC downregulation mechanism. Moreover, the levels of *BAX*, *Caspase3*, *p21*, and *Survivin* also increased in the presence of 30 μM of AA after 48 h in PC3 cells [23]. In this work, our results showed the increase of Caspase3/7 activity and ROS production with the combined use of HIC and AA. Notably, the G1 phase was arrested by the synergic effect of HIC and AA after 48 h. Taken together, our observations suggest that AA and HIC could mediate the cell death in PC3 and DU145 cells through the activation of apoptosis via p53, p21 signaling. AR signal is not the only rationale to explain the anticancer activity of AA in PCa cells. In addition, the presence of HIC + AA potentially inhibited cell proliferation. Therefore, the combination of HIC and AA would be considered as a promising agent in the treatment of AR-negative PCa cells. In summary, the activation

of the P2Y1 receptor by HIC and its combination with AA demonstrated that the HIC might be an attractive agent for the treatment of prostate cancer.

Conclusion

In summary, our results show that the HIC and AA induce apoptosis-mediated cell death through the activation of Caspase3/7 and ROS production. The synergistic effect of HIC and AA affects prostate cancer cells proliferation in a time-dependent manner, and their migration, invasion, colony-forming ability, and cell cycle progression in the G1 phase. More importantly, the combination of two compounds, a P2Y1 receptor agonist and an androgen receptor inhibitor, is found to be a potential combinatorial drug to overcome prostate cancer.

Supplementary Information The online version contains supplementary material available at https://doi.org/10.1007/s10495-022-01716-1.

Acknowledgements We thank Tampere University for providing all instrumental facility.

Author contributions NRC synthesized and characterized the compounds; HL executed the experiments and data analysis. AM and TR involved in technical discussion, quality check and manuscript editing. OY and MK conceived and managed all studies. All the authors contributed to writing the manuscript.

Funding HL acknowledge the TUT-RAE for the project grant support.

Data availability The datasets generated analysed during the current study are available from the corresponding author on reasonable request.

Declarations

Conflict of interest The authors declare that they have no competing interests.

Ethical approval Not applicable.

Informed consent Not applicable.

Consent for publication Not applicable.

References

1. Leitzmann MF, Rohrmann S (2012) Risk factors for the onset of prostatic cancer: age, location, and behavioral correlates. Clin. Epidemiol 4:1–11
2. Siegel RL, Miller KD, Jemal A (2020) Cancer statistics, 2020. CA Cancer J Clin. https://doi.org/10.3322/caac.21590
3. Ruterbusch JJ, Bylsma LC, Barlev A et al (2017) Bicalutamide treatment patterns in elderly prostate cancer patients: a historical cohort study using the surveillance, epidemiology and end results program (SEER)-medicare database. Val Heal 20(5):A127–A128
4. Rathkopf DE, Scher HI (2018) Apalutamide for the treatment of prostate cancer. Expert Rev Anticancer Ther. https://doi.org/10.1080/14737140.2018.1503954
5. Scher HI, Fizazi K, Saad F et al (2012) Increased survival with enzalutamide in prostate cancer after chemotherapy. N Engl J Med. https://doi.org/10.1056/nejmoa1207506
6. Smith MR, Saad F, Chowdhury S et al (2018) Apalutamide treatment and metastasis-free survival in prostate cancer. N Engl J Med. https://doi.org/10.1056/nejmoa1715546
7. Sternberg CN, Castellano D, Daugaard G et al (2014) Abiraterone acetate for patients with metastatic castration-resistant prostate cancer progressing after chemotherapy: final analysis of a multicentre, open-label, early-access protocol trial. Lancet Oncol. https://doi.org/10.1016/S1470-2045(14)70417-6
8. Heinlein CA, Chang C (2004) Androgen receptor in prostate cancer. Endocr Rev 105(34):12182–12187
9. Tan ME, Li J, Xu HE et al (2015) Androgen receptor: Structure, role in prostate cancer and drug discovery. Acta Pharmacol Sin 36(1):3–23
10. Weiner AB, Cohen JE, DeLancey JO et al (2020) Surgical versus medical castration for metastatic prostate cancer: use and overall survival in a National Cohort. J Urol. https://doi.org/10.1097/ju.0000000000000684
11. Garje R, Chennamadhavuni A, Mott SL et al (2020) Utilization and outcomes of surgical castration in comparison to medical castration in metastatic prostate cancer. Clin Genitourin Cancer. https://doi.org/10.1016/j.clgc.2019.09.020
12. Karantanos T, Corn PG, Thompson TC (2013) Prostate cancer progression after androgen deprivation therapy: mechanisms of castrate resistance and novel therapeutic approaches. Oncogene 32(49):5501–5511
13. Pal SK, Patel J, He M et al (2018) Identification of mechanisms of resistance to treatment with abiraterone acetate or enzalutamide in patients with castration-resistant prostate cancer (CRPC). Cancer. https://doi.org/10.1002/cncr.31161
14. Bremmer F, Jarry H, Strauß A et al (2014) Increased expression of CYP17A1 indicates an effective targeting of the androgen receptor axis in castration resistant prostate cancer (CRPC). J Korean Phys Soc. https://doi.org/10.1186/2193-1801-3-574
15. Kluetz PG, Ning YM, Maher VE et al (2013) Abiraterone acetate in combination with prednisone for the treatment of patients with metastatic castration-resistant prostate cancer: US food and drug administration drug approval summary. Clin Cancer Res 19(24):6650–6656
16. Bedoya DJ, Mitsiades N (2014) Expert Review of Anticancer Therapy Abiraterone acetate, a first-in-class CYP17 inhibitor, establishes a new treatment paradigm in castration-resistant

prostate cancer. Expert Rev Anticancer Ther. https://doi.org/10.1586/era.11.196
17. Amm J, Aragon Ching JB (2013) The changing landscape in the treatment of metastatic castration-resistant prostate cancer. Ther Adv Med Oncol 5(1):25–40
18. Bryce A, Ryan CJ (2012) Development and clinical utility of abiraterone acetate as an androgen synthesis inhibitor. Clin Pharmacol Ther 91(1):101–108
19. McKay RR, Silver R, Bhak RH et al (2020) Treatment of metastatic castration resistant prostate cancer with radium-223: a retrospective study at a US tertiary oncology center. Prostate Cancer Prostatic Dis. https://doi.org/10.1038/s41391-020-00271-7
20. US Food and Drug Administration (2018) FDA approves abiraterone acetate in combination with prednisone for high-risk metastatic castration-sensitive prostate cancer. https://www.fda.gov/drugs/informationondrugs/approveddrugs/ucm596015.htm. Accessed 15 June 2020
21. Sipra QUAR, Bin RI, Asghar N et al (2020) Treatment of metastatic castration sensitive prostate cancer (mCSPC) by disease volume: A systematic review and a meta-analysis. J Clin Oncol. https://doi.org/10.1200/jco.2020.38.15_suppl.e17539
22. Fragni M, Galli D, Nardini M et al (2019) Abiraterone acetate exerts a cytotoxic effect in human prostate cancer cell lines. Naunyn Schmiedebergs Arch Pharmacol. https://doi.org/10.1007/s00210-019-01622-5
23. Grossebrummel H, Peter T, Mandelkow R et al (2016) Cytochrome P450 17A1 inhibitor abiraterone attenuates cellular growth of prostate cancer cells independently from androgen receptor signaling by modulation of oncogenic and apoptotic pathways. Int J Oncol. https://doi.org/10.3892/ijo.2015.3274
24. Li WH, Qiu Y, Zhang HQ et al (2013) P2Y2 receptor promotes cell invasion and metastasis in prostate cancer cells. Br J Cancer. https://doi.org/10.1038/bjc.2013.484
25. Shabbir M, Ryten M, Thompson C et al (2008) Characterization of calcium-independent purinergic receptor-mediated apoptosis in hormone-refractory prostate cancer. BJU Int. https://doi.org/10.1111/j.1464-410X.2007.07293.x
26. Wei Q, Costanzi S, Liu QZ et al (2011) Activation of the P2Y1 receptor induces apoptosis and inhibits proliferation of prostate cancer cells. Biochem Pharmacol. https://doi.org/10.1016/j.bcp.2011.05.013
27. Janssens R, Communi D, Pirotton S et al (1996) Cloning and tissue distribution of the human P2Y1 receptor. Biochem Biophys Res Commun. https://doi.org/10.1006/bbrc.1996.0640
28. Le HTT, Rimpilainen T, Konda Mani S et al (2019) Synthesis and preclinical validation of novel P2Y1 receptor ligands as a potent anti-prostate cancer agent. Sci Rep. https://doi.org/10.1038/s41598-019-55194-8
29. Le HTT, Murugesan A, Ramesh T et al (2021) Molecular interaction of HIC, an agonist of P2Y1 receptor, and its role in prostate cancer apoptosis. Int J Biol Macromol 189:142–150. https://doi.org/10.1016/j.ijbiomac.2021.08.103
30. Le HTT, Murugesan A, Candeias NR et al (2021) Functional characterization of HIC, a P2Y1 agonist, as a p53 stabilizer for prostate cancer cell death induction. Futur Med Che 13(21):1845–1864
31. Chou TC (2006) Theoretical basis, experimental design, and computerized simulation of synergism and antagonism in drug combination studies. Pharmacol Rev 58(3):621–681
32. Chou TC, Talalay P (1984) Quantitative analysis of dose-effect relationships: the combined effects of multiple drugs or enzyme inhibitors. Adv Enzyme Regul. https://doi.org/10.1016/0065-2571(84)90007-4
33. Chou TC (2018) The combination index (CI < 1) as the definition of synergism and of synergy claims. Synergy 7:49–50
34. McQuin C, Goodman A, Chernyshev V et al (2018) Cell profiler 3.0: next-generation image processing for biology. PLoS Biol. https://doi.org/10.1371/journal.pbio.2005970
35. Brentnall M, Rodriguez-Menocal L, De Guevara RL et al (2013) Caspase-9, caspase-3 and caspase-7 have distinct roles during intrinsic apoptosis. BMC Cell Biol. https://doi.org/10.1186/1471-2121-14-32
36. Le Thu HT, Murugesan A, Candeias NR et al (2021) Functional characterization of HIC, a P2Y1 agonist, as a p53 stabilizer for prostate cancer cell death induction. Future Med Chem. https://doi.org/10.4155/fmc-2021-0159
37. Redza-Dutordoir M, Averill-Bates DA (2016) Activation of apoptosis signalling pathways by reactive oxygen species. Biochim Biophys Acta Mol Cell Res 1863:2977–2992
38. Simon HU, Haj-Yehia A, Levi-Schaffer F (2000) Role of reactive oxygen species (ROS) in apoptosis induction. Apoptosis. https://doi.org/10.1023/A:1009616228304
39. Fleury C, Mignotte B, Vayssière JL (2002) Mitochondrial reactive oxygen species in cell death signaling. Biochimie. https://doi.org/10.1016/S0300-9084(02)01369-X
40. Feher A, Ötvös K, Pasternak TP, Pettkó-Szandtner A (2008) The involvement of reactive oxygen species (ROS) in the cell cycle activation (G 0 -to-G 1 transition) of plant cells. Plant Signal Behav. https://doi.org/10.4161/psb.3.10.5908
41. Vermeulen K, Berneman ZN, Van Bockstaele DR (2003) Cell cycle and apoptosis. Cell Prolif 36(3):165–175
42. Elmore S (2007) Apoptosis: a review of programmed cell death. Toxicol Pathol 35:495–516. https://doi.org/10.1080/01926230701320337
43. Martin T, Ye L, Sanders A, et al (2014) Cancer invasion and metastasis: molecular and cellular perspective. Metastatic Cancer Clin Biol Perspect
44. Ju A, Cho YC, Kim BR et al (2018) Anticancer effects of methanol extract of Myrmecodia platytyrea Becc leaves against human hepatocellular carcinoma cells via inhibition of ERK and STAT3 signaling pathways. Int J Oncol. https://doi.org/10.3892/ijo.2017.4178
45. Bagnyukova T, Serebriiskii IG, Zhou Y et al (2010) Chemotherapy and signaling: how can targeted therapies supercharge cytotoxic agents? Cancer Biol Ther 10:839–853
46. Ozaki T, Nakagawara A (2011) Role of p53 in cell death and human cancers. Cancers (Basel) 3:994–1013
47. Lossi L, Castagna C, Merighi A (2018) Caspase-3 mediated cell death in the normal development of the mammalian cerebellum. Int J Mol Sci 19(12):3999
48. Zhang JH, Xu M (2000) DNA fragmentation in apoptosis. Cell Res 10:205–211